Optimization and Design for Heavy Lift Launch Vehicles

A Thesis Presented for a
Masters of Science
The University of Tennessee, Knoxville

Paul Andreas Ritter
May 2012

Copyright © by Paul Andreas Ritter
All rights reserved

DEDICATION

This thesis is dedicated to both Jesus Christ and my wonderful family who have both made completing this project possible.

ACKNOWLEDGEMENTS

I would like to thank Dr. Evans Lyne for inspiring and pushing me to work on this project. Without this encouragement, I would not have developed a deeper understanding of the components of launch vehicles and the tools necessary to accurately model such a vehicle. These ideas and inspiration have provided a methodology and work ethic that I will be able to use the rest of my life. I would also like to thank Dr. Robert McAmis and Dr. Kivanc Ekici who serve on the thesis committee.

I would also like to thank NASA for providing me with the opportunity to work with them. Specifically, I am very grateful to Dr. Jonathon Jones and Jason Campbell for their direction and willingness to answer the many questions that I had when developing the modeling code.

There are also numerous people that answered many questions for me and provided encouragement when things got tough. I would like to thank my Mom, Dad, and brother, the Hixson family, Dr. John Blevins, Stephen Phillips, Dale Jackson, Rachel Johnson, Tim Kibbey, and to anyone else who might have offered an encouraging word.

Abstract

The simulation and evaluation of an orbital launch vehicle requires consideration of numerous factors. These factors include, but are not limited to the propulsion system, aerodynamic effects, rotation of the earth, oblateness, and gravity. A trajectory simulation that considers these different factors is generated by a code developed for this thesis titled Trajectories for Heavy-lift Evaluation and Optimization (THEO). THEO is a validated trajectory simulation code with the ability to model numerous launch configurations. THEO also has the capability to provide the means for an optimization objective. Optimization of a launch vehicle can be specified in terms of many different variables. For a heavy lift launch vehicle in this thesis, the goal of optimization is to minimize Gross Lift Off Weight (GLOW). THEO provides the capability to optimize by simulating hundreds of thousands of trajectories for a single configuration through the variation of preset independent variables. The sheer volume of these trajectories provides the means to locate configurations that minimize GLOW. Optimization can also be performed by determining the minimum amount of energy necessary to reach target burnout conditions. The energy requirements are then correlated to the propellant mass which can be used to estimate GLOW. This thesis first discusses the validation of THEO as a simulation program and the properties associated with accurately modeling a trajectory. It then relates how THEO and other developed tools can be utilized to determine a configuration that is optimized to minimize GLOW to orbit for adaptable payload sizes.

Table of Contents

Chapter 1 – Introduction **1**
1.1. Original Thesis Objective 2
1.2. Revised Objective 2
1.3. Thesis Significance 3

Chapter 2 – Trajectory Tool Development and Validation **4**
2.1. Options for Trajectory Modeling 5
2.1.1. Matlab 5
2.1.2. POST 5
2.1.3. Introducing a New Code 6
2.2. THEO Objectives 6
2.2.1. Programming Language Selection 6
2.3. Launch Trajectory Description 7
2.3.1. Relating Pitch and Flight Path Angle 7
2.3.2. Pitch Angle Conditions 7
2.3.3. Vehicle Properties 8
2.4. THEO Validation 8
2.4.1. Validation Constraints 8
2.4.2. Validation Configuration 9
2.4.3. Gravity and Planet Properties 10
2.4.4. Atmospheric Model 10
2.4.5. Level of Trajectory Complexity 12
2.4.6. Equation of Motion 13
2.4.7. Method of trajectory Modeling within THEO 14
2.4.8. Revised Equations of Motion 15
2.4.9. Aerodynamic Coefficients 16
2.4.10. Thrust Profile 18
2.4.11. Validation of Output Data 19
2.5. THEO as an Optimization Tool 25
2.5.1. Defining a Successful Case 25
2.5.2. Additional Independent Variables 26
2.6. Data Output Files 26
2.7. Completed FORTRAN Improvements 27

Chapter 3 – Aerodynamic Considerations and Evaluation **29**
3.1. Atmospheric Model 30
3.2. Aerodynamic Effects 30
3.2.1. Lift 30
3.2.2. Drag 31
3.2.3. Dynamic Pressure 33
3.2.4. Aerodynamic Heating 33
3.2.5. Aerodynamic Acoustics 33
3.2.6. Static Stability 34
3.3. Missile DATCOM 34
3.3.1. Purpose and Capability 34

3.3.2. Limitations 35
3.4. Nose Cone Analysis 35
3.4.1. Shroud Consderations 35
3.4.2. Nose Cone Types 37
3.4.3. Nose Cone Reference Model 38
3.4.4. Nose Cone Performance and Properties 39
3.4.5. Final Fairing Selection 42
3.5. Aerodynamic Coefficient Estimation 43

Chapter 4 – Rocket Propulsion 48
4.1. Rocket Propulsion Systems 49
4.1.1. Liquid 49
4.1.2. Solid 50
4.1.3. Hybrid 50
4.1.4. Nuclear 50
4.1.5. Electric 50
4.2. Rocket Performance 51
4.2.1. Evaluating Thrust 51
4.2.2. Nozzle Inefficiencies 51
4.2.3. Specific Impulse 52
4.2.4. The Rocket Equation 52
4.3. Propulsion System Advantages and Disadvantages 54
4.3.1. Solid Propulsion Systems 54
4.3.2. Liquid Propulsion Systems 56
4.4. Optimization Engine Selections 58
4.4.1. Solid Rocket Boosters 58
4.4.2. Liquid Rocket Engines 59

Chapter 5 – Independent Variables and Computation Considerations 61
5.1. Independent Variables 62
5.1.1. Primary Pitch Event Start Time 62
5.1.2. Length of Primary Pitch Event 63
5.1.3. Primary Pitch Event Pitchrate 66
5.1.4. Stage Propellant Mass 66
5.2. THEO Time Step 69

Chapter 6 – Analysis Methodology and Secondary Tools 71
6.1.Vehicle Optimization Utilizing THEO 72
6.1.1. THEO Decision Logic 72
6.1.2. Three Dimensional Visualization 72
6.1.3. Intersection Curves 74
6.1.4. Variable to Optimize 75
6.2. Rocket Equation Optimization 76
6.2.1. Mathematical Approach 76
6.2.2. Velocity Budget Analysis Approach 77
6.3. Optimization Methods Comparison 80

Chapter 7 – Launch Vehicle Analysis and Results **82**
7.1. Configuration Types 83
7.2. 2.5 Stage RSRM Vehicle 85
7.2.1. 2.5 Stage RSRM Aerodynamic Coefficients 85
7.2.2. Inert Mass Correction 86
7.2.3. 2.5 Stage RSRM General Analysis 87
7.2.4. 2.5 Stage RSRM Refined Analysis 90
7.2.5. 100 mt Payload Requirement for 2.5 Stage RSRM 95
7.2.6. 60 mt Payload Requirement for 2.5 Stage RSRM 97
7.3. 2.5 Stage RSRM V Vehicle 98
7.3.1. 2.5 Stage RSRM V Aerodynamic Coefficients 98
7.3.2. 2.5 Stage RSRM V General Analysis 99
7.3.3. 2.5 Stage RSRM V Refined Analysis 102
7.3.4. 100 mt Payload Requirement for 2.5 Stage RSRM V 104
7.3.5. 60 mt Payload Requirement for 2.5 Stage RSRM V 107
7.4. 2.5 Stage M550 FW3 Vehicle 108
7.4.1. 2.5 Stage M550 Aerodynamic Coefficients 109
7.4.2. 2.5 Stage M550 General Analysis 109
7.4.3. 2.5 Stage RM550 Refined Analysis 111
7.4.4. 100 mt Payload Requirement for 2.5 Stage M550 117
7.4.5. 60 mt Payload Requirement for 2.5 Stage M550 119
7.5. 2.5 Stage P80 Vehicle 121
7.5.1. 2.5 Stage P80 Aerodynamic Coefficients 121
7.5.2. 2.5 Stage P80 General Analysis 121
7.5.3. 2.5 Stage P80 Refined Analysis 124
7.5.4. 100 mt Payload Requirement for 2.5 Stage P80 129
7.5.5. 60 mt Payload Requirement for 2.5 Stage P80 130
7.6. 2 Stage Vehicle 131
7.6.1. 2 Stage Vehicle Aerodynamic Coefficients 132
7.6.2. 2 Stage Vehicle General Analysis 132
7.6.3. 2 Stage Vehicle Refined Analysis 133
7.6.4. 100 mt Payload Requirement for 2 Stage Vehicle 137
7.6.5. 60 mt Payload Requirement for 2 Stage Vehicle 139
7.7. 2 Stage Booster Vehicle 139
7.7.1. 2 Stage Booster Vehicle Aerodynamic Coefficients 139
7.7.2. 2 Stage Booster Vehicle General Analysis 140
7.8. 1.5 Stage RSRM V Vehicle 141
7.8.1. 1.5 Stage RSRM V Vehicle Aerodynamic Coefficients 141
7.8.2. 1.5 Stage RSRM V Analysis 142

Chapter 8 – Conclusion **146**
8.1. Final Results 147
8.2. Continued Study and Improvements 148

Appendices **150**
Appendix A **151**
Appendix B **152**
Vita **162**

List of Tables

Chapter 1
Table 1.1 – Thesis Task Delegation 3

Chapter 2
Table 2.1 – Rocket Validation Configuration 9
Table 2.2 – Earth Standard Properties 10
Table 2.3 – Pitch Event Parameters 19
Table 2.4 – Sample Inputs for Independent Variables 26

Chapter 3
Table 3.1 – Historical Nose Cone and Fairing Comparison 38
Table 3.2 – Specified Missile DATCOM Descriptors 39
Table 3.3 – Nose Cone Mass and Volume Comparison 41
Table 3.4 – Lift and No Lift Comparison 44

Chapter 4
Table 4.1 – Sample Velocity Budget 53
Table 4.2 – Liquid Propellant Properties 57
Table 4.3 – Engine Parameter Comparison 57
Table 4.4 – Liquid Engine Selections 59

Chapter 6
Table 6.1 – Sample Vehicle 78

Chapter 7
Table 7.1 – Initial Configurations 83
Table 7.2 – Independent Variable Specifications 85
Table 7.3 – Inert Mass Adjustment Comparison 87
Table 7.4 – 2.5 Stage RSRM General Analysis Top Configurations 87
Table 7.5 – Pitch Analysis Bounds 88
Table 7.6 – 2.5 Stage RSRM GLOW Minimization Cases 91
Table 7.7 – Revised 2.5 Stage RSRM GLOW Minimization Cases 92
Table 7.8 – 2.5 Stage RSRM Configuration for 130 mt Payload 93
Table 7.9 – 100 mt Derivative of 2.5 Stage RSRM Vehicle 95
Table 7.10 - 60 mt Derivative of 2.5 Stage RSRM Vehicle 97
Table 7.11 - 2.5 Stage RSRM V General Analysis Top Configurations 99
Table 7.12 – 2.5 Stage RSRM V GLOW Minimization Cases 102
Table 7.13 - 2.5 Stage RSRM V Configuration for 130 mt Payload 103
Table 7.14 - 100 mt Derivative of 2.5 Stage RSRM V Vehicle 106
Table 7.15 - 60 mt Derivative of 2.5 Stage RSRM V Vehicle 107
Table 7.16 - 2.5 Stage M550 General Analysis Top Configurations 110
Table 7.17 - 2.5 Stage 3 M550 GLOW Minimization Cases 111
Table 7.18 - 2.5 Stage 3 M550 GLOW Minimization Cases Revised 112
Table 7.19 - 2.5 Stage 4 M550 GLOW Minimization Cases 114
Table 7.20 - 2.5 Stage M550 130 mt Payload Vehicle Selections 115

List of Tables (cont.)

Table 7.21 - 2.5 Stage M550 Configuration for 130 mt Payload 115
Table 7.22 - 100 mt Derivative of 2.5 Stage M550 FW3 Vehicle 117
Table 7.23 - 60 mt Derivative of 2.5 Stage M550 FW3 Vehicle 119
Table 7.24 – 2.5 Stage M550 FW3 Configuration Summary 120
Table 7.25 – 2.5 Stage P80 General Analysis Top Configurations 122
Table 7.26 – 2.5 Stage 7 P80s GLOW Minimization Cases 124
Table 7.27 – 2.5 Stage 8 P80 GLOW Minimization Cases 125
Table 7.28 - 2.5 Stage P80 130 mt Payload Vehicle Selections 126
Table 7.29 - 2.5 Stage M550 Configuration for 130 mt Payload 127
Table 7.30 - 100 mt Derivative of 2.5 Stage P80 Vehicle 129
Table 7.31 - 60 mt Derivative of 2.5 Stage P80 Vehicle 130
Table 7.32 - 2.5 Stage P80 Vehicle Configuration Summary 131
Table 7.33 – 2 Stage General Analysis Top Configurations 132
Table 7.34 – 2 Stage GLOW Minimization Cases 134
Table 7.35 – 2 Stage Configuration for 130 mt Payload 134
Table 7.36 – Saturn V and 2 Stage Vehicle Comparison 136
Table 7.37 – 100 mt 2 Stage Vehicle 138
Table 7.38 – 60 mt 2 Stage Vehicle 139
Table 7.39 – 2 Stage Vehicle Configuration Summary 139
Table 7.40 – 2 Stage Booster General Analysis Top Configurations 140
Table 7.41 – 1.5 Stage RSRM V with Multiplication Factor 142
Table 7.42 – 1.5 Stage RSRM V with Booster Adjustments 143
Table 7.43 – 1.5 Stage RSRM V Vehicle Comparison 144
Table 7.44 – Minimized GLOW for 1.5 Stage Vehicle 144

Chapter 8
Table 8.1 – Overall Configuration Comparison 147

List of Figures

Chapter 2
Figure 2.1 – Vehicle Reference Angles 7
Figure 2.2 – Model Configuration 9
Figure 2.3 – Atmospheric Model Validation 11
Figure 2.4 – Coriolis Effect 14
Figure 2.5 – Aerodynamic Coefficient Validation 16
Figure 2.6 – Aerodynamic Force Validation 17
Figure 2.7 – Thrust Profile Validation 18
Figure 2.8 – Altitude Comparison 20
Figure 2.9 – Velocity Comparison 20
Figure 2.10 – Acceleration Comparison 21
Figure 2.11 – Rate of change of FPA Comparison 21
Figure 2.12 – Velocity Azimuth Comparison 22
Figure 2.13 – Altitude Validation Plot 23
Figure 2.14 – Velocity Validation Plot 23
Figure 2.15 – Acceleration Validation Plot 24
Figure 2.16 – Rate of FPA Validation Plot 24
Figure 2.17 – Velocity Azimuth Validation Plot 25

Chapter 3
Figure 3.1 – Lifting Bodies 31
Figure 3.2 – Base Drag 32
Figure 3.3 – Sample Nose Cone Shapes 36
Figure 3.4 – Nose Cone Analysis Reference Shape 38
Figure 3.5 – Drag Coefficient Profile for Various Nose Cones 39
Figure 3.6 – NACA Nose Cone Foredrag Coefficients 40
Figure 3.7 – Sample Decibel Variation across a Binconic Nose Cone 42
Figure 3.8 – Missile DATCOM Drag Coefficient Estimation 43
Figure 3.9 – Missile DATCOM Lift Coefficient Estimation 44
Figure 3.10 – Altitude, Inertial Velocity, and Inertial Flight Path Angle Comparison 45
Figure 3.11 – Pitch Induced Angle of Attack 46
Figure 3.12 – Lift due to Angle of Attack 46

Chapter 4
Figure 4.1 – RSRM Thrust Profile 54
Figure 4.2 – Grain Cross Sections 55
Figure 4.3 – Propellant Mass Ratio 56
Figure 4.4 – Booster Thrust Profile Comparison 58

Chapter 5
Figure 5.1 – Primary Pitch Event Start Time 64
Figure 5.2 – Length of Primary Pitch Event 65
Figure 5.3 – Primary Pitch Event Pitchrate 67
Figure 5.4 – Stage Propellant Mass 68
Figure 5.5 – THEO Time Increment 70

List of Figures (cont.)

Chapter 6

Figure 6.1 – Vehicle Burnout Altitude 73
Figure 6.2 – Vehicle Burnout Inertial Velocity 73
Figure 6.3 – Vehicle Burnout Inertial FPA 74
Figure 6.4 – Intersection Curve Groups 74
Figure 6.5 – GLOW versus Stage 1 ΔV fraction 79
Figure 6.6 – Stage Reassignment 80

Chapter 7

Figure 7.1 – Sample Vehicle Configurations 84
Figure 7.2 – RSRM Configuration Lift Coefficient Profile 86
Figure 7.3 – RSRM Configuration Drag Coefficient Profile 86
Figure 7.4 – Case 5a Intersection Curves 89
Figure 7.5 – Case 6a Intersection Curves 89
Figure 7.6 – Case 6a Revised Intersection Curves 90
Figure 7.7 – Case a11 Intersection Curves 91
Figure 7.8 – Case a11 Revised Intersection Curves 92
Figure 7.9 – 2.5 Stage RSRM Stability Surface for 130 mt Configuration 93
Figure 7.10 – 2.5 Stage RSRM Aerodynamic Limits Check 94
Figure 7.11 – 100 mt Derivative of 2.5 Stage RSRM GLOW vs ΔV Curve 96
Figure 7.12 – 60 mt Derivative of 2.5 Stage RSRM GLOW vs. ΔV Curve 98
Figure 7.13 – RSRM V Configuration Lift Coefficient Profile 98
Figure 7.14 – RSRM V Configuration Drag Coefficient Profile 99
Figure 7.15 – Case 7b Intersection Curves 100
Figure 7.16 – Case 7b Revised Intersection Curves 101
Figure 7.17 – Case 8b Intersection Curves 101
Figure 7.18 – Case 8b Revised Intersection Curves 102
Figure 7.19 – Case b5 Intersection Curves 103
Figure 7.20 – 2.5 Stage RSRM V Stability Surface for 130 mt Configuration 104
Figure 7.21 – 2.5 Stage RSRM V Aerodynamic Limits Check 105
Figure 7.22 – 100 mt Derivative of 2.5 Stage RSRM GLOW vs ΔV Curve 107
Figure 7.23 – 60 mt Derivative of 2.5 Stage RSRM GLOW vs. ΔV Curve 108
Figure 7.24 – M550 Configuration Drag Coefficient Profile 109
Figure 7.25 – Case 2c Intersection Curves 111
Figure 7.26 – 2.5 Stage M550 Stability Surface for Case c5 113
Figure 7.27 – 2.5 Stage M550 Stability Surface for Case c4a 113
Figure 7.28 - 2.5 Stage M550 Stability Surface for Case c3b 114
Figure 7.29 - 2.5 Stage M550 Aerodynamic Limits Check 116
Figure 7.30 - 2.5 Stage M550 100 mt Stability Surface for Case 17ca 118
Figure 7.31 - 2.5 Stage M550 60 mt Stability Surface for Case 13cb 120
Figure 7.32 – P80 Configuration Drag Coefficient Profile 121
Figure 7.33 – Case 4d Intersection Curves 123
Figure 7.34 – Case 4d Revised Intersection Curves 123
Figure 7.35 - Case 7d Intersection Curves 124
Figure 7.36 - Case 7d Revised Intersection Curves 125

List of Figures (cont.)

Figure 7.37 - 2.5 Stage P80 130 mt Payload Vehicle Selections 126
Figure 7.38 - 2.5 Stage P80 Stability Surface for Case d5a 127
Figure 7.39 - 2.5 Stage P80 Aerodynamic Limits Check 128
Figure 7.40 - 2.5 Stage P80 100 mt Stability Surface for Case 3dd 129
Figure 7.41 - 2.5 Stage P80 60 mt Stability Surface for Case 8de 131
Figure 7.42 – 2 Stage Configuration Drag Coefficient Profile 132
Figure 7.43 - Case 5e Intersection Curves 133
Figure 7.44 – Case e4 Intersection Curves 134
Figure 7.45 - 2 Stage Aerodynamic Limits Check 135
Figure 7.46 – 130 mt 2 Stage Vehicle Stability 136
Figure 7.47 – Saturn V Vehicle Stability 137
Figure 7.48 – 100 mt 2 Stage Vehicle Stability 138
Figure 7.49 - 2 Stage Booster Configuration Drag Coefficient Profile 140
Figure 7.50 – 1.5 Stage RSRM V Configuration Drag Coefficient Profile 142
Figure 7.51 – Modified Thrust Profiles for RSRM V Booster 144
Figure 7.52 – 1.5 Stage RSRM V Aerodynamic Limits Check 145

Chapter 8
Figure 8.1 – Overall Optimized Configuration 149

Nomenclature

English Characters

$\boldsymbol{a}$	= acceleration vector
A	= cross-sectional area
C_D	= drag coefficient
$C_{D,0}$	= zero-lift drag coefficient
C_f	= thrust coefficient
C_i	= drag due to lift coefficient
C_L	= lift coefficient
D	= drag
db	= decibel energy emittance
f	= velocity budget fraction
$\boldsymbol{F}$	= external forces vector
g	= local gravity constant
g_0	= Earth gravity constant
G_o	= Gravitational constant
h	= altitude
I_{sp}	= specific impulse
L	= lift
m	= current mass
m_b	= burnout or payload mass
m_{earth}	= mass of earth
m_{dot}	= mass flow rate
m_i	= inert mass
m_0	= initial mass
m_p	= propellant mass
m_t	= inert and propellant mass
MW	= molecular weight
P	= pressure
$\boldsymbol{P}$	= momentum vector
p_a	= ambient pressure
p_e	= exit pressure
P_s	= local pressure
P_∞	= moving flow pressure
$\dot{q}$	= convective heating rate
r_{eq}	= radius at equator
r_p	= radius at poles
r_0	= local radius from planet center
R	= gas constant
T	= temperature
$\boldsymbol{T}$	= thrust vector
T_c	= combustion temperature
U_s	= local flow velocity
U_∞	= surrounding flow velocity
V	= relative velocity
$\boldsymbol{V}$	= velocity vector
V_e	= exhaust velocity
V_c	= circular velocity
ΔV	= velocity contribution
x_{cp}	= center of pressure
γ	= Flight path angle
Y	= side force

Greek Characters

α	= angle of attack
γ_c	= specific heat ratio
δ	= pitch angle
δ_r	= pressure ratio
ε	= velocity azimuth
ϵ_s	= inert mass fraction for stage s
θ	= longitude
θ_r	= temperature ratio
μ	= bank angle
μ_g	= gravitational parameter
π_s	= payload ratio for stage s
ρ	= density
σ_r	= density ratio
φ	= latitude
ω	= planet angular speed

Chapter 1

Introduction

Chapter 1

Introduction

1.1 Original Thesis Objective

NASA tasked the University of Tennessee with a project to design a heavy lift launch vehicle for future low earth orbital launch missions. The vehicle was required to bring a payload of 60 metric tons to 160 metric tons and to be adaptable for payload masses which may change from one mission to the next. The project consisted of a conceptual design of the vehicle, including the number of stages, engine selection, aerodynamic considerations, and overall vehicle configuration. The propulsion system was to utilize previously designed engines and boosters to provide the thrust required for the different stages. The project was tasked to a number of graduate students and a senior design group with original tasking defined in Table 1.1.

Other initial constraints were defined for the vehicle and trajectory. Vehicle length was limited to 100 m with a core stage diameter limited to 10 m. The target altitude was specified as 400 km above the surface of the earth. Lastly, aerodynamic considerations were limited by a maximum dynamic pressure of 800 psf. Other than these considerations, free reign was given to vary the properties of the vehicle.

Developing such a design requires the capability to model the vehicle aerodynamics and engine performance within an ascent trajectory simulator. The trajectory simulator was originally developed in Matlab by another graduate student. It was validated and had the capability to evaluate a trajectory as an initial value problem with boundary conditions. The initial values of velocity, altitude, flight path angle, latitude, longitude, and heading were used to determine a solution to the final flight path angle, circular velocity, and position. It was intended that the solution be found by re-evaluating the aerodynamic and propulsion characteristics every time the Matlab code was run until the vehicle converged on a solution. Aerodynamic properties were to be evaluated using the Air Force missile aerodynamic simulator called Missile DATCOM. It was expected to provide coefficients that would be considered acceptable for this analysis.

1.2 Revised Objective

It was eventually determined there were some issues with the process that the senior design group was employing, and the configurations that were chosen to reach orbit were in fact insufficient. Although still unclear, there seemed to have been an issue with the pitch program within the trajectory modeling code. It was then necessary to develop a new code capable of accurate modeling of a trajectory.

This new code was deemed necessary to provide the means not only to model a trajectory but also to optimize the different configurations to the required orbit. It was recommended by NASA that the configurations not just reach the target conditions but that they would also minimize the Gross Liftoff Weight (GLOW) of the vehicle. Payload requirements were also redefined for 60 metric tons to 130 metric tons.

The new task became to develop a code that would be validated by NASA and would also optimize the vehicle in terms of this new specification. Considering this specification, the new code was designed to evaluate a trajectory for a configuration and to also vary certain independent variables that would provide the means to search for an optimized case. Once the code was completed, it could then be utilized to optimize launch configurations. This thesis describes the creation of the validated trajectory simulator and optimization of different heavy lift launch vehicles using this tool. Refer to Table 1.1 for a revised task breakdown after the senior design group finished.

1.3 Thesis Significance

This thesis is significant because it contributes to the scientific world in two ways. The first corresponds to the development of a new trajectory modeling code. There are numerous trajectory simulation tools available, but most are designed to optimize a vehicle using advanced mathematical methods. This code provides the means to optimize by graphical interpretation of the results for thousands of independent configurations. It provides this capability along with potential application to vehicles and orbits not specific to heavy-lift and low earth orbits.

The United States is in a current state of indecision and is trying to determine the next step in putting launch vehicles into orbit. Much of this comes from trying to decide which launch vehicles configurations are the most efficient and reliable for placement into orbit. This study contributes to answering these questions by optimizing multiple configurations to the required orbital conditions. The results shed some light to a possible selection for a heavy lift launch vehicle in the near future.

Table 1.1. Task Delegation before and after THEO Creation.

Delegation	Initial			Revised
Task	Myself	Completed by Others	Worked on by Others	Myself
Perform Research	X	X	X	X
Define Engines			X	X
Define Configurations	X		X	X
Evaluate Aerodynamics	X		X	X
Evaluate Engine Performance	X		X	X
Create Trajectory Simulation Tool		X		X
Validate Simulation Tool		X		X
Develop Optimization Methods			X	X
Optimize Configurations	X		X	X
Create 3D Models	X		X	X

Chapter 2

Trajectory Tool Development and Validation

Chapter 2

Trajectory Tool Development and Validation

To evaluate and optimize specified configurations, it is necessary to have a code capable of modeling multiple trajectories. There are modeling programs available, but the selection of the code is driven by the needs of this project. This optimization calls for the analysis of numerous configurations with a range of initial inputs, which easily places the number of simulated trajectories in the millions.

A program that provides reliable data must be utilized to quickly evaluate these trajectories for the optimization of different configurations. Also, as there are many different configurations, it is essential to minimize the amount of time spent creating and gathering the necessary data for the analysis. These two factors drive the decisions for a trajectory modeling code, and lead to the creation of the code Trajectories for Heavy-lift Evaluation and Optimization (THEO).

2.1 Options for Trajectory Modeling

2.1.1 Matlab

The original intention was to utilize an already developed Matlab code with the capability to create and search through a matrix of simulated trajectories for successful cases (Miller, 2011). In terms of capability, it showed a lot of potential but had some issues that could not be corrected. The applied pitch values would not transfer correctly into the equations. As a result, some configurations would fly in an unexpected fashion. Also, when compared to a validated code, this Matlab code could not produce final conditions that would correspond with the final conditions of the exact same configuration in a validated code.

2.1.2 POST

The second option was to use the NASA developed Program to Optimize Simulated Trajectories (POST) for the optimization of the configurations. POST is a three degree of freedom (3DOF) validated Fortran-based program that utilizes a loop of steps to optimize a variable and target certain conditions (NASA, 1970). It uses advanced mathematics to optimize a variable and reevaluates the trajectory with each new step in the loop. The optimized variable is adjusted based on a number of specified dependent and independent variables. The dependent variables are desired target conditions while the independent variables are adjusted to optimize the variable specified (POST Formulation Manual, 1990). For example, an optimized payload mass variable optimization varies the pitch events of a trajectory to reach the specified target conditions of altitude, injection point, and inclination. The program will eventually converge if there is a solution near the initial guess values and if the dependent variables can be met based on the specified optimization variable and the independent variables. This is a useful concept in that many different variables can be individually optimized for a configuration. In this project it would be advantageous to see the optimizations associated with certain variables such as payload or propellant mass.

There are some issues associated with using POST that would make it difficult to implement it for this analysis. As stated earlier, a converged run is dependent on the ability of the optimized variable to converge to the specified dependent variables. If the initial guesses are substantially off, POST will not converge and a manual adjustment of the initial guesses is required to obtain a solution.

Another adverse consideration associated with POST that would limit the amount of data collected is the method at which it evaluates a trajectory with certain inputs. To explain this, consider a run that is optimizing, or in other words, maximizing, the payload mass. POST would require initial guesses for the independent pitch variables and stage mass inputs that would be held constant. An evaluation with different parameters of mass or thrust values would require a completely new run. This can be time consuming as the expected optimization for this project will require the variation of multiple variables (POST Utilization Manual, 1990). A much more user friendly optimization of these configurations would allow for a range of propellant masses and/or pitch properties.

It should also be noted that POST is subjected to government restrictions based on the International Traffic in Arms Regulations (ITAR). With this restraint, the use and resources of POST would have been greatly limited in terms of performing optimizations.

2.1.3 Introducing a New Code

These considerations are limiting in that the two potential trajectory simulation codes are either ITAR regulated or inaccurate. If POST were available it would the obvious choice as it is the only one that has been validated. Even though the Matlab code has some favorable characteristics, it is not reliable. This led me to a decision to create THEO which would be validated and would also utilize some of the techniques employed in the Matlab code that optimize different variables on a much larger scale.

2.2 THEO Objectives

To create a new simulation program, it is essential first to specify the ambition associated with what it will accomplish as it optimizes the trajectory for a configuration. As stated earlier, this analysis requires many different configurations with unique properties. This implies the need to easily adjust parameters such as thrust, specific impulse, size characteristics, propellant properties, etc. Capability for quick user input in simple or complete configuration overhaul satisfies this requirement.

Another objective is to have evaluation techniques that serve the purpose of optimization. It is important to ensure that THEO can promote optimization in a way that offers large capability in terms of data analysis for successful or near to successful configurations. This will provide a benefit as it will reveal patterns associated with the determination of optimized configurations. This topic is discussed in more detail in a later section. THEO is not directly used for optimization, but it provides the data necessary to optimize using analysis tools described in a later chapter. Another necessary evaluation method is a capability for singular trajectory simulation. THEO must also have the option to model a trajectory based on singular input values without optimization. In other words, where would the vehicle end up if the user were to input one value for each specific engine, dimensional, aerodynamic, and pitch property?

2.2.1 Programming Language Selection

Based on these requirements and the considerations of the two available codes, it was determined to develop a new trajectory simulation code in FORTRAN. When compared with Matlab, FORTRAN is inherently faster, which is valuable when evaluating a large number of cases. This choice is also helpful in the validation process because POST is in FORTRAN. Transferring data files and models back and forth between the two codes when written in the same language is relatively simple.

2.3 Launch Trajectory Description

A trajectory is defined as the path of a vehicle determined by the resultant forces acting on the body. This definition can be applied to a number of different vehicles and types of trajectories. As THEO will be tracing a launch trajectory for a number of configurations, one must first understand the format of a launch trajectory and the different events associated with the launch.

2.3.1 Relating Pitch and Flight Path Angle

Before continuing with the outline of a launch, it is important to understand the difference between flight path angle (γ) and pitch angle (δ). Assuming thrust is always aligned with the body axis, pitch angle is defined as the angle of the centerline body axis of the vehicle with respect to the local horizontal of Earth. Flight path angle is different in that it is defined as the angle between the velocity vector and the local horizontal. Figure 2.1 shows a comparison of the two in relation to a rocket. When these angles are not equal, the angle of attack concept is introduced.

$$\alpha = \delta - \gamma \tag{2.1}$$

Angle of attack (α) in Eq. (2.1) is a term that shows the variation of the centerline body axis with respect to the motion of the vehicle. This implies that the motion of the vehicle is not in the direction of the body axis during a pitch event. Misalignment of the two angles induces a lift component on the vehicle that will affect the trajectory.

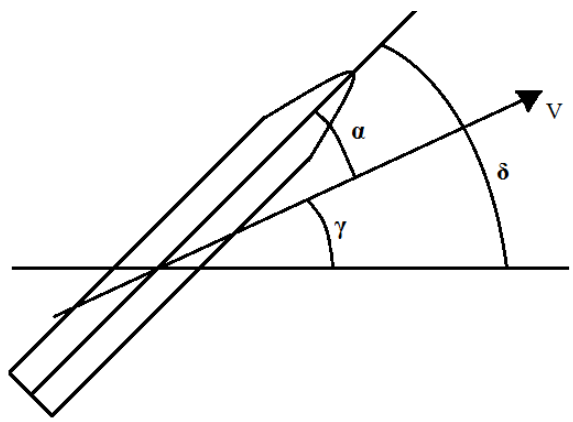

Figure 2.1. Vehicle Reference Angles

2.3.2 Pitch Angle Conditions

Initially, the vehicle is at rest on the launch pad with a specified flight path angle and pitch angle. For these configurations, both parameters are set to 90º on the launch pad. In other words, the vehicle is pointed in a direction perpendicular to the local horizontal plane of the earth. The engines initiate the launch sequence, and the vehicle remains on the pad until the thrust to weight ratio is greater than one. When thrust to weight is greater than one, the rocket lifts off, and remains at the preset γ and δ until the primary pitch event is activated. The next event in the trajectory is the primary pitch event which is a preset occurrence controlled by the avionics system of the rocket. It is represented by a rate of change of the pitch angle. The pitch event is defined as tipping the vehicle in such a way that it will begin the process of rotating from a vertical position to a nearly horizontal position with respect to the earth. This event can be controlled in a few ways. One method is to induce non-trimmed control surfaces that generate a moment on the vehicle due to a misaligned force. Another approach is to utilize thrust vectoring, which

angles the engine nozzles so that a small non-axial component of the thrust forces the pitch event. Once this event is initiated, the vehicle is no longer in motion perpendicular to the local plane of the Earth. The pitch event continues until it reaches a preset vehicle condition. Flight path angle is governed by an ordinary differential equation that is dependent on the local vehicle properties. The equation is presented and explained in more detail in a later section.

After the primary pitch event is completed and all forces are realigned with the body, the vehicle begins the gravity turn portion of the trajectory (Turner, 2000). A gravity turn is an excellent tool and is relatively straightforward in that gravity now forces a continued rotation due to the weight component no longer being aligned with the body axis. Since δ is no longer induced and α is 0, pitch and flight path angle must be equal. During this time they are governed with the equation of motion mentioned earlier for flight path angle (Dukeman & Hill).

This gravity turn event will continue until a secondary pitch event is activated. A secondary event is very similar to a primary event in that it will induce a controlled, moment-induced pitchrate. There can be numerous secondary events, and they are usually designed to assist the vehicle in arriving at the required burnout conditions of velocity, altitude, and flight path angle.

2.3.3 Vehicle Properties

Throughout this whole process, the properties of the vehicle are changing. Mass is a maximum on the ground, while minimum is at burnout. Mass is dependent on the flow rates of the propellants and on the location of inert mass separations associated with the different stages of the vehicle. Other terms, such as velocity, orbital position on the earth, angular descriptions, and altitude all vary with respect to time. An evaluation of all these variables is the process associated with designing and modeling a trajectory.

2.4 THEO Validation

It is imperative this new code be validated with an already developed code that is an up to date tool. POST is the obvious choice here because it has been accurately used in the prediction of trajectories for forty years. The theoretical data simulated by POST has been compared to empirical vehicle trajectory data and verified. As to the question of ITAR regulations, POST became available as I was employed by NASA for a period of seven weeks. My purpose there was to continue the development of this code with verification.

2.4.1 Validation Constraints

An accurate validation of a newly developed code requires identical input conditions to produce a trajectory having both matching burnout conditions as well as matching conditions during the entire launch. The flawless scenario would be a perfect match without differences in the results. POST was developed in 1970 and has been continually updated by hundreds of people to become the all-encompassing program it is today (Formulation Manual, 1990). To bring a simulator to this point would be a substantial task beyond the time constraints of this thesis. As a result, an accuracy goal was set that would be more accessible. The designated target accuracy was set to bring THEO to trajectory and burnout conditions within 5% of the calculated trajectory of POST. Why 5%? It was seen with a preliminary analysis that outputs with a 5% difference do not correspond numerically to a 5% difference in the input values but to a 1% difference. In other words, if certain inputs are adjusted by 5% the outputs will reevaluate to a 25% difference. This is an astounding effect, indicating an input value adjustment must be handled carefully. This one percent is small enough that it approaches a limit in terms of intervals used when optimizing to different inputs. For example, a input pitchrate of 0.40º/s would have 1% adjustment of ±0.0040º/s. This is limiting in that increments of the pitch values only are evaluated every 0.01º/s. The adjustment required is more precise than the input data. It is also expected that the 5% difference is also close enough that it will still show patterns and optimization configurations that correspond to the expectations revealed with POST.

As development of the code progressed, it was getting very difficult to match the output data of the trajectory within the desired 5%. The issue was associated with the inaccuracy of the necessary models within THEO. Atmospheric data, thrust profiles, and aerodynamic data must all be replicated exactly if THEO is to reach the target accuracy. The new goal then became to match all of the input data as closely as possible. The following sections discuss the replication of applicable models in THEO to validate it with POST.

2.4.2 Validation Configuration

For validation purposes it is important to consider all variables and parameters. This is completed by comparing the output data from POST and THEO for all specified validation variables. NASA provided POST trajectory data for a specific configuration that is replicated within THEO. The models for these variables are described within the following sections, and the validation configuration that was input in POST and replicated in THEO is shown in Table 2.1.

The vehicle described in this table is a 2.5 stage vehicle with two Reusable Solid Rocket Motor (RSRM) boosters. Boosters are a standalone system that simply strap onto the core of the vehicle to provide extra thrust, and the RSRM boosters described here were initially used for the Space Shuttle. A 2.5 stage launch vehicle uses three different propulsion systems. The first stage engines provide propulsion from the core of the vehicle at the beginning of launch till the propellant is exhausted. The booster burn (half stage) happens in coincidence with the first stage until booster separation. Stage two engines ignite after the first stage has separated, and burn until the vehicle reaches burnout conditions. An illustration of the vehicle is shown in Figure 2.2.

Table 2.1. Rocket Validation Configuration.

Rocket Configuration Parameters									
		SI		Eng			SI		Eng
Total Mass	2799846	*kg*	6172604	*lbm*	**Stage 1 Engine**	F-1A			
Total Length	100	*m*	328	*ft*	# of Engines	2	-		
Core Diameter	10	*m*	33	*ft*	Thrust/eng	7.50	*MN*	1.69	*Mlbf*
Booster Stage	RSRM				Total Thrust	15.00	*MN*	3.37	*Mlbf*
# of Motors	2	-			Isp	250	*s*		
Thrust/Booster	11.38	*MN*	2.56	*Mlbf*	Propellant	850000	*kg*	1873929	*lbm*
Total Thrust	22.76	*MN*	5.12	*Mlbf*	**Stage 2 Engine**	J-2X			
Isp	266	*s*			# of Engines	3	-		
Mass/Booster	585876	*kg*	1291635	*lbm*	Thrust/eng	2.00	*MN*	0.45	*Mlbf*
Engine Mass	1171752	*kg*	2583271	*lbm*	Total Thrust	6.00	*MN*	1.35	*Mlbf*
Payload Mass	133568	kg	294468	*lbm*	Isp	450	*s*		
Shroud Mass	19674	*kg*	43374	*lbm*	Propellant	500000	*kg*	1102311	*lbm*

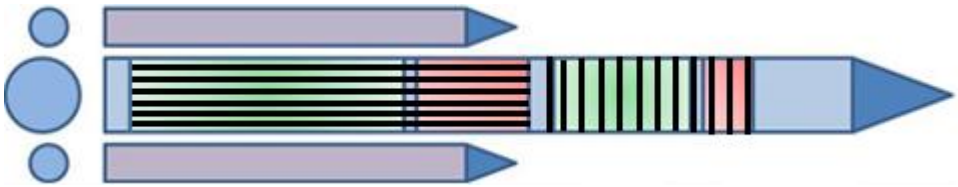

Figure 2.2. Model Configuration. The first stage is designated with black horizontal lines. The second stage propellant is indicated by the vertical lines, and the RSRM boosters are shown as strapped onto the side of the first stage.

2.4.3 Gravity and Planet Properties

To correctly model gravitational properties in the desired planet system, it is important first to calculate a standard gravity constant (g_0) based on the gravitational constant (G_o) which is the average gravity constant over the surface of the earth. This is shown in Eq. (2.2) and has been determined based on the 1984 World Geodetic Mapping performed by the Department of Defense (USA DoD). To represent the average gravity coefficient, the value is estimated at latitude of 45 degrees which is approximately halfway in between the planet's polar (r_p) and equatorial (r_{eq}) radii The standard value is shown in Table 2.2 as well as several other Earth-specific parameters.

$$g_0 = 9.7803267714\left(\frac{1+0.00193185138639\sin^2(45°)}{1-0.00669437999013sin^2(45°)}\right) \tag{2.2}$$

THEO utilizes a simplified oblate model to approximate the geocentric position of the launch vehicle (Weiland, 2010). The geocentric reference frame planet radius is measured from the center of the reference planet to the sea level surface. This radius (r_0) varies with the latitude (ϕ) of the earth as in Eq. (2.3). Rotation of the planet produces a centripetal force that causes the equatorial plane of the planet to bulge out (Stern). This bulge is latitude dependent and varies the planet's radius from the equator to the poles. The average gravity surface constant can then be adjusted based on the instantaneous radius and altitude (h) using Eq (2.4). This equation provides the ability to estimate local gravitational values based on the vehicle's current latitude and radial position.

Notice in Eq (2.4) that if h is equal to zero then $g = g_0$. This statement is valid because the assumption is that g_0 calculated with Eq (2.2) is assumed to be the average gravity constant for the planet. So when h is zero, g is equivalent to the average value.

$$r_0 = \frac{r_{eq}r_p}{\sqrt{r_p{}^2\cos^2(\phi)+r_{eq}{}^2sin^2(\phi)}} \tag{2.3}$$

$$g = g_0\left(\frac{r_0}{r_0+h}\right)^2 \tag{2.4}$$

Table 2.2. Earth Standard Properties

	Metric		English	
Mass of Earth	5.9736E+24	kg	1.3170E+25	lbm
Radius at Poles	6356829	m	20855484.58	ft
Radius at Equator	6378214	m	20925644.49	ft
Gravitational Parameter	6.6726E-11	$m^3/kg\text{-}s^2$	1.0688E-09	$ft^3/lbm\text{-}s^2$
Sea Level Gravity	9.8068	m/s^2	32.17414944	ft/s^2
Rotation	7.29E-05	rad/s		
Surface Density	1.225	kg/m^3	0.002377	$slugs/ft^3$
Surface Temperature	288.15	K	518.67	$°R$
Surface Pressure	101.325	kPA	2116.214811	lb/ft^2

2.4.4 Atmospheric Model

The atmosphere of Earth is modeled with a series of equations that estimates the temperature (θ_r), pressure(δ_r), and density(σ_r) ratios as a function of altitude. These ratios are equal to the related local atmospheric property (T,P,ρ) divided by its sea level standard property (T_o,P_o,ρ_o) as in Eqs. (2.5a) through (2.5c) (Asselin, 1997). The relation in Eq. (2.6) should also be noted as it is used to calculate upper atmosphere temperature ratios.

$$\theta_r = \frac{T}{T_0}; \quad \delta_r = \frac{P}{P_0}; \quad \sigma_r = \frac{\rho}{\rho_0} \tag{2.5a-c}$$

$$\sigma_r = \frac{\delta_r}{\theta_r} \tag{2.6}$$

It is extremely difficult to model the properties of the atmosphere from the surface of the planet to the outer reaches of the atmosphere with one equation. There are many different regions within the atmosphere that have varying properties. As a result, it is broken into sections that can be modeled individually. The model used in THEO was developed by a third party based on the 1976 US Standard Atmosphere Model (National, 1976). The model separates the atmosphere into nine different regions, and estimates the atmosphere from sea level to 500 km (Gyatt, 2011). It is assumed that both density and pressure are negligible after 100 km due to the exponential increase in the mean free path between molecules. Temperature is evaluated up to 500 km as there are heat increases due to radiation. The equations for this THEO model including their constraints are in Appendix A. These equations are validated with tabulated 1976 Standard Atmosphere data as is shown in Figures 2.3a-c.

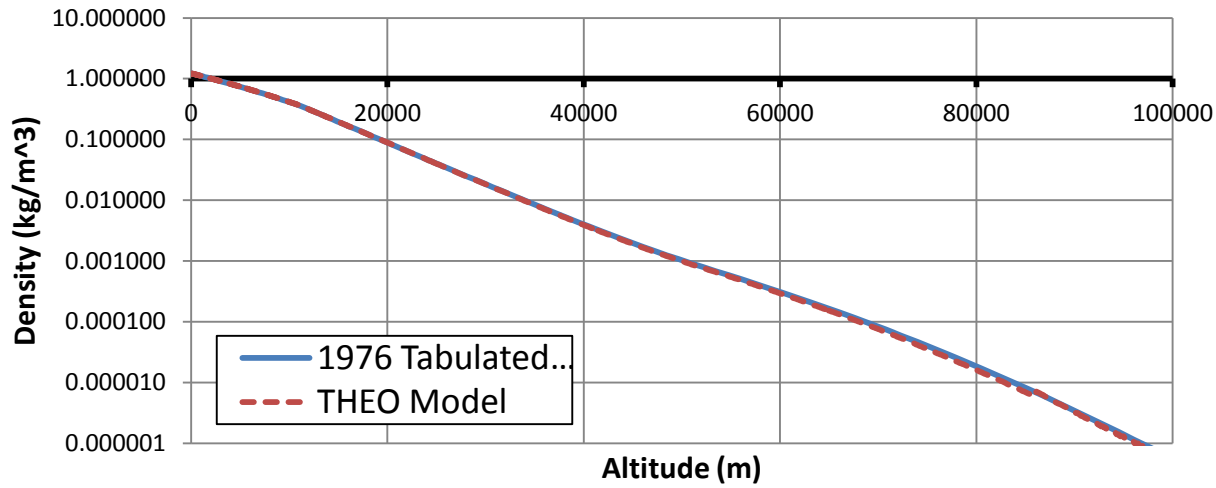

(a)

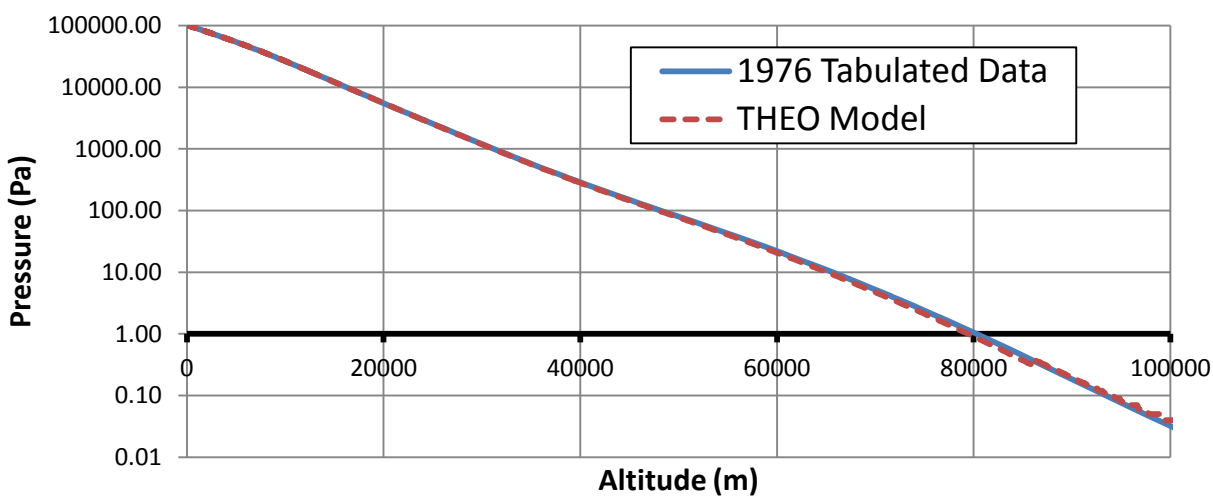

(b)

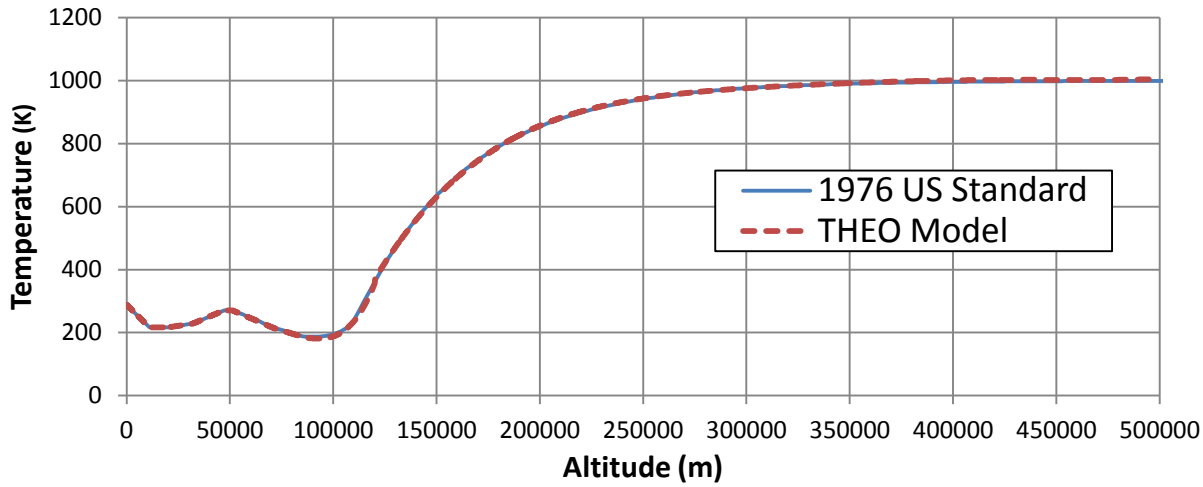

(c)

Figure 2.3a-c. Atmospheric Model Validation. These figures show the validation equation evaluation for density (2a), temperature (2b), and pressure (2c) within the code THEO.

The THEO generated profiles match well with the tabulated data for the 1976 Standard Atmosphere. The three atmospheric properties represented in these figures illustrates that the atmospheric equations used in THEO are an acceptable model.

Atmospheric profiles can also be modeled in THEO with a tabular input. This tabular method is input with the included Fortran data file *atmosphere.dat*. With this option, it is relatively simple to import a specific or desired data set. The data set requires an altitude, density, pressure, and temperature column in metric units in that order. This method is also included to ensure any questions of accuracy that might be associated in using the equation option. The equation option has been tested against the standard atmosphere tabular input and is quite accurate. It is suggested the user utilize the equation option as a primary method for atmospheric modeling. Linear interpolation within the tabular data set increases the computation time by almost five times of what it would take using the equation model. Computation speed is important to THEO as the optimizations involve the evaluation of thousands of trajectories.

2.4.5 Level of Trajectory Complexity

When designing a trajectory modeling code, developers choose to represent the trajectory of the vehicle based on a 3 or 6 DOF equation set. This number represents the number of first order differential equations that govern the path and flight of the specified vehicle.

A 3 DOF trajectory model focuses on evaluating the translational motion of the vehicle using Newton's 2nd Law. It affiliates this translation to the movement of a point mass to the burnout conditions in the standard x,y, and z directions. All forces act on this point.

A 6 DOF set takes this model to the next step. In reality the vehicle will experience another type of movement; specifically, the rotational movement of this vehicle about the specified x,y, and z axes. This motion is the result of a number of different causes. Aerodynamic forces, misaligned thrust vectors, thrust vector controls, gravity, non trimmed control surfaces, and unsymmetrical shapes can all generate moments that contribute to a rotational movement about any one of these three axes (Yechout, Morris, Bossert, & Hallgren, 2003). As can be imagined, this leads the trajectory model to be very complicated. It requires continual reevaluation of mass moments of inertia, resultant moments, center of gravity, and center of pressure. A code of such complexity could take years to develop, and is simply beyond the current requirements of this optimization. As this project is geared toward finding patterns and methods associated with this optimization, a 3 DOF simulation was judged to be adequate.

2.4.6 Equations of Motion

THEO is a 3 DOF trajectory modeling program that progresses through a trajectory by integrating the equations of motion with a user specified time increment. The dynamics of this point mass model are governed by the following set of equations (Eq. 2.7-2.12) (Weiland, 2010).

$$\frac{dr}{dt} = Vsin(\gamma) \tag{2.7}$$

$$\frac{d\phi}{dt} = \frac{Vcos(\gamma)\sin(\varepsilon)}{r} \tag{2.8}$$

$$\frac{d\theta}{dt} = \frac{Vcos(\gamma)\cos(\varepsilon)}{rcos(\phi)} \tag{2.9}$$

$$\frac{dV}{dt} = \frac{Tcos(\propto)}{m} - \frac{D}{m} - gsin(\gamma) + \omega^2 rcos^2(\phi)(\sin(\gamma) - \cos(\gamma)\tan(\phi)\sin(\varepsilon)) \tag{2.10}$$

$$\frac{d\gamma}{dt} = \frac{Tsin(\propto)}{mV} + \frac{Lcos(\mu)}{mV} - \frac{Ysin(\mu)}{mV} - \frac{gcos(\gamma)}{V} + \frac{V}{r}\cos(\gamma) + \tag{2.11}$$
$$+ 2\omega\cos(\phi)\cos(\varepsilon) + \frac{\omega^2 r}{V}cos^2(\phi)(\cos(\gamma) + \sin(\gamma)\tan(\phi)\sin(\varepsilon))$$

$$\frac{d\varepsilon}{dt} = \frac{Lsin(\mu)}{mVcos(\gamma)} + \frac{Ycos(\mu)}{mVcos(\gamma)} - \frac{V}{r}\cos(\gamma)\cos(\varepsilon)\tan(\phi) \tag{2.12}$$
$$+2\omega(\tan(\gamma)\cos(\phi)\sin(\varepsilon) - \sin(\phi) + \frac{\omega^2 r}{Vcos(\gamma)}\sin(\phi)\cos(\phi)\cos(\varepsilon)$$

The preceding equations are derived from an analysis using Newton's 2nd Law. The formulations are based upon a vector summation of the velocity, acceleration, and force in each of the three translational directions. This is valid, for the described vectors are formulated in a relative frame of reference with respect to an inertial frame. An inertial frame is necessary for evaluation using Newton's 2nd Law (Thomson, 1986).

The variable *dr/dt* in Eq. (2.7) describes the rate of change of altitude for the vehicle. This equation is fairly intuitive and indicates that as long as γ is greater than zero, the vehicle will increase in altitude as a function of a component of the velocity vector.

The next two equations describe the rate of change of position of the vehicle with respect to latitude (*dϕ/dt*) and longitude (*dθ/dt*). Both Eqs. (2.8) and (2.9) are evaluated with the instantaneous current values generated with the other four equations of motion.

Equations (2.10) – (2.12) correspond to the variable for acceleration (*dv/dt*), rate of change of flight path angle (*d*γ/dt), and rate of change of velocity azimuth (*dε/dt*). The equation for acceleration is built with a summation of the force components acting on the vehicle as well as any influences that the rotational component of the rotating planet has on the trajectory. The force components of thrust (*T*), drag (*D*), side force (*Y*), and gravity (*g*) all contribute to summations as a component at an angle of α, γ, or bank angle (*μ*). Acceleration is easily understood and is defined as the rate of change of the velocity of the vehicle. The rate of change of flight path angle is the rate of the previously described γ. This variable is the rate at which the velocity vector is turning from a position perpendicular to the earth's surface to horizontal to the earth's surface.

Velocity azimuth (ε) is defined as the planar velocity heading with respect to the equator and the local horizontal surface. This property describes the heading as if the viewer were watching the vehicle from above. For example, if a vehicle was launching from Cape Canaveral with a pitch event to turn the rocket due east, the initial velocity azimuth would be 90º (0º on the unit circle). Since the vehicle cannot travel on a constant inclination orbit with constant latitude, it is required to have a constantly changing azimuth to stay in the correct orbit. Equation (2.12) evaluates this necessary change for ε.

2.4.6a Effects from Rotation of the Earth

The rotational components in these equations should also be noted. Rotational speed of the Earth (ω) has two effects on the vehicle as it moves through the atmosphere to its orbital position. The terms containing 2ω are labeled the Coriolis Effect (Encyclopedia Britannica). This effect includes the impact of the rotation of the earth on the current direction of motion of the vehicle. Consider a non rotating earth and the case of a launch from the North Pole. The trajectory would resemble a line directly from the North Pole to 0º longitude position at the equator. Add the earth rotation with the exact same launch, and the vehicle will miss the target condition as shown in Figure 2.4.

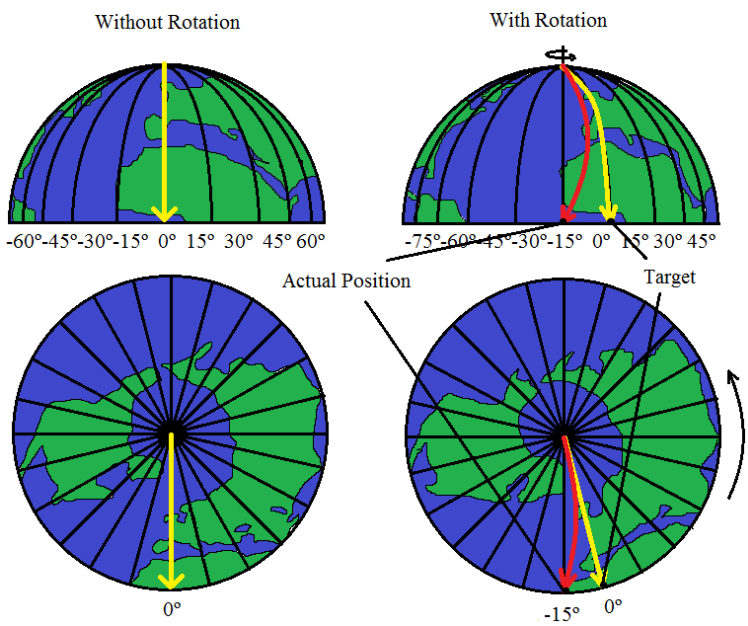

Figure 2.4. Coriolis Effect. Earth rotation consideration (Encyclopedia Britannica).

The $\omega^2 r$ term describes another issue called the Eötvös effect. As a vehicle is traveling from east to west the inertial velocity is the sum of the relative velocity and the velocity component associated with the rotation of the earth at that latitude. This additional velocity component increases the centripetal acceleration of the vehicle, which is equivalent to increasing the acceleration component toward the center of the earth. In other words, the vehicle will have a slightly higher tendency to steer towards the center of the earth (Teunissen).

2.4.7 Method of Trajectory Modeling within THEO

THEO has two capabilities in its execution. It can be used as a tool to help optimize or to determine the burnout conditions of a single trajectory based on the input configuration. When using as tool in optimization, it will search configurations that best reach burnout conditions. When modeling a single trajectory it simply steps the through one complete trajectory until final burnout. Both of these capabilities have the same inner workings when evaluating a trajectory. The differences lie in the number of trajectories and configurations that are simulated and

how THEO organizes the data. This section describes the processes and assumptions associated with the framework for both of these capabilities within THEO.

The events and steps of a general launch trajectory were described in a previous section. Here explains how this methodology of a launch case transfers into THEO and how it handles the many different events. It follows a very systematic process that steps through the trajectory one time increment at a time. Time is represented by increments which are a user specified input that describes the number of time the trajectory is reevaluated each second. When the first iteration is initiated, it reads the user specified inputs and starts cycling through the first iteration. At this point it runs some checks to evaluate the current conditions of time, reference area, thrust, engine properties, aerodynamic coefficients, atmospheric properties, heat rate, mass, and pitch. Some of these variables serve as flags for an event and will activate an event when a certain condition is met.

For example, a pitch event is user defined with three terms: a start time, the length of the pitch, and the pitchrate. During a run, the code translates these times into an iteration number able to notify THEO if the current time falls within the constraints for a pitch event. These will continue until an iteration number for length of the pitch deactivates the specified pitch. This method of flagging is used for multiple events within the process of modeling a trajectory. Another flag example are the individual components of mass or the total mass of the vehicle. When the booster mass has decreased to a specified value, this flag informs THEO that the booster inert mass needs to be released and that the thrust component from booster must be removed. This will also initiate a flag that removes the reference and nozzle exit areas of the boosters. The same type of mass flag is used when all fuel is burned in the stage 1 and stage 2 portions of the trajectory. A last important flag is associated with the release of the shroud which is controlled by the instantaneous heat rate. When the heating reaches a specified minimum, the shroud will release. This is described in more detail in the aerodynamic chapter.

2.4.8 Revised Equations of Motion

The equations of motion have been defined, but there is an assumption made in THEO that should be mentioned. Side force (*Y*) is an angle induced force that acts perpendicular to lift, drag, and weight, and is parallel to the local surface of the earth. It is induced by bank angle (μ), which is similar to angle of attack except that it lies on the horizontal plane. This term is assumed negligible in THEO because it is expected that an asymmetric launch vehicle would avoid the extra complications associated with side force. This is verified with POST, as the ouput from POST shows the side force is negligible. The updated set is shown in Eqs. (2.13)-(2.15) assumes that side force and bank angle are zero.

THEO will evaluate the translational conditions for each increment using these equations, and will continue to check the flags with updated parameters. Iterations will progress until burnout, or when the total mass of the propellant is equal to zero.

$$\frac{dV}{dt} = \frac{Tcos(\propto)}{m} - \frac{D}{m} - gsin(\gamma) + \omega^2 rcos^2(\phi)(\sin(\gamma) - \cos(\gamma)\tan(\phi)\sin(\varepsilon)) \tag{2.13}$$

$$\frac{d\gamma}{dt} = \frac{Tsin(\propto)}{mV} + \frac{L}{mV} - \frac{gcos(\gamma)}{V} + \frac{V}{r}\cos(\gamma) + 2\omega\cos(\phi)\cos(\varepsilon) + \frac{\omega^2 r}{V}cos^2(\phi)(\cos(\gamma) + \sin(\gamma)\tan(\phi)\sin(\varepsilon)) \tag{2.14}$$

$$\frac{d\varepsilon}{dt} = -\frac{V}{r}\cos(\gamma)\cos(\varepsilon)\tan(\phi) + 2\omega(\tan(\gamma)\cos(\phi)\sin(\varepsilon) - \sin(\phi) + \frac{\omega^2 r}{Vcos(\gamma)}\sin(\phi)\cos(\phi)\cos(\varepsilon) \tag{2.15}$$

2.4.9 Aerodynamic Coefficients

Aerodynamic coefficients describe the relation between aerodynamic forces and pressure forces on the vehicle. These forces that are evaluated based on aerodynamic coefficient estimation have an effect on the resultant force of the vehicle at any point in time. This implies that an error in the aerodynamic properties can affect the desired burnout conditions of altitude, inertial velocity, and flight path angle. To ensure consistent aerodynamic profiles for this validation, drag and lift coefficients are approximated based on the POST aerodynamic data (Campbell, 2010). This POST input deck uses an aerodynamic model for a 2.5 stage vehicle, illustrated in Figure 2.2. The aerodynamic coefficient approximation of that model is compared to POST in Figures 2.5a and 2.5b. The lift coefficient data that is generated in POST is a function of angle of attack and Mach number. It is difficult to replicate this data in THEO as a function of two variables, but Figure 2.5c verifies that lift coefficients in THEO are proportional to angle of attack. At any angle of attack in Figure 2.5c and corresponding Mach number, the lift coefficient is induced in Figure 2.5a. It is not understood why POST indicates that a positive lift coefficient induces a negative angle of attack, but this was replicated to validate THEO with POST. No one at NASA was able to explain this inconsistency. The aerodynamic forces applied by POST and THEO are in Figures 2.6a and 2.6b.

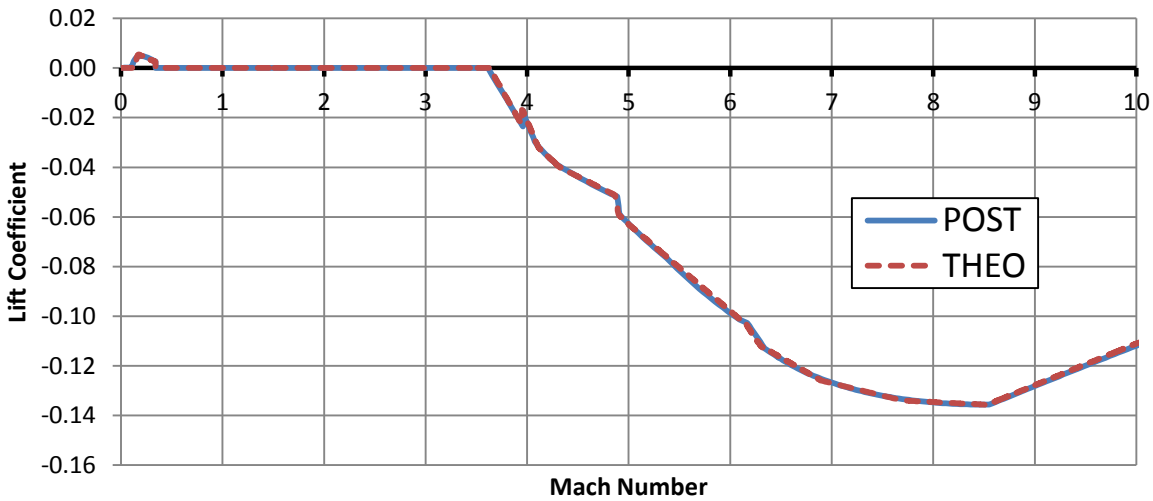

(a)

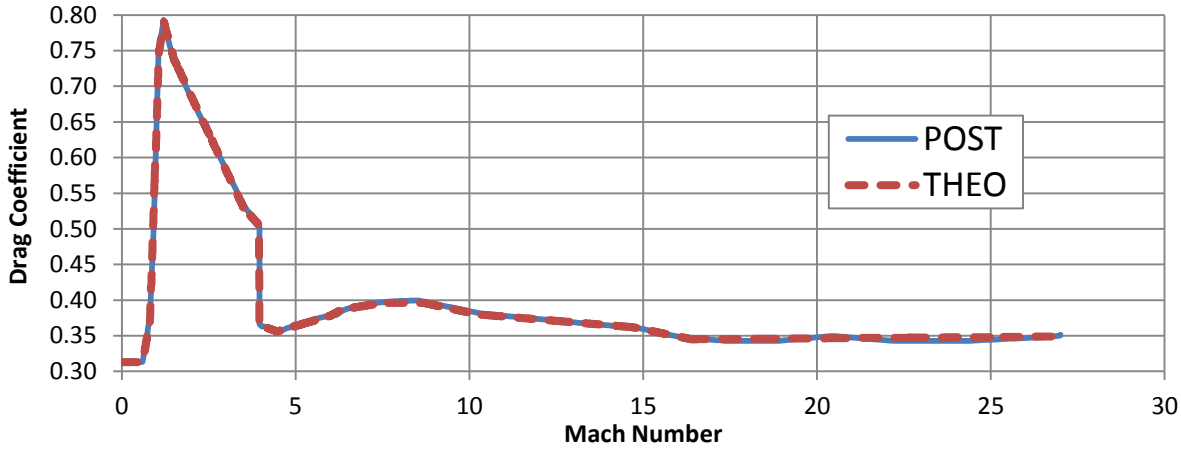

(b)

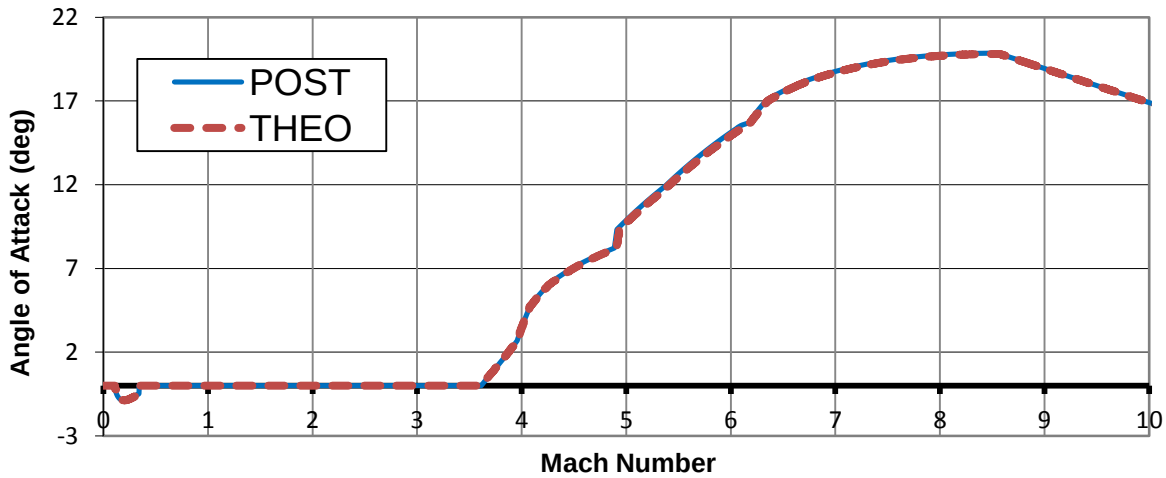

(c)

Figure 2.5a-c. Aerodynamic Coefficient Validation.

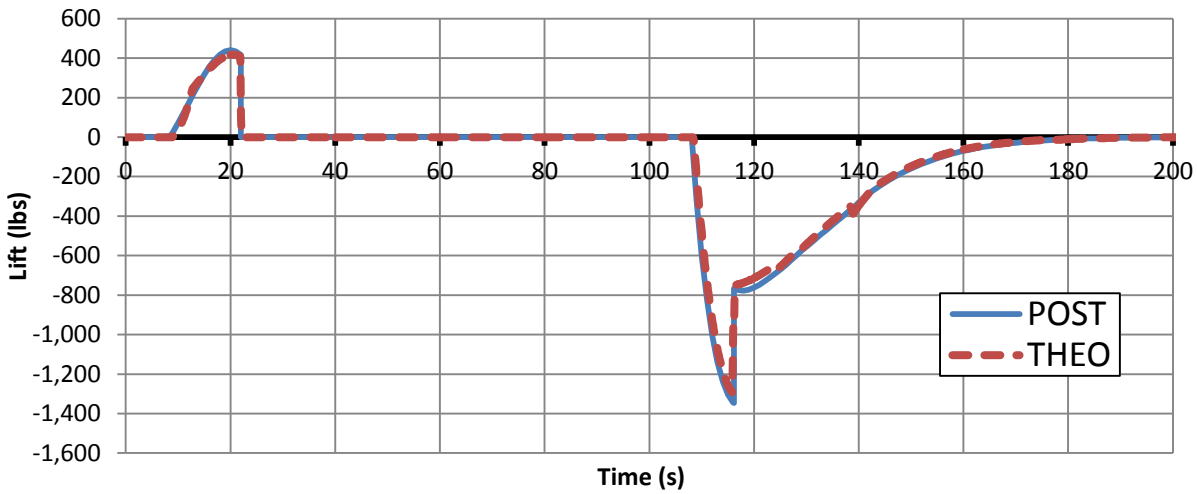

(a)

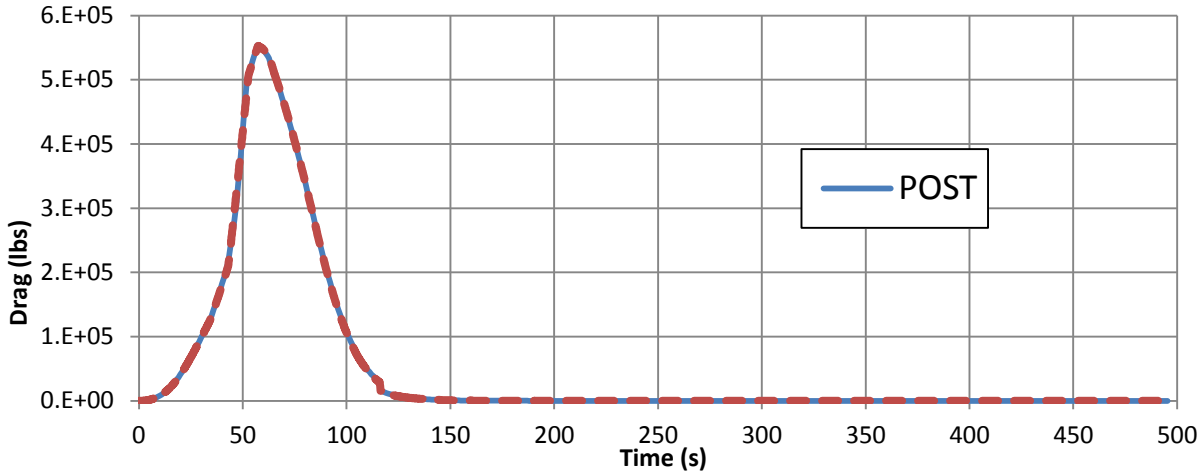

(b)

Figure 2.6a-b. Aerodynamic Force Validation.

2.4.10 Thrust Profile

The thrust profiles for this configuration consist of three different steps (2.5 stages) within the trajectory. Table 2.1 shows the parameters for the thrust profile in this configuration. Figure 2.7 illustrates both the individual and the total thrust profiles for comparison with POST. The first step, or the booster stage, consists of two Reusable Solid Rocket Motors (RSRMs). These boosters have a time dependent thrust and mass flow rate profile. The profile corresponds to an attempt to minimize dynamic pressure in the early stages of flight. It should be noted that there are seven different boosters than can implemented in THEO by the user. The type and number of boosters are selected in the terminal input when running THEO. Each has a thrust and mass flow rate profile approximation based on tabular data obtained from NASA (Kibbey & Campbell, 2010). These boosters are either currently developed or in the development process within the confines of the American governmental or private space industry. These different boosters are discussed more in the propulsion section of this report. Figure 2.7 shows the corresponding thrust values for both POST and THEO and how they coincide. The profiles in this figure illustrate that the thrust inputs to POST and THEO are the same.

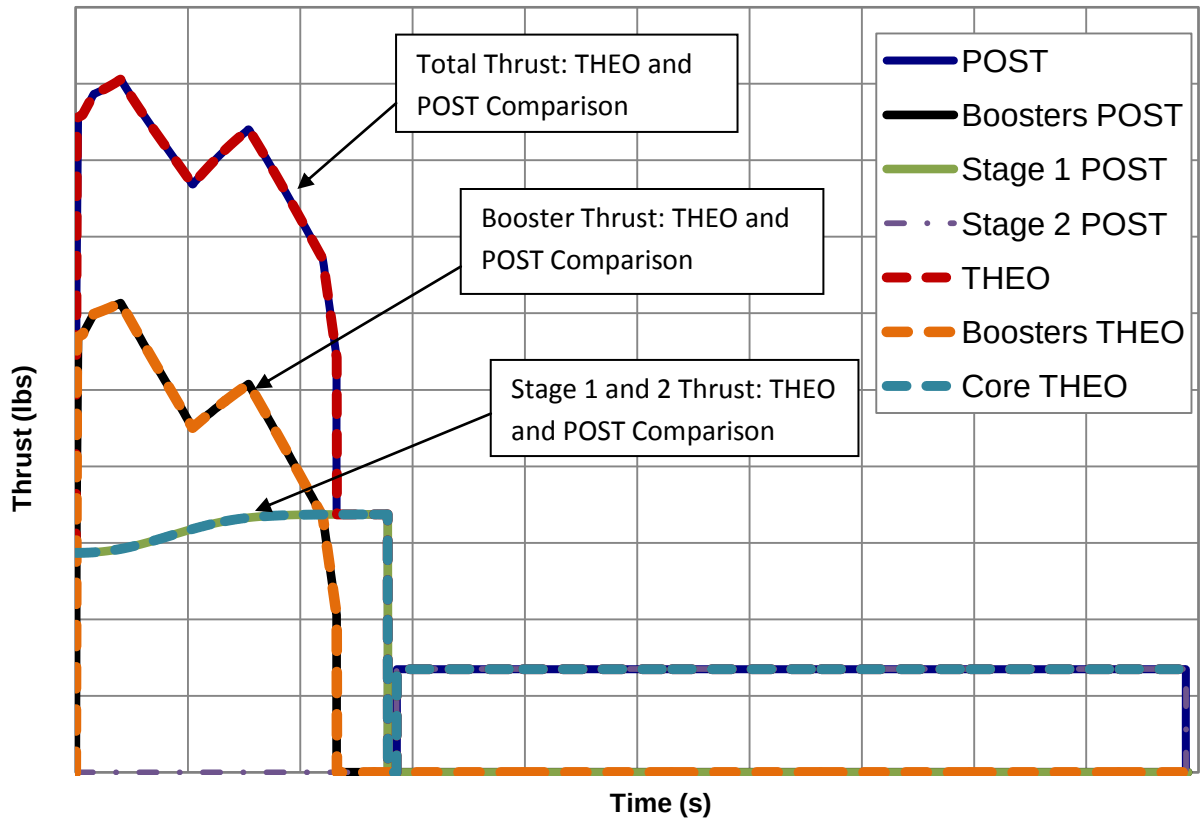

Figure 2.7. Thrust Profile Validation. This illustrates consistency of the thrust profile of THEO with respect to POST. Scale for axis is removed due to ITAR regulations.

Stages 1 and 2 thrust profiles correspond to a constant vacuum thrust liquid propulsion system. The engine parameters of thrust, mass flow rate, and specific impulse are referenced to the engine specifications for the F-1A and the J-2X for stages 1 and 2 respectively. Stage 1 has 2 F-1A engines and stage 2 has 3 J-2X engines. The thrust curves for these stages are a total thrust, accounting for all engines.

It should be noted the stage 1 profile is not a constant value. This is a result of thrust loss due to the inability of the flow to expand to an optimum condition. If the engine is unable to expand flow to the desired

optimum condition of vacuum pressure, the local atmospheric pressure acts on the exit area, reducing the vacuum thrust value produced by the engine (Sutton & Biblarz, 2010). This thrust reduction continues as long as there is a substantial atmospheric pressure. In the case of this trajectory, the pressure loss is negligible at approximately 100 s. This term acts on any engine firing, including the boosters (Turner, 2000). Figure 2.7 shows the booster profiles and the pressure reduced thrust values are correctly employed to validate THEO against POST.

2.4.11 Validation of Output Data

The previous sections have discussed the variables and properties necessary for validation and have outlined the methodology used in THEO. Input data and necessary atmospheric and earth standard models were described, and the backbone of the code was introduced in Equations 2.7-2.12.

POST ran the specified configuration in Table 2.1 and optimized the variable payload to the orbital altitude of 208000 m (682406 ft). The maximized payload was determined to be 133568 kg (294468 lb). The independent variables for this configuration are five different pitch events varied by POST to bring the vehicle to the optimized burnout conditions. They are shown in Table 2.3.

Table 2.3. Pitch Event Parameters

	Pitchrate (deg/s)	Start Time (s)	Duration (s)
Primary Event	-0.413814	8.5	13.5
Secondary Event 1	0.0117503	108	25
Secondary Event 2	-0.0116578	133	50
Secondary Event 3	-0.0915362	183	75
Secondary Event 4	-0.164918	258	237

A complete replication of pitch and vehicle properties within THEO is compared to the POST data in Figures 2.8 - 2.12. Notice that the burnout altitude in Figure 2.8 has a percent difference of 11.4% between the POST value and THEO generated data. The only other plots that have a significant difference are Figures 2.11 and 2.12. The discrepancy for early in Figure 2.12 is the result of a necessary assumption described later. The difference in the variable relative rate of γ in Figure 2.11 is due to the method by which POST models the launch before the primary pitch event. A condition within POST allows for the rate of γ to be evaluated before the first pitch event, and as a result it begins to tip over before the pitch event. It is possible that this early tip is due to the inertial rate of γ that considers the rotation of the earth. As described earlier, THEO handles this situation differently by intuitively holding the conditions of a relative γ at a vertical position until the first pitch event is initiated. This introduces a problem because at the same start time the rate of γ for both simulation tools is quite different. THEO's rate of change of γ is more negative and as a result the velocity vector will turn over faster when compared to the POST data. To account for this, a time correction is introduced into THEO that changes the start time from 8.52 s to 8.7 s. This essentially implies that THEO must initiate its first pitch event 0.18 sec late for it to correctly model the difference in γ.

Reevaluating THEO with this consideration is shown in Figures 2.13 – 2.17. These new plots demonstrate this start time adjustment has corrected the trajectory to match POST. Not only was the rate of change of γ corrected, but so was altitude, indicating that the start time issue was the source of both sources of error. Additional data output plots are shown Figures B1-B16 in Appendix B. Output data was provided in English units, and for ease of comparison these figures are in English units. All of the charts replicate the POST trajectory well, but a few them have points that should be noted.

Figure 2.13 shows the altitude comparison of the models. The final condition is remarkably close and has a percent difference of only 0.274% while the original goal for this difference was 5%. Also, notice the burnout conditions for velocity in Figure 2.14. Both the relative and inertial velocities are extremely close and have a percent difference of 0.0626%.

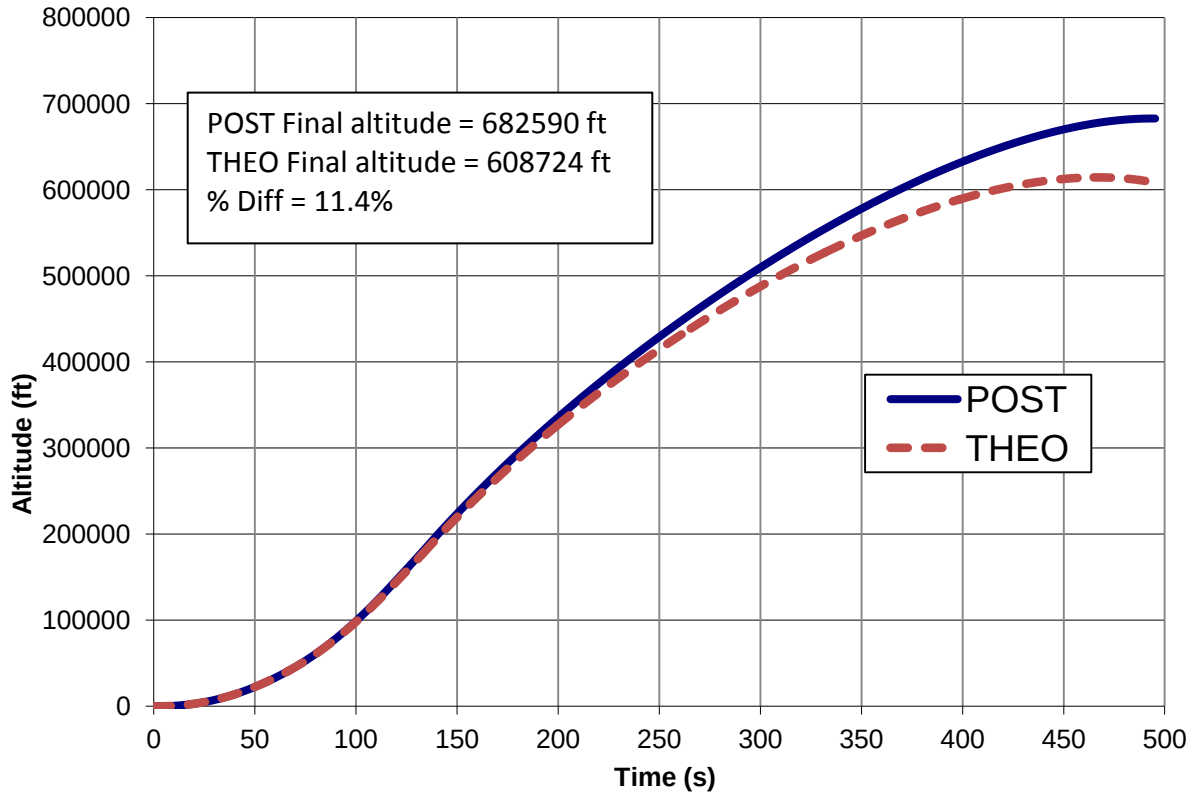

Figure 2.8. Altitude Comparison

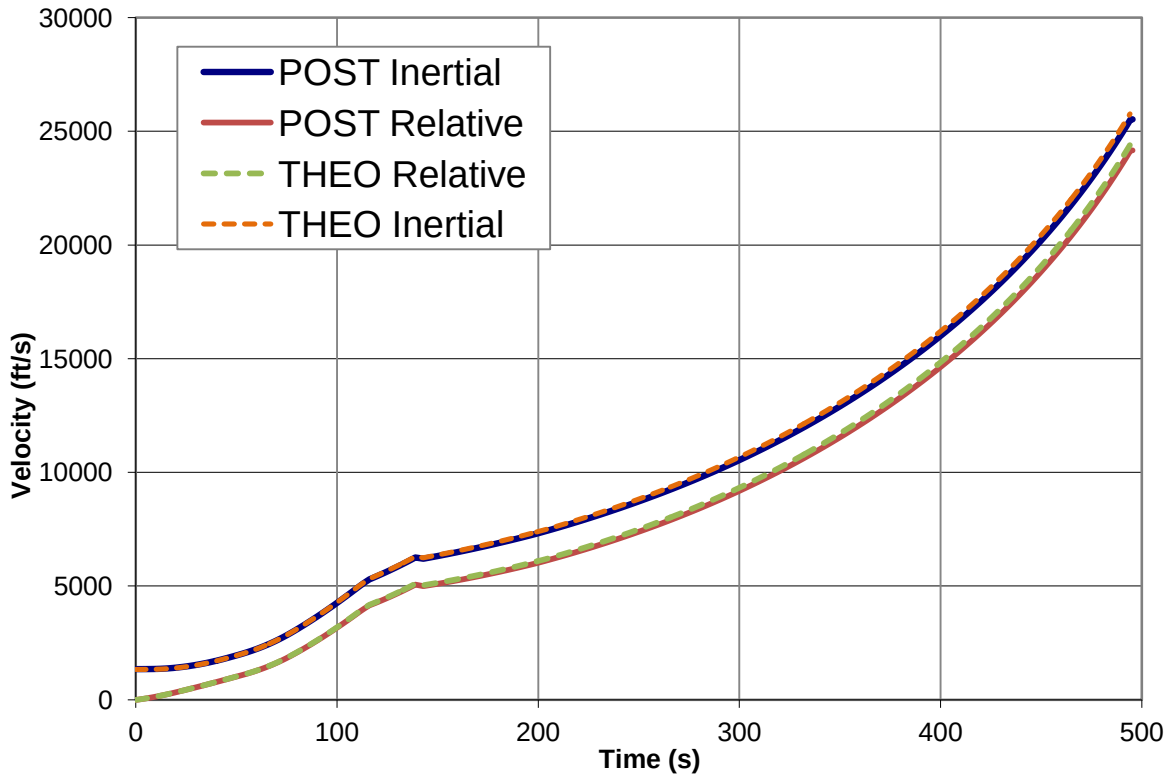

Figure 2.9. Velocity Comparison.

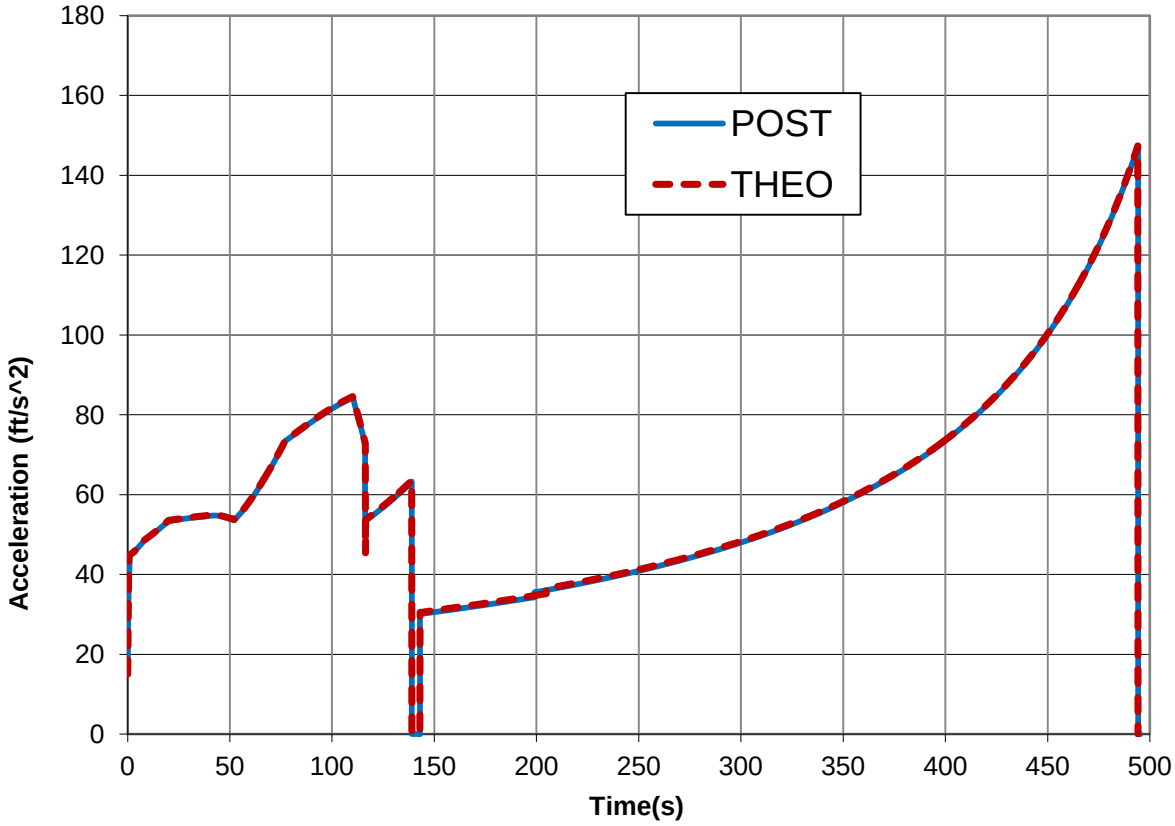

Figure 2.10. Acceleration Comparison.

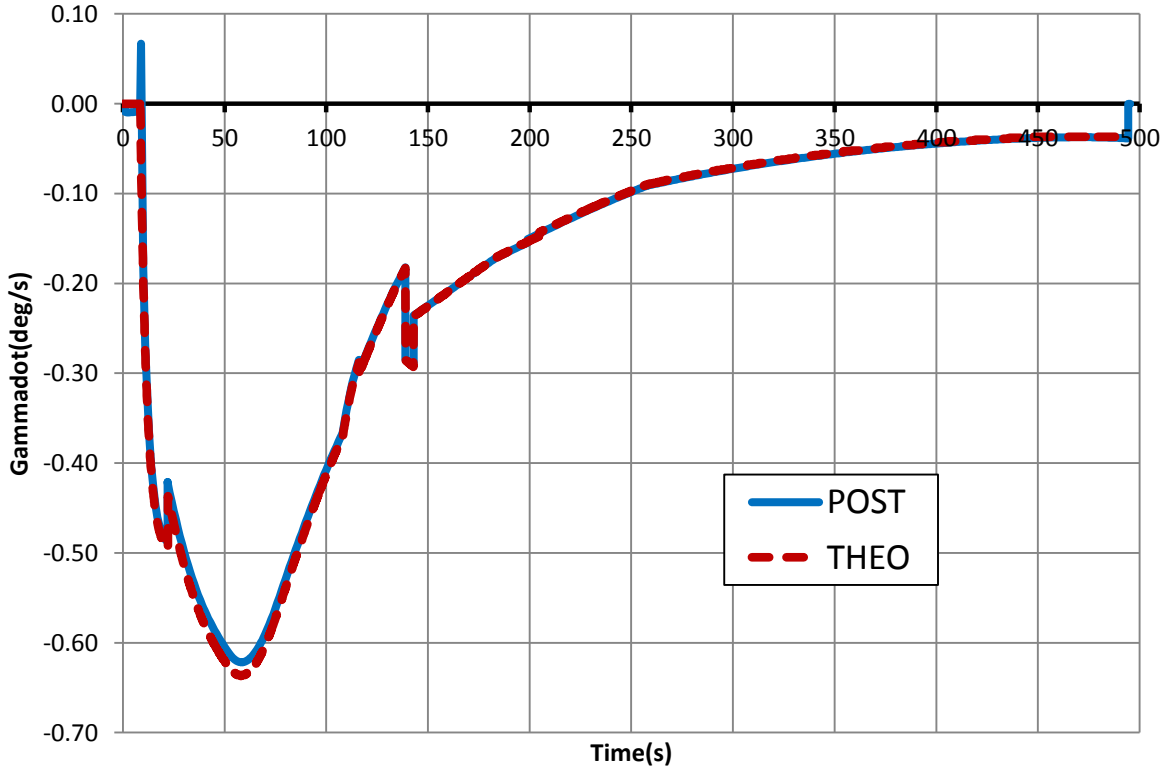

Figure 2.11. Rate of Change of Relative Flight Path Angle Comparison.

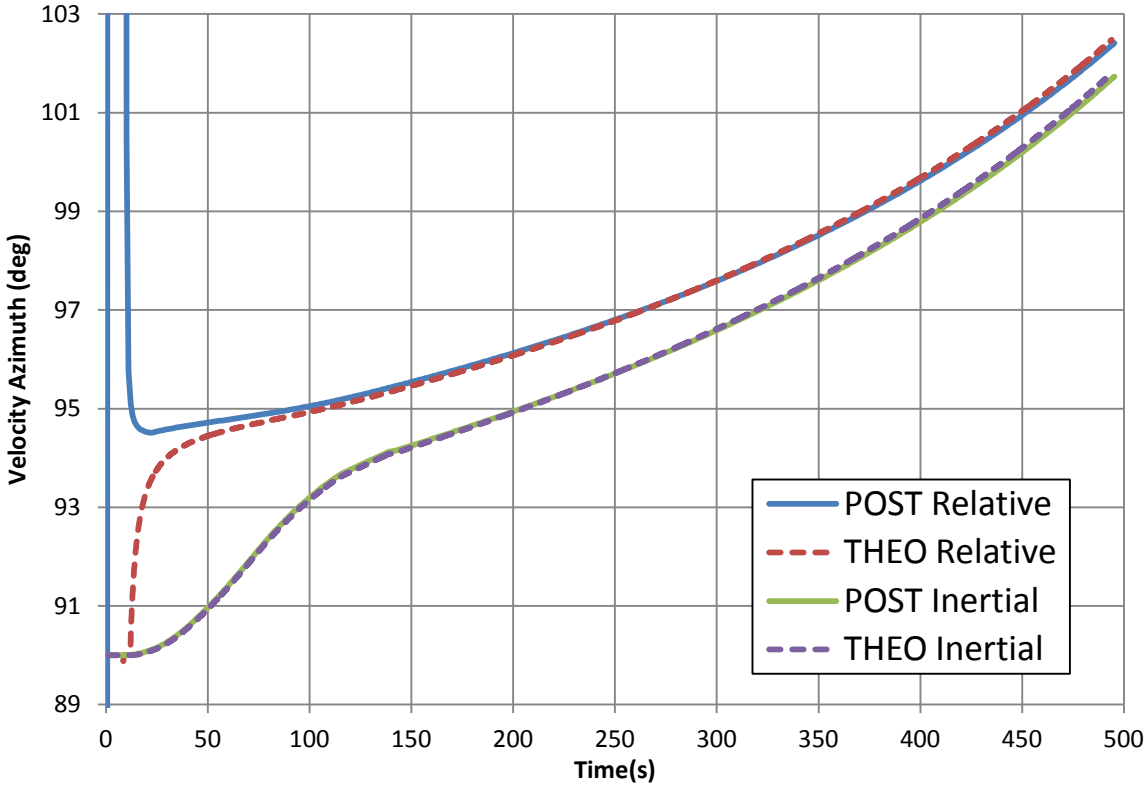

Figure 2.12. Velocity Azimuth Comparison.

The resultant acceleration of the vehicle is shown in Figure 2.15. The POST acceleration variable *asm* is labeled the resultant measurable acceleration of the vehicle (Utilization Manual, 1990). There are two differences between *asm* and the acceleration calculated in Eq (2.10). The first is that the measurable acceleration does not consider an α dependent component of thrust, but includes the total thrust. In other words the cos(α) multiplier is removed for this variable. The other difference stems from the term 'measurable'. *Asm* includes the gravity component of the acceleration. For example, if a person were in this rocket, the measurable acceleration to them would be gravity in addition to the resultant acceleration of the rocket. The adjustments match the THEO data with the POST output acceleration variable and indicate that acceleration is calculated correctly.

In Eq. (2.15) notice the *1/cos(γ)* included in the Eötvös effect portion of the equation. This equation evaluates the rate of change of ε, and can blow up substantially when γ is within ±1º of 90º. Affirmation of this is found in the POST curve in Figure 2.17 for a time less than 10 s. This presents a problem for THEO, for at launch the vehicle is at γ=90º, which would force the equation to infinity. THEO has no way to mathematically understand an undefined variable. Using trial and error, the mathematical issue is avoided by eliminating the Eötvös term in Eq. (2.14) until γ is less than or equal 89.37º. The flight path angle adjustment correctly aligns the velocity azimuth with the expected POST profile without any adverse effects.

These figures show that THEO is capable of modeling a trajectory comparable to POST. The accuracy goal was reached and surpassed substantially, indicating that any assumptions made within THEO were acceptable or similar to an assumption that POST makes. This analysis demonstrates that THEO is a valid tool for simulating trajectories and aiding in determining optimized configurations.

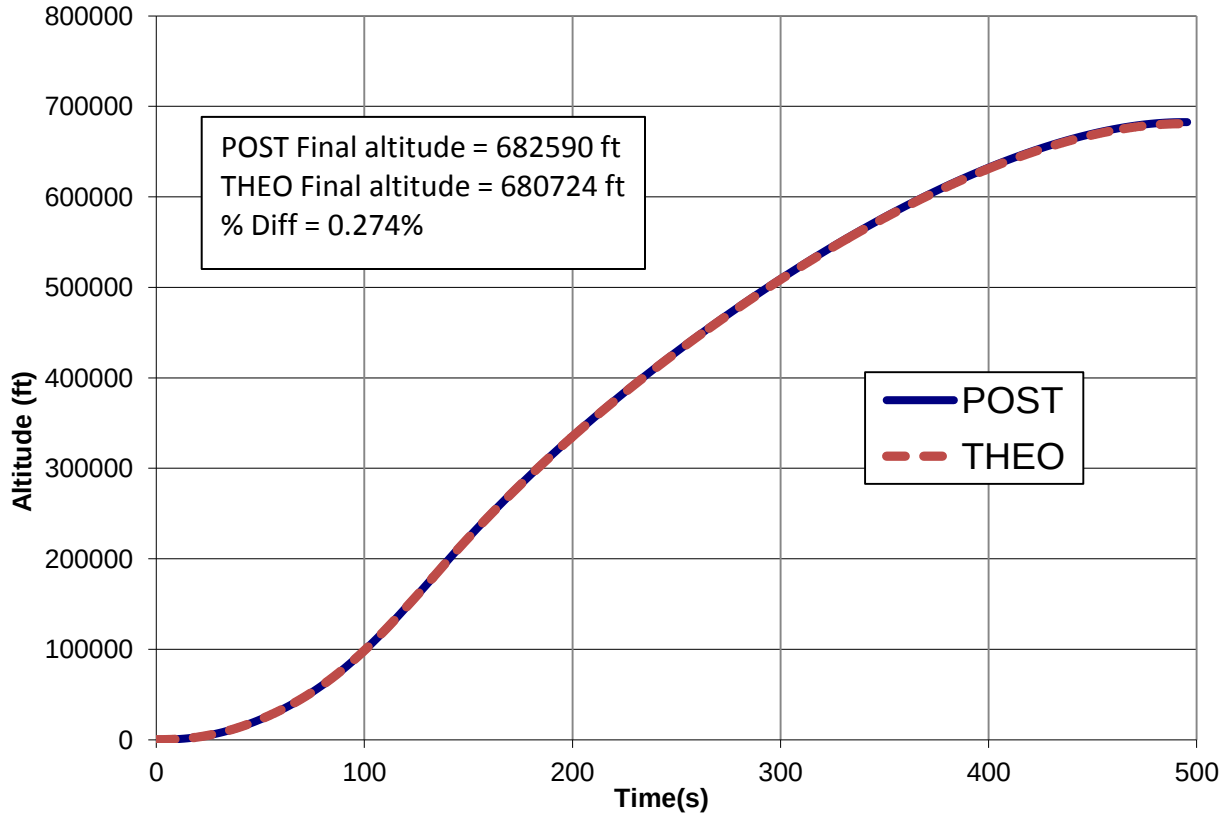

Figure 2.13. Altitude Comparison Validation Plot.

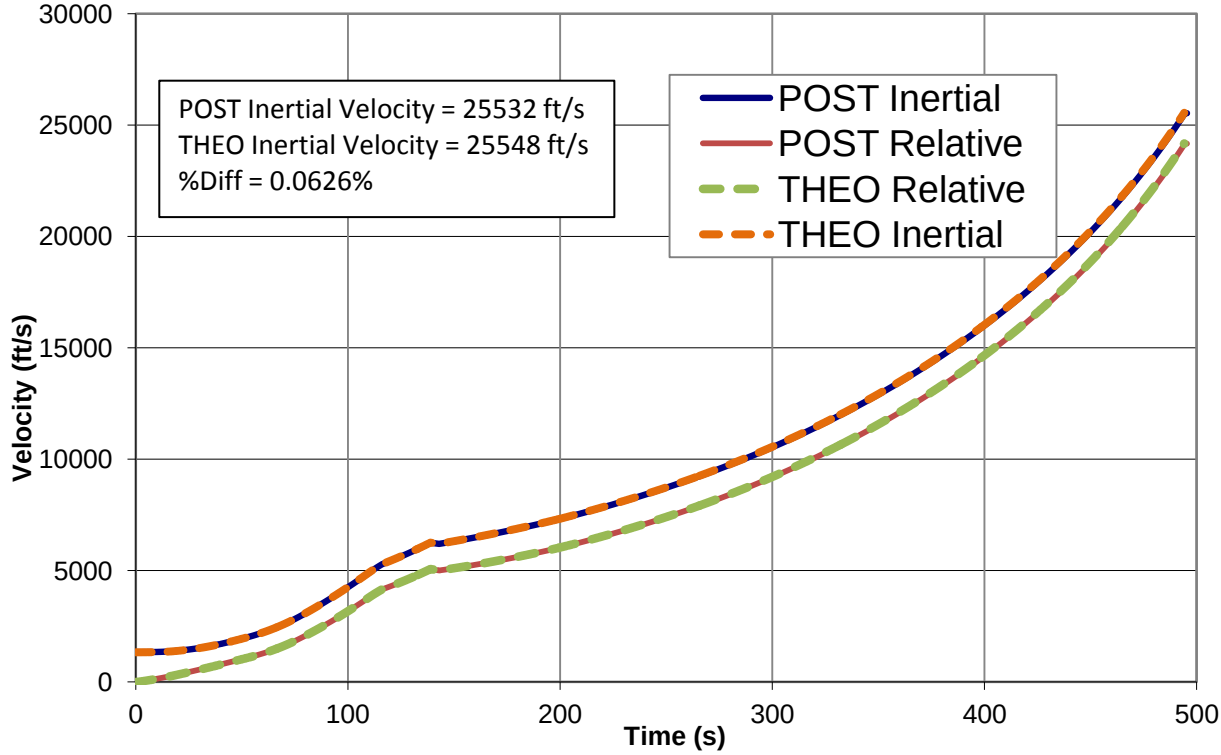

Figure 2.14. Velocity Comparison Validation Plot.

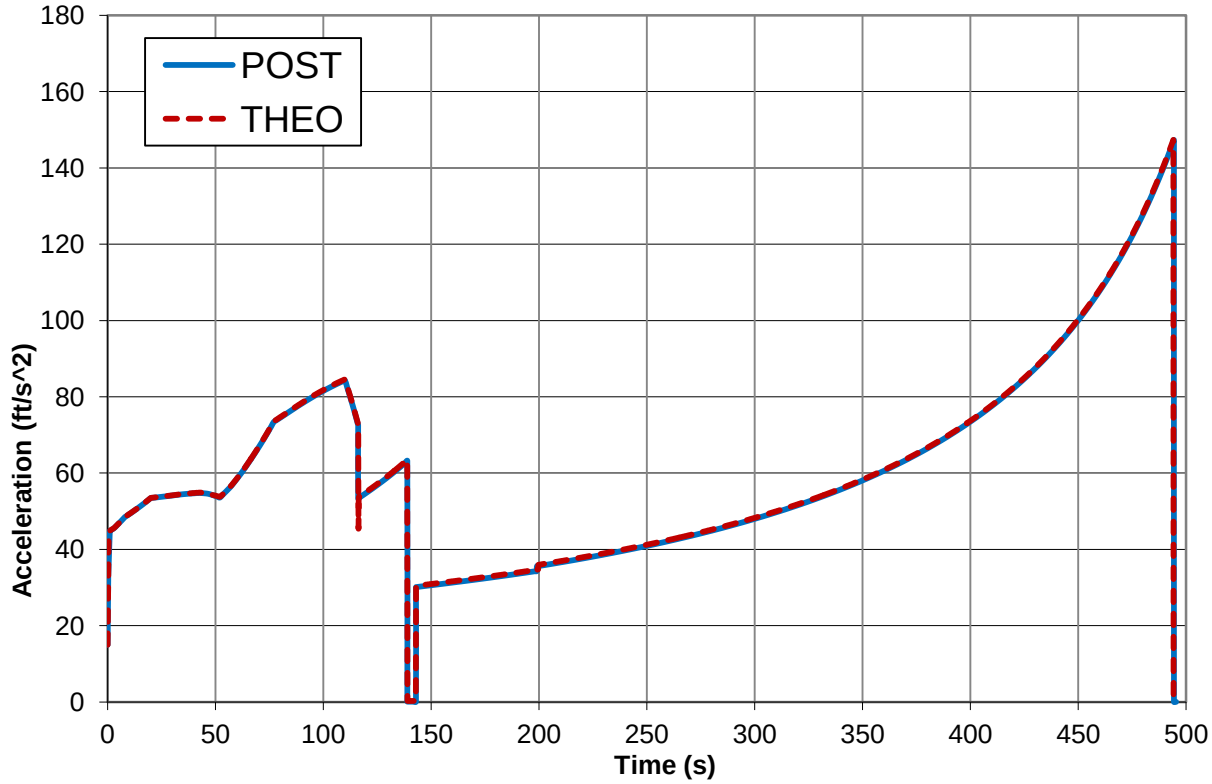

Figure 2.15. Acceleration Validation Plot.

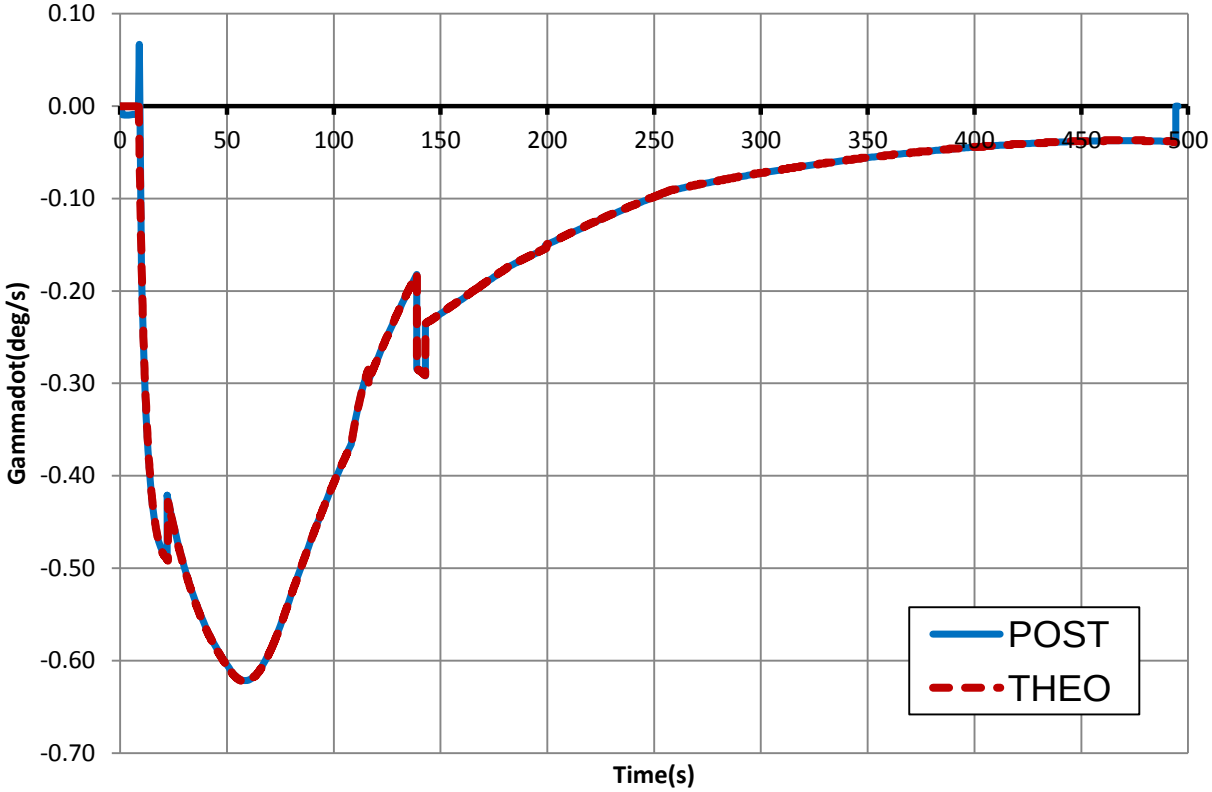

Figure 2.16. Rate of Change of Relative Flight Path Angle Validation Plot.

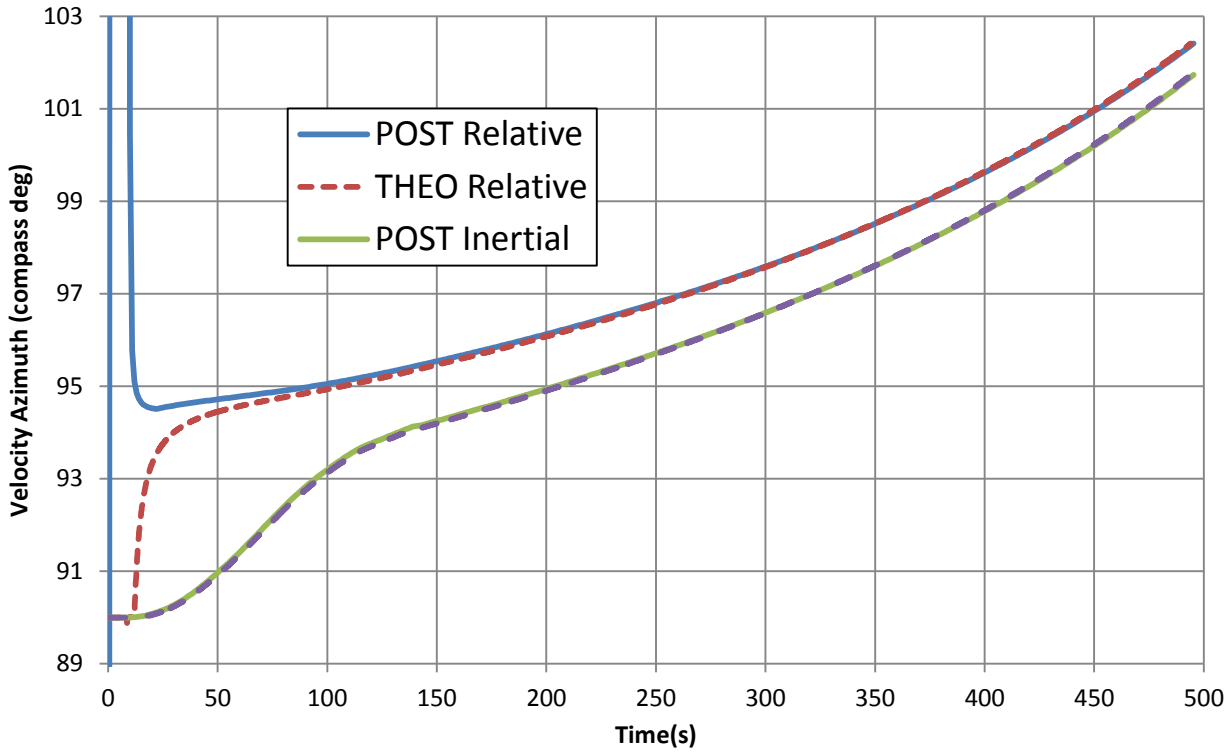

Figure 2.17. Velocity Azimuth Validation Plot.

2.5 THEO as an Optimization Tool

The use of THEO follows a mathematically simple process. The inner workings of a trajectory within the procedure follow the same process as described in Section 2.4.9. It will provide the means to optimize by generating results for many different trajectories based on 5 different independent variables that are varied throughout a run. It uses the concept of DO loops to simulate different trajectories based on these independent variables. For example, consider the independent variable of stage 1 propellant mass for a 2.5 stage vehicle. As a tool, THEO will vary this term based on a user input minimum, maximum, and interval. If the user wants to test the results of varying the stage 1 mass from 600000 kg to 800000 kg in 50000 kg intervals, THEO is able to present the results of all the cases in a matrix that can be analyzed. A description of analysis methods using THEO and other tools is described in a later chapter.

2.5.1 Defining a Successful Case

Before moving on, it is necessary to explain how this code determines the top cases out of all the user specified runs. The definition of a top case in this code is: a case that best fulfills the burnout conditions of the desired orbital position. The burnout condition is defined by three variables; altitude, inertial velocity, and inertial flight path angle. These three target variables have the ability to demonstrate if the vehicle has reached the desired orbit and can stay in orbit. For a vehicle to lie in a circular orbit at a specified altitude, it must have an orbital velocity as shown in Eq. (2.16), where μ_g is the gravitational parameter and r is the geocentric planet radius plus the altitude. To ensure this, THEO will search for a case that matches the inertial velocity of the vehicle to the required velocity at that altitude.

$$\boldsymbol{V_c} = \sqrt{\frac{\boldsymbol{\mu_g}}{\boldsymbol{r}}} \tag{2.16}$$

There is one more check THEO performs on the vehicle to verify its final condition. Flight path angle is the direction of the velocity vector, and because of this, a vehicle will not be able to fly in a circular orbit unless this angle is close to 0º. By considering this angle, it describes the maximum amount of kinetic energy that has been put into the orbital direction. A flight path angle close to zero at the desired altitude ensures energy is not being wasted in a vertical direction but that there is only kinetic energy in the desired dirtection. To be considered a partially successful case, the minimum requirements for inertial flight path angle of the vehicle must be no greater than 5º and no less than -2º with respect to the horizontal. These three variables are essential to determining if a case has the potential to be optimized. A successful case is one that has burnout velocity and altitude fulfilled within 0.5% of the desired condition and a burnout flight path angle within ± 0.5 º of a horizontal angle. For an altitude of 400000 m and an orbital velocity of 7670 m/s the tolerance would be ± 2000 m and ± 38.4 m/s. This is described in more detail in a later chapter.

2.5.2 Additional Independent Variables

In addition to the stage 1 propellant mass, there are four other parameters that can be varied when determining an optimized case. They are stage 2 propellant mass and the primary pitch parameters of start time, length of pitch, and pitchrate. These are all specified in the same way as stage 1 propellant mass with a minimum, maximum, and interval. With five different variables running different sets of data, the number of trajectories can add up very quickly. Table 2.4 shows an example of an interval set for these five different variables. The total number of calculated trajectories is the product of the number of configurations within each variable. As Table 2.4 illustrates, the number of calculated trajectories grows if varying all five variables. Depending on the computer, server, or compiler, THEO will evaluate multiple trajectories per second. Using f90 on a UNIX server, THEO evaluates anywhere from 10-30 trajectories per second.

THEO searches through all the calculated trajectories and selects cases that fulfill minimum requirements of inertial flight path angle, velocity, and altitude. This group is placed in the output file *pitch2.out* and presents cases that come closest to required burnout conditions. The top case selected from this group is the one that best fits the desired criterion.

Table 2.4. Sample Inputs for Independent Variables.

	Minimum	Maximum	Interval	# Configuration
Pitch Start time (s)	8.7	18.7	1	11
Pitch Length (s)	4.5	15.5	1	12
Pitchrate (deg/s)	-0.21	-0.47	0.01	25
Stage 1 Propellant Mass (kg)	300000	1000000	50000	15
Stage 2 Propellant Mass (kg)	300000	900000	50000	13
THEO Computation Speed	22	traj/s		
Total Configurations	643500			

2.6 Data Output Files

There are three files that output when running an optimization. The first is called *pitch.out*. This file contains the burnout conditions of every simulated trajectory, and depending on the total number of trajectories can be a substantial amount of data. This file is essential to optimization as it can be used in a data analysis plotting tool described later to visualize patterns with the whole data set.

The aforementioned file *pitch2.out* contains the top cases out of *pitch.out* that come close to achieving desired burnout conditions that were described in section 2.5.1. This reduces the amount of data for the user. Also, this file has the same output syntax as *pitch.out*.

The last file *mav.out*, is used as output for both targeting and optimization. This file outputs the trajectory at every time increment for the singular run or for the top case. This data can immediately be copied and pasted into an excel file called *output case.xlsx*. This makes it very simple for the user to visualize the trajectory results on a graph.

2.7 Completed FORTRAN Improvements

The computation speed is about 22 trajectories per second for an f90 compiler on the University of Tennessee UNIX server. This is an improved value from the original 10 trajectories per second. This improvement is due to a few minor adjustments within THEO. Trigonometric functions are time consuming functions when compared to a normal floating point operation. There were some redundant trig function calculation within THEO, and eliminating them improved the performance by 20%-30%. Another substantial time improvement was made with an adjustment to the linear interpolation subfunction. Originally, to locate the index for interpolation in an input data file, the subfunction would search through the data file from position (1,1) until it reached the desired value. This search time was limiting the computation of THEO. To minimize this, the subfunction would instead save the index of the previous position, and start searching for the index near the previous one. This is comparable to the idea of bounding a search. These two adjustments were able to more double the performance of the computation time of THEO.

Chapter 2 References

Asselin, M. (1997). *An Introduction to Aircraft Performance.* American Institute of Aeronautics and Astronautics. Reston: AIAA.

Brauer, G. L., Cornick, D. E., Olson, D. W., Peterson, F. M., & Stevenson, R. (1990). *Program to Optimize Simulated Trajectories (POST) Formulation Manual.* NASA.

Brauer, G. L., Cornick, D. E., Olson, D. W., Peterson, F. M., & Stevenson, R. (1990). *Program to Optimize Simulated Trajectories Utilization Manual.* NASA.

Campbell, J. (2010). *POST Input Case.* Huntsville.

Conklin, G., Coughenour, J., Golden, M., Harper, A., Merriweather, M., Miller, R., & Mitchell, R. (2011). *Heavy Lift Conceptual Design.* Senior Design , Knoxville.

Dukeman, G. A., & Hill, A. D. (n.d.). *Rapid Trajectory Optimization for the Ares I Launch Vehicle.* NASA, Huntsville.

Encyclopedia Britannica. (2012). *Coriolis force*. Retrieved from Encyclopedia Britannica Online: http://www.britannica.com/EBchecked/topic/137646/Coriolis-force

Gyatt, G. (2011). *The Standard Atmosphere*. Retrieved from http://web.me.com/gyatt/atmosculator/The%20Standard%20Atmosphere.html/#ERRATA

Kibbey, T. P., & Campbell, J. J. (2010). *Catalog of Solid Rocket Motor Designs Available for Heavy-Lift Propulsion.* Huntsville.

Miller, R. (2011). main_launch.

NASA. (1970). Program to Optimize Simulated Trajectories.

National Oceanic and Atmospheric Administration; NASA, US Air Force. (1976). *U.S. Standard Atmosphere 1976.* Washington D.C.

Stern, D. D. (n.d.). *The Rotating Earth*. Retrieved from Educational Web Sites on Astronomy, Physics, Spaceflight and the Earth's Magnetism: http://www-istp.gsfc.nasa.gov/stargaze/Srotfram1.htm

Sutton, G. P., & Biblarz, O. (2010). *Rocket Propulsion Elements* (8th Edition ed.). Hoboken, NJ: John Wiley & Sons, Inc.

Teunissen, C. (n.d.). *The Eotvos Effect*. Retrieved from The physics of rotation: http://www.cleonis.nl/physics/phys256/eotvos.php

Thomson, W. T. (1986). *Introduction to Spaceflight Dynamics.* New York: Dover Publications, Inc.

Turner, M. J. (2000). *Rocket and Spacecraft Propulsion* (1st Edition ed.). (R. A. Marriot, Ed.) Chichester, UK: Praxis Publishing Ltd.

USA DoD. (n.d.). *Department of Defense World Deodetic System 1984.*

Weiland, C. (2010). *Computational Space Flight Mechanics.* Berlin, Germany: Springer-Verlag.

Chapter 3

Aerodynamic Considerations and Evaluation

Chapter 3

Aerodynamic Considerations and Evaluation

Orbital launch vehicle design is complicated by the influence of an atmosphere. An atmosphere is described as a layer of gases that surrounds a celestial body as a result of the gravity of the specified body. These present gases form a combination of fluids that can hinder or assist the movement of any object within the atmosphere. This movement through an atmosphere is affected by a number of different aerodynamic quantities such as lift, drag, friction, dynamic pressure, heating, acoustics, and stability. These properties are generated as a reaction of any object with the surrounding fluid and must be evaluated to account correctly for an acceptable prediction of any simulated trajectory. This chapter will discuss the methods and assumptions used to account for these aerodynamic effects and provide some insight into minimizing negative results on the vehicle.

3.1 Atmospheric Model

There are numerous models for Earth's atmosphere. The selection of the 1976 U.S. Standard Atmosphere Model for THEO was based on availability and accuracy (National Oceanic and Atmospheric Administration; NASA, 1976). The most recent models are restricted by ITAR regulations, so the 1976 Standard model is the most recent version available without restriction.

Earth's atmosphere contains a mixture of numerous gases that consist mostly of nitrogen, oxygen, carbon dioxide, helium, and argon. This combination provides us with air, the fluid medium through which all air vehicles must travel. This fluid introduces the aforementioned aerodynamic quantities of lift, drag, friction, dynamic pressure, heating, acoustics, and stability. These properties can be evaluated based on the altitude dependent atmospheric variables of density (ρ) and pressure (P).

3.2 Aerodynamic Effects

3.2.1 Lift

Lift is defined as the force that is generated perpendicular to the lifting surface as a result of velocity difference between the surface and fluid. The force is a result of a pressure difference between the bottom and top of the lifting surface, and is in the direction of the decreasing pressure gradient and proportional to this gradient (Bertin, 2002). Lift can be induced on any shape moving through a fluid medium, but this section will describe how lift acts on two specific shapes. The first shape generates lift using a non-symmetric airfoil as shown in Figure 3.1a. When placed in a fluid flow at zero angle of attack (α), this airfoil will generate lift. This is a result of the differing surface shapes on both the top and bottom of the airfoil. The shape is designed so that the moving air over the top the airfoil will have a higher velocity than the airflow on the bottom. According to a simplified version of Bernoulli's equation, Eq. (3.1), this increase in the flow velocity from U_∞ to U_s decreases the static pressure (P_s) from ambient conditions (P_∞) and creates lift in the direction of the decreasing pressure gradient (White, 2006). An airfoil or non-symmetric shape will generate lift as long as it is not at its zero lift position.

$$P_s = \frac{1}{2}\rho_\infty\left(U_\infty{}^2 - U_s{}^2\right) + P_\infty \tag{3.1}$$

Figure 3.1. Lifting Bodies. Airfoil designed to generate lift while an axisymmetric body is for zero lift

A symmetrical body is different from the described airfoil in that both the top and bottom surfaces have the same shape. When designing a launch vehicle, this can often be the case as many of them are axisymmetric. At a zero angle of attack, the vehicle in Figure 3.1b will also have axisymmetric airflow on the outer surface of the vehicle. This implies a zero pressure gradient from the top to the bottom of the vehicle. Lift is only induced when this axisymmetric configuration is moved to a nonzero angle of attack. As launch vehicles only have an angle of attack during a pitch event, an axisymmetric case will only generate lift during these events.

In terms of atmospheric properties, lift (L) is proportional to density (ρ), as shown in Eq. 3.2. It is also governed by the vehicle properties of area (A), lift coefficient (C_L), and velocity (V). When calculating the lift of a wing, area is defined as the plan surface area. For axisymmetric launch vehicles, the area is defined as the frontal cross sectional area (NASA, 1970). Lift coefficient is the ratio of lift aerodynamic force to the pressure forces associated with the vehicle, and for the case of the configurations of this project has the potential to be determined using Missile DATCOM (McDonnell, 2008). Velocity in this equation is defined as the velocity of the vehicle with respect to the surrounding fluid.

$$L = C_L \, {}^1\!/_2 \, \rho V^2 A \tag{3.2}$$

It should be noted that lift can either impede or assist the launch of a vehicle into orbit. As the lift is normal to motion of the vehicle, it can affect both the horizontal and vertical motion of the vehicle, as illustrated in Eqs. (2.13) - (2.15). If lift has a positive vertical component, the resultant force on the vehicle is at a slightly higher angle, which can efficiently bring the vehicle to the target altitude. If there is a negative vertical component from lift, then the opposite is true and the vehicle can be impeded from reaching its target altitude.

3.2.2 Drag

Drag is a force that opposes the direction of motion of a vehicle through a fluid. In terms of atmospheric effects on a launch vehicle, drag has the most significant negative effect on the performance. There are many different types of drag, and all act in a way to impede the motion a vehicle. The drag types considered for the launch configurations are zero lift drag, drag due to lift, friction drag, pressure drag, and base drag (Anderson Jr, 1999). These drag components on a launch vehicle can be broken up into three classes.

3.2.2.a Total Drag

The first class is simply labeled *drag* and for this project consists of zero lift drag coefficient ($C_{D,0}$) and lift induced drag coefficient (C_i). Zero lift drag is the total drag of the vehicle when it has the condition of zero lift, and drag due to lift is the coefficient of the vehicle when it is not at a zero lift condition. The total drag coefficient (C_D) is the summation of these two components.

The equation for evaluating drag is very similar to lift, as shown in Eq. (3.3). Drag (D) is also dependent on air density (ρ), cross sectional area (A), and velocity (V) relative to the air (Anderson Jr, 1999). The difference between the two equations comes with estimation of the drag coefficient. Missile DATCOM is used to calculate C_D and is evaluated based on skin friction, zero lift drag, and base drag. The direction of drag calculated in this equation is always opposite of the vehicle's velocity vector.

$$D = C_D \, {}^{1}\!/_{2} \, \rho V^2 A \tag{3.3}$$

3.2.2.b Pressure Drag

Pressure drag is associated with thrust but is introduced here because it is important to understand how this drag component degrades the engine thrust. Pressure drag is defined as the effect on the engine performance due to the local atmospheric pressure (Turner, 2000). The performance of an engine is maximized when the exhaust can expand exactly to the local atmospheric conditions. This corresponds to minimizing energy loss as a result of pressure difference between the nozzle exit pressure and the ambient pressure. When the ambient pressure is greater than the nozzle exit pressure, there is a drag term that acts in the negative thrust direction . Some refer to this as a pressure thrust term. Since this term is in specific conjunction with the thrust axis, it is discussed in more detail in the propulsion chapter.

3.2.2.c Base Drag

The next drag consideration is base drag. Base drag is the result of aerodynamic interaction between the base of the launch vehicle and the surrounding fluid and/or exhaust flow. Figure 3.2 shows two different cross section nozzle exits. Figure 3.2a shows the end of the rocket body tapering into the nozzle edge. Figure 3.2b does not taper into the nozzle edge, and as a result, the end of the nozzle has a flat doughnut shape that affects the momentum of the involved fluid. At the doughnut edge of the nozzle, there is a velocity gradient between the airflow and the high- speed combustion fluid of the rocket. This gradient develops an unsteady vortex mixing region that creates a low pressure on the base of the vehicle. This low pressure increases the vehicle drag and is a function of the local pressure and the cross sectional area of the mixing region (Sutton & Biblarz, 2010).

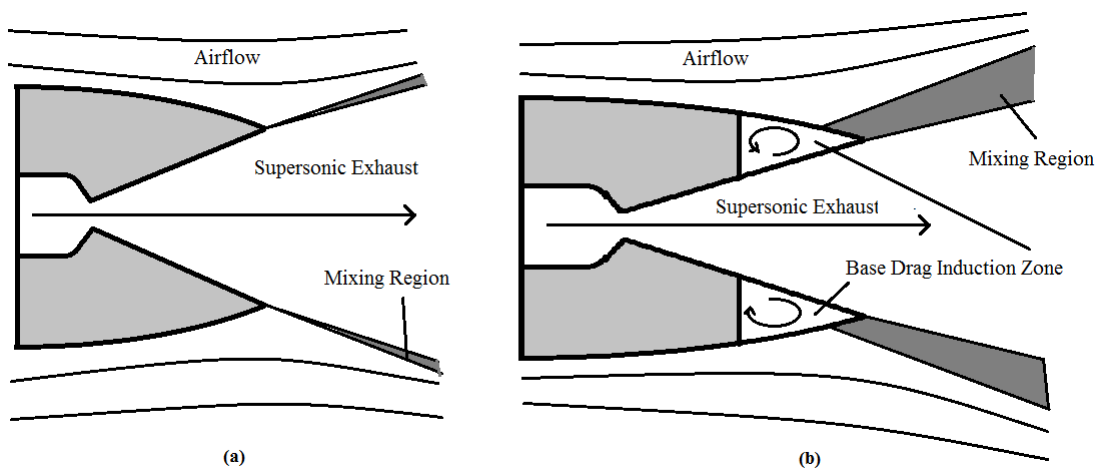

Figure 3.2. Base Drag. A rocket body that tapers off to the nozzle eliminates base drag (Sutton).

3.2.3 Dynamic Pressure

Dynamic pressure (q_∞) is a term from Bernoulli's equation which describes the pressure acting on the vehicle as result of the surrounding airflow. This term is critical as it provides an indicator for the maximum aerodynamic stress a launch vehicle can sustain and is shown in Eq. (3.4). Launch vehicles are designed to withstand aerodynamic loading to a certain point, but this strength is limited by the necessity to minimize liftoff weight. An increase in strength of the vehicle also requires an increase in the weight. Rockets, especially heavy lift launch vehicles, produce millions of Newtons of thrust, and the structure has to be able to withstand the accelerations and velocities associated with atmospheric flight. As the velocity of the vehicle increases, the dynamic pressure on the vehicle increases. If pressure continues to increase, the vehicle will reach a region where it can no longer handle the loads. This will cause a critical failure, and the vehicle will break apart. Limiting the dynamic pressure avoids this potential failure by avoiding overstress of the vehicle.

$$q_\infty = {}^{1}/_{2}\,\rho V^2 \tag{3.4}$$

There are three parts to dynamic pressure that describe this point of structural failure. The first constraint has English units, and is a maximum dynamic pressure of 800 psf. This number represents the maximum allowable q_∞ for a vehicle at an angle of attack of up to 6º. The maximum angle of attack is the second constraint and is defined to limit the majority of aerodynamic loads to the axial structure within the vehicle and only applies up to an altitude of approximately 100 km. An α greater than 6º, generates moments that are capable of critical failure.

These two constraints introduce a third constraint called $q_\infty\alpha$. This describes the limit of the product of the two, and this term can never be greater than 4800 º-psf. These constraints have been specified by Dr. John Blevins at NASA Marshall Space Flight Center and are the terms that correspond to the structural limitations associated with materials used in today's launch vehicles.

It should also be noted that once the vehicle has proceeded to a region of negligible atmosphere, the vehicle is no longer constrained to a 6º angle of attack. At ρ~0, the dynamic pressure will be approximately zero, indicating that no aerodynamic forces or moments act on the vehicle.

3.2.4 Aerodynamic Heating

The friction between the surrounding fluid and the vehicle results in considerable convective heating. This must be considered as it is important to keep the contents in the payload bay and the rocket protected during the atmospheric region of flight. The shroud protects the payload and guidance systems of the rocket and must be used until the convective heating effects become negligible. Equation 3.5 shows the 3-sigma free molecular heat rate ($\dot{q}$) for the nose cone is a function of dynamic pressure (q_∞), velocity (V), and the k factor (k_f) which is equal to 2. The heat rate has units of (Btu/(ft^2-s)), dynamic pressure is in (psf), and velocity in (m/s). This is the equation used in the POST input deck and is comparable to other documented equations (Kelley & Rochelle). Effects are considered negligible when the heat rate is less than or equal to 0.1 Btu/(ft^2-s) (Isakowitz, Hopkins, & Hopkins Jr., 2004). To decrease the mass of the vehicle in flight, the shroud is released when this heat rate minimum is achieved.

$$\dot{q} = q_\infty V k_f * (0.00128593\,{}^{Btu}/_{ft-lb}) \tag{3.5}$$

3.2.5 Aerodynamic Acoustics

Acoustic effects are the next consideration that results from the interaction of the fluid with the vehicle. Acoustics play an important role for two reasons. The first is that there are enormous amounts of energy emitted by the shroud as it interacts with the surrounding air. This is often the result of a major aerodynamic event such as an

oscillating shock wave that is induced by zones of separated flow. These events often correspond to the adverse pressure gradients associated with sharp corners or steep curves that define the shape of certain nose cones. This is very important to consider as a high energy emittance level can severely damage equipment and be harmful for humans. Typical values can range in between 120 db and 165 db for a heavy lift launch vehicle. Consideration of this factor is discussed in more detail in the nose cone analysis.

The second effect of acoustics on a launch vehicle involves associated vibrations. Every object has a natural frequency at which it prefers to oscillate. If an object is oscillating at this frequency and the amplitude is high enough, the object can tear itself apart. This can happen if the acoustic vibrations are in sync with the launch vehicle's natural frequency. It is important to consider these acoustical limitations when designing a configuration. For the extent of this analysis, this effect can be assumed negligible, primarily because most of the configurations have attached boosters that tend to increase the resistance of the vehicle to approaching this natural frequency.

3.2.6 Static Stability

Static stability is the last atmospheric effect that must be considered when designing a rocket. Static stability can generally be defined as the tendency of an air vehicle, after a flight perturbation, to develop aerodynamic forces and moments that return the vehicle to a steady state flight condition (Yechout, Morris, Bossert, & Hallgren, 2003). Consider a thrust-vectoring induced pitch event. During the event, there is a thrust component that has altered the vehicle from its steady state orientation. The steady state orientation usually corresponds to the three conditions of zero angle of attack, thrust alignment with the body axis, and trimmed vehicle surfaces. Static stability of the vehicle would be described as the ability of the aerodynamic moments on the launch vehicle to rotate it back to the steady state orientation once the pitch event has been completed. If this can be achieved, then the vehicle can be considered statically stable.

For another illustration, consider the trajectory of an arrow being shot from a bow. An inexperienced archer can often release the arrow in such a way that it has an angle of attack as soon as it leaves the bow. It has been perturbed from its steady state orientation. If the arrow is statically stable, the fins on the back of the arrow will introduce a restoring moment to rotate it back to $\alpha=0$.

The physical requirements for static stability are that the center of pressure should be located on the vehicle so the aerodynamic forces generate a restoring moment. As the vehicle rotates around the center of gravity of the vehicle, this suggests that the center of pressure (x_{cp}) must be aft of the center of gravity. This will result in a statically stable vehicle (Bertin, 2002).

It should be noted that with current technology, having a statically stable launch vehicle is no longer a necessity. There have been some substantial improvements in the area of nozzle thrust vectoring. This ability allows the guidance system for the rocket to actively control and adjust the orientation and account for any induced perturbations. The Ares I crew launch vehicle was a relatively unstable design, but had advanced thrust vectoring capable of keeping it in a steady orientation (Brandon, Derry, Heim, Hueschen, & Bacon).

3.3 Missile DATCOM

3.3.1 Purpose and Capability

This is the tool used to evaluate the aerodynamic properties for the different configurations within this analysis. It is a FORTRAN-based program that was initially created by the McDonnell Douglas Corporation and has been updated by the U.S. Army Aviation and Missile Research, Development and Research Center (AMRDEC) and the Air Vehicles Directorate of the Air Force Research Laboratory (AFRL/RB). It was designed with the purpose to provide a missile aerodynamic design tool that would provide suitable accuracy necessary for preliminary design and provide the user with means to model different configurations easily.

A vehicle is modeled by creating a case that compiles a group of input cards to build the model based on the expected flight conditions and desired geometry. Multiple cases can be run within the input deck to model different phases of a trajectory. This makes it relatively simple to simultaneously model the launch phase, booster separation, and stage 1 separation of a single configuration. The flight conditions are generally specified with altitude, Mach number, and angle of attack. Based on the inputs, Missile DATCOM can calculate the aforementioned aerodynamic properties of C_L, C_D, and x_{cp} (Auman, Doyle, Rosema, Underwood, & Blake, 2008).

3.3.2 Limitations

There are a few limitations associated with the use of this program. The first is modeling the strap on boosters for a launch configuration. Since, this program was created to model missiles, it does not have a booster capability. The boosters can be approximated, though, using the input card *inlet*. As some missile designs incorporate jet engines on the sides of the core missile, Missile DATCOM was given the capability to model this. The boosters for this analysis can be modeled with these jet engines by covering any inlets and specifying the shape of the engine to match the dimensions of any of the boosters. This trick for modeling boosters proved to be a good estimation as some of the aerodynamic properties adjusted accordingly to these shapes. This is only option as the other types of protuberance input cards are specifically for fins and small geometric shapes.

Another issue was noticed when complex user-inputted nose cone shapes were tested. There were some unexpected values that seemed to go against the intuition associated with lift and drag coefficients. It was eventually assumed this problem was a result of the relative simplicity of Missile DATCOM.

There are also issues associated with estimating the lift coefficients for a heavy lift vehicle. As will be shown later, the lift coefficients approximated by Missile DATCOM are approximately an order of magnitude off of the expected value.

3.4 Nose Cone Analysis

This section addresses the selection of the nose cone. As it is the precursor to the rest of the vehicle, it can subsequently be a deciding factor in whether or not the vehicle can fly effectively. There are a few factors that generally contribute to design decisions for the nose cone configuration. These contributing factors are mass, volume, ease of manufacturing, aeroacoustics, and aerodynamic properties. There are many different types of nosecones, and each of them has advantages and disadvantages associated with the shape.

3.4.1 Shroud Considerations

A favorable aerodynamic property in this section translates to a minimized drag coefficient. The drag coefficient is affected by edges, curves, area, surface roughness, and the property of the surrounding fluid. This shroud analysis will look at a few different configurations that vary across these parameters. For simplicities sake, surface roughness and the fluid properties (as a function of altitude) are held constant. This is a fair assumption as the surface roughness can be scaled if necessary, and the flight path is restricted to Earth's atmosphere.

When designing a launch vehicle, a major objective is to minimize the ratio of initial to final mass (i.e. make payload as much of the mass as possible). This can best be done by minimizing the mass of all components, and in this case minimizing the shroud mass. The mass of a three dimensional shape is a function of the product of surface area and thickness. When the surface area is minimized, so is the mass. The conical nose cone has the lowest surface area and would be the optimal case if the shroud were chosen based on mass alone. Does the conical nose cone have favorable aerodynamics and aeroacoustics, and what is a good balance between minimizing mass and aerodynamic properties? These are questions the next few sections will address and evaluate.

Volume available within the shroud is an important factor because it dictates how much space is available for payload or avionics equipment. A cross section profile is shown in Figure 3.3a and 3.3b that compares different nose cones' shapes. The x axis represents the axial position with zero being the nose cone tip, and the y axis illustrates the radial position of each nose cone as a function of the axial position. Generally volume is an important consideration, but NASA did not include any bounds in terms of a minimum shroud volume, and as such volume is not a deciding factor for the final nose cone.

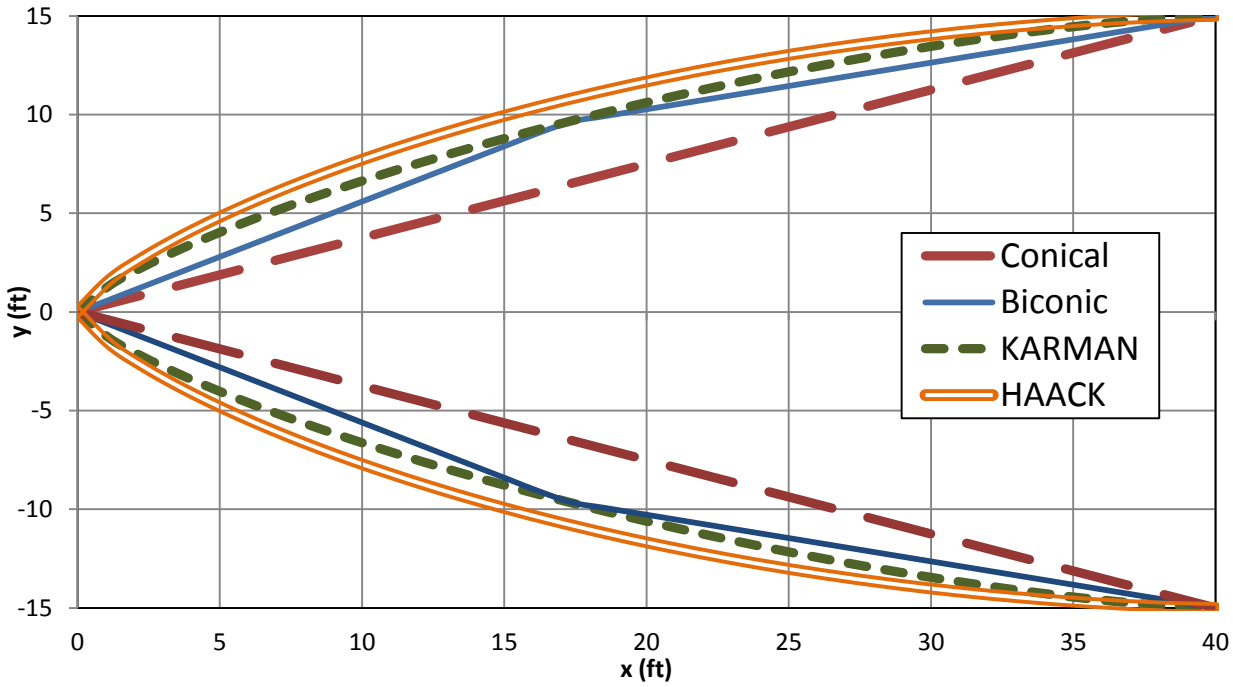

(a)

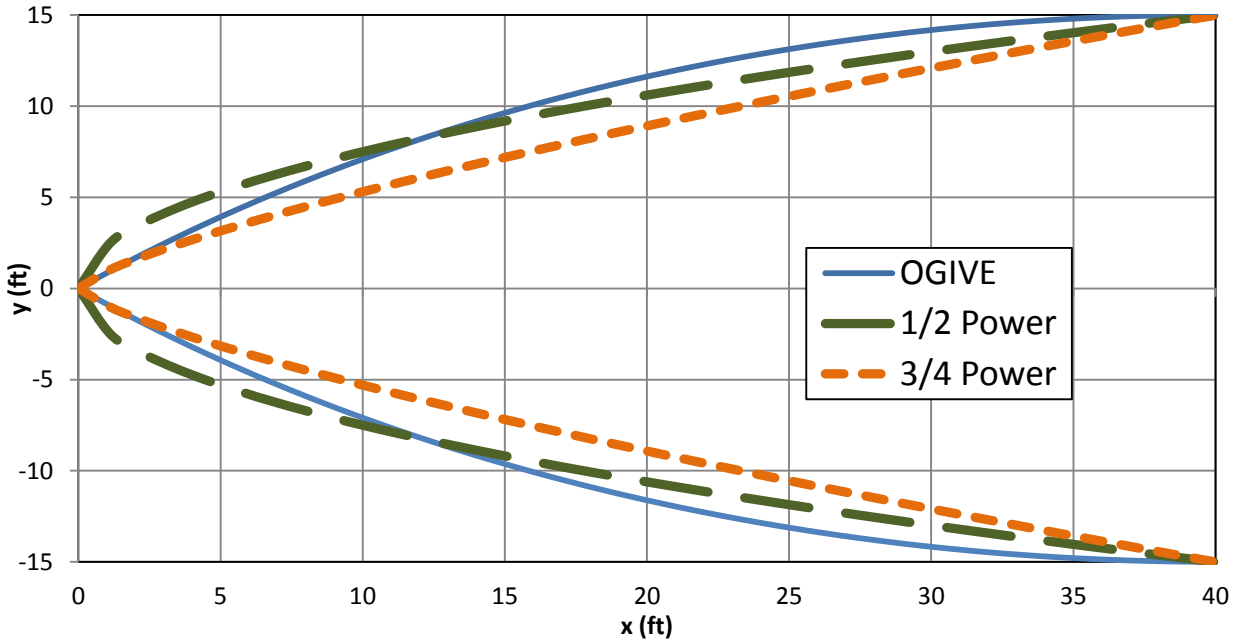

(b)

Figure 3.3a-b. Sample Nose Cone Shapes.

3.4.2 Nose Cone Types

There are five basic nose cone shapes that designers consider to be viable options. They are the Conical, Ogive, Power series, Karman, and Haack configurations. Each of them is described here to illustrate their shape and some of the basic advantages and disadvantages. Refer back to Figure 3.3 for a visual representation. The nose cones are modeled with equations that evaluate the local radius (*y*) as a function of local axial postion (*x*), overall nose cone length (*L*), and the base radius (*R*) (Crowell Sr., 1996).

The conical configuration is the simplest nose cone and as the name indicates, is simply a cone. It is relatively easy to manufacture and is described with Eq. (3.6). As mentioned before, this nose cone is important because it provides a minimum reference value for shroud mass. Any other nose cone with the same base radius and length will have a greater mass. The conical class configuration can be modified to increase the number of conic sections. This modified shape is called the biconic and consists of a cone stacked on top of the frustum of another cone. It is still relatively easy to construct and has potential aerodynamic advantages as well as a larger volume. The sharp corners do introduce some problems acoustically as there can be oscillating shock waves with supersonic flow. Additionally, this shape can be modified further by adding more conic sections resulting in triconic, 4-conic, and 5-conic shapes.

$$y = \frac{xR}{L} \tag{3.6}$$

The next nose cone is called an Ogive and has a shape formed from a segment of a circle which smoothly meets with the rocket body. It is used because the base of the Ogive shroud meets smoothly with the main body of the rocket. Simply put, this eliminates any discontinuities that would otherwise exist from a sharp edge generated where the shroud and rocket body meet. The radius (*y)* can be represented at any point as in Eq. (3.7).

$$y = \sqrt{\left(\frac{R^2+L^2}{2R}\right)^2 - (L - x^2)} + R - \left(\frac{R^2+L^2}{2R}\right) \tag{3.7}$$

The Power series is a nose cone type that can be described by rotating a parabolic shape around an axis. This shape can be modified by changing the exponent of the parabola (*n*) from 0 to 1 as in Eq. (3.8). Increasing *n* towards one decreases the bluntness while decreasing n to 0 turns the shroud tip into a point. There is a small discontinuity at the rocket body and cone interface, but the *n* power can be modified to minimize these effects. The ½ and ¾ power nose cones are compared in this analysis.

$$for\ 0 \leq n \leq 1: y = R\left(\frac{x}{L}\right)^n \tag{3.8}$$

Haack and Karman nose cones are different because they are not constructed geometrically but designed mathematically to minimize drag. These minimizations are constrained by two different factors. In a Haack configuration, the constraints are length and volume while the Karman configuration is constrained by length and diameter.

Table 3.1 shows a comparison of fairings and nose cones used on current and historical launch vehicles. These six cases serve to provide a historical basis when choosing the final nose cone type. The first two use an unspecified nose cone profile, but based on published pictures, it is expected they use either a ¾ Power or an Ogive curve. The Titan IVB is approximately the same size as the previous cases but uses the biconic nose cone (Isakowitz, Hopkins, & Hopkins Jr., 2004). It is difficult to compare these three vehicles directly to the one in this project because there is a big difference in payload requirement. The Ares V and Saturn V use the Biconic also, and since the payload requirements are much closer to 130 mt, these two vehicles serve as a acceptable historical comparison (Sumrall & McArthur).

Table 3.1. Historical Nose Cone and Fairing Comparison.

	Nose Cone & Fairing				
	Type	Diameter	Length	Mass	Payload
	-	m	m	kg	kg
Delta IV Heavy	*unknown*	5.1	19.1	3520	21892
Atlas V 500	*unknown*	5.4	23.4	4649	17590
Ariane 5	OGIVE	5.4	17	2900	20000
Titan IVB	Biconic	5.08	26.2	6300	21680
Ares V	Biconic	10	21.68	13736	130000
Saturn V	Biconic	6.6	18.8	-	119000

3.4.3 Nose Cone Reference Model

When performing the analysis, it is important to consider what is being evaluated and how that data can be used. This initial analysis has two purposes. The purpose first being to determine which nose cone has the best drag properties, while the second is to provide preliminary drag coefficients for use in the optimization.

To provide a usable preliminary drag profile a body length is added to the nose cone. In essence, the drag coefficients will simply be modeled to represent an early version of the rocket design and provide a reasonable estimation for initial drag inputs. The reference length is limited by the maximum design length of 100 m specified by NASA. The diameter of the vehicle was adjusted from 10 m to 9.14 m based on preliminary calculations performed by the senior design group. To provide a starting point for the fairing length, it is matched to the historical Ares V vehicle with a length of 22 m. The nose cone is the section of the fairing that corresponds to the nose cone profiles described in the previous section, and is assumed to have a length of 12 m. The L/D ratio for the nose cone is 3.28. The other 10 m is necessary to provide extra room for the payload, and separates from the vehicle with the nose cone. An illustration is shown in Figure 3.4. Missile Datcom requires an approximated Roughness Height Rating (RHR) to evaluate surface drag effects. Assuming the surface is a dip galvanized metal, the Missile Datcom manual suggests a RHR of 2000 millionths of an inch (Auman, Doyle, Rosema, Underwood, & Blake, 2008).

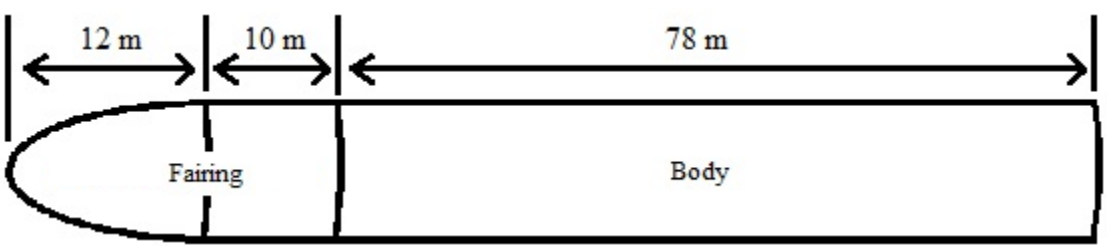

Figure 3.4. Nose Cone Analysis Reference Shape. Not to scale.

To evaluate the aerodynamic properties of this vehicle at a point in the atmosphere, Missile DATCOM requires three atmospheric descriptors. These descriptors are Mach number, altitude, and angle of attack. Instead of attempting to make educated guesses as to what the values are, it is helpful to find a comparable vehicle that already this information generated. The Saturn V is a comparable vehicle with a similar trajectory, and as such, the preliminary Mach numbers and altitude can be used to approximate the vehicle in Figure 3.4. With the Saturn V Mach number and altitude descriptors shown in Table 3.2 it is now possible to estimate the drag profiles for the different nose cone configurations. Remember that the goal of this section is only to determine which nose cones perform best with the specified reference length, and the Saturn V data should reveal this. Notice the evaluation ends at Mach # = 8.05. This is due to the fact that heavy lift launch vehicles generally reach negligible atmospheric effects by the time it is in the low hypersonic region of Mach 4 to Mach 8.

Table 3.2. Specified Missile DATCOM Descriptors.

Subsonic											
Mach #	0.51	0.55	0.61	0.65	0.7	0.75	0.8	0.86	0.92	0.95	0.98
Altitude(m)	3168	3508	4061	4457	4877	5320	5786	6276	6789	7054	7326
Supersonic											
Mach #	1.01	1.05	1.49	2.02	2.51	3.05	3.52	4	4.55	5.05	5.52
Altitude(m)	7700	8000	11401	16097	20251	24976	29063	33529	39113	13542	15256
Mach #	6.04	6.52	7.05	7.48	8.05						
Altitude(m)	54210	57620	61102	63758	69120						

3.4.4 Nose Cone Performance and Properties

An analysis in Missile DATCOM of the different nose cones with a reference length is shown in Figure 3.5 (McDonnell Douglas Corporation; 2008). These curves illustrate the drag coefficient as a function of Mach number. Angle of attack in this flight region is on the order of 0.1 and as such, is assumed to have no effect on the drag profile. Immediately the Ogive and Haack shapes differentiate themselves aerodynamically. The drag coefficients associated with these two are often 10 % - 20 % higher than the other shapes. The conical shape has a very high C_D peak in the transonic region. This is likely due to the sharp tip, and must be carefully considered as this is typically a region of high dynamic pressure, drag, and acoustic effects. Notice the biconic shroud provides an improvement in drag over the conical shape from the transonic to hypersonic flight regime. Adding an inflection point to the conical shape increases the tip angle which in turn has a positive effect on the drag profile.

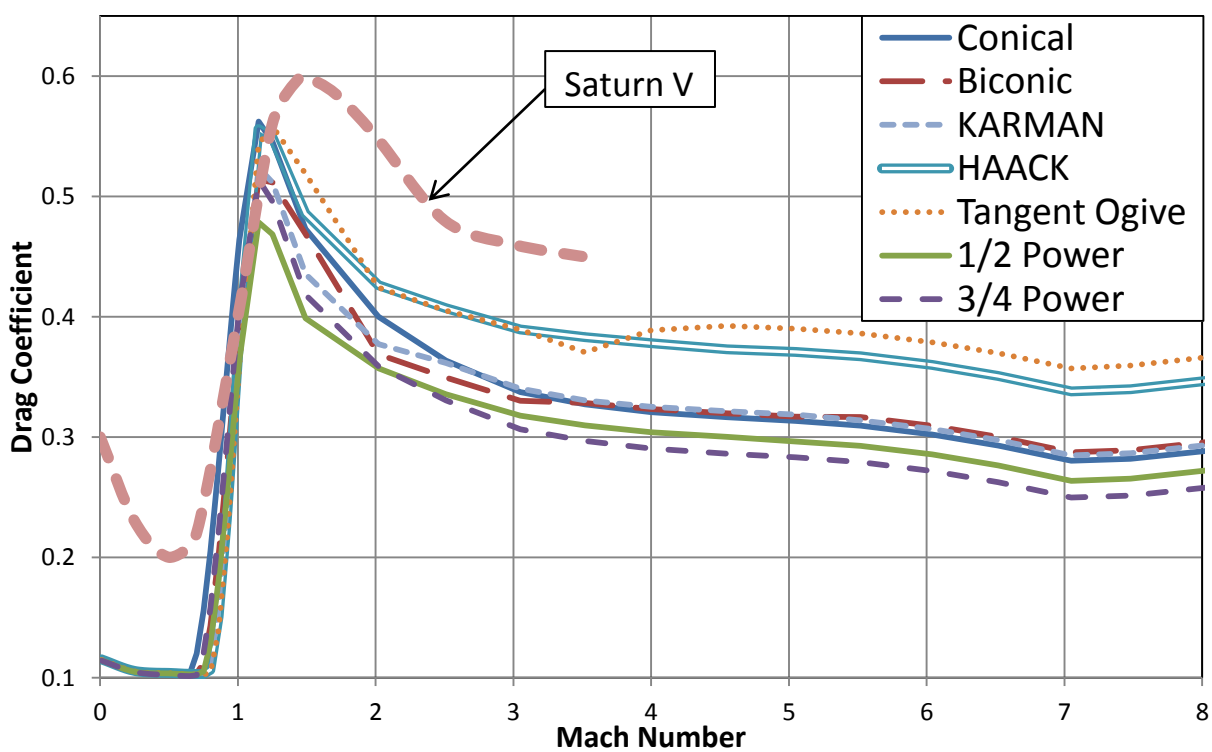

Figure 3.5. Drag Coefficient Profile for Various Nose Cones.

The Karman and ¾ Power configurations have similar initial C_D values but then separate with the latter shape having the best overall drag coefficient. The ½ Power configuration has the best transonic region drag coefficient but then rises to follow the ¾ Power design as a close second. The transonic region is a region of high concern as atmospheric effects are a maximum at this point. By the time a launch vehicle reaches Mach 3-5, drag effects have become negligible as the dynamic pressure has become low.

For comparison, an estimated Saturn V drag profile is also shown in Figure 3.5 (Braeunig, 2010). The estimation from this source only evaluates drag up to M = 3.5. The drag profile for subsonic through supersonic flight regions for the Saturn V is higher than the other configurations. This is expected as the nose cone shapes modeled in Missile Datcom are simply stacked on top of a plain cylinder. The Saturn V curve is a model that takes into account the fins and Saturn V geometry. These extra components intuitively result in a higher drag profile.

To aid in validating the Missile Datcom estimation for different nose cone shapes in Figure 3.5, NACA generated foredrag coefficients for three nose cone shapes are shown in Figure 3.6 (Perkins, Jorgensen, & Sommer, 1958). The foredrag represents the total drag minus the base drag, and as a result, the foredrag coefficient is less than the total drag coefficient. Even though the magnitude of drag coefficients differs between the two figures, the profiles are comparable. As expected the conical shape starts off with a high drag coefficient and decreases below the Ogive and Haack shapes as Mach number increases. The Ogive and Haack configurations are very similar to the Missile Datcom results except for the transonic region. According to the NACA data, these two shapes start off low and then increase to a higher values. It is possible that this inconsistency is associated with the reference length that is added onto the shapes in Figure 3.5 or by the addition of the base drag component. The NACA data does verify the Missile Datcom is capable of approximating drag coefficients for simple vehicles.

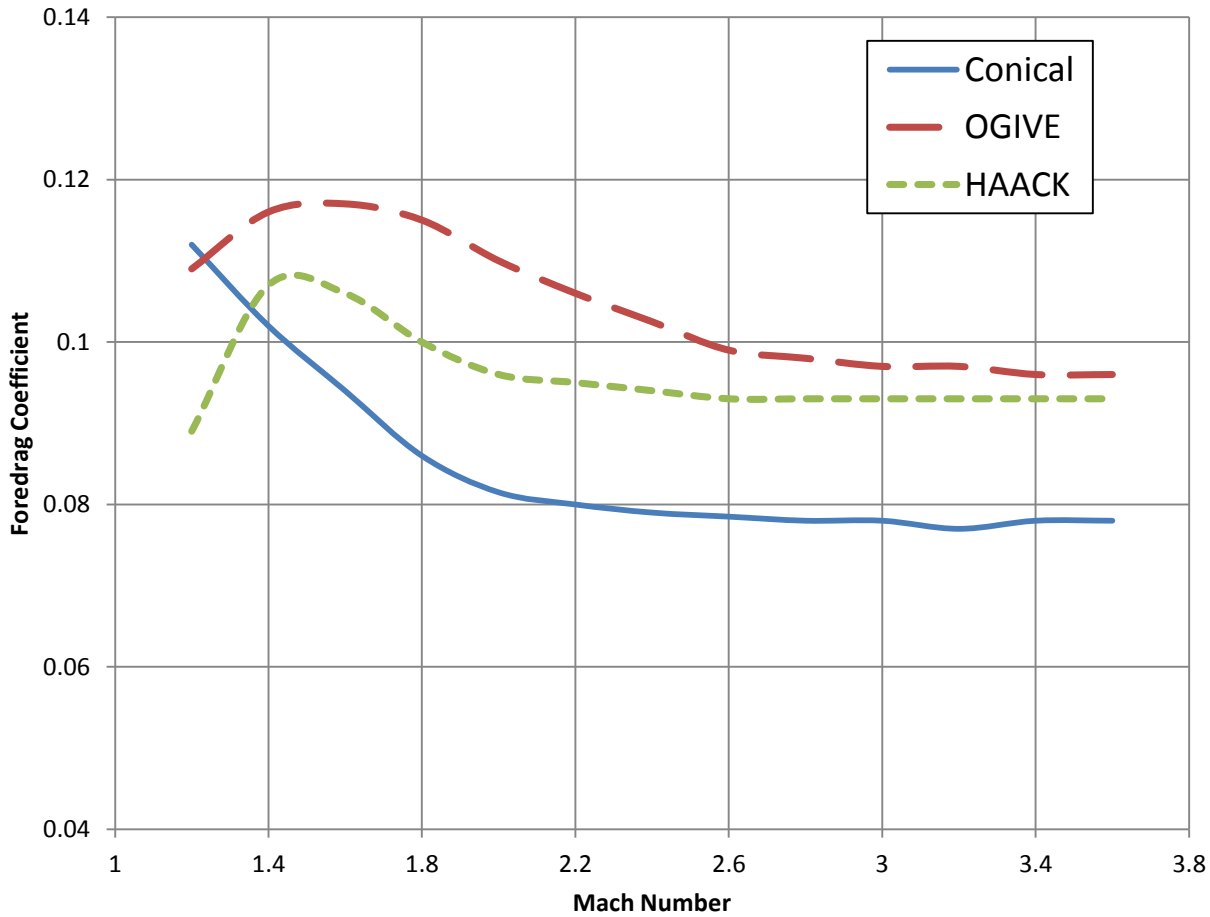

Figure 3.6. NACA Nose Cone Foredrag Coefficients. For L/D = 3.

Table 3.3 shows the surface area and available volume for payload of the nose cones in Figure 3.5. Surface area is determined by integrating the shape around a central axis. Volume in this table is defined as the volume enclosed by the nose cone that is available for payload and/or equipment. Mass would be determined by multiplying the surface area times a thickness and material density. In today's nose cone designs, the structure is made of a light honeycomb material designed to withstand aerodynamic loading. As honeycomb density and thickness values are unavailable, this table does not include a mass estimation. Even though mass is not available for the different nose cones, surface area can serve as an indicator as to which nose cones will have a higher mass. Surface area is proportional to mass, and as such a higher surface area will result in a higher mass.

Table 3.3. Nose Cone Mass and Volume Comparison.

Cone Type	Surface Area	% Diff.	Volume	% Diff.
-	m^2	-	m^3	-
Conical	187.07	0%	278	0%
Biconic	221.77	17%	370	28%
Ogive	252.63	30%	455	48%
Haack	256.88	31%	462	50%
Karman	238.82	24%	412	39%
1/2 Power	241.90	26%	412	39%
3/4 Power	210.19	12%	332	18%

It first should be understood that the absolute minimum mass and volume for a shroud is with the conical case. This is noticed in Table 3.3, but is confirmed by the fact that the shortest distance between two points (the tip and base) is a straight line. This coincides with the least amount of surface area and therefore the smallest mass and volume. The conical nose cone provides a good reference shape, and the percent difference in Table 3.3 describes the difference in volume and surface area of each nose cone when compared to the conical shape.

Both Ogive and Haack configurations have approximately 30 percent more surface area than the conical type and a higher surface area than any of the other configurations. As a result of this and the low aerodynamic performance for these two nose cone types, they are removed from any of the potential configurations for the rocket designs. Remember from Table 3.1 that the Ariane V and possibly the Atlas V and Delta IV use an Ogive shape. It is possible in spite of high mass and drag properties, designers chose this shape to maximize volume.

Before continuing in the decision making process, there is a concept that is necessary to introduce. Heavy lift launch vehicles are unique in that the amount of thrust being produced by the engines dwarfs the associated drag on the vehicle. The Saturn V has a total first stage thrust of approximately 38702 KN and a maximum drag value of 460 KN (Braeunig, 2010). The thrust is approximately two orders of magnitude greater than this aerodynamic force. This indicates that a small difference in nose cone drag coefficient will have a negligible effect on the vehicle. When faced with multiple configurations where some have better drag coefficients but a higher surface area and mass, it is advantageous to choose the shape that promotes a lower Gross Lift Off Weight (GLOW).

The conical shape nose cone is the lightest, but is not a recommended choice due to the volume consideration mentioned earlier. Heavy lift vehicles have to carry a very large payload, and this payload must be able to fit within the payload bay that is contained within the fairing. A majority of the nose cone is reserved for this purpose so that the cylindrical sections of the vehicle can contain the propellant without requiring a higher vehicle radius. A conical shape limits this payload volume and is removed from consideration.

The four other configurations are reasonably close to each other in terms of aerodynamic properties, and it is difficult to distinguish the best configurations. In an effort to minimize surface area and mass both the Karman and ½ Power shapes can be eliminated. The ¾ Power type is the best nose cone at this point in the analysis. It has only a 12 % increase in surface area over the conical shape as compared to 17% associated with the biconic configuration. It is also has slightly more favorable drag coefficient curve.

3.4.4.a Acoustic Considerations

Maximum acoustic levels are correlated with unsteady aerodynamics, the strength of a shock, and the level of separation of the flow from the surface. These effects become substantial in the transonic region as there is the potential for significant adverse pressure gradients that will induce oscillating shock waves and large acoustic energy release (John & Keith, 2006). A NASA fairing trade study provides some insight as to where these effects are strongest and to which nose cone configurations they correspond (Lepsch & Cerro, 2008).

In this study, the pressure distribution surrounding the fairing is analyzed to determine which shapes have a high probability for flow shock oscillations. The smallest overall adverse pressure gradients were associated with the biconic and the ½ Power shape. The ½ Power shroud was already removed from the potential nose cones due to weight implications, and since the NASA study does not include acoustic evaluation for a ¾ Power, the data evaluation for it must be assumed incomplete. This leaves us with the biconic nose cone shape. It should be noted that the biconic shape has the third highest maximum acoustic output at 161.6 dB but this event is fortunately contained locally at the point of the oscillating shock wave.

There is a unique acoustic property associated with biconic nose cone shapes. It is an inherent quality that results in a high maximum decibel level but a low average. Since adverse pressure fluctuations only act locally, there are regions where acoustic levels are much lower as shown in Figure 3.7. The linear region between a nose tip and the inflection point promotes a favorable pressure gradient and reduces the acoustic value to 141 dB. Due to this, the biconic shape can serve as a safe and effective nose cone. It should be noted that the final case selected by the NASA study is the Tangent Ogive shape (Lepsch & Cerro, 2008).

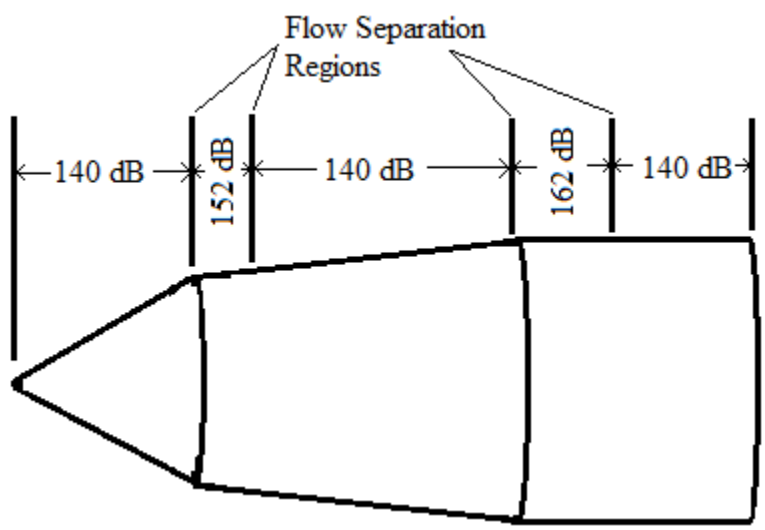

Figure 3.7. Sample Decibel Variation across a Biconic Nose Cone

3.4.5 Final Fairing Selection

There are multiple considerations that come into play when selecting a nose cone shape for a fairing on a heavy lift launch vehicle. The requirements deemed necessary are that the nose cone minimize mass, have sufficient volume, and provide a safe acoustical environment. Based on the study for this thesis, the shape that best fulfills these requirements is the biconic nose cone. It is the lightest case with a low average acoustic levels and high volume. This decision is consistent with historical data as the Saturn V and Ares V in Table 3.1 were designed with biconic nose cones. Even though the trade study chose the Ogive shape, it was determined to use the biconic shape to minimize the weight of the nose cone. The final fairing mass is assumed to be 19674 kg and is selected based on a POST input deck supplied by NASA (Campbell, 2010).

3.5 Aerodynamic Coefficient Estimation

The validation of THEO in Chapter 2 involved replicating the aerodynamic coefficients used in the POST simulation. This was done by extracting the aerodynamic output data from POST and integrating it into THEO. The aerodynamic data shown in Chapter 2 is not created by Missile DATCOM but experimentally tabulated from NASA during wind tunnel testing (NASA, 1970). This section discusses a comparison between the NASA developed aerodynamic data and Missile DATCOM to determine if it is a usable aerodynamic tool. Figures 3.8 and 3.9 compare both the drag and lift coefficient data for the two different aerodynamic sources.

The vehicle represented in the NASA tabulated data is a 2.5 stage vehicle with two large boosters. To validate Missile Datcom as an aerodynamic tool, the same vehicle was created in DATCOM to determine if was capable of modeling heavy lift launch vehicles. The dimensions and properties of this vehicle are not revealed here due to ITAR regulations.

Notice that Missile DATCOM models the wind tunnel drag coefficient profile in Figure 3.8 moderately well. It creates a curve that follows a profile similar to the data from the wind tunnel experiments. The largest difference is in the hypersonic region from approximately Mach 4 all the way to the burnout condition. This region is of little importance as density is low and aerodynamic effects are approximately negligible. The error for this approximation most likely originates in attempting to recreate the vehicle model with boosters or atmospheric conditions within the input deck of Missile DATCOM. It is difficult to exactly match the dimensions and properties of the vehicle because of the limited capability and complicated input files associated with this preliminary analysis tool. There also could be some differences between the flow properties used in the wind tunnel and those simulated in Missile DATCOM. In spite of these errors, DATCOM does prove to be an acceptable tool when approximating experimental data for drag coefficient.

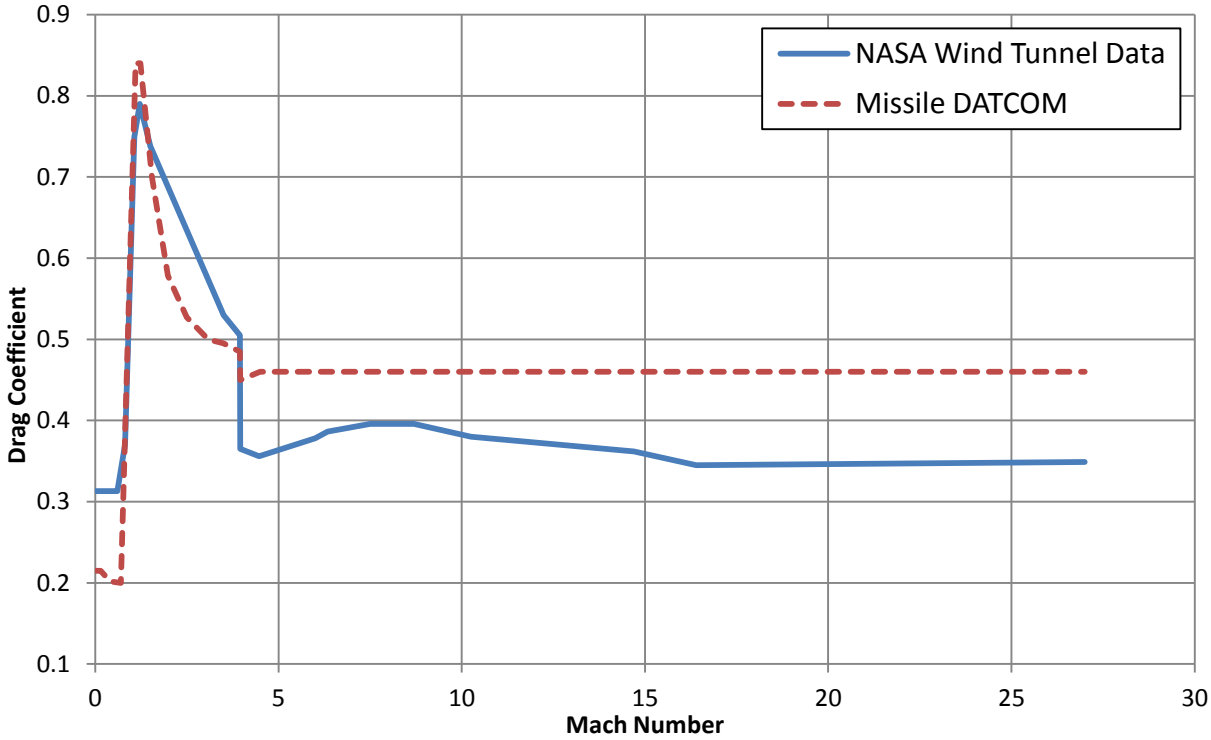

Figure 3.8. Missile DATCOM Drag Coefficient Estimation. Is comparable to NASA wind tunnel test data.

The lift comparison is much less reliable, as illustrated in Figure 3.9. The Missile DATCOM prediction is approximately an order of magnitude off and is a poor representation. It is limited in its ability to calculate lift coefficients for such a large launch vehicle and as such cannot be used to estimate the lift coefficients for the configurations in this project. This presents a problem as there are no other aerodynamic tools available for lift coefficient estimation. An attempt was made to locate historical lift data for vehicles similar to those in the optimization, but this data is unavailable or extremely difficult to find. Two of the vehicles that are analyzed in this optimization project are 2.5 stage vehicles with two large boosters. They resemble the vehicle NASA used in the wind tunnel to generate the lift data, and as such, they can use the same aerodynamic lift data. This thesis attempts to optimize seven different configurations, and there are still five without lift data.

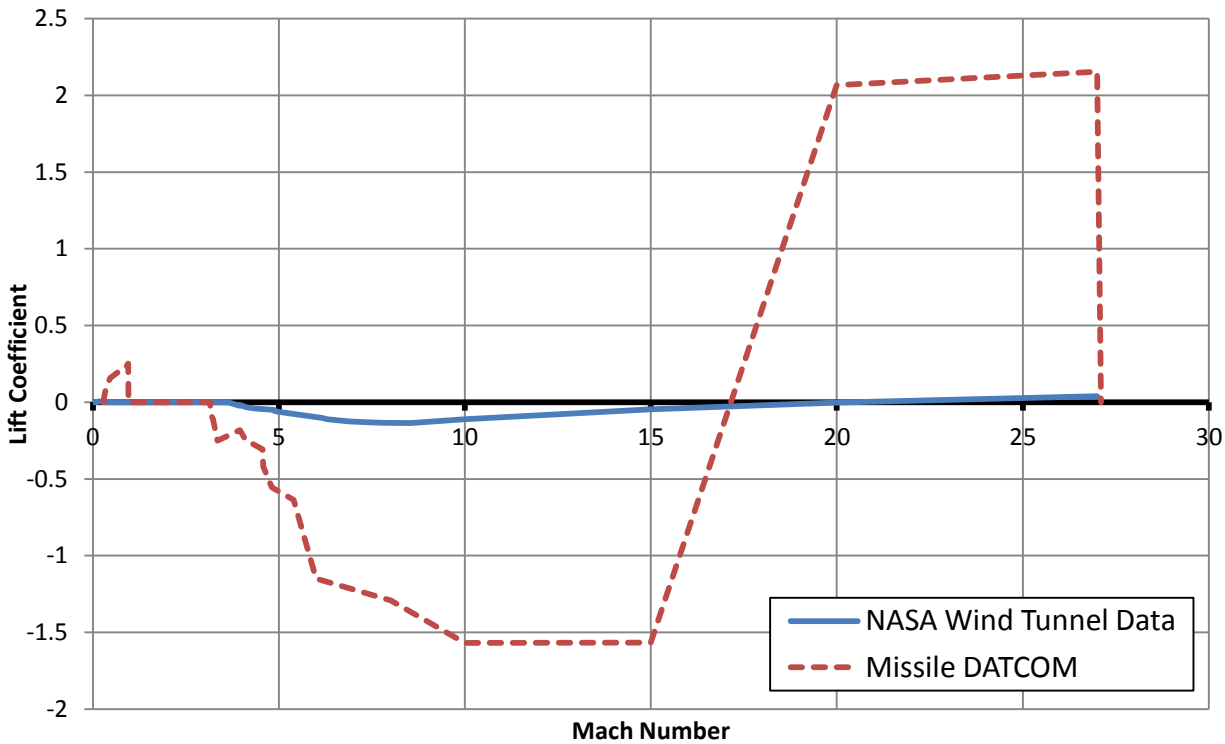

Figure 3.9. Missile DATCOM Lift Coefficient Estimation. Comparison shows profile is unreliable.

The next question to ask is, how much does lift affect the overall trajectory of a heavy lift launch vehicle? To determine this, a reference 2.5 stage vehicle is run in THEO that can use the NASA tabulated wind tunnel data. It is run once with the lift on, and again with the lift turned off. The results are compared in Figure 3.10a-c for the three variables of altitude, inertial velocity, and inertial flight path angle. The variables for the lift and no lift conditions are matched right on top of each other. Table 3.4 displays a comparison of the burnout conditions, the maximum dynamic pressure, and the launch time.

Table 3.4. Lift and No Lift Comparison.

	With Lift	No Lift	
Altitude	399821	399529	*m*
Burnout Velocity	7667.4	7668	*m/s*
Flight Path Angle	-0.2580	-0.2680	*deg*
Max Dynamic Pressure	799.6	799.7	*psf*
Time for Launch	596.1	596.1	*s*

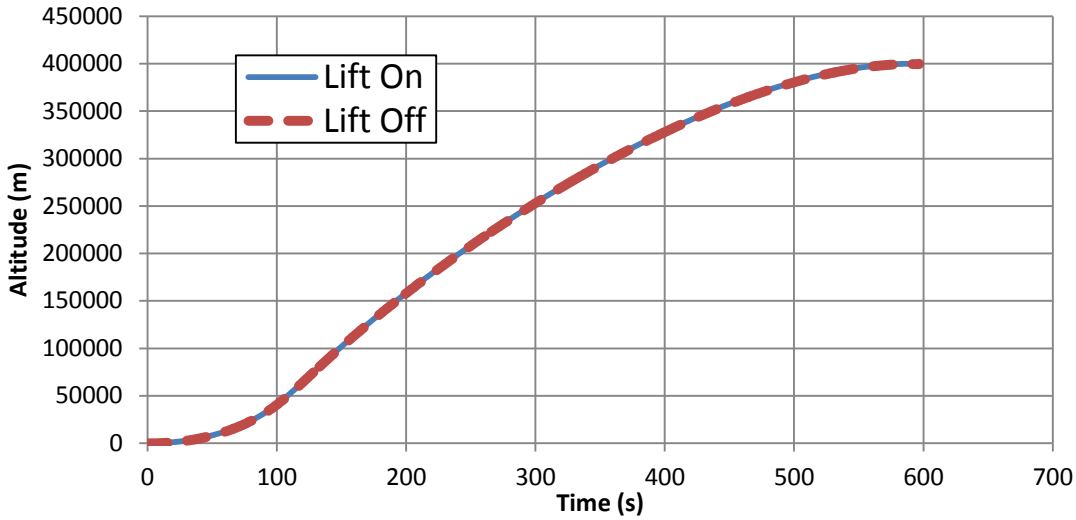

(a)

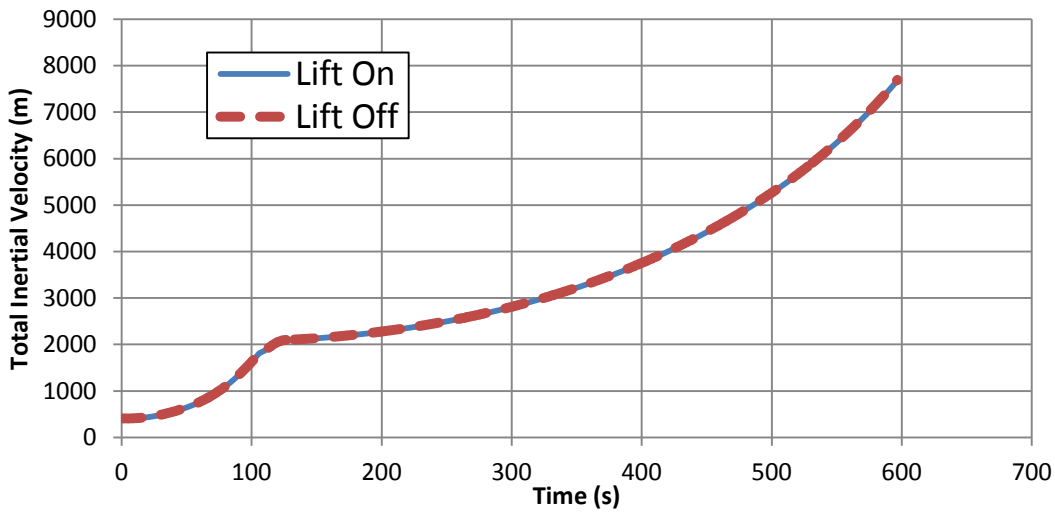

(b)

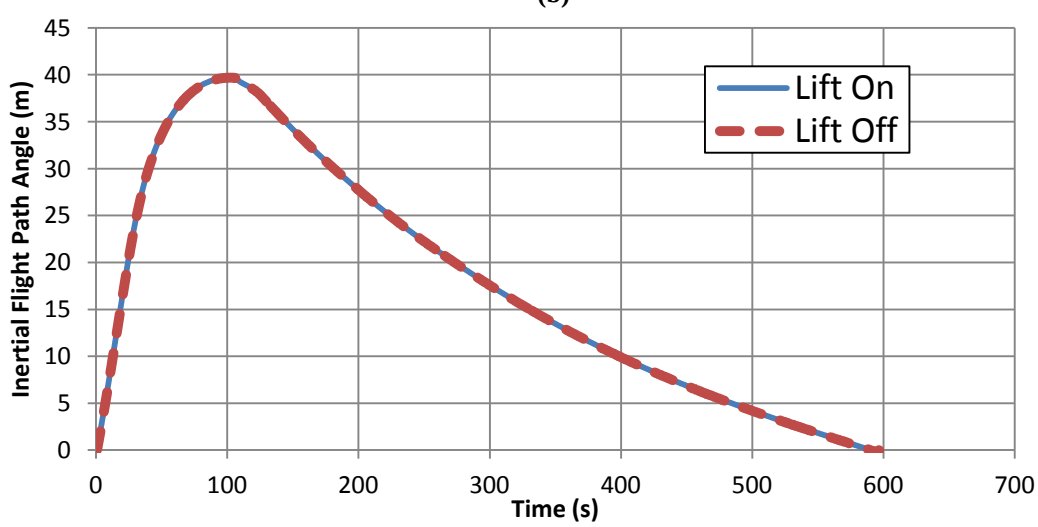

(c)

Figure 3.10a-c. Altitude, Inertial Velocity, and Inertial Flight Path Angle Comparison.

The three burnout conditions in Table 3.4 indicate that lift has a very small effect on the trajectory of the vehicle. Does this make sense conceptually? Lift is generated only when the vehicle has an angle of attack within the atmosphere. For a heavy lift launch vehicle, there is only an angle of attack when a pitch event is programmed into the trajectory. There are usually five pitch events when using THEO, but only a portion of them take place within the measurable atmosphere. Figure 3.11 shows the angle of attack for the trajectory, and notice how the lift in Figure 3.12 corresponds to the angle of attack. When the secondary pitch events are initiated at 108 s, the lift is generated but shifts to zero as the density decreases. Even though there is an angle of attack past 140 s, there is no lift due to atmospheric conditions. Figure 3.10a-c shows that lift has a very small effect on a heavy lift vehicle, and as a result, the assumption is made for all vehicles not resembling the NASA 2.5 stage case that lift can be neglected.

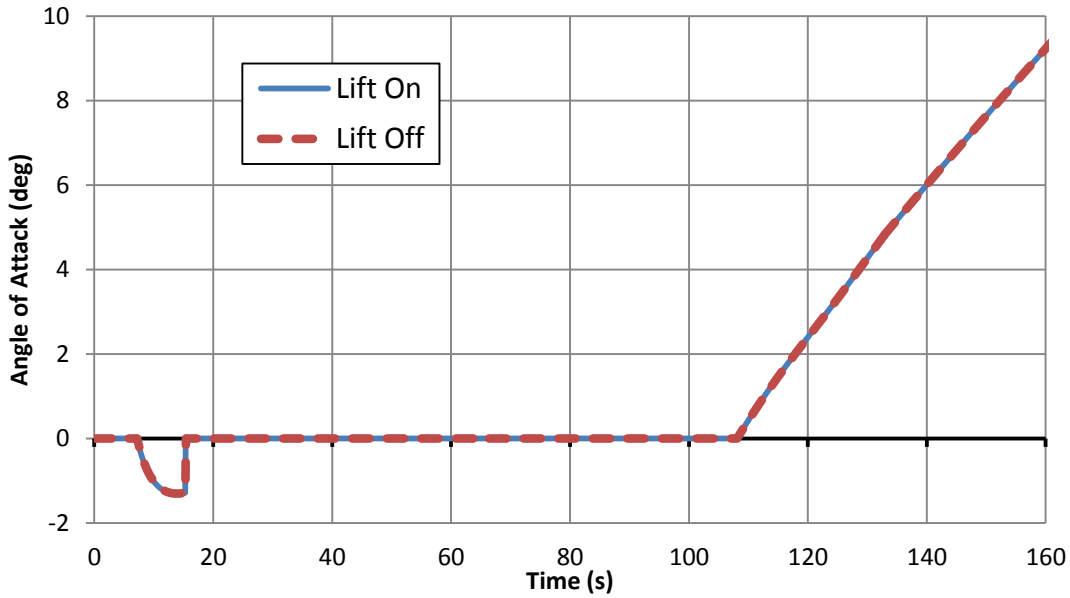

Figure 3.11. Pitch Induced Angle of Attack. Corresponds with lift.

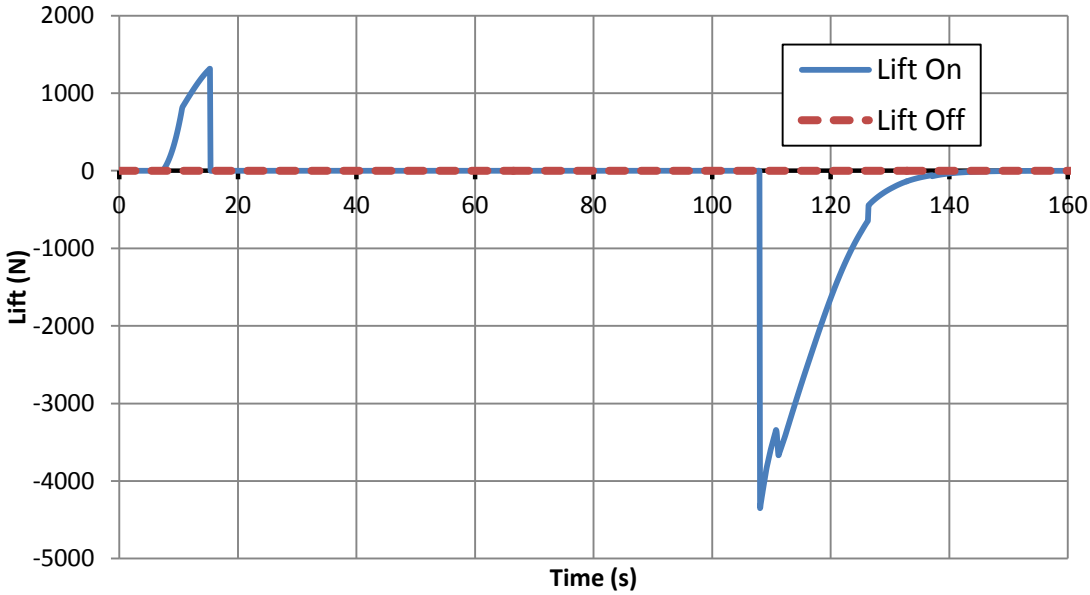

Figure 3.12. Lift due to Angle of Attack.

Chapter 3 References

Anderson Jr, J. D. (1999). *Aircraft Performance and Design.* Boston: WCB/McGraw-Hill.

Auman, L., Doyle, J., Rosema, C., Underwood, M., & Blake, W. (2008). *Missile DATCOM User's Manual - 2008 Revision.* Air Force Research Laboratory.

Bertin, J. J. (2002). *Aerodynamics for Engineers* (4th Edition ed.). Upper Saddle River, NJ: Prentice-Hall, Inc.

Braeunig, R. A. (2010, July). *Rocket and Space Technology*. Retrieved from Saturn V Launch Simulation: http://www.braeunig.us/apollo/saturnV.htm

Brandon, J. M., Derry, S. D., Heim, E. H., Hueschen, R. M., & Bacon, B. J. (n.d.). *Ares-I-X Stability and Control Flight Test: Analysis and Plans.* Hampton: NASA Langley Research Center.

Campbell, J. (2010). *POST Input Case.* Huntsville.

Crowell Sr., G. A. (1996). *The Descriptive Geometry of Nose Cones.*

Isakowitz, S. J., Hopkins, J. B., & Hopkins Jr., J. P. (2004). *International Reference Guide to Space Launch Systems* (Fourth ed.). Reston, VA: AIAA.

John, J. E., & Keith, T. G. (2006). *Gas Dynamics* (3rd Edition ed.). Upper Saddle River, NJ: Pearson Prentice Hall.

Kelley, R. L., & Rochelle, W. C. (n.d.). *Atmospheric Reentry of a Hydrazine Tank.* Houston.

Lepsch, R., & Cerro, J. (2008). *Ares V Geometry Trade Study* . NASA.

McDonnell Douglas Corporation; Air Force Reasearch Laboratory. (2008). Missile Datcom. Ohio.

NASA. (1970). Program to Optimize Simulated Trajectories.

National Oceanic and Atmospheric Administration; NASA, US Air Force. (1976). *U.S. Standard Atmosphere 1976.* Washington D.C.

Perkins, E. W., Jorgensen, L. H., & Sommer, S. C. (1958). *Investigation of the Drag of Varios Asially Symmetric Nose Shapes of Fineness Ratio 3 for Mach Numbers from 1.24 to 7.4.* NACA.

Sumrall, J. P., & McArthur, C. (n.d.). *Ares V: Designing the Heavy Lift Capability to Explore the Moon.* Huntsville: NASA.

Sutton, G. P., & Biblarz, O. (2010). *Rocket Propulsion Elements* (8th Edition ed.). Hoboken, NJ: John Wiley & Sons, Inc.

Turner, M. J. (2000). *Rocket and Spacecraft Propulsion* (1st Edition ed.). (R. A. Marriot, Ed.) Chichester, UK: Praxis Publishing Ltd.

White, F. M. (2006). *Viscous Fluid Flow* (3rd Edition ed.). Boston, MA: McGraw Hill.

Yechout, T. R., Morris, S. L., Bossert, D. E., & Hallgren, W. F. (2003). *Introduction to Aircraft Flight Mechanics.* (J. A. Schetz, Ed.) Blacksburg, VA.

Chapter 4

Rocket Propulsion

Chapter 4

Rocket Propulsion

Propulsion is defined as the act of manipulating energy in such a way to provides movement to an object. This movement can be classified in many different ways, but usually corresponds to acceleration, a direction change, or overcoming forces that impede motion (Sutton & Biblarz, 2010). There are many different variants of propulsion systems that can provide movement to an object, but only a few have the capability for use in heavy lift launch vehicles to orbit . A launch vehicle must operate at subsonic and supersonic speeds in both atmospheric and vacuum conditions, indicating that most air-breathing propulsion devices like jet and piston engines would be inoperative for the vacuum portion of the flight. There is a branch of vehicles called rocket based combined-cycle (RBCC) or turbine based combined-cycle (TBCC) engines that utilize a combination of air-breathing and stored propulsion systems (Olds & Saks, 1997). These engines have a lot of potential but are still heavily in the research and development phases.

All that is left is rocket propulsion, a type of propulsion that is completely dependent on producing thrust based on stored energy. History has affirmed this decision as all manner of orbital launch vehicles have some sort of rocket engine. The Saturn V, the Space Shuttle, Soyuz, Delta IV, and Ariane are a few examples of historical rocket vehicles that have been used or are in use for bringing payloads to orbit. This chapter will provide a summary as to which types of rocket propulsion systems will be used in the configurations in this analysis to bring the required payload to orbit. Also, one of the objectives of this project is to utilize propulsion technologies and hardware that are currently available or at a phase in design that could make them available in the near future. This propulsion analysis will discuss different engines and boosters available that will best fit the thrust and engine requirements.

4.1 Rocket Propulsion Systems

There are several different rocket technologies available. All have characteristics that are tuned to different purposes. A comparison of these characteristics is essential to eliminate propulsion propellant systems incapable of heavy lift launch vehicles.

4.1.1 Liquid

The first is a liquid propulsion system. This is usually a bipropellant system with a fuel and oxidizer. The fuel and oxidizer are both liquids and are separated when stored. When the launch is initiated, they are fed through a system of pumps and feed lines until they combine in the combustion chamber of the rocket. The reaction in this chamber creates a large energy release in the form of heat. These hot combustion gases must escape and follow the path to the converging diverging nozzle where they accelerate to the exhaust velocity. This type of propulsion system is very efficient as it has the highest performance of any of the chemical propulsion systems and is able to extract a higher percentage of chemical energy than some of the other methods (Humble, Henry, & Larson, 1995). It is also highly controllable as there are start and stop capabilities along with thrust modulation. One of the disadvantages of for liquid propulsion is some of the liquids have very low density, resulting in higher volume containment chambers. This tends to have a negative effect on the mass and volume of the vehicle (Sutton & Biblarz, 2010).

4.1.2 Solid

Solid propulsion engines are the oldest form of rocket propulsion. They have been used since the age of the Chinese dynasties and have been refined and enhanced ever since then. They consists of a solid molded propellant at a certain geometry within the combustion chamber. This solid contains both the oxidizer and fuel and is cast to optimize the flow out of the nozzle. Once the propellant is ignited, the energy release is driven to the nozzle where it accelerates to the specified exhaust velocities (Turner, 2000). Compared to other systems, solid rockets are relatively simple and do not require much hardware, which makes the production process simple and relatively cheap. They also have high thrust values which are necessary for the early stages of heavy lift launch vehicles. Performance is typically lower than other systems as the energy density of the propellant is not as high as other methods (Sutton & Biblarz, 2010).

4.1.3 Hybrid

Hybrid propulsion systems are a combination of the two previously mentioned systems. The hybrid is very similar to a liquid engine except for the oxidizer or fuel is kept as a solid in the combustion chamber. This eliminates the piping and storing associated with either the fuel or oxidizer. Essentially, the hybrid is able to combine some of the best aspects associated with solid and liquid systems. The solid propellant decreases the overall complexity, while the liquid propellant increases the percentage of energy extraction. Unfortunately, the combining of these two methods introduces some issues such as unexpected mixing and low amplitude vibrations that can be destructive. There has not been enough development in this area, and there are no hybrid systems available that provide the necessary thrust required for a heavy lift launch vehicle. This system shows significant potential, but until more development is completed, the hybrid system is not considered a viable candidate for this study (Humble, Henry, & Larson, 1995).

4.1.4 Nuclear

Nuclear propulsion is another type of rocket engine. It is similar to a liquid propulsion system except for the heat addition. In a liquid system, the heat addition is the result of very high temperature combustion gases, where as for nuclear propulsion the heat comes from a nuclear fission reaction that is then exchanged to the liquid propellant for acceleration through the nozzle (Sutton & Biblarz, 2010). This system has the capability for high performance; however, technological and political implications limit the use of this system in any vehicle. No launch vehicles have flown with this type of engine.

4.1.5 Electric

The last major type of a rocket propulsion system is an electric propulsion system. It uses electricity to accelerate the propellant of the vehicle. This system can add energy to a particle by using solid resistance elements, arc discharge, or by ionizing the particles. These particles are then accelerated through the nozzle by a magnetic field at exhaust velocities much higher than any of the other rocket propulsion systems. This implies a very efficient system capable of running as long as there is propellant and electrical energy. With solar panels, this method has the potential for long lasting energy necessary for powering the particle acceleration process. There is one characteristic that makes this system unrealistic for a launch vehicle. Even though the exhaust velocity of the particles is very high, there are less exhaust particles when compared to a chemical propulsion system. This means the overall thrust is low, and implies this system is more suited for low thrust maneuvers outside the atmosphere (Humble, Henry, & Larson, 1995).

4.2 Rocket Performance

4.2.1 Evaluating Thrust

The creation of thrust is a result of the change in momentum due to the transformation of chemical heat energy into kinetic energy. For both solid and liquid propellant systems the combustion and exiting processes are identical. In the instant after the chemical reaction, the stationary gases contain enormous amounts of heat energy which are released by the expansion and movement of the gas towards the nozzle. The flow reaches Mach 1 at the throat and continues to accelerate through the length of the diffuser. The reaction force between the accelerating flow and the nozzle is the result of the pressure of the expanding gas acting on the diffuser surface area. This force is the thrust term and is generated solely from this reaction (Sutton & Biblarz, 2010).

Another way of considering the thrust ($\boldsymbol{T}$) generated from exhaust flow is to analyze it with a simplified version of Newton's 2nd Law (Eq. (4.1)) . This law of conservation of momentum shows thrust is a term dependent on the rate of change of momentum and any other acting forces ($\boldsymbol{F}$). In this case, thrust is the result of a vector momentum exchange. Any object with velocity ($\boldsymbol{V}$) and mass (m) has momentum ($\boldsymbol{P}$) as defined in Eq. (4.2). In the case of a rocket engine, the exhaust molecules are ejected at a certain velocity ($\boldsymbol{V_{ex}}$) with a certain mass, resulting in

$$\frac{dP}{dt} = \frac{d}{dt}(m\boldsymbol{V}) = \boldsymbol{T} + \boldsymbol{F} \tag{4.1}$$

$$\boldsymbol{P} = m\boldsymbol{V} \tag{4.2}$$

momentum. In flight, the vehicle has equal and opposite momentum to the exhaust particles. One of the requirements of a system is for the momentum to remain constant. This implies that if the momentum of the exhaust particles changes in a negative direction, the vehicle will have to positively increase its momentum by the same amount. Change in momentum is defined in Eq. (4.3). Equation 4.4 shows the change in momentum with respect to time is dependent on mass flow rate ($\dot{m}$) and exhaust velocity. This principle can then be applied to Newton's 2nd Law as in Eq. (4.5). Conceptually, this is important because instead of looking at momentum in terms of individual mass particles, it relates the thrust to a mass flow rate. This simplicity makes it possible to represent all exhaust molecules exiting the nozzle (Humble, Henry, & Larson, 1995).

$$d\boldsymbol{P} = dm\boldsymbol{V_e} \tag{4.3}$$

$$\frac{d\boldsymbol{P}}{dt} = \frac{dm}{dt}\boldsymbol{V_e} \tag{4.4}$$

$$\boldsymbol{T} = \frac{d\boldsymbol{P}}{dt} - \boldsymbol{F} = \dot{m}\boldsymbol{V_e} - \boldsymbol{F} \tag{4.5}$$

4.2.2 Nozzle Inefficiencies

The extra force term ($\boldsymbol{F}$) in Eq. (4.5) represents a pressure drag loss. This term was introduced in the aerodynamics chapter and corresponds to a thrust loss due to the ambient pressure conditions. Differences in the exit and ambient pressure can adversely affect the performance of the rocket.

The ideal situation for a maximum momentum exchange with the working fluid and nozzle corresponds to complete gas expansion, which happens to be vacuum pressure. This expansion results in a maximum pressure force acting on the nozzle. Unfortunately, this is limited by the length of the nozzle, as full expansion of the flow would require an infinite nozzle. The requirements for a nozzle of this magnitude introduce unacceptable weight and size conditions for the engine. It is better to design the nozzle in such a way that it functions within the

atmosphere at close to optimum conditions. The optimum atmospheric condition for exhaust flow is that exit pressure at the nozzle be equal to the local ambient pressure.

If the exiting pressure is less than the ambient pressure this is called over-expanded flow. Over-expanded flow can be degrading to the flow as it creates an adverse pressure gradient. This adverse pressure gradient can cause flow separation that will remove the flow from the inner surface of the nozzle. Remember that the exhaust fluid in a nozzle provides a reaction force as long as it is in contact with the nozzle. If this contact is decreased by a separation, the momentum exchange can be much less. This results in pressure thrust loss defined in Eq. (4.6) where thrust is dependent on exit pressure (p_e), ambient pressure (p_a), and nozzle exit area (A_e) as well as mass flow and exhaust velocity. This term is included in the thrust calculations within THEO.

$$\boldsymbol{T} = \dot{\mathrm{m}}\boldsymbol{V_e} - (p_e - \mathrm{p_a})\mathrm{A_e} \tag{4.6}$$

If the exit pressure is greater than the ambient condition the result is under-expanded flow. If the flow expansion is not completed within the nozzle it must continue the expansion outside of the nozzle. This indicates that if the nozzle were slightly longer it would be able to exchange momentum with working fluid for a longer time period. Since most nozzles cannot adjust to the changing local ambient pressure, they are usually designed to be slight under-expanded. This avoids the possible separations associated with over-expanded flow (Sutton & Biblarz, 2010).

4.2.3 Specific Impulse

There is a parameter in rocket propulsion useful when comparing different types of propellants and engines. It is called specific impulse (I_{sp}) and is shown in Eq. (4.7) as a function of $\dot{m}$ mass flow rate, thrust, and sea level gravity. This term has units of seconds and describes the change in momentum available per unit weight of the fuel. This is in essence an efficiency term that describes how much the propulsion system can change the momentum of a vehicle based on the propellant and engine. Specific impulse can also be determined with exhaust velocity as in Eq. (4.8). Typical I_{sp} values are 260 s - 300 s for solid rockets, and 320 s – 460 s for liquid engines (Sutton & Biblarz, 2010).

$$I_{sp} = \frac{T}{\dot{\mathrm{m}}g_0} \tag{4.7}$$

$$I_{sp} = v_e g_0 \tag{4.8}$$

These numbers show specific impulse is much higher in liquid systems than in solid systems. Why not use liquid systems for all components on these heavy lift configurations? This has to do with the actual density of the propellants. Many liquid fuel and oxidizers have low density. This means sufficient amounts of liquid fuel require large storage containers within the vehicle. This can increase the size of the vehicle which in turn, increases drag effects as well as inert mass components. Solid propellants have very high densities, and as a result are useful for conserving space and mass. A configuration that contains both systems is able to utilize positive aspects of both.

4.2.4 The Rocket Equation

The rocket equation was engineered by Konstantin Tsiolkovsky to prove space travel is possible (Turner, 2000). The basic derivation uses a simplified version of Eq. (4.5), assuming there are no external forces such as pressure loss, drag, or gravity. Equation 4.9 is the simplified equation in vector notation and Eq. (4.10) shows the scalar version. The scalar version can be used because there are no external forces and only two directions. The negative is used to account for the opposing directions of the exhaust and vehicle velocity.

$$\dot{m}\boldsymbol{V_e} = \boldsymbol{ma} \tag{4.9}$$

$$\boldsymbol{m}\frac{\boldsymbol{dv}}{\boldsymbol{dt}} = -\boldsymbol{V_e}\frac{\boldsymbol{dm}}{\boldsymbol{dt}} \tag{4.10}$$

Rearranging this equation yields Eq. (4.11), which can then be integrated with respect to the mass and velocity of the vehicle. Evaluating the definite integral using the initial and final conditions of both mass and velocity yields the rocket equation as in Eq. (4.12). This equation shows the change in velocity (ΔV) of a vehicle is a function of the engine exhaust velocity (V_{ex}), and the ratio of the initial mass (m_0) to final mass (m) .

$$-V_{ex}\int_{m_0}^{m}\frac{dm}{m} = \int_0^{V_b} dv \tag{4.11}$$

$$\Delta V = V_{ex}\ln\left(\frac{m_0}{m}\right) \tag{4.12}$$

This equation is incredibly useful as it describes how much propellant is necessary to bring a vehicle to burnout velocity. In a way, it illustrates how the energy available within the propellant corresponds to changing the velocity of the vehicle. This equation can also be applied to multiple stages by evaluating the burnout velocity for each stage and summing them together.

Equation 4.12 can be adjusted to account for the losses associated with different forces and events that act on the vehicle. This introduces what is called the velocity budget of a vehicle. Velocity budget reveals how much ΔV from the propellant is required to reach orbital velocity and overcome all of the associated losses with traveling to orbit (Humble, Henry, & Larson, 1995). The terms that are considered in the budget are drag, steering, gravity and the rotation of the earth where each is represented by a ΔV term as in Eq. (4.13). Each of the force terms can be translated into ΔV by dividing each by mass and integrating with respect to time for the entire launch procedure. This is shown in Eq. (4.14).

$$\Delta V_{req} = \Delta V_{LEO} + \Delta V_{Steering} + \Delta V_{Drag} + \Delta V_{Gravity} + \Delta V_{rotation} = \Delta V_{Prop} \tag{4.13}$$

$$\Delta V_{req} = \sqrt{\frac{\mu}{r}} + \int_0^t \frac{T}{m}(1-\cos\alpha)dt + \int_0^t \frac{D}{m}dt + \int_0^t \frac{W}{m}\sin\gamma\, dt + \omega r\cos\phi\, dt = \int_0^t \frac{T}{m}dt \tag{4.14}$$

To reach orbit at the required injection velocity, the total ΔV within the propellant must at the very least equal the required ΔV. Table 4.1 shows typical velocity budget values for two different vehicles with a 400 km burnout orbit. Notice the differences associated with ΔV_{req} when secondary pitch events are used. These values were generated in THEO using Eqs. (4.13) and (4.14). For comparison, the Saturn V ΔV_{req} is shown (Saturn Flight Evaluation Working Group, 1973). The difference in ΔV_{req} for the Saturn V and 2 stage vehicle is due to different mission requirements

Table 4.1. Sample Velocity Budget. 2.5 Stage Vehicle with secondary pitch events and 2 stage vehicle with no secondary pitch event and gravity turn for entire burn. In (m/s).

Vehicle	ΔV_{LEO}	ΔV_{steer}	ΔV_{drag}	$\Delta V_{gravity}$	ΔV_{rot}	ΔV_{req}	ΔV_{prop}
2.5 Stage	7670.8	78.7	45.8	2205.7	-444.0	9556.9	9613.4
2 Stage	7670.8	0.0	25.5	3065.2	-441.7	10319.9	10300.9
Saturn V	7645.8	-	-	-	-	9312	-

4.3 Propulsion System Advantages and Disadvantages

This section goes into more detail as to the different characteristics and properties of the solid and liquid propulsion systems. As these two systems are the potential candidates as propulsion components for the launch vehicle, it is important to understand in more detail the benefits and shortcomings associated with each system

4.3.1 Solid Propulsion Systems

These launch systems are treated differently for heavy lift launch vehicles. In a heavy lift launch vehicle, solid propellant rockets are almost always built as a stand-alone system. In other words, they are built as boosters; which are strap on, high thrust, independent systems. This provides a lot of variability as it is relatively simple to attach them to a configuration to provide extra thrust if needed.

Solid propulsion rockets are unique in that they contain both the fuel and oxidizer in the combustion chamber. This requires that the propellant be cast to a grain shape. The grain shape can be designed to best fit a number of different factors. It can be shaped to provide a constant thrust, variable thrust, short burn time, and long burn time. These factors are governed by the mass flow rate through the nozzle which is in turn a function of the exposed surface area of the propellant. A larger grain surface area exposes more propellant to the ignition process and provides a higher burn rate (Turner, 2000).

The grains are tailored to specific mission designs. For example, the Reusable Solid Rocket Motor (RSRM) booster used on the Space Shuttle is designed to provide thrust during the atmospheric phase of the launch. During this phase, high dynamic pressures can potentially damage the craft. This is avoided by introducing a thrust bucket into the grain of the design as shown in Figure 4.1. The thrust bucket is the result of surface area manipulation to reduce the thrust during the expected high pressure regions.

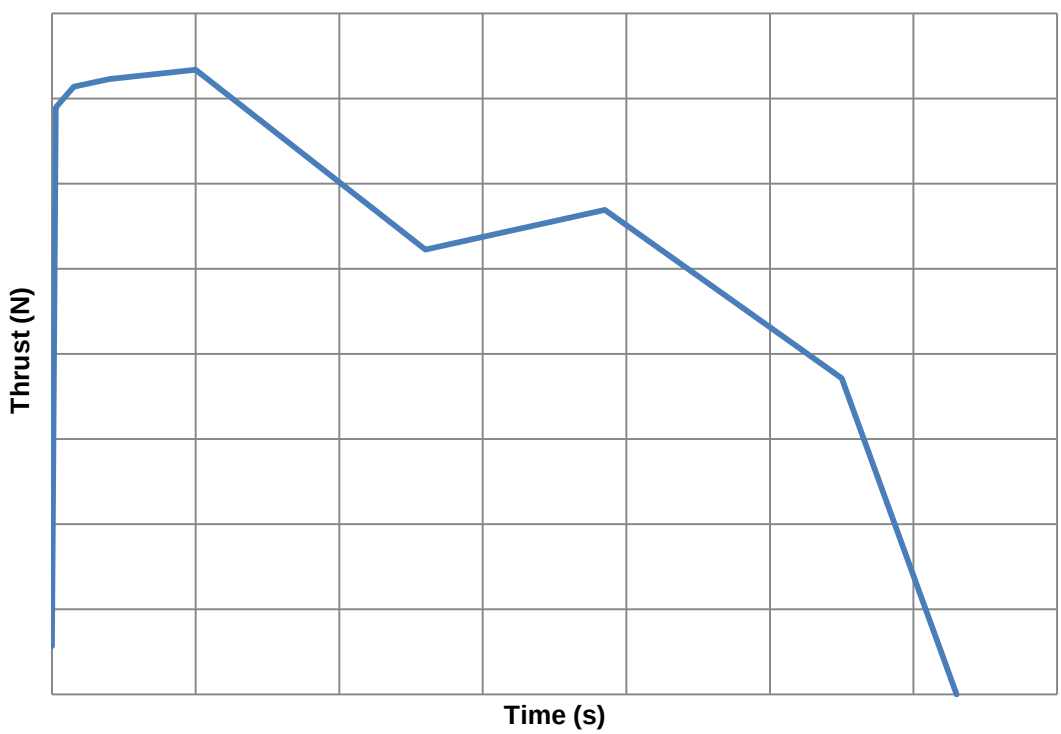

Figure 4.1. RSRM Thrust Profile. Shows thrust bucket to reduce atmospheric effects. Axis removed for ITAR regulations (NASA).

Figure 4.2 shows sample grain geometries that correspond to a different purpose. Type (a) has a cylindrical surface that gradually increases in thrust. The surface area linearly increases with time indicating a linear increase in the mass flow rate and thrust. Type (b) is a geometry that promotes approximate constant thrust using the rectangular shaped imprints. As time progresses, the imprints slowly wear away while the radius of the cylinder continues to increase. The third case (c) is a constant thrust profile. As one surface area is increasing linearly, the other is decreasing linearly. This formation is difficult to manufacture as suspending the central cylinder can introduce complications. Type (d) represents an advanced profile. It starts at very high thrust values and slowly decreases until all the fins have burned away. After that, the profile linearly increases with the changing circumference of the outer cylinder (Turner, 2000). These few cases have demonstrated the capability of a grain, and how they can be used in many different situations.

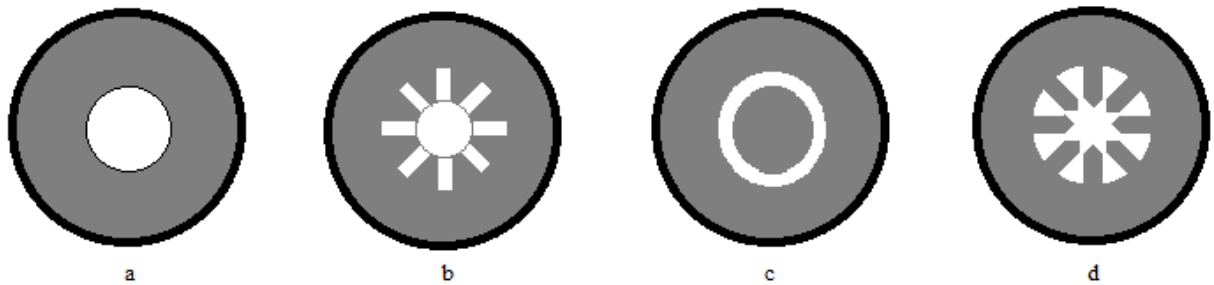

Figure 4.2. Grain Cross Sections. Each cross section is designed to fulfill a specific thrust profile purpose.

There is an issue associated with certain solid rocket grains that can decrease the overall performance. Some solid rockets are very large and cannot be cast all at once. Instead, they are cast in lengthwise segments and are then connected at joints. This is the case in both the RSRM and Hydroxy-terminated Polybutadiene and Composite Case booster (HTC) (Kibbey & Campbell, 2010). These joints introduce a perturbation in the flow of the combustion chamber, which can induce vortices that affect the overall momentum of the flow. There has not been a significant amount of research on this subject, but is a consideration when utilizing multi-segment booster types. This can be avoided by using monolithic or single segment grains.

Another issue with solid propulsion systems is that there is a lack of stop/start capability once the ignition process has initiated. This is the result of both the oxidizer and fuel being contained within the propellant grain. There is no way to separate one from the other to halt the oxidation process. This can present an issue if there is ever a problem during launch.

One of the most favorable qualities of a solid rocket is the simplicity associated with hardware. As all the propellant is contained within the combustion chamber, there is no need for pumps, feed lines, and extra power sources associated with liquid configurations. This provides high reliability and eliminates some inert mass which can put the fuel to a total mass ratio between 0.85 and 0.91. This ratio is acceptable, but overall is usually slightly less than the fuel to total mass ratio of a liquid propulsion system. Figure 4.3 shows the effects of fuel to total mass ratio (*MR*) for a single stage vehicle on final vehicle velocity. As MR increases, the maximum achievable burnout out velocity also increases. Maximizing this ratio can greatly increase the performance of a rocket (Sutton & Biblarz, 2010).

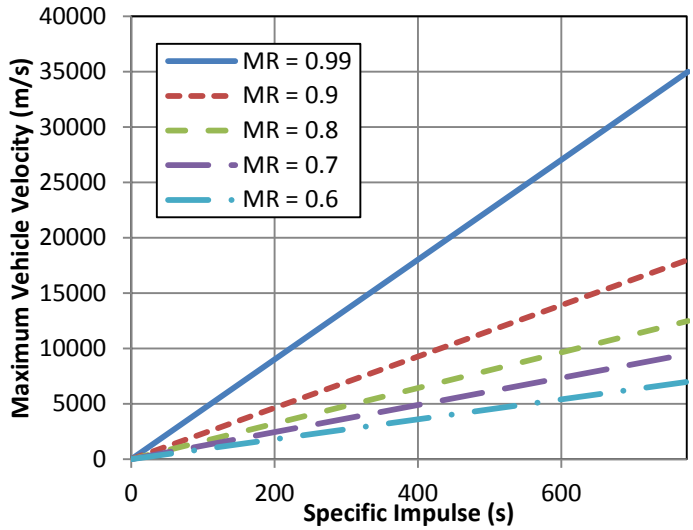

Figure 4.3. Propellant Mass Ratio. (Sutton and Biblarz).

4.3.2 Liquid Propulsion Systems

Inherently, these systems are more complicated than solids, but they tend to provide more versaility and capability. Since the fuel and oxidizer are located in different tanks, it is necessary to transport them to the combustion chamber. This requires a complex system of feed lines, piping, and injectors that must provide the fuel and oxidizer at correct mixture ratios and chamber pressures. Driving up the pressure of these components requires a turbopump that is often powered by a smaller combustion chamber within a rocket. In turn, this uses some of the propellant. The system is incredibly complicated but is necessary for maximum energy extraction. This resulting high efficiency is evident in the specific impulse for liquid systems.

There are many different types of fuels and oxidizers, but most efficient combinations have at least one cryogenic component. This introduces more complications that usually increase the inert mass of a liquid propulsion stage. The liquid must be insulated, and all the piping must be designed so that it can expand and contract without any leaking. This also means that due to evaporation, the rocket propellant cannot be stored in the tanks for long periods of time. This is very different from solid boosters, as they can be stored ready to launch for months and even years.

As there are numerous different combinations for an oxidizer and fuel, it is important to consider a few important factors when selecting. Combustion temperature plays a significant role when determining the thrust and exhaust velocity for certain combinations. Equation 4.15 shows exhaust velocity (v_e) and therefore I_{sp} are dependent

$$v_e = C_f \left[\gamma \left(\frac{2}{\gamma+1} \right)^{(\gamma+1)/(\gamma-1)} \frac{MW}{RT_c} \right]^{-1/2} \tag{4.15}$$

on the properties of molecular weight (MW), the gas constant (R), the ratio of specific heats (γ_c), and combustion temperature (T_c). These variables describe the properties of the fuel and oxidizer combination in the exhaust gases. The thrust coefficient (C_f) is also an important factor as it considers the properties of the nozzle. Exhaust velocity depends on the square root of the combustion temperature. This varies slightly, depending on the surrounding pressure, but is mostly dependent on the chemical energy available for release. This is specific to the properties of the fuel and oxidizer (Turner, 2000). Table 4.2 shows properties of different fuel and oxidizer combinations. Notice the liquid fluorine combination has the highest combustion temperature and exhaust velocity. Even though performance of this combination is high, it produces extremely toxic byproducts and cannot be used.

Table 4.2. Liquid Propellant Properties. (Turner, 2000)

Oxidizer	Fuel	O/F Ratio	T_c (K)	Density (kg/m^3)	V_e (m/s)
O_2	H_2	4.83	3251	0.32	4550
O_2	RP1	2.77	3701	1.03	3580
F_2	H_2	9.74	4258	0.52	4790
N_2O_2	MMH	2.37	3398	1.20	3420
N_2O_2	N_2O_4+UDMH	2.15	3369	1.20	3420

Notice, even with the lowest combustion temperature, the liquid oxygen/hydrogen combination still has the second highest exhaust velocity. This is a result of the molecular weight of the exhaust gas. Eq. (4.15) implies a propellant with higher molecular weight adversely affects the exhaust velocity. The opposite is true for a low molecular weight. As a result of conservation of momentum, this higher molecular weight implies a lower velocity.

Liquid propulsion engines are designed to fulfill a certain purpose. Propellant combinations with lower specific impulse tend to function better in the 1st stage of a vehicle, where high thrust is necessary to overcome the weight and aerodynamic forces. Higher specific impulse values tend to function better in a second or third stage when the goal is simply to increase the velocity of the vehicle without having to overcome large forces (Braeunig, 2008).

These factors all come into play when an engine is being designed. The engines are designed to operate for a specific function based on the properties of the propellant. Table 4.3 shows a number of active and retired engines with a specific fuel and oxidizer combination. Notice the Space Shuttle Main Engine (SSME) and how the specific impulse relates to the mission requirements. It was designed to fire in conjunction with the RSRM boosters for the entire duration of the space shuttle launch. There is large difference in the sea level and vacuum-specific impulse. This is so the motor can focus on overcoming adverse forces early in the launch and then utilize the high specific impulse later in the flight to speed up the shuttle. Another example is the engine used on the Saturn V launch vehicle. The F-1 motor was used in stage 1. It has a low specific impulse suited to the purpose of a very high thrust motor. The J-2 is the second and third stage motor for the Saturn V, and accelerates the vehicle efficiently with high specific impulse (Saturn Flight Evaluation Working Group, 1973). The application of applying certain engines to certain stages is used in this heavy lift launch vehicle optimization as it tends to indicate which engine types function best for a certain purpose.

Table 4.3. Engine Parameter Comparison. Performance comparison for different engines (Turner, 2000).

Engine	Propellant	O/F Ratio	Vac. Th (N)	I_{sp} Vac. (s)	I_{sp} SL (s)	Chamber P (bar)
Vulcain	LO_2/LH_2	6.2	1075000	431	310	105
SSME	LO_2/LH_2	6	2323000	455	363	204
J-2	LO_2/LH_2		1052000	425	200	
F-1	LO_2/Kerosene	2.27	7893000	304	265	70
RS-27	LO_2/Kerosene	2.25	1043000	295	264	48
RD 170	LO_2/Kerosene	2.63	8060000	337	309	245

Unlike solid propulsion systems, liquids have stop and start capability. This is done by cutting off the flow for both the oxidizer and fuel. This is very useful for attitude adjustment and orbital motors, and is also advantageous if there is a need for engine shutdown. It is also possible to adjust the flow rates within the feed lines indicating an active control thrust modulation. There is the potential to use this control for thrust buckets in atmospheric flight regimes. This is usually left to solid motors, as a liquid propulsion system has the highest performance when operating at design flow conditions (Sutton & Biblarz, 2010).

4.4 Optimization Engine Selections

The solid and liquid propulsion systems used in this project must be selected based on designs currently in use, retired, or are in development and nearing availability. This section details the solid and liquid propulsion systems used in the heavy lift launch vehicle optimization. These selections are made based on the considerations presented in the previous sections that outline the benefits and issues associated with using either type of system.

4.4.1 Solid Rocket Boosters

There are four different solid propulsion boosters chosen to provide example of in modeling of a heavy lift launch vehicle. Together, they cover a range of capability in terms of different designs. The approximation thrust profiles used in THEO for these four boosters are shown in Figure 4.4- Figure 4.5. The first booster is the RSRM. It is a four segment motor with an ammonium perchlorate oxidizer and aluminum powder fuel (Alliant Techsystems). The RSRM motor has proven to be a very reliable booster as it has been used by NASA for the past thirty years. It has high thrust necessary for a heavy lift launch, and as the building facilities are still available today, it is a very economical choice. Figure 4.4 shows a comparison of the four booster selections.

The second booster is the newest variant of the RSRM called the RSRM V. It is an updated five segment version of its smaller brother, and has an improved thrust profile. The RSRM V is currently in the final testing phases and should be ready for flight in a couple years. As this is a design the United States will potentially use for future launch vehicles, it is important to include in the analysis.

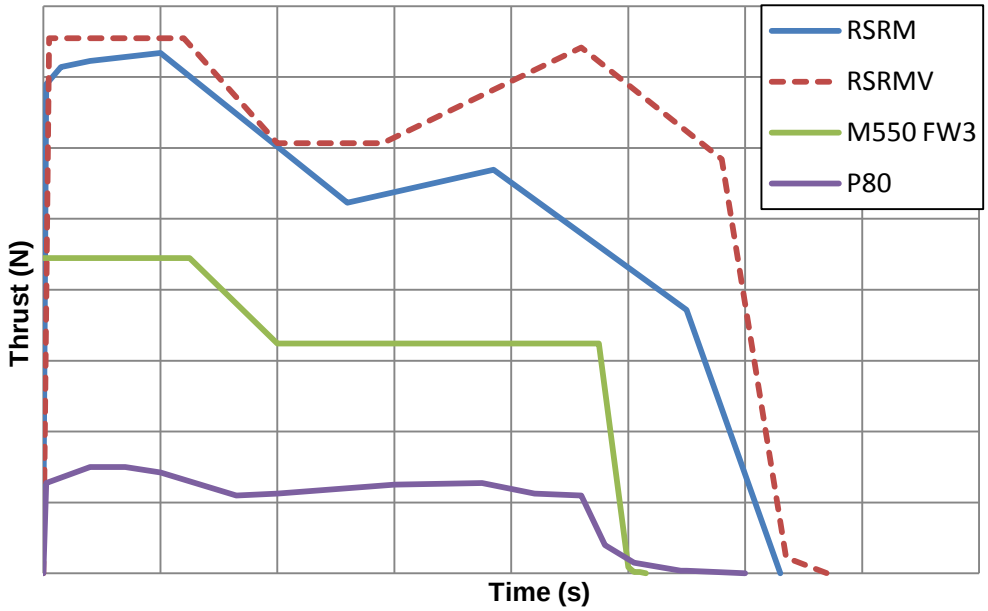

Figure 4.4. Booster Thrust Profile Comparison. These profiles correspond to the booster profiles in THEO. Axis removed from figure due to ITAR regulations.

The next booster considered is of the monolithic variant, which is a single segment rocket booster. It is called the Monolithic 550 FW3 and is must less complicated than any of the RSRM solid motors. It also has a much lower mass than the RSRM family and a lower thrust profile. This introduces a significant variability as the number of boosters can be varied to match the desired payload range necessary for this project. It is expected that a variation of 2-4 boosters could be used to bring the maximum payload of 130 mt to orbit.

The last is a small booster called the P80. It has very low thrust and low mass. A successful launch might require 6 to 8 of these boosters. This is of interest in a similar way to the Monolithic 500 because researchers are interested in the variability and cost savings of using light, high-number booster configurations (Kibbey & Campbell, 2010).

In the testing of these different cases, some of the boosters are applied as the first stage of the launch vehicle. So, instead of having a 1st stage liquid core this configuration might use 3 Monolithic 550s. There is some interest from NASA as to what the results of a configuration like this might look like.

4.4.2 Liquid Rocket Engines

The liquid propulsion systems considered are shown in Table 4.4 with their engine properties. The F-1 used on the Saturn V is an incredibly powerful rocket engine that has the high thrust necessary for the 1st stage of the launch. The F-1A is the latest version of the F-1 that was developed but never put into production. It has improved engine properties and is more capable than the F-1 (Sutton & Biblarz, 2010). Another liquid engine is the SSME. This engine is one of the most efficient rocket engines that ever designed. It does have lower thrust than the F-1A, but can be overcome by adding more engines. This engine type is of interest particularly to NASA as they now have a number of SSME engines that are inactive (Isakowitz, Hopkins, & Hopkins Jr., 2004). The new variant of the J-2 called the J-2X is much more efficient than its counterpart and has a higher specific impulse and thrust (Lamm, 2007). The specific impulse is lower than then SSME, but the J-2X is less expensive to manufacture than the SSME.

Table 4.4. Liquid Engine Selections. Engine Selections for use in project analysis .

	Thrust (N)	Vac I_{sp} (s)	SL I_{sp} (s)	O/F Ratio	T_{burn} (s)	P_c (bar)	D_{exit} (m)	A_{exit} (m^2)	m_{brnout} (kg)	Fuel
F-1	6909000	304	265	2.2674	165	70	3.76	11.103645	9153	LO_2/Kerosene
F-1A	8896440	300	-	-	158	70	3.61	10.235387	-	LO_2/Kerosene
J-2X	1310000	448	-	5.5	465	90	3.05	7.3061664	2472	LO_2/LH_2
SSME	2170000	455	363	6	480	204.08	2.4	4.5238934	3177	LO_2/LH_2

Chapter 4 References

Alliant Techsystems. (n.d.). The Space Shuttle Reusable Solid Rocket Motor.

Braeunig, R. A. (2008). *Rocket Propellants*. Retrieved from Rocket and Space Technology: http://www.braeunig.us/space/propel.htm

Humble, R. W., Henry, G. N., & Larson, W. J. (1995). *Space Propulsion Analysis and Design.* (R. W. Humble, Ed.) New York: The McGraw-Hill Companies, Inc.

Isakowitz, S. J., Hopkins, J. B., & Hopkins Jr., J. P. (2004). *International Reference Guide to Space Launch Systems* (Fourth ed.). Reston, VA: AIAA.

Kibbey, T. P., & Campbell, J. J. (2010). *Catalog of Solid Rocket Motor Designs Available for Heavy-Lift Propulsion.* Huntsville.

Lamm, T. (2007). *J-2X Engine.* Pratt and Whitney Rocketdyne.

Olds, J., & Saks, G. (1997). A Conceptual Design Tool for RBCC Engine Performance Analysis. *1997 Space Technology & Applications International Forum (STAIF-97).* Albuquerque: AIP.

Saturn Flight Evaluation Working Group. (1973). *Saturn V Launch Vehicle Flight Evaluation Report - AS-512 Apollo 17 Mission.* Huntsville: Marshall Space Flight Center.

Sutton, G. P., & Biblarz, O. (2010). *Rocket Propulsion Elements* (8th Edition ed.). Hoboken, NJ: John Wiley & Sons, Inc.

Turner, M. J. (2000). *Rocket and Spacecraft Propulsion* (1st Edition ed.). (R. A. Marriot, Ed.) Chichester, UK: Praxis Publishing Ltd.

Chapter 5

Independent Variables and Computation Considerations

Chapter 5

Independent Variables and Computation Considerations

The data generated by THEO for optimization is defined by specified variables and steps. There are five different independent variables that can be used when modeling configurations, and they are start time, length, and pitchrate for the primary pitch event, stage 1 propellant mass, and stage 2 propellant mass. An evaluation is completed by varying these five different independent variables to determine if the vehicle can reach the desired target conditions of altitude, inertial velocity, and inertial flight path angle. Remember from earlier that the desired burnout conditions are an altitude of 400 km, and inertial velocity of 7670 m/s, and a flight path angle of 0 deg. As explained in Chapter 2, determining configurations that achieve orbit is done by utilizing loops within THEO to compare the results of different trajectories. These different trajectories are created using a range of input values for the previously mentioned variables, and are specified by the user with a minimum, maximum, and interval. The interval is defined as the step size between the minimum and maximum. For example, if the user were to input minimum, maximum, and interval pitch start time as [7.5 7.8 0.1] s, THEO would simulate different configurations with a start time of 7.5, 7.6, 7.7, and 7.8 s. This same format is applied to all five variables.

The results are then organized based on how close a particular run comes to the target burnout conditions. THEO will then select, with its limited decision making procedures, the configuration that it considers to best reach the target conditions.

This selection is rather limited since it only reveals the data associated with that specific case. There is another method that utilizes the data in *pitch.out* and *pitch2.out* to reveal how adjusting the independent variables affects the burnout conditions of the vehicle. Before approaching this concept, Chapter 5 discusses considerations associated with selecting input values and intervals for the independent variables.

5.1 Independent Variables

When selecting minimum, maximum, and interval values for the optimization, it is essential to consider any limitations that might be associated with selections. These limitations can apply to physical impracticalities and even to accuracy considerations. Whatever the case, using THEO to simulate numerous trajectories requires careful selection of these independent variables. This section will provide some guidelines as to making an initial guess for these three different values for each variable.

5.1.1 Primary Pitch Event Start Time

The minimum start time for the primary pitch event is defined by two conditions. The first is that the launch vehicle must clear the tower before it can begin the event. As the launch vehicle must be no taller than 100 m, it is assumed that the tower is the same height. Depending on the thrust to weight ratio, this will generally happen between 5 and 10 s. It requires simple experimentation to determine where this point lies for a specific configuration.

When NASA launches the Space Shuttle, the first pitch event is initiated as soon as the vehicle clears the launch tower. The Shuttle does so to convert as much of the thrust into horizontal velocity as soon as possible. THEO does not make this assumption, as the heavy lift launch vehicle and Shuttle are very difficult vehicles. The heavy lift launch vehicle is much heavier than the shuttle, and it is possible that initiating the pitch event later is necessary to reach target conditions.

The second condition relates to the idea that the start time variable can be somewhat of an unstable input. This was introduced in Chapter 2 as a very small change in the start time was seen to substantially affect the burnout conditions of the launch vehicle. This implication is supported in Figure 5.1, where plots show the burnout conditions for a reference launch vehicle as a function of primary pitch event start time. The other four independent variables are held constant to show the effect of changing pitch event start time. With these plots, it is possible to see the effects of a start time that is too early and too late. An early start time forces the vehicle over prematurely, steering it back into the atmosphere and away from the target conditions. A late pitch time will place the vehicle on track to a high altitude, but with a less than adequate circular velocity. This is a result of the majority of energy being expelled into overcoming gravity instead of increasing the velocity of the vehicle.

Figure 5.1 also shows the effects of changing the interval step size for start time. This is imperative to ensure an adequate step size is used to search for successful configurations. It is also a goal to use a large step size that will minimize computation time. These charts shed some insight as to where the medium is between minimizing step size and computation time. When determining if an interval set is a good representative, it is important to consider discontinuities similar to the velocity jump at approximately 7.5 s in Figure 5.1b. An interval set needs to be able to identify points similar to this. It is obvious that both intervals 5 s and 10 s do not recognize the discontinuity in the plot and also do not accurately represent the curve. An interval of 1 s does approximate the curve well, but just like the previous two, it does not recognize the discontinuity. Both intervals of 0.5 s and 0.1 s satisfy these conditions and as to cut down on computation time, it is suggested to use an interval of 0.5 s.

5.1.2 Length of Primary Pitch Event

The method for determining limitations for length of the primary pitch event can be handled in a similar fashion. First, consider how NASA handles pitch length in POST. The POST input deck validating THEO uses a dynamic pressure flag to determine the length of the pitch event. Specifically, when the dynamic pressure reaches 150 psf, POST deactivates the pitch event. I could find no justification for this flag specification, and resolved to consider primary pitch length based on the user input independent variable loops.

The requirements for pitch length are that it must be long enough for the vehicle to transition from a vertical to horizontal orientation but short enough the vehicle will not turn back into the atmosphere. There are no specific lengths to define these points, but it is possible to understand how the vehicle might behave when subjected to different pitch lengths.

Figure 5.2 shows the effects on burnout conditions when applying a different pitch length to the same configuration. The other four variables are held constant to solely show the effect of varying the pitch event length. These plots show that adjusting the pitch length when it is less than approximately 15 s can have a substantial effect on the burnout conditions. The high slopes of the curves before 15 s are an indicator of this. After 15 s, the curves for all three burnout conditions become relatively stable. This a result of how it is possible for the pitchrate to coincide with the gravity turn. Consider the situation of a primary pitch event with a start time of 5 s and a length of 10 s. After this event is completed at 15 s, gravity will take over and continue to turn the vehicle until a secondary pitch event is activated. The aforementioned stability occurs when the induced pitchrate resembles the gravity turn pitchrate. If this is the case, a longer pitch length does not have much of an effect on the burnout conditions.

Consideration of the interval step size for length of the pitch event is also shown in Figure 5.2. Using the same logic as for start time interval step size, it is determined an interval of 1 s is adequate. The data from this interval represents the curve well and also reduces computation time as compared to using an interval of 0.5 s.

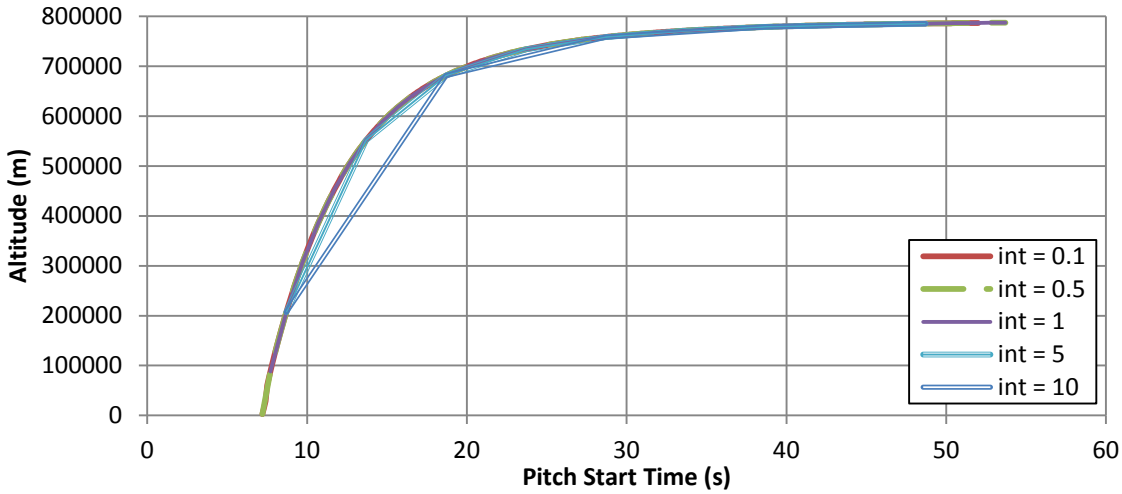

(a)

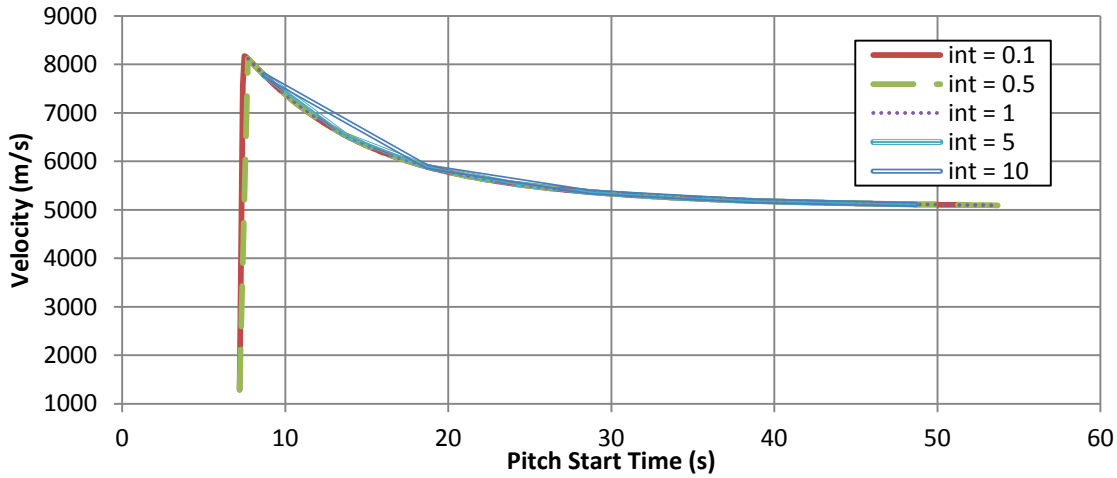

(b)

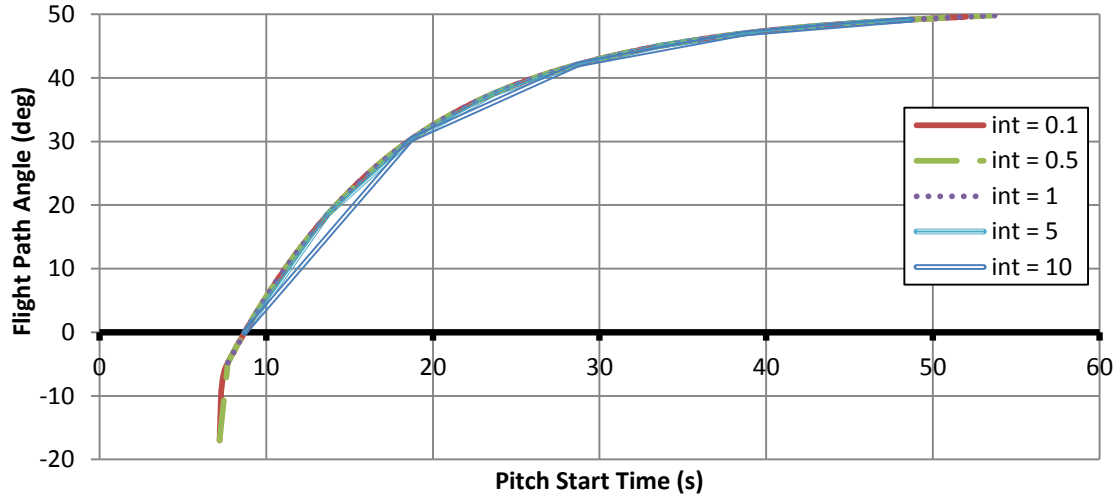

(c)

Figure 5.1a-c. Primary Pitch Event Start Time. These plots illustrate burnout conditions of a launch vehicle as a function of start time. Plots also show the curve fit associated with a specified interval.

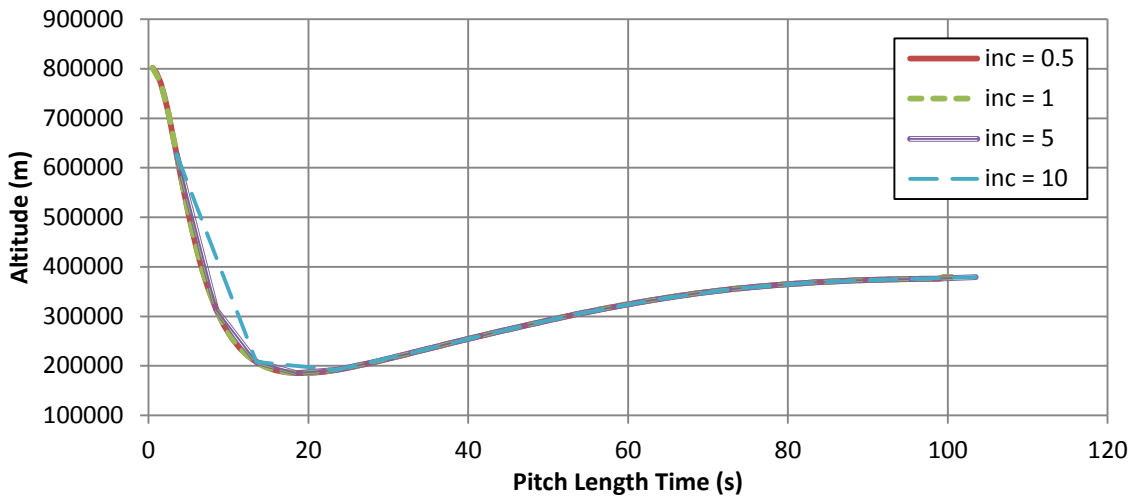

(a)

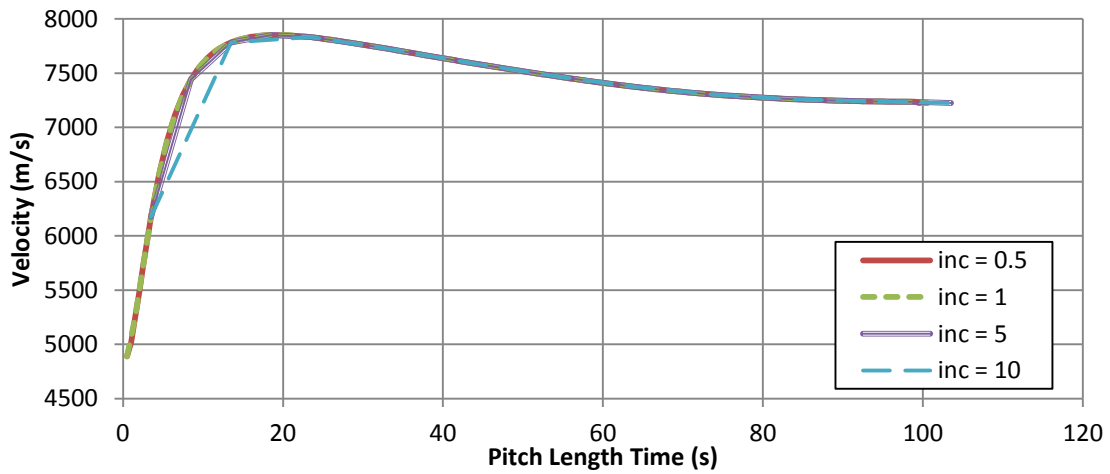

(b)

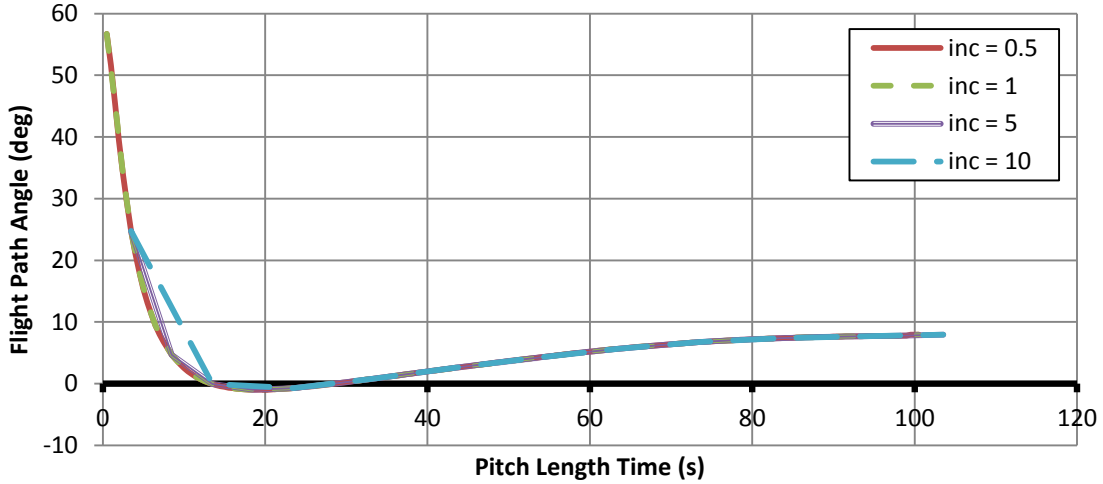

(c)

Figure 5.2a-c. Length of Primary Pitch Event. These plots illustrate the burnout conditions of a launch vehicle as a function of primary pitch length. Plots also show the curve fit associated with a specified interval.

5.1.3 Primary Pitch Event Pitchrate

As in THEO, the pitchrates within POST are specified as an independent variable. The independent variables are varied within POST using a projected gradient algorithm to optimize the payload mass for the target conditions. THEO also follows a similar method but uses the much simpler procedure of varying the pitchrate based on user input.

In a similar way to pitch length, it is important to ensure the pitchrate is high enough to eventually bring the vehicle to the necessary orientation and low enough to keep the launch vehicle from turning back into the atmosphere. Another consideration is the effect of pitchrate on angle of attack. One of the limitations for atmospheric flight is that the angle of attack for the vehicle must be no higher than 6º. The pitchrate must be kept below a point that would cause the angle of attack to increase past the structural limitation of 6º.

The plots in Figure 5.3 show the effect of different pitchrate intervals on the burnout conditions. The ideal choice would be the interval of 0.001 deg/s. Unfortunately, this is not practical as a typical pitchrate can range anywhere in between 0.01 deg/s and 0.80 deg/s. It is computationally inefficient to use such a small interval with such a large range. This leaves the interval 0.01 deg/s, which is slightly less accurate but is the only remaining interval that has the ability to catch the discontinuity.

5.1.4 Stage Propellant Mass

The last two independent variables within POST are stage 1 and stage 2 propellant mass, and there is a constraint associated when assigning a maximum for both stage propellants. The thrust to weight ratio for the vehicle must be greater than one within the first two seconds of launch. If the propellant mass is high enough, a thrust to weight ratio less than one will prevent the vehicle from ever leaving the launchpad.

Figure 5.4 shows the effects of varying both stage 1 and 2 propellant mass. The horizontal plane in the different plots represents the desired burnout condition. The intersection of this horizontal plane with the surface in each plot represents a point where that particular burnout condition has been reached. These surfaces show how adjusting the propellant mass for each stage can cause the actual burnout condition to drift away from the desired burnout condition. Notice, there are two different intersections curve on both Figure 5.4a and 5.4b. Figure 5.4b shows there are two regions where the launch vehicle will reach target velocity. The first is on the backside of the surface where there is a very steep slope. The second region is a more stable region as it has a shallower slope. Figure 5.4a also shows that there are two regions where there is an intersection of the altitude burnout conditions to the desired horizontal plane. A later chapter will address the topic of distinguishing which intersection points and curves could be optimized solutions for the launch vehicle. These plots simply illustrate the possibilities when viewing the final condition of the vehicle as a function of propellant mass. The recommended interval for propellant mass is 50000 kg for a broad analysis, and 10000 kg for a fine analysis.

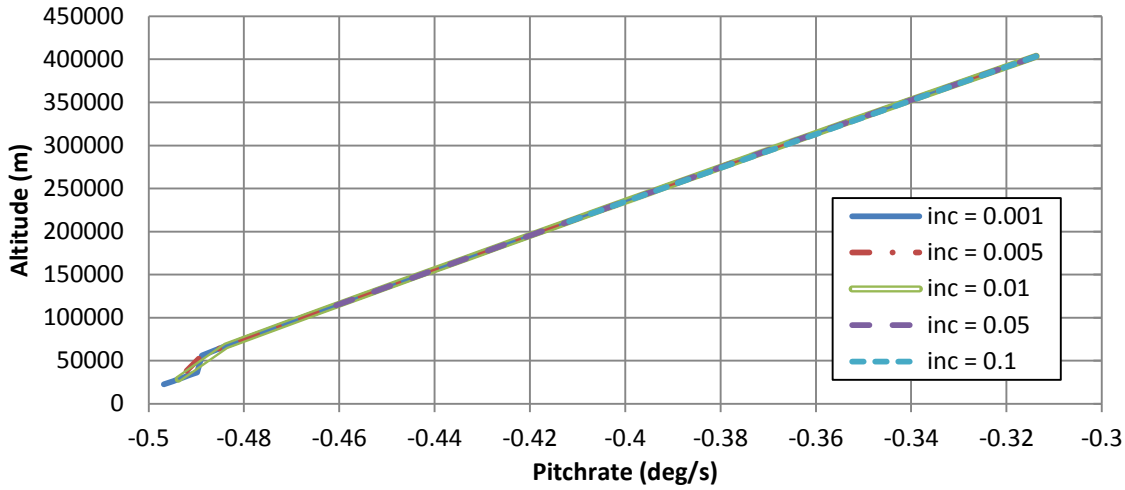

(a)

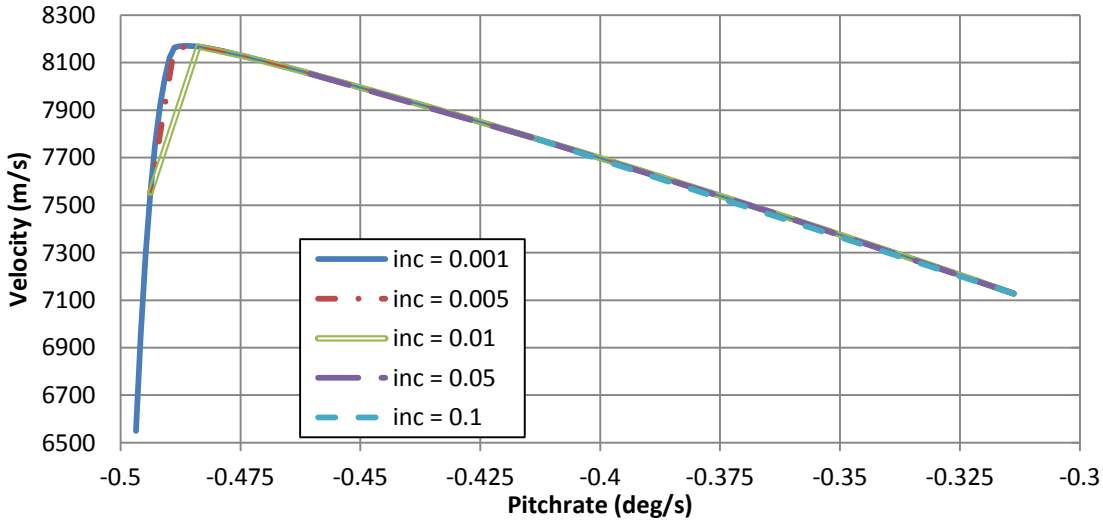

(b)

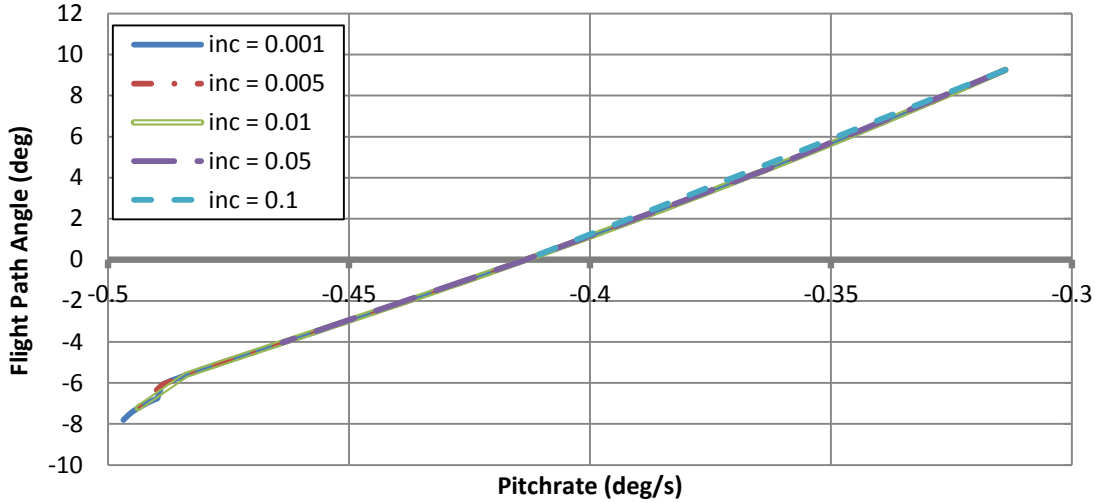

(c)

Figure 5.3a-c. Primary Pitchrate. These plots illustrate the burnout conditions of a launch vehicle as a function of primary pitch length. Plots also show the curve fit associated with a specified interval.

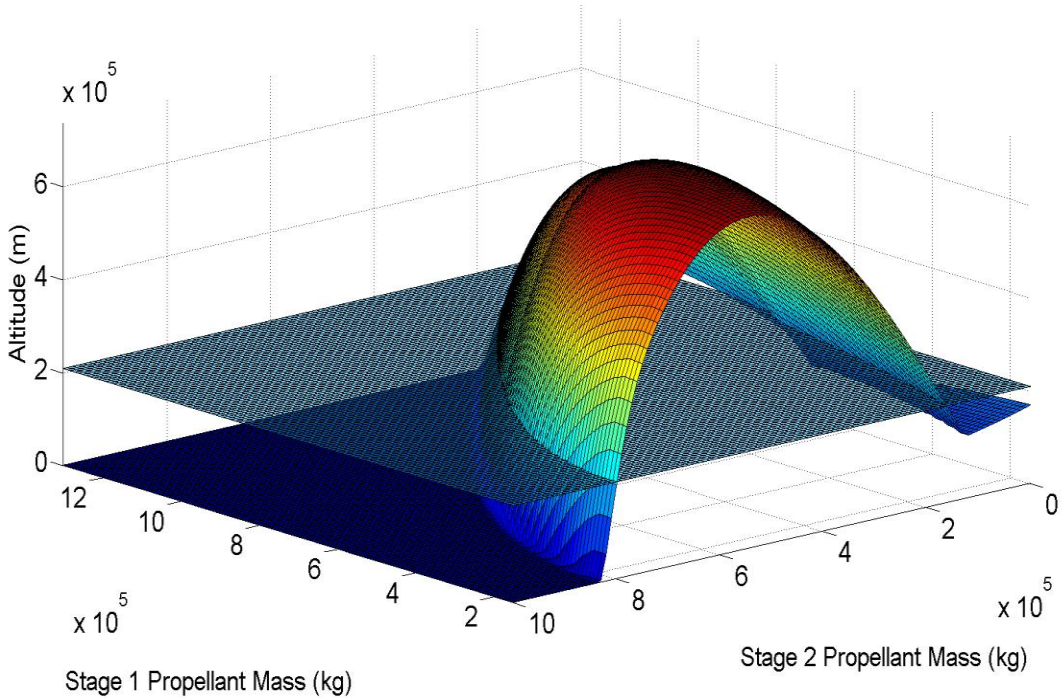
x 10^5
Altitude (m)
6
4
2
0
12
10
8
6
4
2
x 10^5
Stage 1 Propellant Mass (kg)
10
8
6
4
2
0
x 10^5
Stage 2 Propellant Mass (kg)

(a)

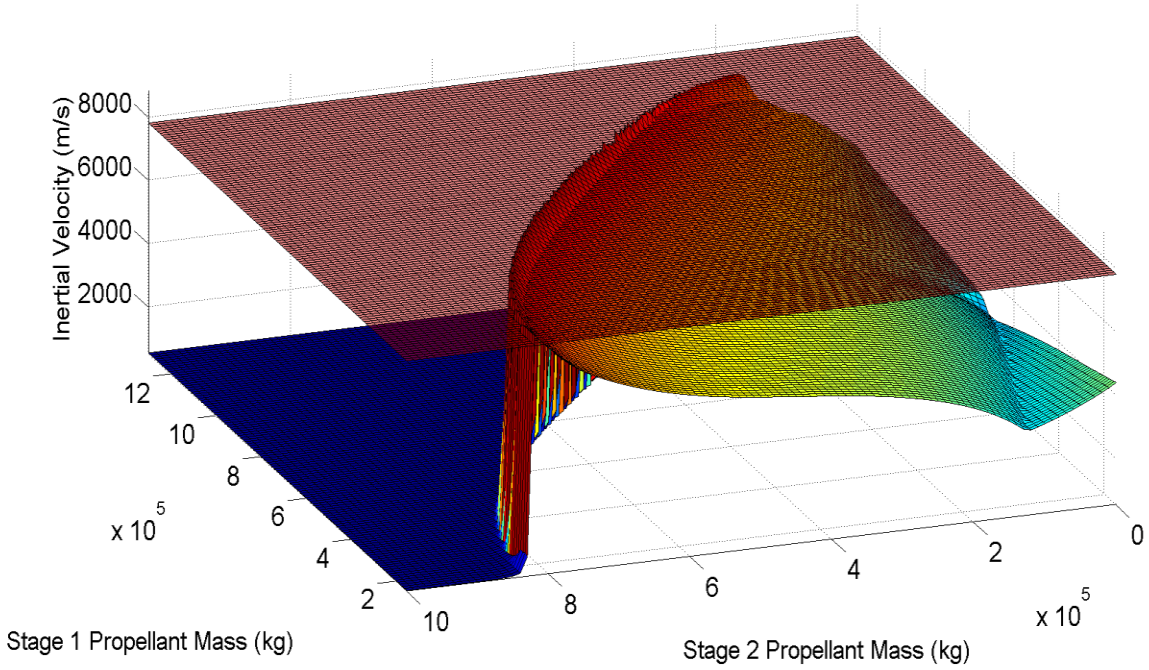
Inertial Velocity (m/s)
8000
6000
4000
2000
12
10
8
6
4
2
x 10^5
Stage 1 Propellant Mass (kg)
10
8
6
4
2
0
x 10^5
Stage 2 Propellant Mass (kg)

(b)

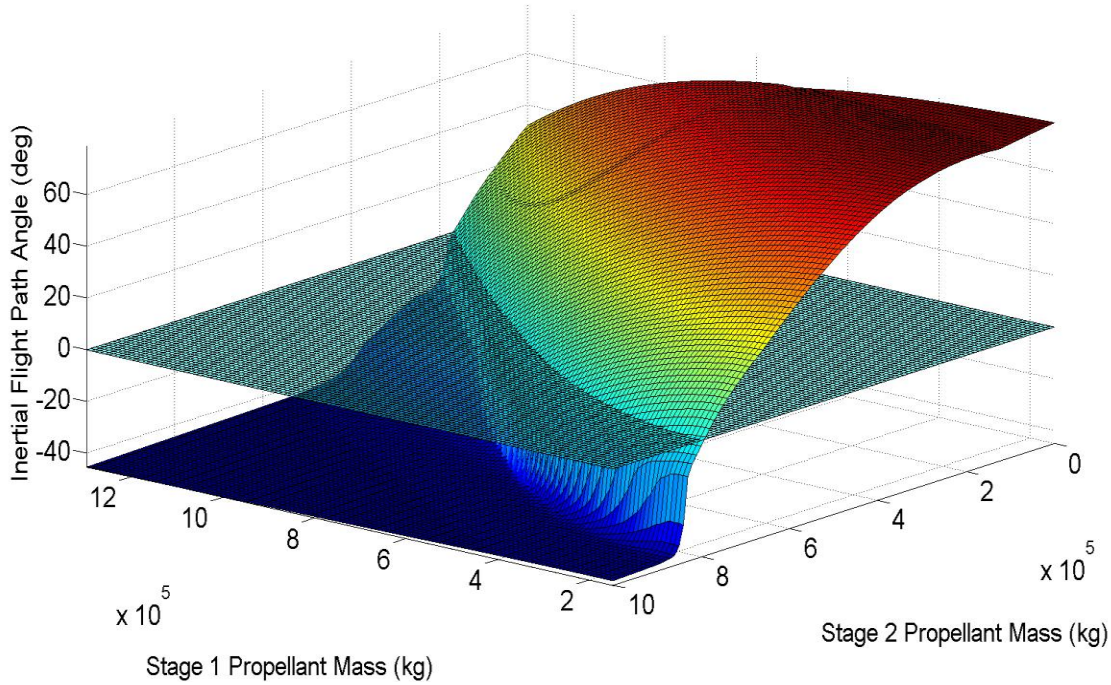

(c)

Figure 5.4a-c. Stage Propellant Mass. These three plots illustrates how changing the propellant masses for a launch vehicle affects the burnout conditions.

5.2 THEO Time Step

The time increment within THEO is a user input value that specifies the number of iterations per second, or the number of times per second the trajectory is evaluated. Figure 5.5 shows the impact of increasing the time increment and the resulting decrease in accuracy. Notice that for all three burnout conditions, the accuracy decreases substantially as the time increment is increased to greater than 0.1 s. Using a time increment less than this greatly increases the computation time with little adjustment in the accuracy. As a result of both of these factors, it is recommended to use dt = 0.1s.

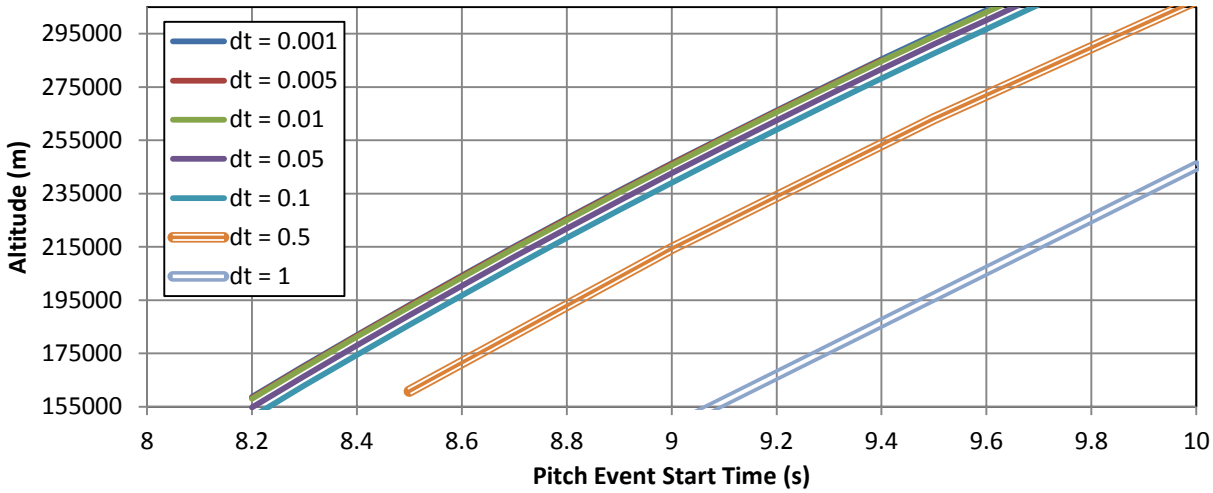

(a)

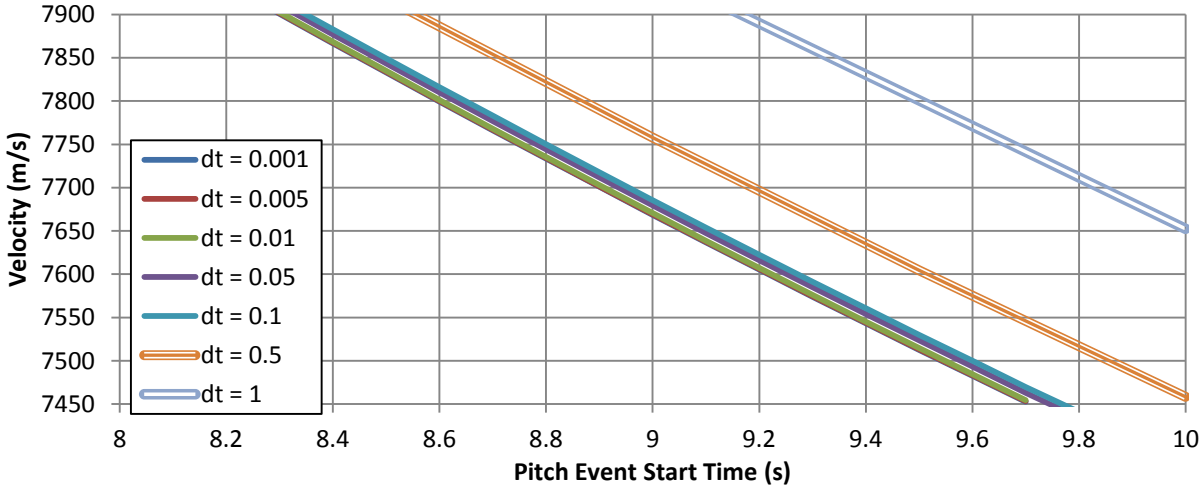

(b)

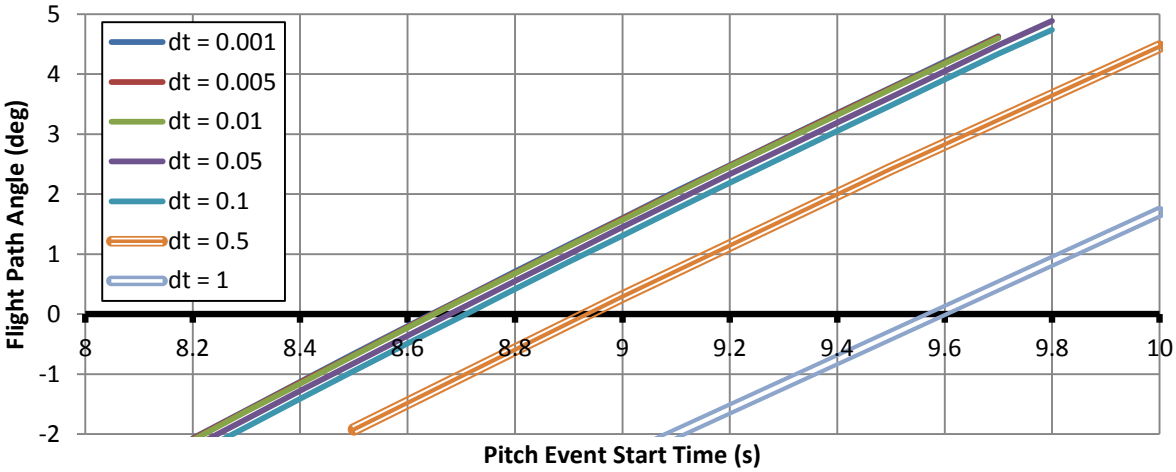

(c)

Figure 5.5a-c. THEO Time Increment. These plots show the effect of changing the time increment on the burnout conditions. Accuracy increases with a decreasing increment.

Chapter 6

Analysis Methodology and Secondary Tools

Chapter 6

Analysis Methodology and Secondary Tools

There are three different methods for optimizing a launch vehicle configuration for this project. The first employs the capability of THEO to simulate thousands of trajectories. By organizing the data from these trajectories in an effective manner, it is possible to determine an optimized configuration. The second method uses a mathematical analysis that optimizes by using the rocket equation as a constraint. The third method is a variant of the mathematical approach that provides a visual representation of determining the minimum amount of energy necessary to bring a payload to orbit. This chapter describes these methods and the tools used to employ them.

6.1 Vehicle Optimization Utilizing THEO

6.1.1 THEO Decision Logic

The selection method by THEO is a target condition based logic, and essentially, will select what it determines to be the top configuration. As revealed in an earlier chapter, this is defined as the configuration to best reach the target conditions of altitude, inertial flight path angle, and inertial velocity. Using this selection process is not considered an optimization. Remember from Chapter 2 that POST mathematically optimizes (maximizes or minimizes) the specified variable by varying the independent variables to the target conditions (NASA, 1970). THEO does not have this mathematical capability, but instead generates data for numerous configurations. The question is, how can this data be used to optimize a launch vehicle to an orbital position? The key is to analyze the data generated by THEO graphically.

6.1.2 Three Dimensional Visualization

The independent variables were outlined in the previous chapter, and the plots in Figure 5.4 are an example of using a visualization tool to organize the output data. There are five independent variables, and as such it is impossible to graphically visualize the effects of all five variables at once. It is instead completed by breaking the data into effective groups for analysis.

A three dimensional (3D) plot allows the user to view data as a function of two variables. By holding three of the variables constant, the effects of changing two independent variables can be represented graphically. To do this, a Matlab program was created that can sort through the output data from THEO and organize it based on the two user-specified independent variables. For example, consider the case of a 2.5 stage vehicle with a stage 1 propellant mass of 1550000 kg, a stage 2 propellant mass of 600000 kg and a pitch start time of 7.7 s. This Matlab code can, as in Figure 6.1-6.3, illustrate the effects of varying the pitch length and the pitchrate on the burnout conditions. Just as in Figure 5.4, these plots also contain a horizontal plane. This plane indicates the desired burnout condition for that particular configuration, and an intersection between the 3D surface and this plane implies a potential solution.

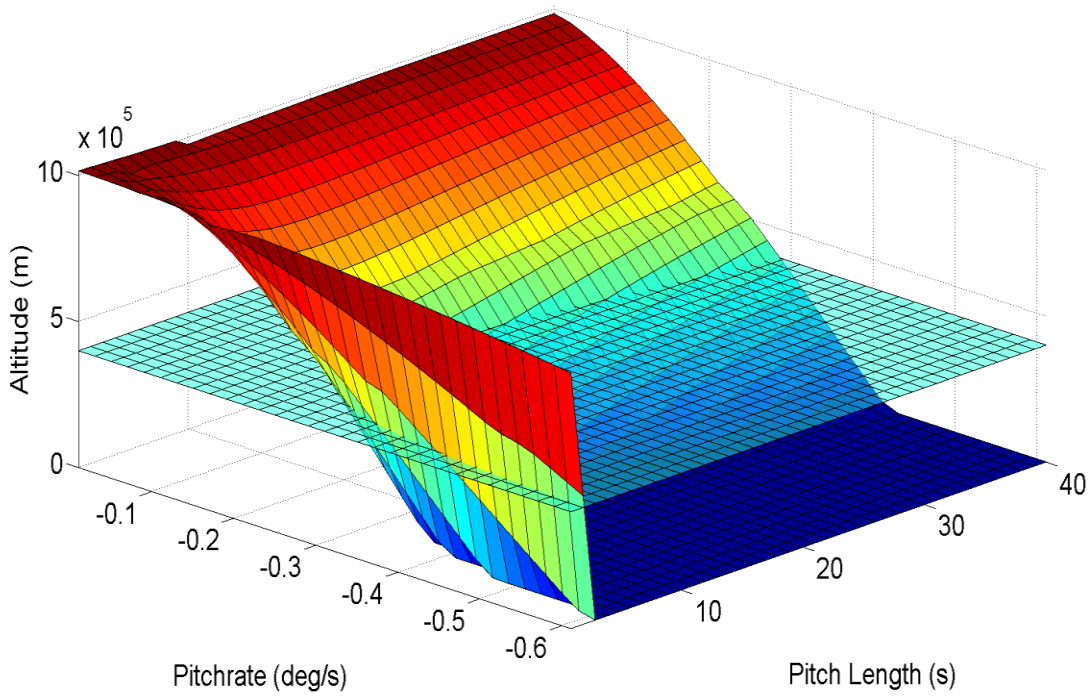

Figure 6.1. Vehicle Burnout Altitude. Function of pitch length and pitchrate.

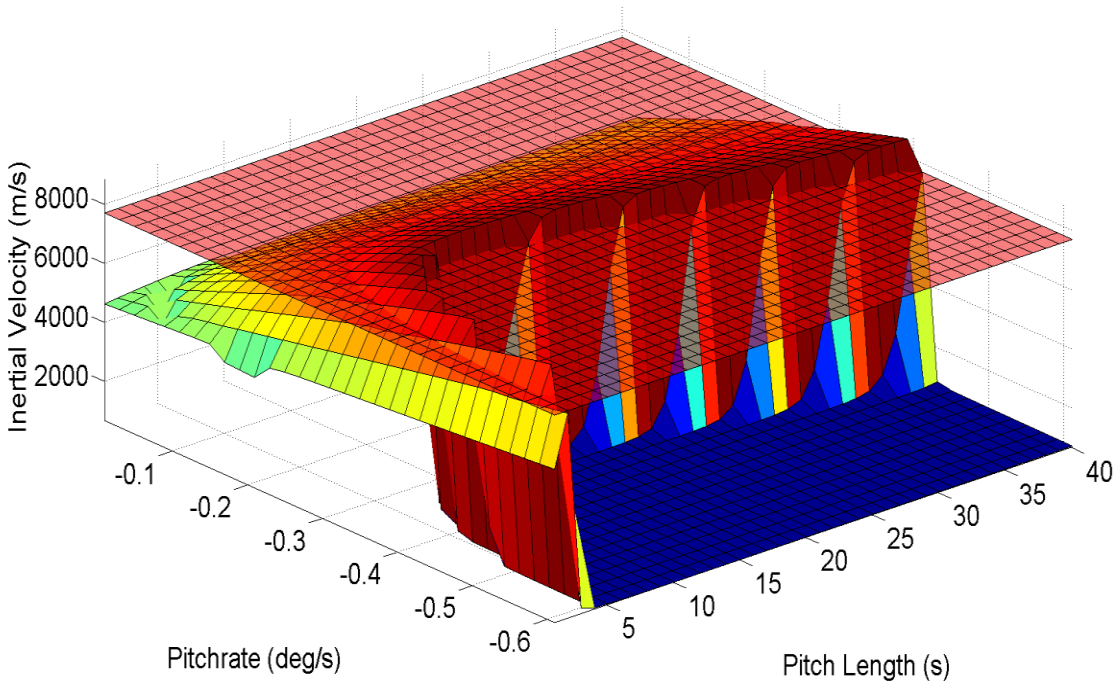

Figure 6.2. Vehicle Burnout Inertial Velocity. Function of pitch length and pitchrate.

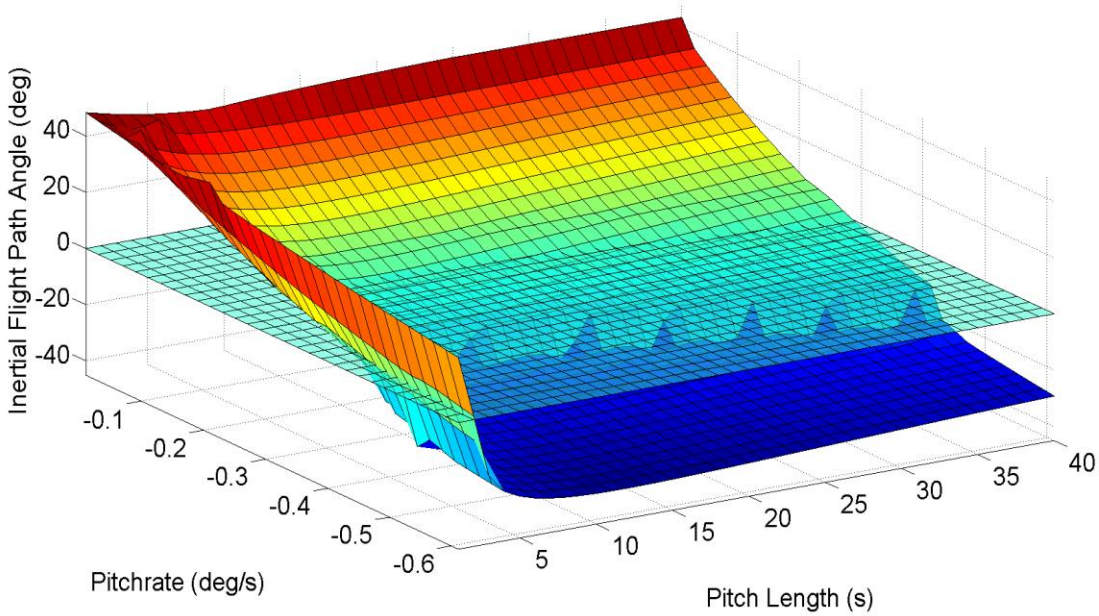

Figure 6.3. Vehicle Burnout Inertial Flight Path Angle. Function of pitch length and pitchrate.

6.1.3 Intersection Curves

Remember that to be in the desired target orbit, a vehicle must satisfy three target conditions at burnout. An intersection on one of the surfaces does not imply that the vehicle has satisfied all three conditions. There must be an intersection on all three of these at the same value for pitchrate and length of pitch. This check is difficult and inaccurate to perform visually, so another code was created to approximate and plot the intersection curves for altitude, inertial velocity, and flight path angle, as in Figure 6.4.

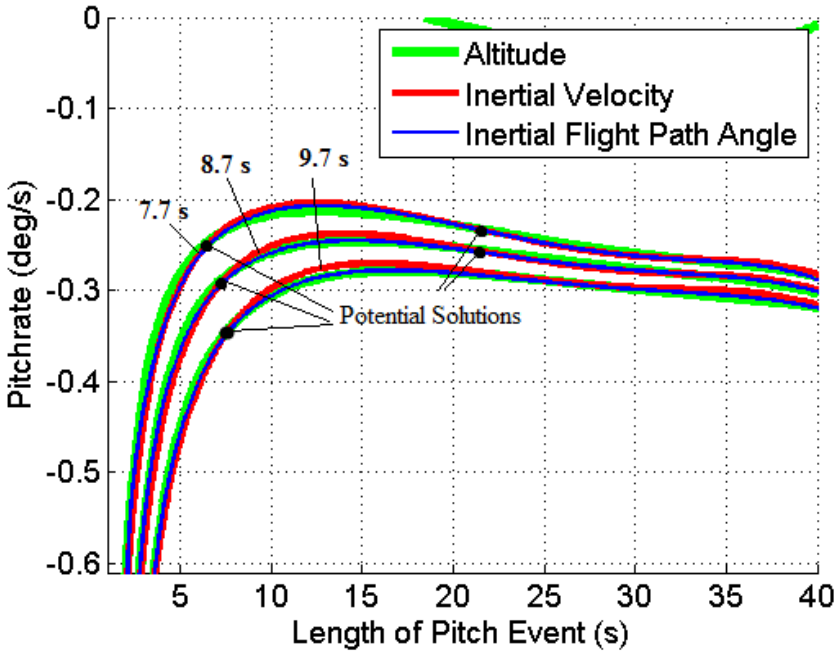

Figure 6.4. Intersection Curve Groups. Start time of 7.7 s, 8.7 s, and 9.7 s.

Each of these groups of curves represents the intersection curves for a specific pitch event start time. Possible solutions are shown at an intersection of all three conditions. The approximation is done by creating a fourth order polynomial that models the surface for each burnout condition. Abnormalities within the data are avoided by localizing the polynomial to the location of the intersection between the plane and surface. Using this step ensures the R^2 value is always above 0.987 and almost always above 0.99. This implies this process is a fair approximation, and is an acceptable indicator as to where solutions might exist. This tool can also be used to estimate the intersections when using stage propellant as the independent variables.

This second code improves the capability of the analysis by allowing the user to see a visual representation of three different independent variables. Each of the intersection curve groups are dependent on a single start time, and groups with a specific start time can be plotted in conjunction with other start time groups. Plotting multiple start time groups is very useful as it shows how the curve shifts when the start time is adjusted. Instead of looking at one solution point on a single curve, multiple groups indicate a region where solutions might exist.

6.1.4 Variable to Optimize

These tools provide the means to determine the location of a potential optimized solution. Before continuing with this discussion, it is important first to clarify what is meant by optimization. There are many properties or variables that can be optimized for a launch vehicle. For example, optimizing aerodynamics might imply minimizing drag or dynamic pressure while optimizing payload might entail maximizing payload based on engine performance or pitch parameters. Another possibility, which is the consideration used in this design analysis, is to optimize the Gross Lift off Weight (GLOW) for a given payload and target orbit. GLOW, which is specified in kilograms, is the mass of the launch vehicle on the launchpad. When considering this variable, it is often the goal in a heavy lift design to minimize this value. GLOW can be considered proportional to cost, and as the lift off mass goes up, so does the cost. As directed by advisors at NASA, it was suggested to consider minimizing this value as the major consideration in optimization to the target conditions. This minimization can also be compared to maximizing the payload mass fraction where mass fraction is the ratio of burnout payload mass to gross lift off mass.

It is also imperative to consider aerodynamic effects on the vehicle. In this analysis, these aerodynamic effects are not necessarily being optimized, but it is essential to ensure dynamic pressure and angle of attack values stay below specified maxima of 800 psf and 6º. Otherwise, a possible failure could occure. These aerodynamic constraints can often be controlled simply by the primary pitch event, but it is important these be checked throughout the analysis.

As GLOW corresponds directly to the stage propellant and inert masses for the vehicle, it is possible to see how THEO can be used to find an optimized case. By varying the independent variables within THEO, it is possible to locate possible regions where a minimized configuration might exist. This search can then be refined utilizing the tools described in the previous sections. These tools, through an iterative process, can provide the means, through surface and plane intersections, to determine the primary pitch properties necessary to minimize the stage propellant masses while achieving required burnout conditions. This process is described in detail in the next chapter in conjunction with an example configuration.

6.2 Rocket Equation Optimization Process

The rocket equation method also seeks to minimize GLOW, but approaches it from a different standpoint. The amount of energy required to reach orbit can be estimated based on known properties of circular velocity and the forces involved with flight to orbit though the atmosphere. The rocket equation reveals the minimum amount of propellant necessary to reach these specified energy requirements.

6.2.1 Mathematical Approach

There are two methods to analyzing the vehicle based on propellant requirements. The first is a mathematical approach that uses a form of a derivative of the rocket equation to optimize GLOW. This method is complex and is limited to series stage vehicles (vehicles with no boosters). Parallel staging complicates the analysis mathematically as it is difficult to optimize a propulsion system with multiple systems burning in conjunction. The relative simplicity of the two stage configuration allows for optimization using the Lagrange multiplier.

Inert mass fraction (ϵ_s) for stage s in Eq. (6.1) is defined as the ratio of the structural inert mass (m_i) to the total mass (m_t) for that stage. Payload ratio (π_s) is the ratio of payload mass (m_{s+1}) of the sth stage to initial mass (m_s) of that stage as shown in Eq. (6.2). The initial mass of the stage (m_s) is defined as the mass of the vehicle after a separation from stage $s-1$, or in the case of stage 1, equal to GLOW. Payload mass for stage s is equal to the initial mass of stage $s+1$. Equation 6.3 is the overall payload ratio (π_b) which is the burnout payload (m_b) divided by the lift off mass (m_1). Overall payload ratio is determined with the product of N payload ratios from N stages (Weisel, 1997).

$$\epsilon_s = \frac{m_i}{m_t} \tag{6.1}$$

$$\pi_s = \frac{m_{s+1}}{m_s} \tag{6.2}$$

$$\pi_b = \frac{m_b}{m_1} = \prod_{s=1}^{N} \pi_1 \, \pi_2 \ldots \pi_N = \prod_{s=1}^{N} \pi_s \tag{6.3}$$

Using Eq. (6.1) and (6.2), the rocket equation outlined and discussed in Chapter 4 can be rearranged to be a function of mass ratios as in Eq. (6.4). The equation represents the summation of velocity contribution (ΔV) from each of the different stages. Remember the total ΔV, or V_b, is the summation of the contribution from each stage. Equation 6.4 indicates each stage is only a function of payload ratio, inert mass fraction, and exhaust velocity for that specific stage.

$$V_b = -\sum_{s=1}^{N} V_{es} \ln(\epsilon_s + (1 - \epsilon_s)\pi_s) \tag{6.4}$$

Minimizing GLOW (m_1) for a vehicle is the goal of the optimization. This term is not present in Eq. (6.4), but is present within the denominator of the term π_b. Maximizing the payload ratio π_b will minimize the GLOW of a vehicle. Equation 6.3 is maximized with the constraint of Eq. (6.4). Since the equation for V_b has a natural log it is helpful to perform the optimization by translating π_b into a natural log as well. This is valid because natural log is an increasing function and maximizing π_b is equivalent to maximizing $ln(\pi_b)$ (Weisel 213). Equation 6.5 is Eq. (6.3) rewritten in natural log form.

$$\ln \pi_b = \sum_{s=1}^{N} \ln \pi_s \tag{6.5}$$

The best way to handle this optimization is to use a method developed by Joseph Lagrange. Solving the constraint equation (Eq. (6.4)) for zero, multiplying by the Lagrange multiplier λ, and then adding to the quantity to optimize produces Eq. (6.6). This equation is valid as the insertion of the constraint is merely the insertion of a complicated way for writing zero. Considering π_s as independent, the partial derivative is shown in Eq. (6.7).

$$\ln \pi_b = \sum_{s=1}^{N} \left(\ln \pi_s + \lambda \left[\frac{\mathrm{V_b}}{\mathrm{N}} + \mathrm{V_{es}}(\epsilon_\mathrm{s} + (1-\epsilon_\mathrm{s})\pi_\mathrm{s}) \right] \right) \tag{6.6}$$

$$\frac{\partial \ln \pi_b}{\partial \pi_s} = \frac{1}{\pi_s} + \frac{\lambda \mathrm{V_{es}}(1-\epsilon_\mathrm{s})}{\epsilon_s + (1-\epsilon_s)\pi_s} = 0 \tag{6.7}$$

This equation represents the partial derivative for N stages, and the simple way to solve this equation would be to solve for π_s if the payload ratios were independent from each other. Unfortunately, not all payload ratios are independent from each other, but this can be remedied by utilizing λ. Choosing λ so the dependent payload ratio is zero allows for the remaining equations to be set equal to zero. Since the rest of the variables are independent, each of the equations can be treated individually, which reveals the maximized payload ratio to be Eq. (6.8). Equation 6.8 for optimized payload ratio still has the unknown variable λ. Inserting Eq. (6.8) into Eq. (6.4) provides the nonlinear relation, Eq. (6.9).

$$\pi_s = \frac{-\epsilon_s}{(1-\epsilon_s)(1+\lambda V_{es})} \tag{6.8}$$

$$V_b = -\sum_{s=1}^{N} V_{es} \ln(\epsilon_s - \frac{\epsilon_s}{1+\lambda \mathrm{V_{es}}}) \tag{6.9}$$

Assuming a two stage vehicle, it becomes Eq. (6.10), a relation with only one unknown, λ. All other variables are specified for each configuration. Unfortunately, to the author's knowledge, this equation cannot be solved explicitly. Using an iterative process or a solver in Matlab, λ can be determined numerically for specific exhaust vehicle properties. This can be adjusted to a three stage vehicle by include an additional term.

$$V_b = -\left[V_{e1} \ln\left(\epsilon_1 - \frac{\epsilon_1}{1+\lambda V_{e1}} \right) + V_{e2} \ln\left(\epsilon_2 - \frac{\epsilon_2}{1+\lambda V_{e2}} \right) \right] \tag{6.10}$$

Once λ is determined, the optimized payload ratios can be determined for each stage using Eq. (6.8). The payload ratios then reveal how much propellant is necessary for the minimized case. Determining λ can be troublesome sometimes, but once it has been determined, it provides very useful values as to the propellant mass for minimized GLOW.

6.2.2 Velocity Budget Analysis Approach

The third optimization method is termed the velocity budget analysis. It is similar to the Lagrange multiplier mathematical approach, but is capable of analyzing more data and presenting it in a more intuitive fashion. Velocity budget analysis is similar in that it also determines how much energy in terms of propellant mass is necessary to bring the vehicle to target orbital conditions. Remember from Chapter 4 the velocity budget describes the amount of energy required in terms of ΔV to reach orbital velocity while overcoming drag, gravitational, and steering losses. If the total ΔV is known for a certain configuration, it is possible to back-track and determine how much propellant is necessary for the specified budget. This is possible using Eq. 6.11, which shows how propellant mass can be determined based on specific impulse (I_{sp}), payload mass at burnout (m_b), inert mass ratio (ϵ), and ΔV (Humble, Henry, & Larson, 1995).

$$m_{prop} = \frac{m_b\left[e^{\left(\frac{\Delta V}{I_{sp}*g_0}\right)}-1\right](1-\epsilon)}{1-\epsilon*e^{\left(\frac{\Delta V}{I_{sp}*g_0}\right)}} \tag{6.11}$$

Equation 6.11 is derived from a combination of the rocket equation, the inert mass fraction, and the propellant mass fraction. It describes the propellant mass required for a one stage vehicle or for one stage within a multiple stage vehicle. Total propellant for a multiple stage vehicle is estimated by calculating m_{prop} for each stage and summing them together. Estimation of the propellant for each stage requires the ΔV contribution and vehicle properties be known for each of the stages. One method to approaching this is to make an initial guess for each stage, perform the calculation, revaluate the initial guess, and iterate the process to minimize the lift off mass. It is simpler to make use of a method that uses a graphical approach.

Consider a 2 stage vehicle with a total ΔV of 10300 m/s. This value is from the example in Table 4.1, and provides an acceptable starting point. Instead of trying to guess how the minimized vehicle might split up the velocity budget, it is advantageous to consider every possible combination. This is done by viewing ΔV in terms of a fraction (f_i) as in Eq. (6.12). In other words, a f_i fraction of the ΔV fulfillment lies with stage i and a (1-f_i) fraction corresponds to stage $i+1$. Effectively, this forces one of the stage's ΔV to be a function of the other. A vehicle with f_1 = 1would correspond to a single stage vehicle.

$$\Delta V_i = \Delta V_{total} * f_i \tag{6.12}$$

Table 6.1. Sample Vehicle.

	I_{sp}	ϵ	f	m_b
	s	-	-	kg
Stage 1	300	0.06	0.4	-
Stage 2	448	0.08	0.6	60000

Consider the vehicle with the parameters defined in Table 6.1. This table shows the specific impulse (I_{sp}), inert mass fraction (ϵ), velocity budget fraction (f), and the payload mass (m_b). It has a stage 1 fraction (f_1) of 0.4, indicating that 40% of the velocity budget is from stage 1. This implies the remaining 60 % comes from stage 2. When sizing a vehicle, it is necessary to start with the uppermost stage as the payload is already known. Using Eq. (6.11), the required stage 2 propellant mass is 252,438 kg with an inert mass of 21,951 kg. The summation of the stage 2 masses as well with the burnout payload becomes the payload for stage 1. Evaluation of stage 1 shows the required propellant mass is 1,268,977 kg with an inert mass of 80,999 kg. The total mass is 1,684,365 kg.

Evaluating this particular case reveals no information as to whether or not it is the minimum GLOW for this configuration. Instead the minimum is determined by varying f_1 from 0 to 1. Plotting GLOW versus the ΔV fraction for stage 1 in Figure 6.5 reveals that a minimum of 1,567,213 kg exists at f_1 of 0.28 and f_2 of 0.72. This presents the question, is this configuration the minimized final solution? Not necessarily, because there are physical limitations that can be difficult to overcome. Since a goal of this project is to use preexisting engines, it is important to ensure thrust to weight ratios are sufficient at lift off. If the vehicle is too light, acceleration and maximum dynamic pressure will be high, and if the vehicle is too heavy, it will never reach altitude. It is also important to consider thrust to weight ratios in the second stage for higher values of f_2. Stage 2 engines are often much less powerful than first stage engines, and if the second stage propellant too heavy, the vehicle will fall back to Earth. Considerations such as these are checked by running the minimum configurations in THEO. Evaluations within THEO reveal these complications and provide indications as to how the propellant masses and/or engines can be adjusted to make the configuration physically plausible. THEO also provides a more accurate total ΔV requirement which is then iterated back into Eq. (6.11).

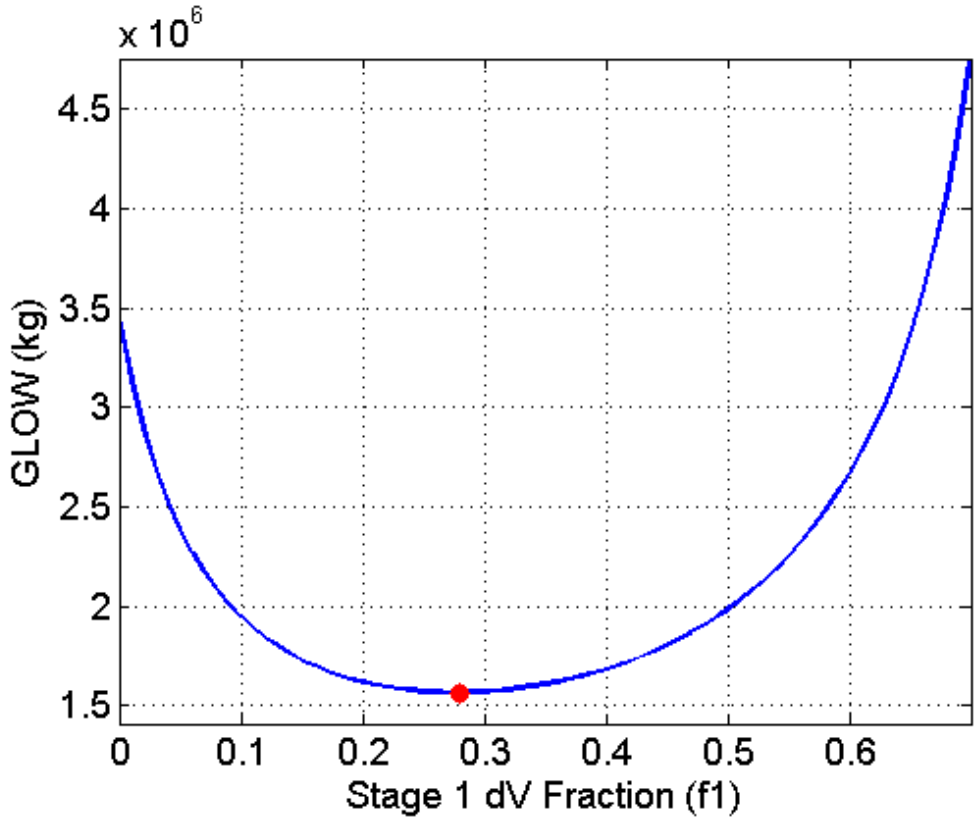

Figure 6.5. GLOW versus Stage 1 ΔV fraction.

This plot is very useful because it not only describes where a minimum exists, but also how stable the configuration is. Stability here is defined as the capability of the vehicle to maintain low GLOW with variations in f_i. For example, in between f_1 of 0.1 and 0.5, a change in stage 1 ΔV does not have a substantial effect on GLOW. Beyond these limits, the curve is very steep, indicating an almost exponential growth in the lift off mass. Even though a configuration with f_1 equal to 0.65 is theoretically capable of bringing the payload to orbit, GLOW has to be doubled to approximately 3300000 kg. This enormous requirement will consequentially increase the cost of the vehicle.

When performing the reevaluation of physical impracticalities using THEO, it is important to go back and check the position of the new vehicle on the GLOW vs f_i plot. If the physically plausible vehicle lies in a relatively stable position, then it can be considered a possible solution for the configuration.

It should be noted this method can also be applied to a 2.5 stage vehicle. It is complicated, but can be simplified with a few assumptions. The first step is instead to consider it a three stage vehicle by breaking down the first stage into sections. This combination burn is redefined as the booster and the first stage while they burn together and labeled stage A in Figure 6.6. It is mathematically difficult to determine the individual ΔV of two different stages burning at the same time, so this trick simplifies the analysis. Specific impulse (I_{spavg}) for the entire new 1st stage is averaged using the mass flow rates ($\dot{m}$) and exhaust velocity (V_{ei}) for each system as in Eq. (6.13). Using this engine property in Eq. (6.11) reveals how much propellant ($m_{booster+core}$) is necessary for the ΔV of this new 1st stage. The inert mass ratio is also reevaluated by dividing the total inert mass for the booster and core by the total propellant for this new first stage.

$$I_{spavg} g_0 = \bar{V}_{eavg} = \frac{\dot{m}_0 V_{e0} + \dot{m}_1 V_{e1}}{\dot{m}_0 + \dot{m}_1} \tag{6.13}$$

The mass of the booster propellant (m_{boost}) is already known, so determining the propellant required (m_1) from what used to be called stage 1 is simply a matter of subtracting booster propellant from the total required for ΔV of the combined system. This is shown in Eq. (6.14) and.

$$m_1 = m_{booster+core} - m_{boost} \tag{6.14}$$

Stage B is now defined as the portion of the original stage 1 of the core that has propellant left after the separation of the boosters. It is usually small, but can be large depending on the burn time of the boosters. The final stage becomes stage C, and remains unchanged in terms of engine properties. Figure 6.6 provides an illustration as to the breakdown of a 3 stage assumption.

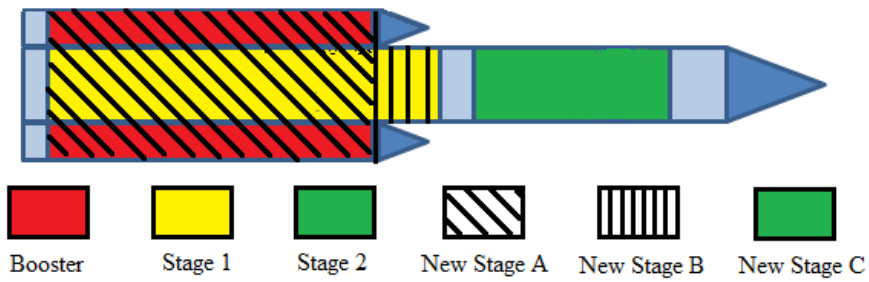

Figure 6.6. Stage Reassignment. Necessary for ΔV estimation of 2.5 stage vehicle.

The process for determining minimized GLOW for the 2.5 stage representation is very similar to the 2 stage vehicle. It requires starting with the final payload and working towards the first stage. The only difference is that there is an additional independent variable that is the result of three ΔV contributions. So, instead of just varying f_1, the minimum case is now revealed by varying f_1 and f_2. Selecting the minimum case is then as simple as viewing the results on a 3D plot with the new stage 1 and 2 mass fractions as the independent variables. It should also be noted that this velocity budget method does not consider the dynamic pressure and angle of attack constraints. The user must be sure to check these constraints during the analysis to be sure that the specified limits are not surpassed.

6.3 Optimization Methods Comparison

This chapter has discussed methods and tools for optimizing launch vehicles to orbit. The first optimization method utilizes THEO by searching through a number of simulated trajectories for a minimized case. The results are then refined and confirmed using intersection groups developed from 3D surfaces. This method has substantial capability but is very time consuming, and as such, is only used on the 130 mt payload requirement configurations. As will be discussed later, it is important that the lower payload requirement configurations are variants of the heavier payload configurations. With this objective, the velocity budget method is utilized to determine if the original configuration can be modified to other payloads. The velocity budget curve helps the user by providing an initial region as to where a solution might exist. These methods are described in more detail in the results section as it helpful to see the process explained in conjunction with an example. The mathematical method is validated, but has limited capability in that it can only evaluate the absolute minimum propellant requirements. This is a hindrance because the minimum configuration often is physically impractical. As a result, the method is not used as an optimization technique.

Chapter 6 References

Humble, R. W., Henry, G. N., & Larson, W. J. (1995). *Space Propulsion Analysis and Design.* (R. W. Humble, Ed.) New York: The McGraw-Hill Companies, Inc.

NASA. (1970). Program to Optimize Simulated Trajectories.

Weisel, W. E. (1997). *Spaceflight Dynamics* (2nd Edition ed.). Boston, MA: Irwin/McGraw-Hill.

Chapter 7

Launch Vehicle Analysis and Results

Chapter 7

Launch Vehicle Analysis and Results

There are seven heavy lift launch configurations in this analysis, and this chapter details the procedure for optimization as well as the results for each case. The optimization is not as simple as searching through cases to determine which best satisfy the target burnout conditions. It requires a process that is very purposeful. The next few sections will explain further and present the optimized results for each configuration.

7.1 Configuration Types

The seven different configurations are described in Table 7.1. These configurations are selected because they have unique properties with a range of different boosters and stage configurations. They can be broken up into three different categories. One of the categories is a 2 stage arrangement. This type has two different propulsion systems which are stacked one on top of the other. The first stage is usually designed to perform efficiently for lift off and low altitude propulsion where the second stage is usually designed to bring the vehicle to orbital velocity. There is a sub group within this category called a 2 stage booster. This type employs the use of a prefabricated booster such as the Reusable Solid Rocket five segment Motor (RSRM V) as the first stage of the vehicle. NASA has put a lot of research into designing solid rocket boosters, and the analysis of these boosters as a first stage is definitely of interest. The next category is 2.5 stage vehicles. These vehicles are very similar to 2 stage vehicles except that there are a number of boosters strapped on that burn parallel to the first stage of the vehicle. The boosters generally separate before 1st stage cutoff which is where the ½ label comes from. The third type is a 1.5 stage configuration. This is very similar to a 2.5 stage except that there is no 2nd stage and the 1st stage fires for the entire launch. The Space Shuttle is an example of this type of vehicle. Illustrations of these vehicle types are shown in Figure 7.1.

A payload to orbit of 130 mt, 100 mt, and 60 mt is considered for each of these configurations. Each configuration is initially optimized to the maximum payload. If successful, each case is then optimized to the smaller payload requirements. Not all of them will be capable of handling the different payload requirements. This analysis reveals the difference between those which are suited towards bringing the maximum payload to orbit, those that have an all around capability, and those that are not suited at all for heavy lift launch. The inert mass estimation in Table 7.1 is only for the first stage and is based on a Saturn V comparison. Inert mass representation here is very simple and is later refined for to provide a more detailed model.

Table 7.1. Initial Configurations.

		Stage 1 Engines		Inert Mass	Stage 2 Engines		Booster Stage	
Configuration	Class	Type	Number	*kg*	Type	Number	Motor	Number
A	2.5 Stage	F-1	2	125000	SSME	2	RSRM	2
B	2.5 Stage	F-1A	3	125000	SSME	3	RSRM V	2
C	2.5 Stage	F-1A	3	125000	J-2X	5	M550 FW3	3
D	2.5 Stage	F-1A	3	125000	SSME	3	P80	7
E	2 Stage	F-1A	5	125000	J-2X	5	-	-
F	2 Stage Booster	RSRM	3	20000	SSME	4	-	-
G	1.5 Stage	SSME	5	125000	-	-	RSRM V	2

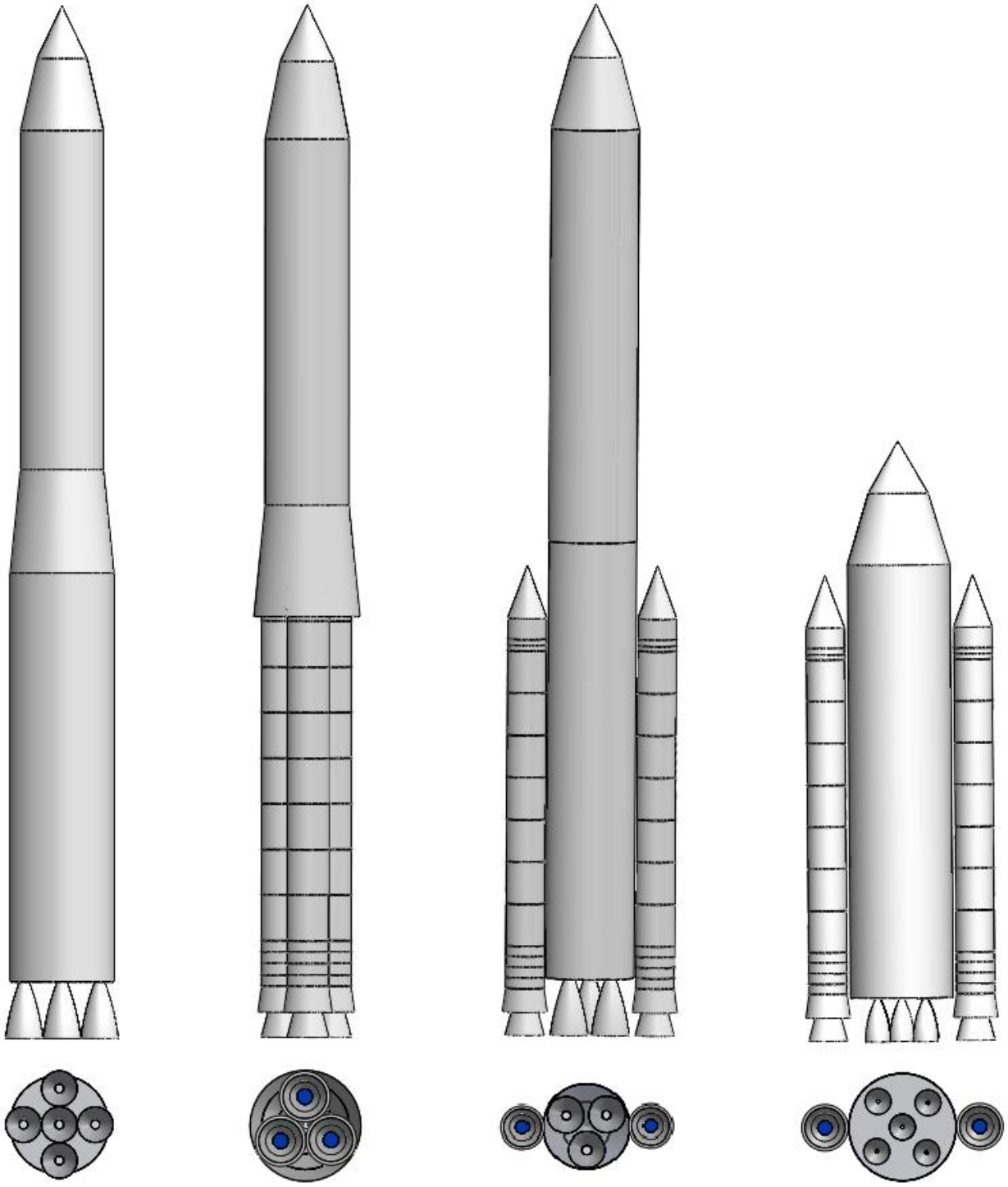

(a) **(b)** **(c)** **(d)**

Figure 7.1a-d. Sample Vehicle Configurations. The illustrations here show a side view and bottom view for the 2 stage (a), 2 stage booster (b), 2.5 stage (c), and 1.5 stage (d) sample vehicles described in the previous section.

7.2 2.5 Stage RSRM Vehicle

Consider configuration A from Table 7.1 with a 130 mt payload. It uses the RSRM for the booster stage, the F-1 for the stage one engines, and the SSME for the stage two engines. The first step is to perform a general analysis to reveal preliminary information as to where potential solutions might exist. It answers the initial question: is it even possible for this configuration to come close to the target burnout conditions? This initial analysis is done by varying the independent variables as specified in Table 7.2. The maximums and minimums in this table are based on the limitations discussed in Chapter 5. Notice some of the intervals are higher than the suggested intervals in Chapter 5. If the intervals are too precise for this broad analysis, disk space and computation time approach unreasonable values. The server location is capable of storing the results for approximately 250,000 different trajectories. Table 7.2 consists of approximately 200,000 different cases, and requires four hours to complete the simulation. Anything much more becomes impractical because of computation time. The intervals are later refined to match the guidelines specified in Chapter 5.

Table 7.2. Independent Variable Specifications.

	Primary Pitch Event			Propellant Mass	
	Start Time	Length	Pitchrate	Stage 1	Stage 2
	s	*s*	*deg/s*	*kg*	*kg*
Minimum	7.2	1	-0.1	1100000	500000
Maximum	14.2	21	-0.65	1600000	900000
Interval	1	2	-0.05	50000	50000

As mentioned earlier, burnout conditions for a launch vehicle are described with the three conditions of altitude, inertial velocity, and inertial flight path angle. It is necessary to satisfy all three conditions for a successful orbit. The target orbit for this launch is a 400 km circular orbit which requires an orbital velocity of approximately 7670 m/s and an inertial flight path angle of 0º. Any variation from this velocity and flight path angle represents a different orbit. A successful configuration has at least the velocity satisfied within ± 40 m/s, the flight path angle within ± 0.5 deg, and altitude within ± 2000 m of the desired burnout altitude.

The first general analysis for this vehicle reveals it is incapable of reaching the desired burnout conditions. The thrust to weight ratio for the vehicle is insufficient resulting in a vehicle that cannot reach required orbital altitude, velocity, and flight path angle. A series of upgrades are made to the vehicle to give it the capability of reaching orbit. The adjustments consist of modifying the 2 F-1 engines to 3 F-1A engines, and the 2 SSME engines to 3 SSME engines.

7.2.1 2.5 Stage RSRM Aerodynamic Coefficients

Figures 7.2 and 7.3 represent the aerodynamic data for the vehicles associated with 2.5 stage RSRM configuration. The lift coefficient profile in Figure 7.2 is only used for the 130 mt configuration and is NASA tabulated data as explained in Chapter 3. The 100 mt and 60 mt payload configurations are assumed to have zero lift as a result of the verification in Chapter 3 that lift has a negligible effect on the results of a trajectory. The drag coefficient profile for the different payload configurations is shown in Figure 7.3. The 130 mt payload configuration uses a higher drag coefficient due to the attached boosters. The size of the 100 mt and 60 mt payload configurations is expected to be similar, and as a result, the drag coefficient profiles are assumed to be the same.

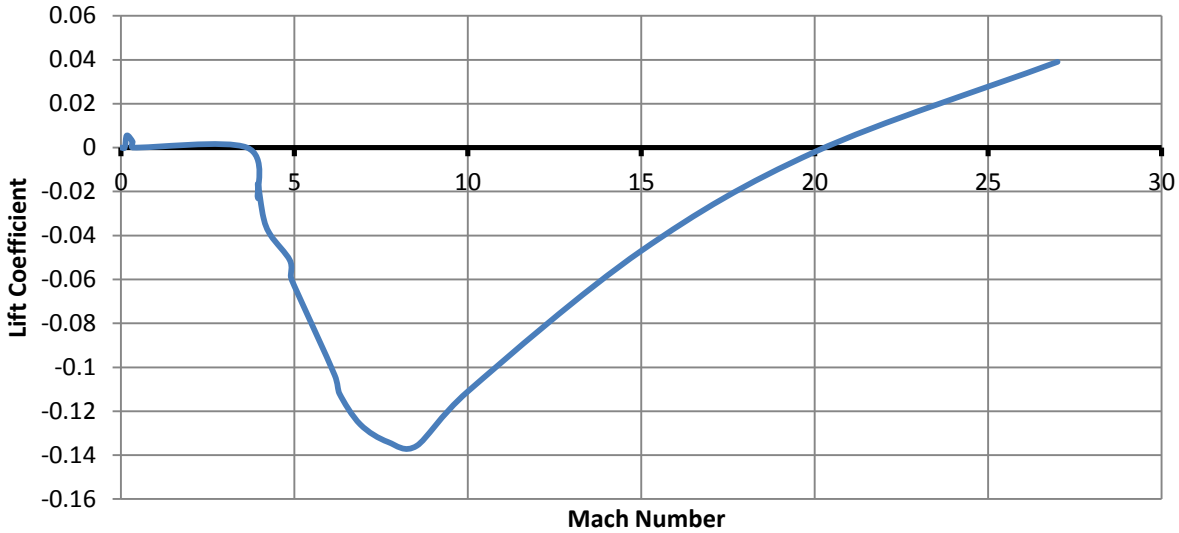

Figure 7.2. RSRM Configuration Lift Coefficient Profile

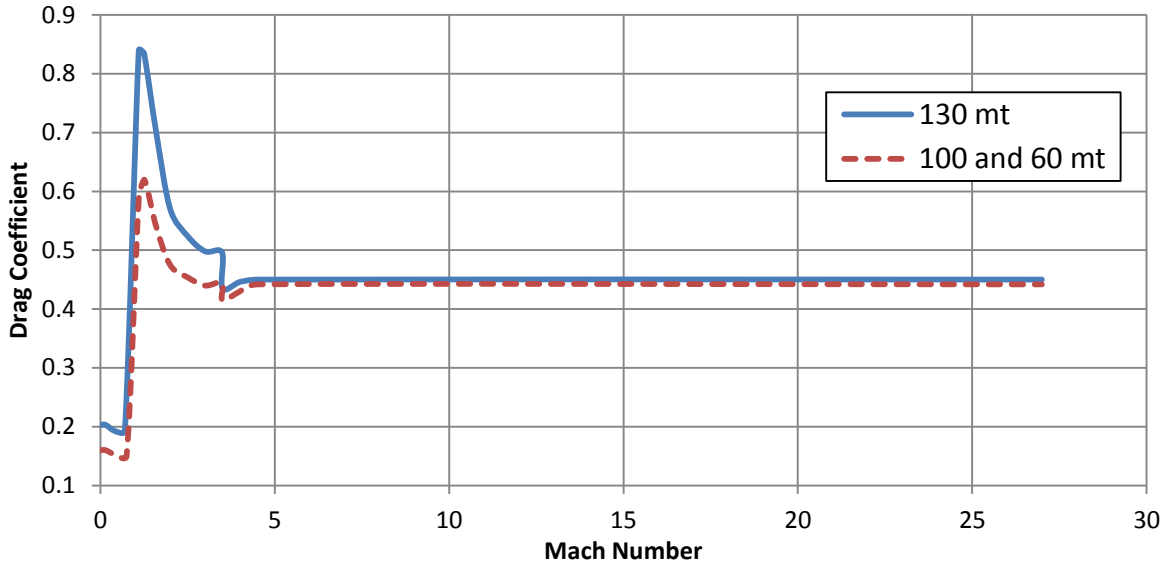

Figure 7.3. RSRM Configuration Drag Coefficient Profile

7.2.2 Inert Mass Correction

An assumption had been made earlier within THEO that needs to be adjusted for the further evaluation of configurations. As shown in Table 7.1, the only inert mass specified is for stage one, and is a value based on a comparison with the Saturn V. This is insufficient as there should be justification for inert mass allocation as well as stage two inert mass consideration. This is adjusted by adding a structural inert mass fraction ratio from a reference (Humble, Henry, & Larson, 1995). The selections for these fractions are based on trend data that puts the mass fraction for stage one at approximately 0.06 and the mass fraction for stage 2 at 0.08. Inert mass fraction (ϵ_s) for stage s in Eq. (7.1) is defined as the ratio of the structural inert mass (m_i) to the sum of the inert mass and propellant

mass (m_p) for that stage. This can be rearranged to determine the inert structural mass for each stage as in Eq. (7.2). These mass fractions provide THEO with the capability to evaluate the inert mass based on the changing variables of the stage propellants. The total dry mass of the vehicle is considered to be the sum of structural inert masses.

$$\epsilon_s = \frac{m_i}{m_t} = \frac{m_i}{m_p + m_i} \tag{7.1}$$

$$m_i = \frac{\epsilon_i m_p}{1 - m_p} \tag{7.2}$$

Table 7.3. Inert Mass Adjustment Comparison.

	Saturn V	Inert Mass Fraction		
	m_i	Propellant	f_i	m_i
	kg	kg	-	kg
Stage 1	125000	1500000	0.06	95745
Stage 2	-	600000	0.08	52174
Total	125000	2100000	-	147919

Table 7.3 shows the revised inert mass assumption increases the total dry weight of the vehicle from 125 mt to 148 mt. This is an issue as the regions that were determined to contain potential solutions are no longer sufficient. Mass that could have potentially been devoted to propellant is now present in the form of structural and engine components. This revision shifts the solutions in such a way that more propellant is required to achieve orbit.

7.2.3 2.5 Stage RSRM General Analysis

A new analysis with inert mass revision and the engine upgrades mentioned earlier produces initial configurations that reach orbit. Table 7.4 shows the top configurations that best satisfy the burnout conditions. In these tables GLOW is the sum of the propellant, inert, payload, shroud, and booster masses.

Table 7.4. 2.5 Stage RSRM General Analysis Top Configurations

	Independent Variables						Burnout Conditions			
	Propellant Mass		Primary Pitch Event				Inertial Property			
	Stage 1	Stage 2	Start Time	Length	Pitchrate	GLOW	FPA	Velocity	Altitude	Max Q
Case	kg	kg	s	s	deg/s	kg	deg	m/s	m	psf
1a	900000	700000	7.2	19	-0.7	3039748	-0.02	7443.9	398737	951
2a	1000000	650000	7.2	21	-0.7	3091784	0.73	7600.9	400044	930
3a	1050000	650000	7.2	15	-0.7	3144975	0.64	7607.9	403941	892
4a	1100000	650000	8.2	19	-0.65	3198167	0.22	7669	401797	857
5a	1150000	650000	9.7	21	-0.65	3251358	-0.08	7719.5	402361	823
6a	1150000	700000	7.2	15	-0.45	3305706	-1.51	7625.6	396906	778
7a	1200000	700000	7.7	21	-0.4	3358897	-1.66	7651.4	401009	747
8a	1250000	700000	9.2	7	-0.65	3412089	-1.98	7693.7	399302	719

In terms of burnout conditions, it is obvious that configuration *4a* is the top choice. It fulfills all burnout conditions within the required 0.5%. This choice is not necessarily the optimized case as it has not yet been shown to minimize GLOW. The purpose of these eight cases is to provide a starting point in searching for the optimized case. They indicate a region where it is possible a group of solutions might exist. The next few steps show the method for analyzing these regions and determining if they minimize GLOW.

Cases *1a – 3a* are the three lightest of the cases, but notice the burnout conditions are not at the required specifications. Inertial velocity is outside of the specified bounds for all three cases. An insufficiency in this area can be the result of two things. The first possibility is that the pitch properties do not correspond well with the mass of the vehicle, and a slight adjustment of the three independent pitch parameters or the secondary pitch events can potentially bring the vehicle to within the required 0.5% of the desired burnout conditions. The other is that there is simply not enough energy within the propulsion system to bring the vehicle to orbital requirements. This can be adjusted by increasing the propellant mass as this increases the total energy available within the vehicle.

As minimized GLOW corresponds to a minimized propellant mass the obvious initial search region corresponds to a search near the lightest case. This is an acceptable starting place, but it is also important to consider the indicator of dynamic pressure. Cases *1a – 5a* all exceed the specified constraint of 800 psf. A high dynamic pressure in this case indicates that the thrust to weight ratio in the atmospheric region of flight is too high. One solution to this would be to remove a first stage engine, but as discussed earlier, two first stage engines and two boosters provide insufficient thrust to bring the payload to burnout conditions.

The only other option is to consider cases with slightly more propellant because as mass increases, the thrust to weight ratio and maximum dynamic pressure will decrease. This trend is shown in Table 7.4 as maximum dynamic pressure decreases while GLOW increases for cases *1a – 8a*. Finding the best case is dependent on locating a balance for a vehicle with the lowest possible GLOW and a dynamic pressure that does not surpass specified limits during launch.

Case *5a* is just above the dynamic pressure limit, and case *6a* is just below the limit. This suggests that a minimized case might exist somewhere in between. The first step to searching for the minimized case is to perform a pitch analysis on *5a* to determine if the pitch properties match well with the vehicle. This is completed by varying the pitch properties for the case at a constant propellant mass with pitch bounds as shown in Table 7.5. This particular step indicates whether or not case *5a* is capable of reaching burnout conditions. Using the intersection curve tool from Chapter 6, it is possible to locate a configuration that fulfills burnout conditions. For a case to be successful, all three burnout conditions must intersect at a single point. Figure 7.4 illustrates the curve groups for a pitch start time of 6.7, 8.7, 10.7, and 12.7 s. For a start time of 6.7 s there is a region where the curves intersect and indicate that there is a solution for this configuration. These plots also show that the intersection groups diverge further from each other as the start time increases.

Table 7.5. Pitch Analysis Bounds

	Start Time	**Length**	**Pitchrate**
	s	*s*	*deg/s*
Minimum	6.7	1	-0.01
Maximum	12.7	40	-0.81
Interval	0.5	1	-0.05

Case *6a* is shown in Figure 7.5 and illustrates the results of increasing propellant by 50 mt. The groups have diverged substantially as the propellant has increased, which as stated earlier, can be the result of either insufficient energy in the vehicle or secondary pitch events that do not fit this particular vehicle. Notice that the altitude and inertial velocity curves stay relatively close together in each group. It is the inertial flight path angle curve that diverges away. This serves to indicate that the pitch properties are not the best fit for this particular vehicle. A revision of the fourth secondary pitch rate to -0.149918 deg/s is shown in Figure 7.6. This revision shows that correction of the secondary pitch profile brings the vehicle to curve groups that intersect.

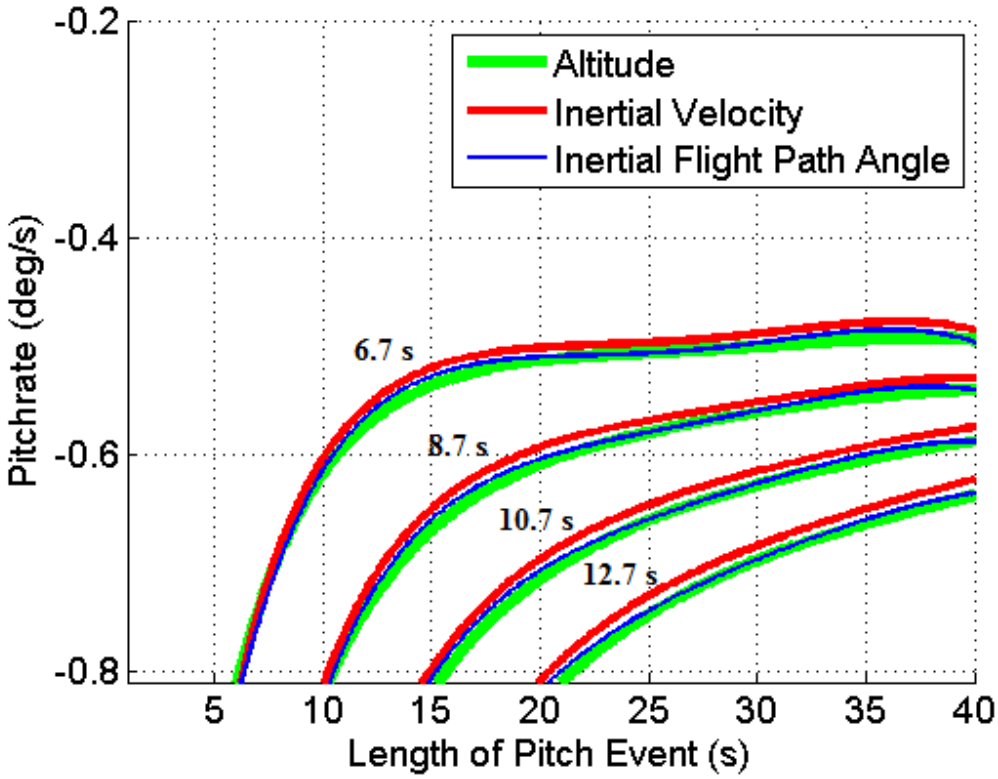

Figure 7.4. Case *5a* Intersection Curves. Burnout curve groups for start time of 6.7-12.7 s.

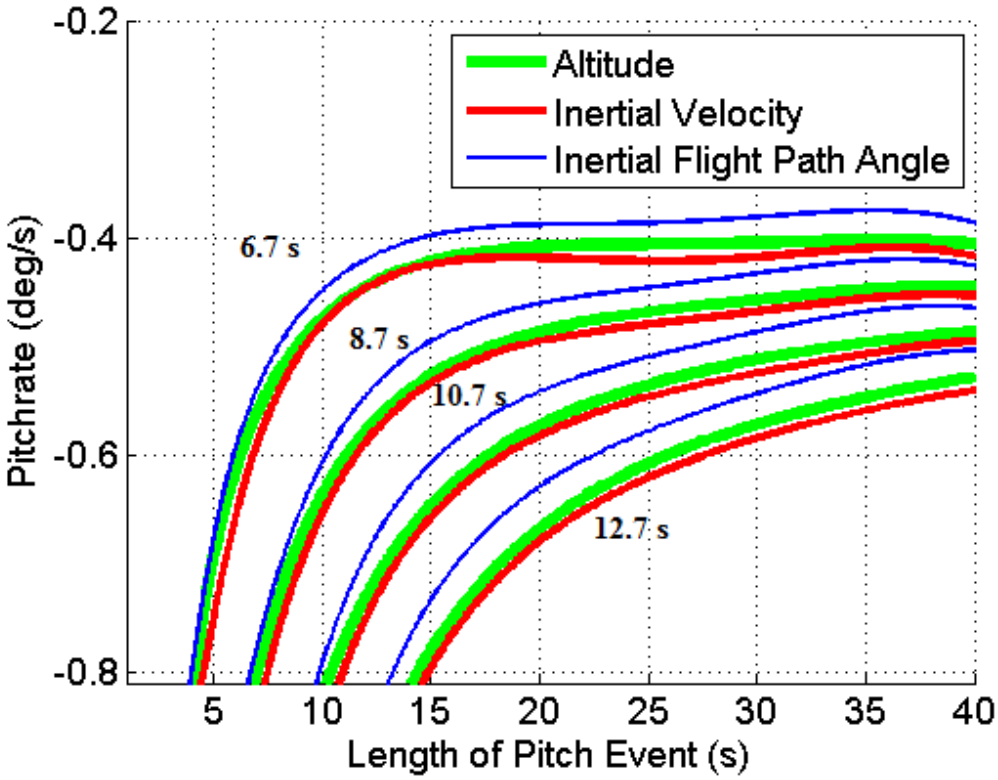

Figure 7.5. Case *6a* Intersection Curve. Burnout curve groups for start time of 6.7-12.7 s.

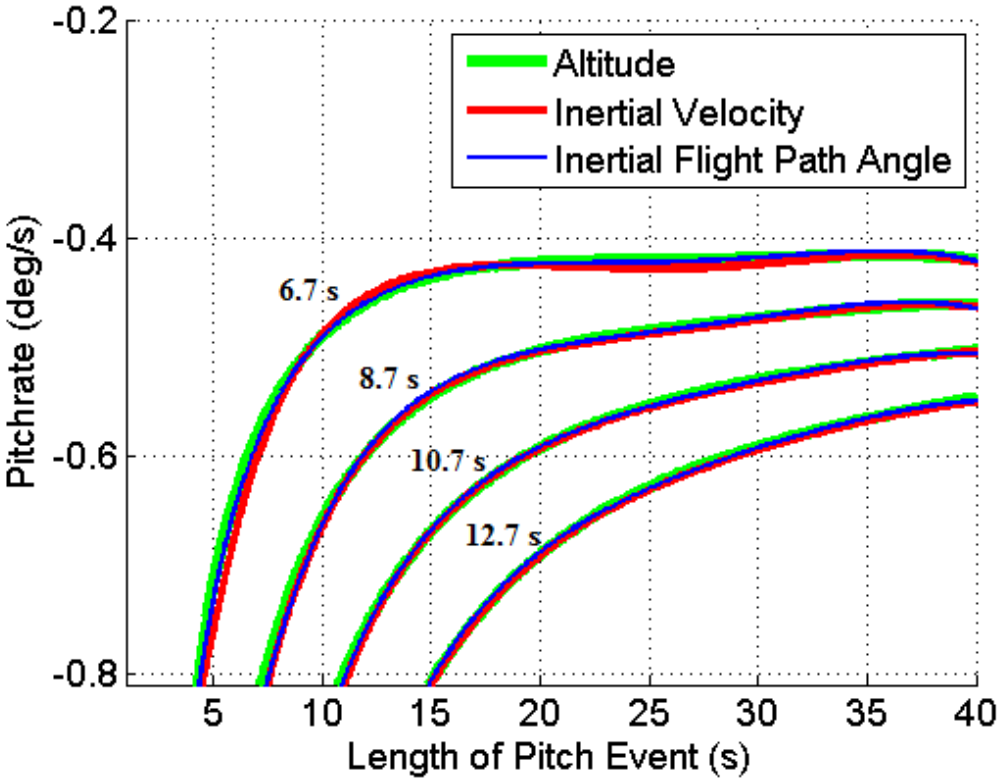

Figure 7.6. Case *6a* Revised Intersection Curves. Adjusted secondary pitchrate.

7.2.4 2.5 Stage RSRM Refined Analysis

The next step in the analysis is to determine if a configuration exists in between case *5a* and *6a* that minimizes GLOW. This is done with THEO by performing a refined analysis of different configurations with propellant masses in between those of case *5a* and *6a*. The top configurations in terms of burnout conditions for this analysis are shown in Table 7.6. Notice that the majority of the cases have a maximum dynamic pressure that is beyond the specified limit, which effectively eliminates them as possible candidates. The highlighted cases are the ones that correspond to an acceptable max dynamic pressure.

None of the cases that are below the minimum for dynamic pressure fulfill the necessary 0.5% for all three target burnout conditions. This implies that a pitch analysis is necessary to determine if the secondary pitch events should be revised. The top three lightest cases are *a4*, *a14*, and *a11*. Case *a11* has a burnout inertial velocity that is closest to the desired conditions, indicating that the energy available in the propellant has the best match in this case. This is an important consideration as it implies that a simple pitch adjustment could bring the vehicle within the desired burnout flight path angle. Case *a11* is also a good case to start with, because unlike *a4* and *a14*, there is some room for the maximum dynamic pressure to increase if the pitch analysis reveals that it is necessary.

The pitch analysis is shown in Figure 7.7, and just like the previous pitch analysis, the inertial flight path angle curve is offset. To remedy this, the fourth secondary pitch event is adjusted to -0.154121 deg/s. Modification of this term shifts the intersection groups to the results shown in Figure 7.8. The curve groups show that this case is capable of reaching the desired burnout conditions at multiple pitch specifications. The new secondary pitch rate is also applied to case *4a* and *a11*, and the results in Table 7.7 illustrate that this correction brings all three cases to desirable burnout conditions. Notice also in this table that the maximum dynamic pressure increases slightly for all three cases, affirming the earlier assumption of using case *a11* instead of *a4* and *a14*.

Table 7.6. 2.5 Stage RSRM GLOW Minimization Cases. Minimized configurations based on Case 4a.

	Independent Variables						Burnout Conditions			
	Propellant Mass		Primary Pitch Event				Inertial Property			
	Stage 1	Stage 2	Start Time	Length	Pitchrate	GLOW	FPA	Velocity	Altitude	Max Q
Case	*kg*	*kg*	*s*	*s*	*deg/s*	*kg*	*deg*	*m/s*	*m*	*psf*
a1	1130000	660000	9.2	26	-0.6	3240951	-0.33	7688.7	399226	826
a2	1130000	670000	10.7	23	-0.7	3251821	-0.68	7678	396518	817
a3	1130000	680000	6.2	28	-0.4	3262690	-0.79	7642	400697	808
a4	1130000	690000	8.7	15	-0.6	3273560	-1.05	7621.9	400046	799
a5	1140000	660000	6.2	17	-0.5	3251589	-0.46	7705.6	397196	821
a6	1140000	670000	6.7	13	-0.5	3262459	-0.57	7673.1	401738	811
a7	1140000	680000	7.2	13	-0.5	3273328	-0.97	7663.9	396934	803
a8	1140000	690000	7.7	12	-0.6	3284198	-1.12	7632.9	399687	793
a9	1150000	660000	6.7	20	-0.5	3262228	-0.3	7694.6	403850	814
a10	1150000	670000	6.7	26	-0.5	3273097	-0.6	7679.4	402523	804
a11	1150000	680000	6.7	20	-0.5	3283967	-0.97	7666.6	398834	796
a12	1150000	690000	6.7	12	-0.47	3294836	-1.2	7642.7	399260	787
a13	1160000	660000	10.2	24	-0.61	3272866	-0.38	7707.7	403368	806
a14	1160000	670000	7.7	17	-0.52	3283735	-0.68	7690.2	401903	798
a15	1160000	680000	6.7	20	-0.44	3294605	-0.98	7673.1	400564	789
a16	1160000	690000	8.2	27	-0.46	3305475	-1.26	7650.9	399270	780

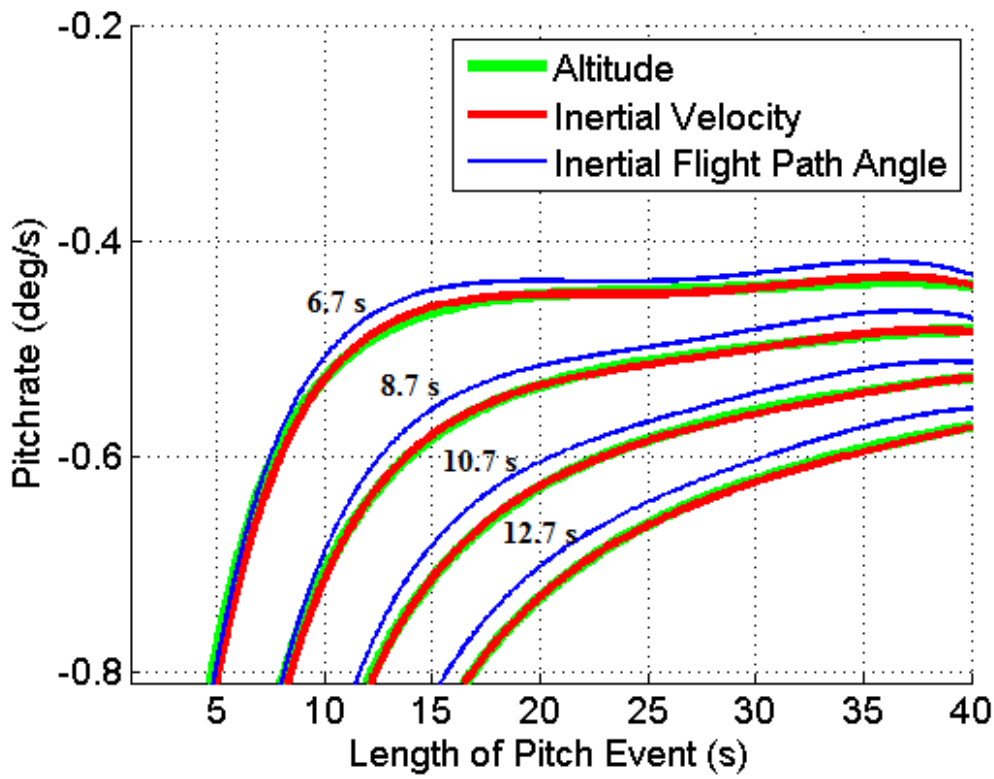

Figure 7.7. Case *a11* Intersection Curves. Burnout curve groups for start time of 6.7-12.7 s.

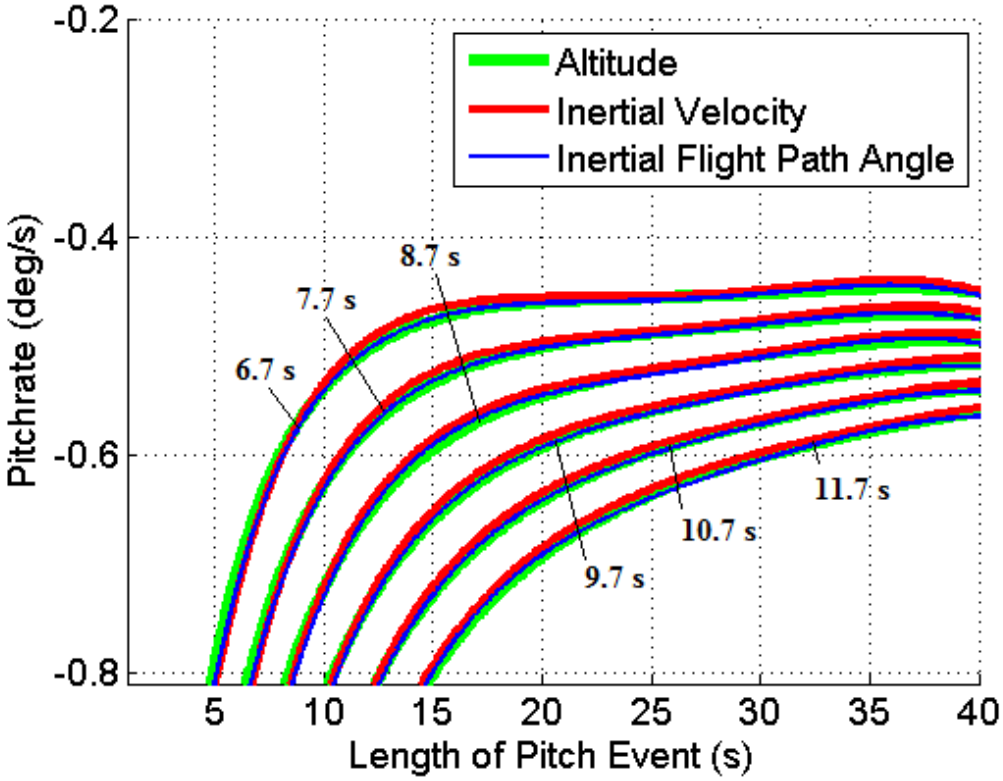

Figure 7.8. Case *a11* Revised Intersection Curve. Adjusted secondary pitchrates.

Table 7.7. Revised 2.5 Stage RSRM GLOW Minimization. With secondary pitchrate revision.

	Independent Variables						Burnout Conditions			
	Propellant Mass		Primary Pitch Event				Inertial Property			
	Stage 1	Stage 2	Start Time	Length	Pitchrate	GLOW	FPA	Velocity	Altitude	Max Q
Case	*kg*	*kg*	*s*	*s*	*deg/s*	*kg*	*deg*	*m/s*	*m*	*psf*
a4	1130000	690000	8.7	15	-0.593	3273560	-0.05	7649.6	400645	801
a11	1150000	680000	6.7	20	-0.459	3283967	0.05	7690.6	400472	798
a14	1160000	670000	7.7	17	-0.532	3283735	0.20	7724.5	399964	801

The final selection for this configuration with minimized GLOW is case *a11*. It has been shown to be optimized in terms of GLOW by performing a series of procedures that ensure the amount of propellant is minimized and that the pitch properties are well suited to the configuration. It has also been shown to fit within the required aerodynamic constraint of 800 psf. Table 7.8 provides a description of the optimized vehicles properties for the 130 mt payload case. The dimensions have been sized based on the volume propellant requirements as well as the room required for the engines and payload. The room necessary for the engines is based on dimensions specific to each engine, and it is also assumed that the payload bay fills the nose cone as well as 10 m into the body of the vehicle.

Table 7.8. 2.5 Stage RSRM Configuration for 130 mt Payload.

	Length	Diameter	Propellant	Inert	Engine	# Engines	Burnout Alt	400000	m
	m	*m*	*kg*	*kg*	*(Shape)*	-	Burnout Vel	7691.3	m/s
Booster	35.05	3.75	1003399	168354	RSRM	2	Burnout FPA	-0.011	*deg*
Stage 1	25.88	8.50	1150000	73407	F-1A	3	Max Q	798.1	*psf*
Stage 2	51.89	8.50	680000	59133	SSME	3	GLOW	3283966	*kg*
Shroud	12.19	8.50	-	19674	Biconic	-	Start Pitch	6.7	*s*
Total	89.96	-	-	-	2.5 Stage	-	Pitch Length	20	*s*
	Secondary Pitch Revision			4th	-0.154582	*deg/s*	Pitchrate	*-0.459*	deg/s

For this configuration to be a potential candidate, it must be shown to be stable in terms of a GLOW versus ΔV analysis. This necessary analysis provides the means to illustrate if a slight change in the ΔV fraction for each stage will require a significant change in GLOW for the vehicle. As described earlier, this is done by plotting GLOW as a function of the ΔV contribution for two different stages of flight in a 2.5 stage vehicle. A ΔV analysis of case *a11* is shown in Figure 7.9.

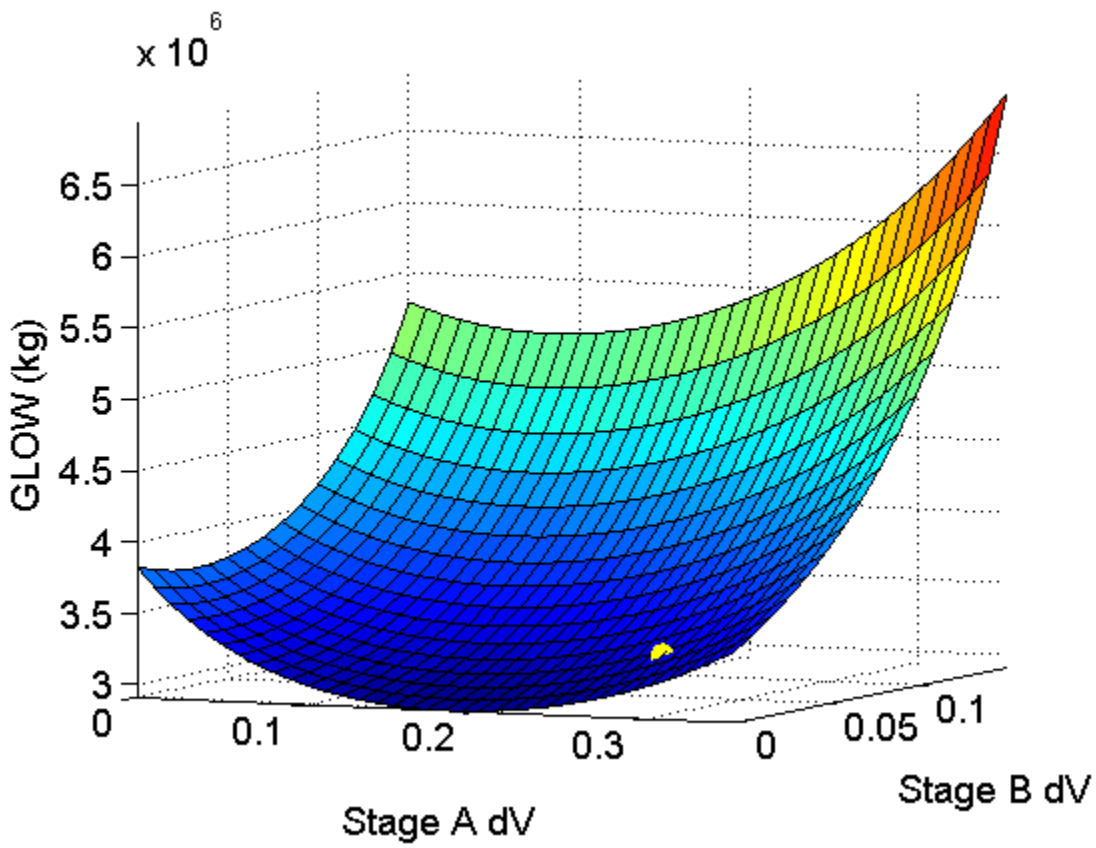

Figure 7.9. 2.5 Stage RSRM Stability Surface for 130 mt Configuration.

This surface shows that the vehicle is somewhat stable in terms of this ΔV property. The location is indicated by the yellow dot in the figure. The axis labeled *Stage A dV* signifies the portion of the launch where the core engines and boosters burn together. *Stage B dV* represents the contribution of the core after the boosters have separated. The position of the dot indicates that a modification of these stage contribution fractions will have a slight but not significant effect on GLOW. Lastly Figure 7.10a-c verifies that this configuration did not surpass any limits for the constraints of angle of attack, dynamic pressure, and angle of attack*dynamic pressure.

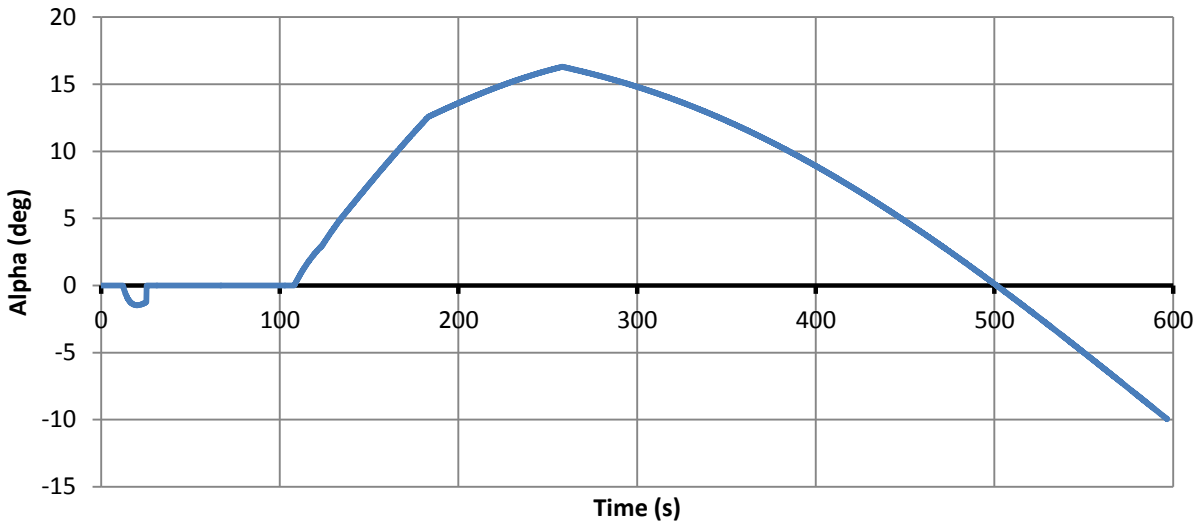

(a)

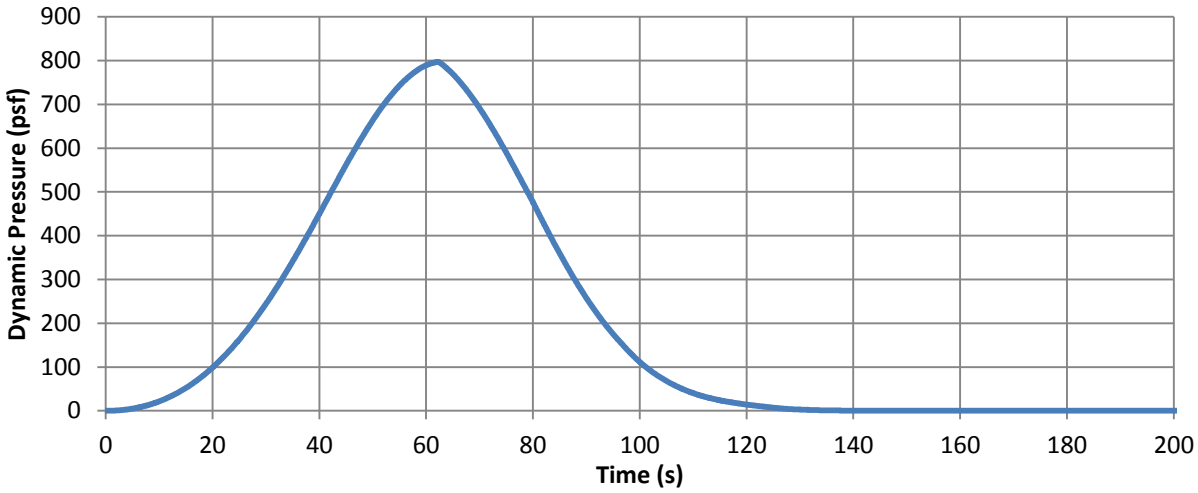

(b)

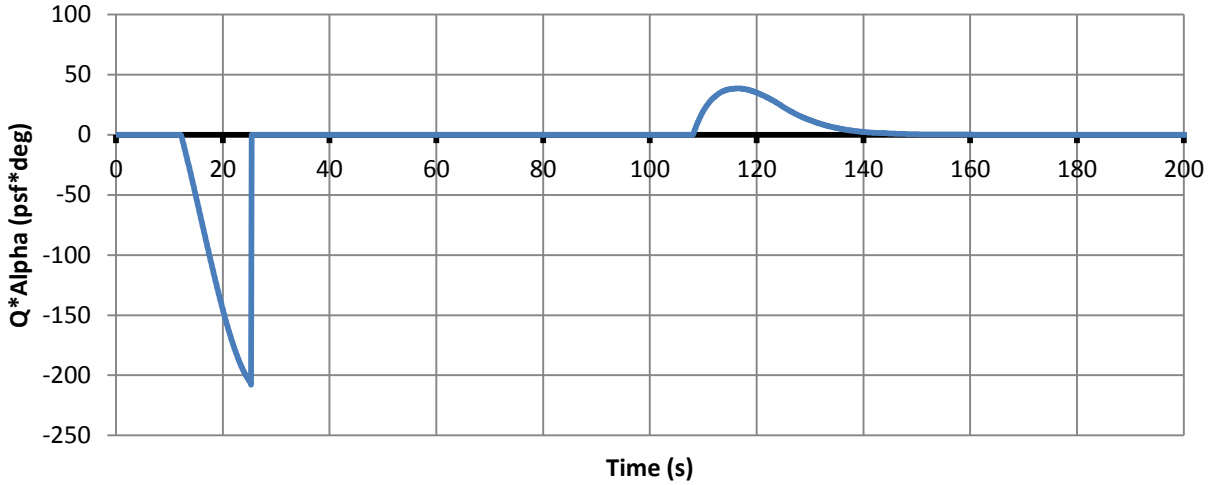

(c)

Figure 7.10a-c. 2.5 Stage RSRM Aerodynamic Limits Check.

7.2.5 100 mt Payload Requirement for 2.5 Stage RSRM

The next step is to determine if this configuration can be modified to fulfill payload requirements of 100 mt and 60 mt. The 130 mt configuration with boosters is very capable as the boosters are well suited to bringing a heavy payload to orbit. This capability is due to the high thrust and large amounts of propellant associated with RSRM boosters. These same qualities can also serve as a hindrance when attempting to scale the higher payload version to that of 100 mt or 60 mt. Considering the size of these particular boosters, it is a safe assumption to state that any configuration with a payload smaller than 130 mt will most likely fly with two or no boosters. As it is impractical to fly with one booster, these are the only two options

The requirement for this analysis is to determine a vehicle with adaptable payload capabilities that has optimized the 130 mt configuration. In other words, can the capabilities of the vehicle be adjusted without making many significant design changes to the original model? This concept is an objective because minimizing changes can decrease cost. For example, if the same size propellant tank for stage one can be used on both the 100 mt and 130 mt configurations, the entire process of design and development is simplified. Engineers only have to design one tank, and parts for two different vehicles can be manufactured together. It is beneficial to employ this concept in the smaller payload configurations instead of attempting to minimize the GLOW. This is done for all 100 mt and 60 configurations.

An analysis for the lower payload requirements is an iterative process that repeats two different steps to search for a solution. The process begins by running a particular configuration in THEO to determine its capability. If it is unsuccessful, then the propellant requirements for the particular payload are evaluated using the velocity budget analysis in Chapter 6 and then run again in THEO. These steps will continue until a capable solution is reached or when the configuration diverges away from the original vehicle.

Minimizing changes in the vehicle can potentially be done by removing the boosters from the vehicle shown in Table 7.8 and determining if the original stage one and two are capable of bringing 100 mt to orbit. The results of this analysis are shown in Table 7.9 and illustrate the steps to determining if simply removing the boosters would bring a smaller payload to orbit. An initial test in THEO of the vehicle in Table 7.8 minus the boosters is unable to fly due to a low thrust to weight ratio. An adjustment is made in case *1aa* by adding one F-1A engine. The adjustment brings the vehicle to the desired altitude and flight path angle, but the velocity component is insufficient. An attempt to remedy this is made in case *2aa* by adding one SSME, but the configuration is still unable to bring the payload to required orbital velocity. This velocity deficiency can also be seen in the columns labeled Required ΔV and Available ΔV.

Table 7.9. 100 mt Derivative of 2.5 Stage RSRM Vehicle.

		Propellant			Engine				ΔV		Inertial Burnout			Max
Case	GLOW	Stage 1	f_1	Stage 2	Stage 1		Stage 2		Req	Avail	Vel.	Alt.	FPA	Q
-	*kg*	*kg*	-	*kg*	*Type*	*#*	*Type*	*#*	*m/s*	*m/s*	*m/s*	*m*	*deg*	*psf*
1aa	2082215	1150000	-	680000	F-1A	4	SSME	3	10042	9680	7302	400782	-0.17	919
2aa	2082215	1150000	-	680000	F-1A	4	SSME	4	9819	9680	7525	399590	0.55	937
3aa	2212747	1150000	-	800000	F-1A	4	SSME	4	10242	9837	7258	400541	-0.50	812
4aa	2082279	1200000	0.259	630000	-	-	-	-	9777	-	-	-	-	-
5aa	2197803	1510000	-	434000	F-1A	4	SSME	3	9485	9662	7839	401032	0.04	909
6aa	2328538	1711983	0.4	356597	-	-	-	-	9777	-	-	-	-	-
7aa	2328544	1711983	-	356597	F-1A	4	SSME	3	9413	9669	7915	399471	3.00	831
8aa	2328544	1711983	-	356597	F-1A	4	SSME	2	9284	9666	8039	400942	0.23	852
9aa	2410892	1823404	0.425	323308	-	-	-	-	9777	-	-	-	-	-
10aa	2410893	1823404	-	323308	F-1A	4	SSME	1	9651	9670	7660	399440	-2.68	775
11aa	2410892	1823404	-	323308	F-1A	4	SSME	1	9783	9668	7527	399769	-0.30	803
12aa	2410893	1823404	-	323308	F-1A	4	J-2X(88.5%)	2	9542	9582	7684	399420	0.38	797

*Shaded rows indicate use of velocity budget analysis to evaluate propellant requirements.

Remember from Chapter 3 that the energy contained within a propellant can be described in terms of the velocity required to overcome hindering effects and reach orbital velocity. The energy available in the propellant is shown here as the energy or ΔV that would be required to bring that particular configuration to orbital conditions. This can serve as an indicator as to why the vehicle's performance is lacking. Also notice the maximum dynamic pressure for both of these cases is above the specified limit.

An attempt is made in case *3aa* to increase the ΔV available by adding propellant to the second stage. No improvements are made by this propellant addition. The addition of a fifth SSME engine to correct this velocity deficiency would be impractical as using that many SSMEs on the second stage is impractical for such an expensive engine. These first three cases show that the original configuration is incapable of bringing the 100 mt payload to orbit. The next step is to determine if the payload can be brought to orbit by performing only slight modifications to the vehicle. Examples of these small modifications might be adjusting the size of the propellant tanks or further changes to the number of engines on each stage.

Dynamic pressure serves as an important indicator at this point. Notice cases *1aa* and 2*aa* have maximum dynamic pressure values above the specified maximum. The thrust to weight ratio is too high which can be reduced by decreasing the number of stage one engines or by increasing the initial GLOW of the vehicle. A decrease in the number of stage 1 engines is impractical as it would also require a decrease in GLOW. According to the minimum GLOW specified in Figure 7.11, there is not room for the necessary decrease in GLOW that would coincide with the removal of an engine. The minimum in this figure specifies the required energy in terms of propellant, and anything less than this would be incapable of reaching orbit. The remaining option decrease the thrust to weight ratio is to increase the propellant. This is done be shifting the vehicle configuration along the curve shown in Figure 7.11. Shifting to the right will increase the contribution of stage 1 to the total ΔV required and will aid in determining if adjustments in the propellant will provide a successful case.

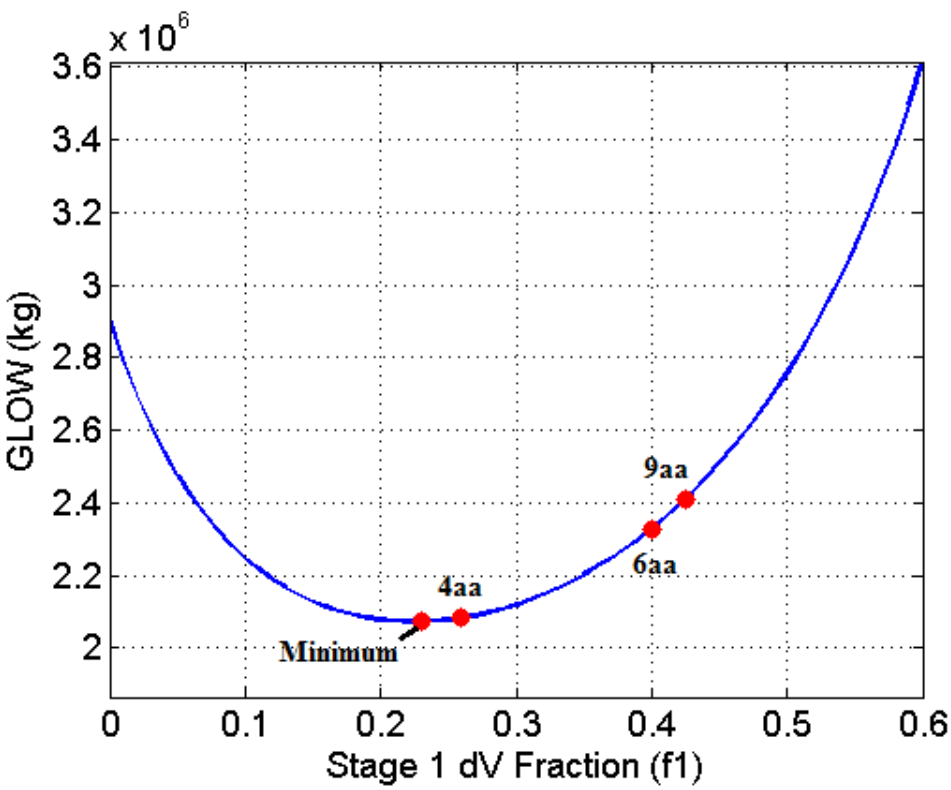

Figure 7.11. 100mt Derivative of 2.5 Stage RSRM GLOW vs. ΔV Curve.

The highlighted rows in Table 7.9 represent the propellant requirements based on the stage 1 ΔV fraction that is specified in the column labeled f_1. Increasing f_1 changes the velocity contribution from each stage which in turn adjusts the amount of propellant and increases GLOW. Case *4aa* represents only a slight shift in f_1, and as result, still has a relatively high maximum dynamic pressure when evaluating the new propellant requirements in THEO, as shown in case *5aa*. The next step brings f_1 to 0.4 with a resultant decrease in dynamic pressure. The burnout velocity of case *7aa* is approximately 250 m/s over the required burnout velocity. A second stage engine is removed in case *8aa*, but the velocity component is still too high. Also notice that the maximum dynamic pressure is still above 800 psf. The next shift moves f_1 to 0.425 and indicates propellant masses as shown in case *9aa*. One second stage engine is removed as the burnout velocity in the previous case surpassed the necessary burnout condition. Case *10aa* is the first that is able to maintain an acceptable dynamic pressure but unfortunately, is not able to bring the vehicle to the necessary zero degree flight path angle. A pitch adjustment is made with the results shown in case *11aa*. Pitch corrections bring the vehicle to the necessary flight path angle, but reduce the burnout velocity. This implies that a successful case exists somewhere in between having one or two SSME engines. This middle ground can be accomplished by exchanging the second stage engine for two J-2X engines running at 88.5% thrust.

This analysis has shown flying the core of 130 mt configuration for 100 mt ton payloads is not a plausible case with the specified engines and propellant masses. The changes necessary to bring the vehicle to orbit are too substantial, and case *12aa* does not resemble the original configuration except for the stage 1 engine type.

7.2.6 60 mt Payload Requirement for 2.5 Stage RSRM Vehicle

An analysis of the 60 mt configuration is shown in Table 7.10. Case *1ab* is an evaluation using the core 130 mt configuration. The results show that this case has excessive energy within the propellant. This is further verified by performing a GLOW versus ΔV analysis as shown in Figure 7.12. Minimum GLOW for the vehicle is approximately 550 mt lower than case *1ab*, which indicates that this case wastes fuel and that the propellant should be decreased. An attempt is then made in case *2ab* to modify the stage 2 propellant without adjusting the stage 1 tank. A ΔV fraction of 0.435 on the curve in Figure 7.12 allows this and reveals the stage 2 propellant amount required. The new propellant amounts are then put into THEO with the results shown in case *3ab*. Inertial velocity is again surpassed as well as the dynamic pressure limit. This indicates the available engines and propellant amounts do not correspond well with each other, and a new search begins with f_1 of 0.22 which is the minimum specified in Figure 7.12. Case *5ab* and *6ab* utilize the minimum GLOW specified in *4ab*, but both are insufficient in terms of reaching burnout velocity. In an attempt to overcome this and the still high dynamic pressure, the configuration shifts with case *7ab* to a f_1 of 0.45. The result of this new propellant amount is evaluated in THEO as case *8ab*, but the velocity is again overshot. This configuration is gradually diverging away from the original core specifications. Consideration of this indicates that the vehicle for a 60 mt payload cannot be produced from components that were used in the 130 mt payload case.

Table 7.10. 60 mt Derivative of 2.5 Stage RSRM Vehicle.

		Propellant			Engine				ΔV		Inertial Burnout			Max
Case	GLOW	Stage 1	f_1	Stage 2	Stage 1		Stage 2		Req	Avail	Vel.	Alt.	FPA	Q
-	*kg*	*kg*	-	*kg*	*Type*	#	*Type*	#	*m/s*	*m/s*	*m/s*	*m*	*deg*	*psf*
1ab	2042214	1150000		680000	F-1A	4	SSME	3	9784	10825	8701	400040	0.27	980
2ab	1510832	1150000	0.435	186530	-	-	-	-	9777	-	-	-	-	-
3ab	1505832	1150000		186530	F-1A	3	SSME	1	9042	9655	8269	400761	-0.01	1155
4ab	1261131	653907	0.220	446946	-	-	-	-	9777	-	-	-	-	-
5ab	1264169	653907		454469	F-1A	2	SSME	3	10349	9647	6954	400514	5.05	617
6ab	1264169	653907		454469	F-1A	3	SSME	2	9941	9665	7390	399508	-0.43	1289
7ab	1549935	1202346	0.450	175873	-	-	-	-	9777	-	-	-	-	-
8ab	1549935	1202346		175873	F-1A	3	SSME	1	9062	9660	8254	399259	-0.03	1115

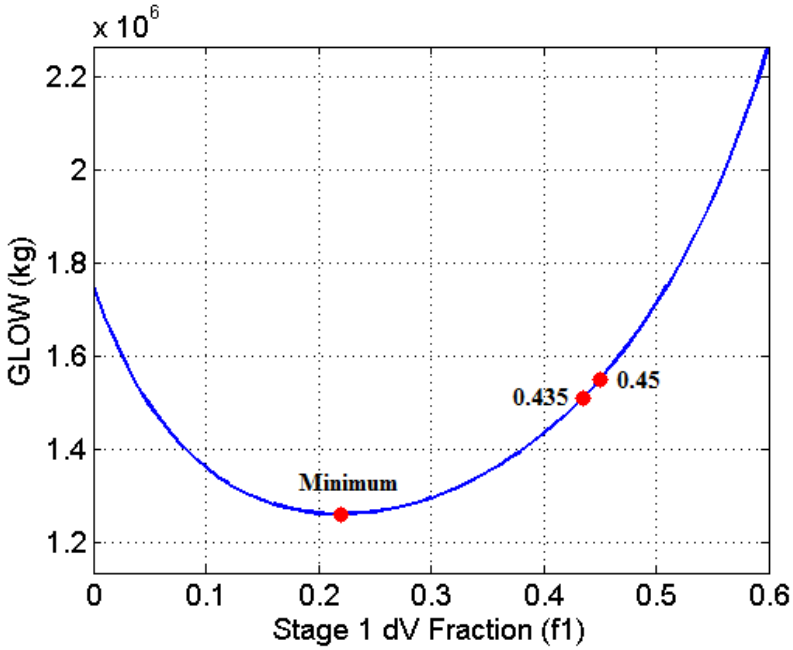

Figure 7.12. 60mt Derivative of 2.5 Stage RSRM GLOW vs. ΔV Curve.

7.3 2.5 Stage RSRM V

The next configuration is very similar to the 2.5 Stage RSRM except the booster stage is replaced by the RSRM V. It has more segments and as a result is designed to produce more thrust than the RSRM for the same burn time. Higher thrust from the boosters implies that less thrust might be necessary in the core engines to bring the vehicle to orbit. As such, it is important to consider the different stage 1 engine configurations.

7.2.1 2.5 Stage RSRM V Vehicle Aerodynamic Coefficients

The aerodynamic profiles for this configuration are shown in Figure 7.13 and 7.14, and the same aerodynamic assumptions are made in this vehicle as were for the previous vehicle.

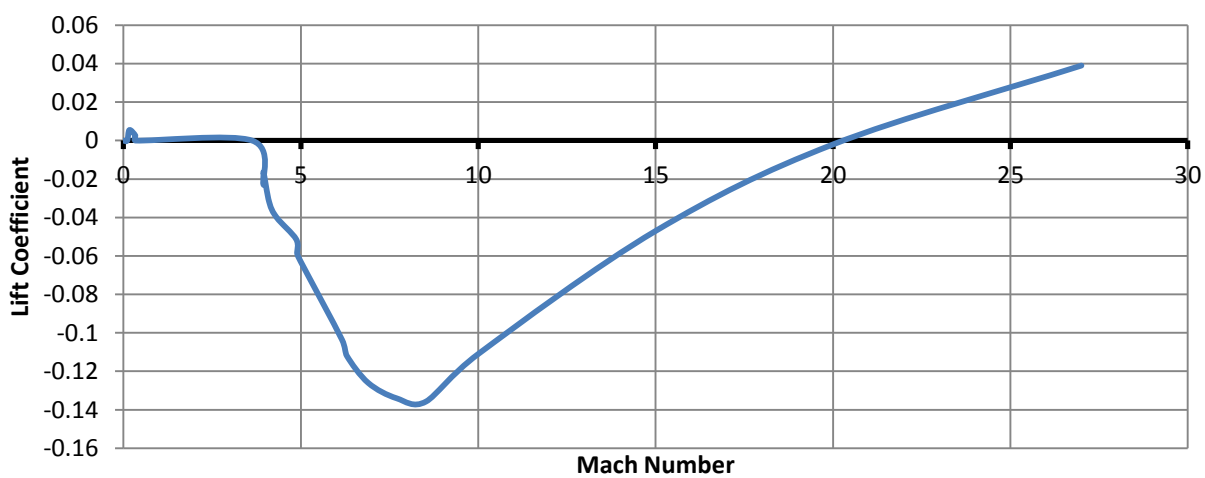

Figure 7.13. RSRM V Configuration Lift Coefficient Profile

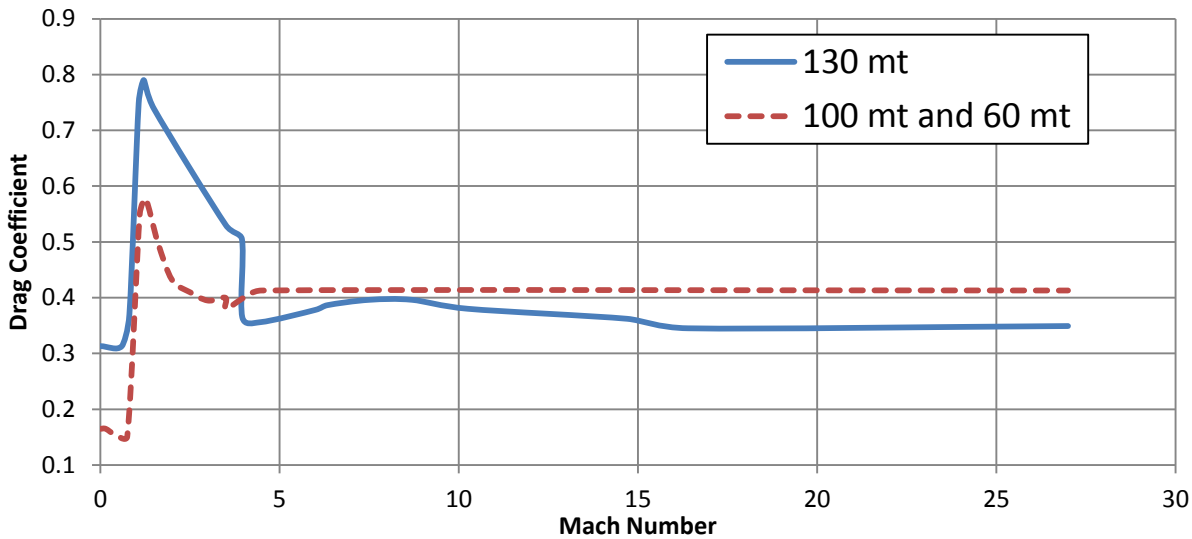

Figure 7.14. RSRM V Configuration Lift Coefficient Profile

7.3.2 2.5 Stage RSRM V General Analysis

A general analysis of the vehicle with two and three first stage engines is shown in Table 7.11. Cases *1b-5b* are the top cases for a vehicle with two F-1A engines, 2 RSRM V boosters, and 3 SSME engines. The first three cases lack in burnout velocity and flight path angle which is a result of insufficient energy contained within the propellant. Case *4b* is a much better match with the required inertial velocity, but the flight path angle is still significantly offset. Flight path angle is brought within the bounds in case *5b* using a pitch adjustment, but unfortunately the inertial velocity is affected. This implies that this configuration is incapable of reaching desired burnout conditions.

Table 7.11. 2.5 Stage RSRM V General Analysis

	Independent Variables						Burnout Conditions			
	Propellant Mass		Primary Pitch Event				Inertial Property			
	Stage 1	Stage 2	Start Time	Length	Pitchrate	GLOW	FPA	Velocity	Altitude	Max Q
Case	*kg*	*kg*	*s*	*s*	*deg/s*	*kg*	*deg*	*m/s*	*m*	*psf*
-	Booster: 2 RSRM V Booster		1st Stage Engine: 2 F-1A				2nd Stage Engine: 3 SSME			
1b	1000000	550000	12.2	17	-0.3	3270099	4.2	7593.5	397663	596
2b	1050000	550000	10.2	19	-0.2	3323290	4	7613.5	398161	577
3b	1100000	550000	13.2	3	-0.7	3376482	3.79	7628.3	398041	559
4b	1200000	500000	7.2	21	-0.1	3428517	4.51	7693.1	403359	548
5b	1200000	500000	7.2	21	-0.0895	3428517	0.289	7582.5	398855	537.3
-	Booster: 2 RSRM V Booster		1st Stage Engine: 3 F-1A				2nd Stage Engine: 3 SSME			
6b	900000	650000	6.2	11	-0.7	3272413	2.35	7741.1	397781	893
7b	900000	700000	8.2	15	-0.65	3326760	1.25	7669.3	400479	843
8b	1000000	700000	7.2	21	-0.45	3433143	0.71	7731.3	398623	787
9b	1000000	750000	14.2	17	-0.7	3487491	-0.32	7623.9	396770	745
10b	1050000	700000	7.2	5	-0.65	3486335	0.66	7739.6	403649	759
11b	1100000	750000	6.2	3	-0.45	3593874	-0.66	7653.9	398475	697
12b	1150000	750000	10.2	7	-0.5	3647066	-0.89	7673.7	396133	676

To compensate for this, an upgrade is made with the addition of a third F-1A engine. The top results for a general analysis of this configuration are shown in cases *6b-12b*. Results show that adding a third engine to the first stage has made the configuration much more capable. All of these cases are substantially closer to fulfilling all required burnout conditions. Notice that cases *6b* and *7b* have a maximum dynamic pressure above the specified limit indicating their ineligibility as a selection for the final configuration. Case *8b* has a maximum dynamic pressure slightly below 800 psf and as a result, indicates that the minimum GLOW configuration exists in between case *7b* and *8b*. Any of the cases following *8b* are quite capable, but notice that GLOW tends to increase substantially with decreasing dynamic pressure. This situation is very similar to the 2.5 stage configuration with RSRM boosters in that the key to locating the optimized vehicle is to determine a balance between a maximum dynamic pressure and a minimized GLOW.

Before continuing with the analysis, notice that the inertial flight path angle for case *7b* and *8b* is slightly outside the specified bounds of ± 0.5º. A pitch analysis should be performed to determine if the remedy for this issue lies in adjusting the secondary pitch properties. A pitch analysis of case *7b* is shown in Figure 7.15. The inertial flight path intersection curve is offset from both the inertial velocity and altitude curves. This suggests that a secondary pitch event adjustment should bring all three intersection curves together. The reevaluation of the intersection curve plot is shown in Figure 7.16 with the fourth secondary pitchrate adjustment to -0.154918 deg/s.

A pitch analysis for case *8b* is illustrated in Figure 7.17. Just as in the previous case, the inertial flight path angle curve is separated from the curve group. This is remedied with the same pitchrate adjustment made in the previous case to -0.154918 deg/s. A re-evaluation of the intersection curves are shown in Figure 7.18 show that the deficiency can be fixed by adjusting the pitch properties. These two cases bound the configurations that exist between them and as a result pitch adjustments made to *7b* and *8b* will also apply to those in between.

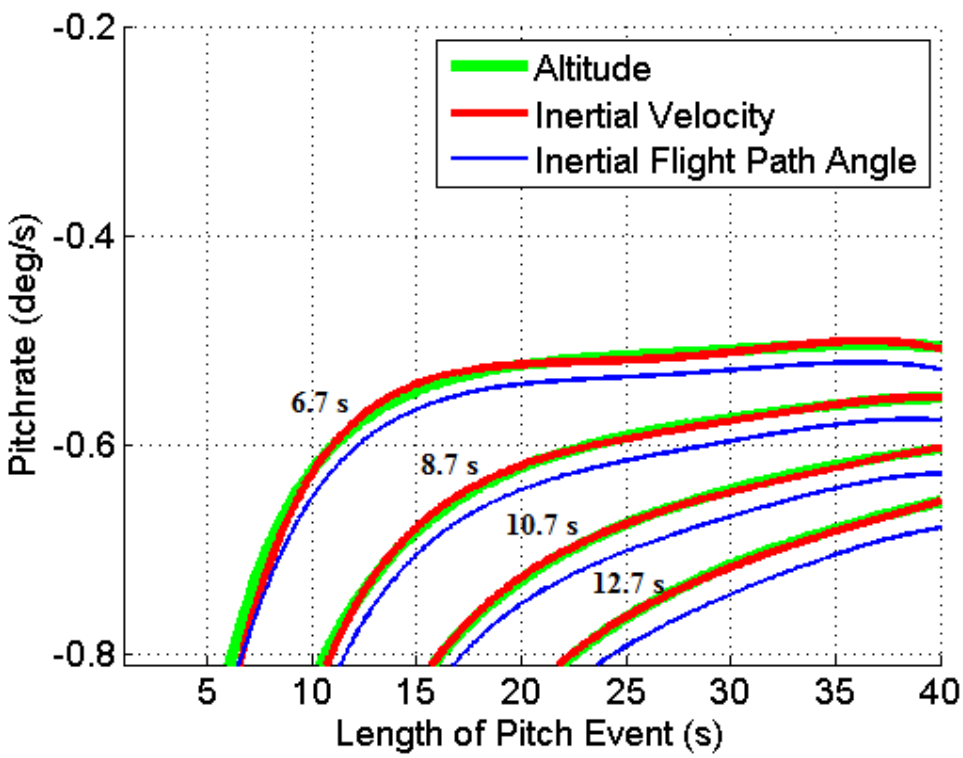

Figure 7.15. Case 7b Intersection Curves. Burnout curve groups for start time of 6.7-12.7 s.

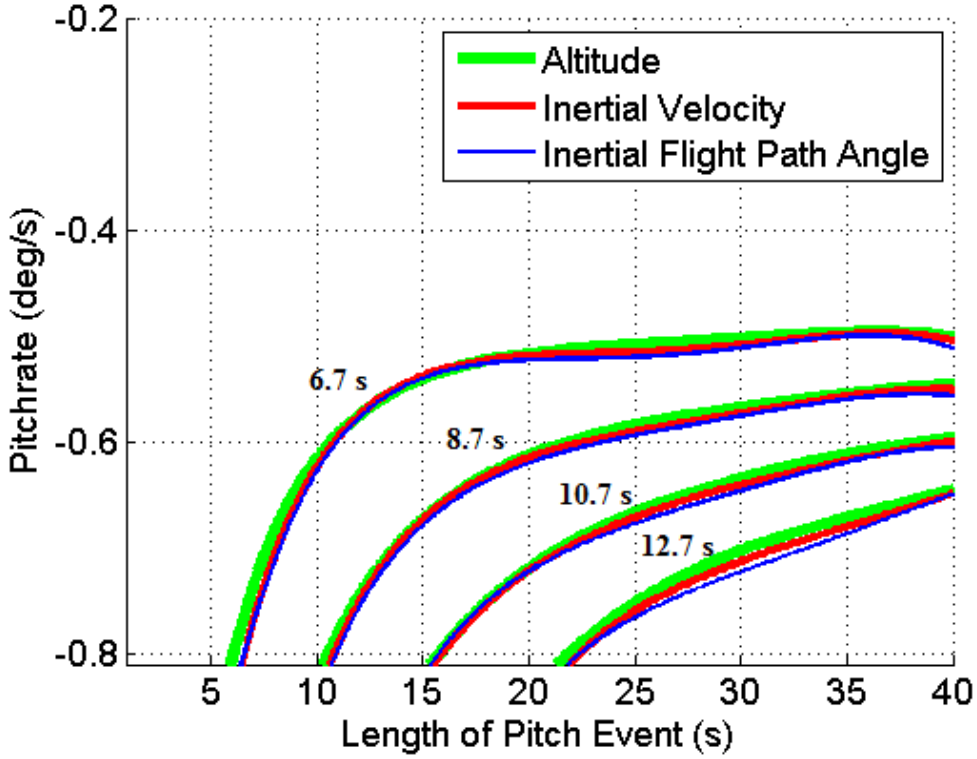

Figure 7.16. Case *7b* Revised Intersection Curves. Adjusted secondary pitchrate.

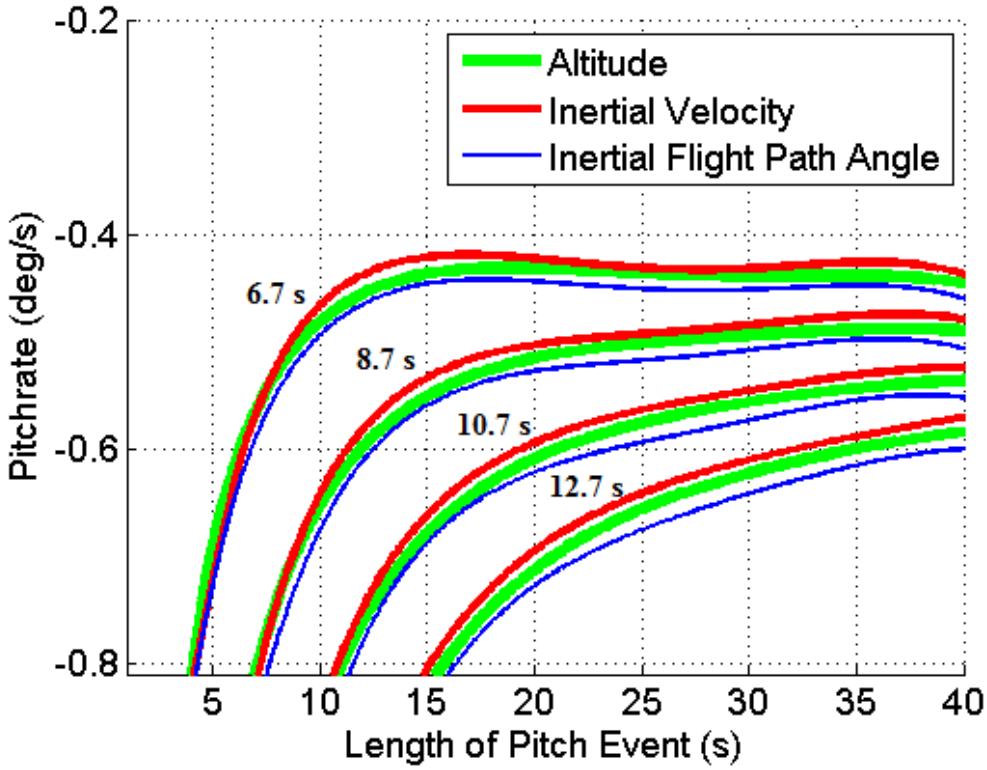

Figure 7.17. Case 8b Intersection Curves. Burnout curve groups for start time of 6.7-12.7 s.

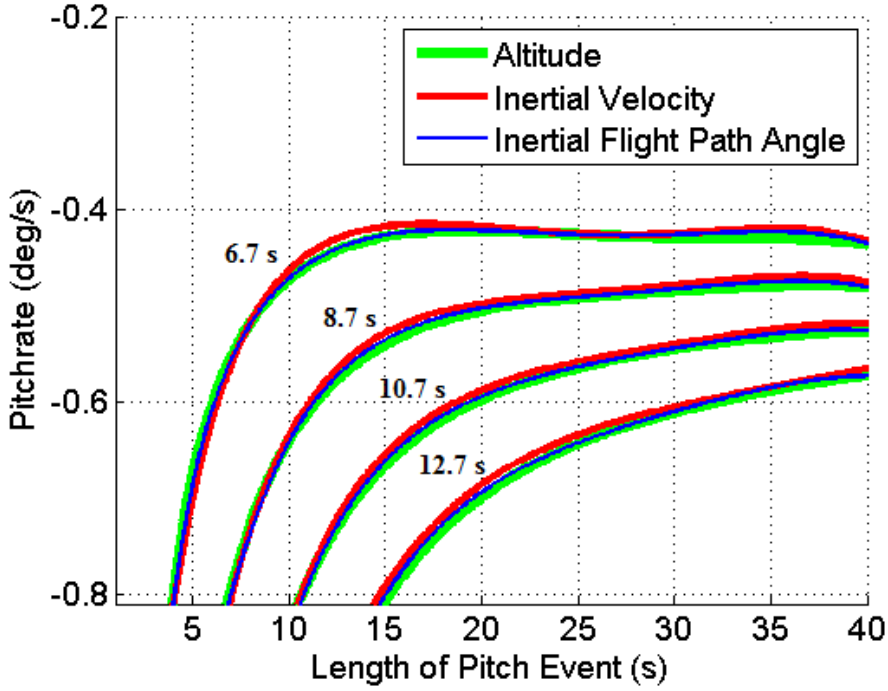

Figure 7.18. Case 8b Revised Intersection Curves. Adjusted secondary pitchrate.

7.3.3 2.5 Stage RSRM V Refined Analysis

To locate the optimized configuration the results of a refined analysis of cases *7b* and *8b* are shown in Table 7.12. The results are a sample of the many derivatives capable of reaching target conditions, but represent those with the lightest GLOW and those closest to the dynamic pressure limit. The large amount of successful cases suggests that this type of configuration is quite capable in achieving orbit, a desirable property when launching variable payloads. The cases are listed in order of increasing GLOW. By a comparison of the GLOW and dynamic pressure columns, it is obvious that case *b5* is the optimized solution for this 2.5 stage vehicle type. This case is the first to achieve a dynamic pressure below the specified limits and because GLOW is inversely proportional to dynamic pressure, it is minimized. The intersection curve analysis in Figure 7.19 verifies the pitch properties of b5.

Table 7.12. 2.5 Stage RSRM V GLOW Minimization Cases. Minimized configurations from 7b and 8b.

	Independent Variables						Burnout Conditions			
	Propellant Mass		Primary Pitch Event				Inertial Property			
	Stage 1	Stage 2	Start Time	Length	Pitchrate	GLOW	FPA	Velocity	Altitude	Max Q
Case	*kg*	*kg*	*s*	*s*	*deg/s*	*kg*	*deg*	*m/s*	*m*	*psf*
b1	960000	700000	6.7	8	-0.6	3390590	0.14	7679.5	402147	806
b2	950000	710000	6.7	11	-0.5	3390821	-0.24	7671.9	396030	804
b3	980000	690000	6.7	15	-0.475	3400997	0.12	7723.5	397241	804
b4	970000	700000	6.2	12	-0.45	3401228	0.09	7683.9	402222	800
b5	960000	710000	7.2	8	-0.6	3401460	-0.22	7670	398304	798
b6	950000	720000	6.2	10	-0.45	3401691	-0.35	7640.8	399719	794
b7	980000	700000	6.2	7	-0.525	3411867	-0.04	7696	399781	795
b8	970000	710000	7.2	9	-0.55	3412098	-0.22	7670	399801	792
b9	960000	720000	6.7	17	-0.425	3412329	-0.41	7646.2	399521	789
b10	990000	700000	6.2	6	-0.55	3422505	-0.03	7695.7	401325	789

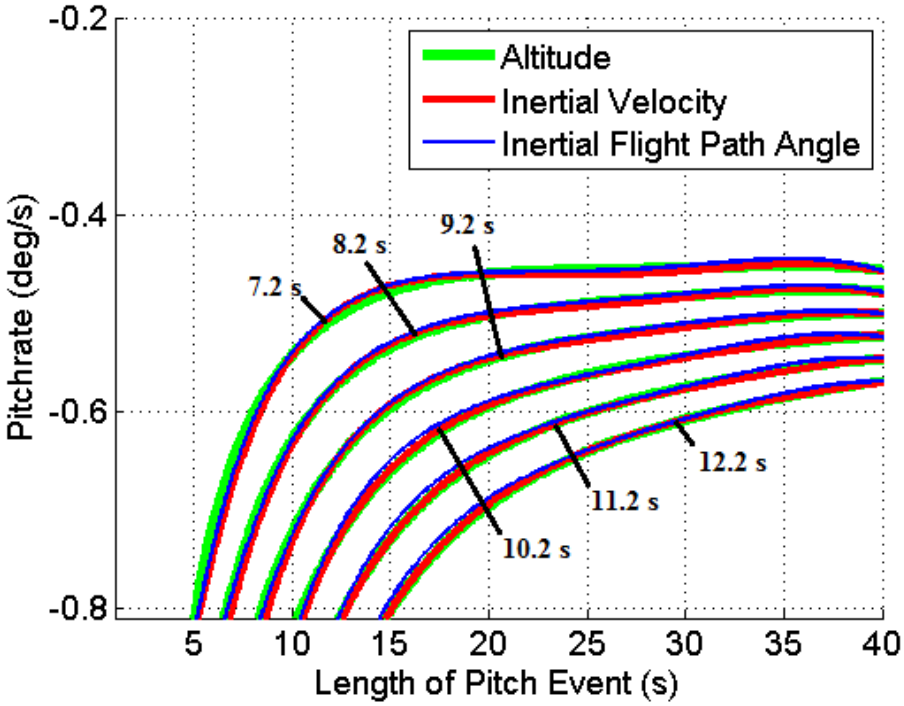

Figure 7.19. Case b5 Intersection Curves. Burnout curve groups for start time of 7.2-12.2 s.

A check is then performed on the radius of the vehicle to determine if the vehicle can be further optimized. This check reveals that to better accomdate the propellant volume, the radius of the first and second stage can be reduced from 4.25 m to 4.1 m. Any smaller and the decrease in drag as a function of cross sectional area forces the vehicle to slightly surpass the maximum dynamic pressure limit. Also, the burnout altitude is slightly off but can be corrected by performing a slight adjustment to the 4th secondary pitch event. This event governs the final altitude of the vehicle and an adjustment from -0.154918 deg/s to -0.155749 deg/s corrects it to 400 km. The final configuration with the corrected radius and secondary pitchrate is shown in Table 7.13.

Table 7.13. 2.5 Stage RSRM V Configuration for 130 mt Payload.

	Length	Diameter	Propellant	Inert	Engine	# Engines	Burnout Alt	400000	m
	m	*m*	*kg*	*kg*	*(Shape)*	-	Burnout Vel	7666.9	m/s
Booster	43.19	3.75	1253457	204116	RSRM V	2	Burnout FPA	-0.253	*deg*
Stage 1	24.80	8.20	960000	61279	F-1A	3	Max Q	799.6	*psf*
Stage 2	58.50	8.20	710000	61742	SSME	3	GLOW	3401459	*kg*
Shroud	12.19	8.20	-	19674	Biconic	-	Start Pitch	7.2	*s*
Total	95.49	-	-	-	2.5 Stage	-	Pitch Length	8	*s*
	Secondary Pitch Revision			4th	-0.155749	*deg/s*	Pitchrate	*-0.600*	deg/s

It is also important to show the GLOW stability in terms of the ΔV contribution from the different propulsion stages. A plot of this relation is shown in Figure 7.20. This vehicle is unique in that the stage 1 propellant is completely burned before the RSRM V booster separation. The boosters continue to burn after the 960 mt of propellant for the F-1A engines is exhausted, implying that the boosters also burn in conjunction with the SSME engines. *Stage A dV* in Figure 7.20 corresponds to the F-1A and Booster burn, and *Stage B dV* coincides with the burn of the Boosters and the SSME engines.

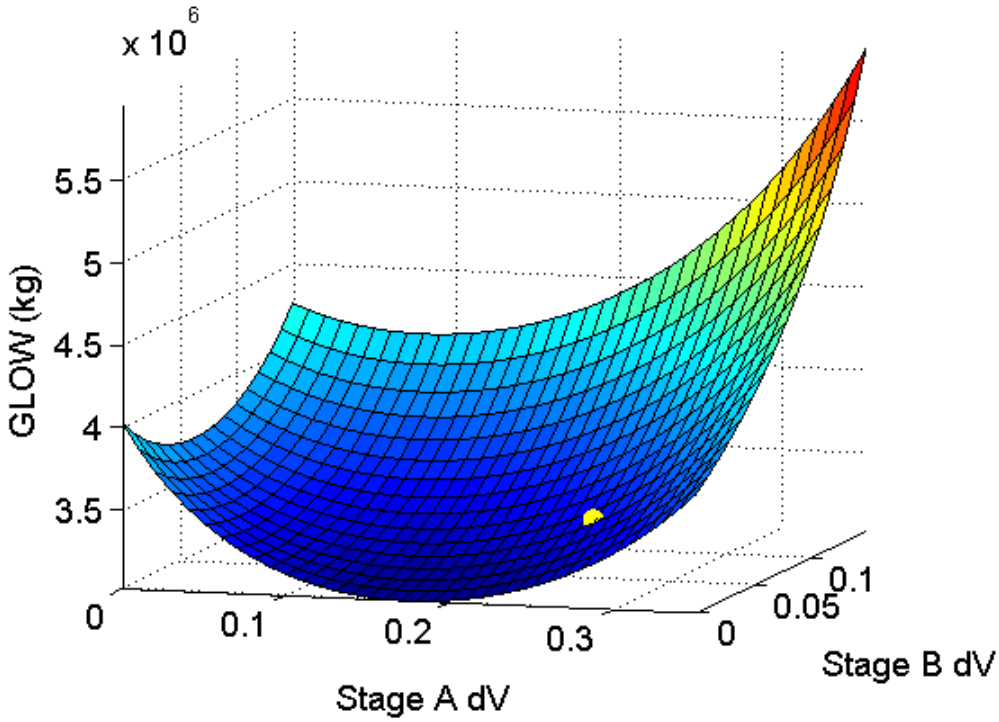

Figure 7.20. 2.5 Stage RSRM V Stability Surface for 130 mt Configuration.

It is important to consider the possible impracticalities of this situation. The majority of 2.5 stage vehicles go through three steps in the propulsion system. The first step consists of the boosters and first stage engines burning together. Step two also includes the first stage engines but considers them only after the boosters have separated from the vehicle. Lastly, the third step consists of the second stage engines firing until the propellant is exhausted. As stated earlier, the 2.5 stage vehicle described in Table 7.13 is slightly different than this description because the RSRM V boosters separate after the stage 1 propellant is exhausted. This complicates the design as it is necessary to allow the boosters to burn in coincidence with the first and second stage. There are ways to modify the vehicle so that this capability can be met, but that will not be discussed here. It is instead important to recognize that an attempt to minimize GLOW for this vehicle increases the complexity of the vehicle as a result of the booster coincident burn. Consideration of this increased complexity should be taken into account when deciding the final top configurations from Table 7.1. Lastly, Figures 7.21a-c illustrate that the aerodynamic constraints of angle of attack, dynamic pressure, and angle of attack*dynamic pressure were not surpassed in the trajectory.

7.3.4 100 mt Payload Requirement for 2.5 Stage RSRM V Vehicle

Remember the goal for lower payload requirements is to determine if slight adjustments to the 130 mt configuration are capable of bringing lower payloads to orbit. It was stated that this can best be done by removing boosters and minimizing adjustments to the core vehicle. This section discusses an attempt to determine if this is possible for this particular configuration. Table 7.14 outlines the cases used to determine if the vehicle described in Table 7.13 is capable of being adjusted for a payload of 100 mt. The analysis is performed in multiple steps. The first is to estimate the propellant masses as a function of the ΔV contribution from the different stages using the procedure outlined in Chapter 6. This velocity budget method is very important because it provides a visual representation as to how adjusting the adjusting the contribution of a particular stage to the total ΔV affects GLOW of the vehicle. These propellant masses are then simulated in THEO to determine if they are in fact capable of bringing the vehicle to desired orbital conditions.

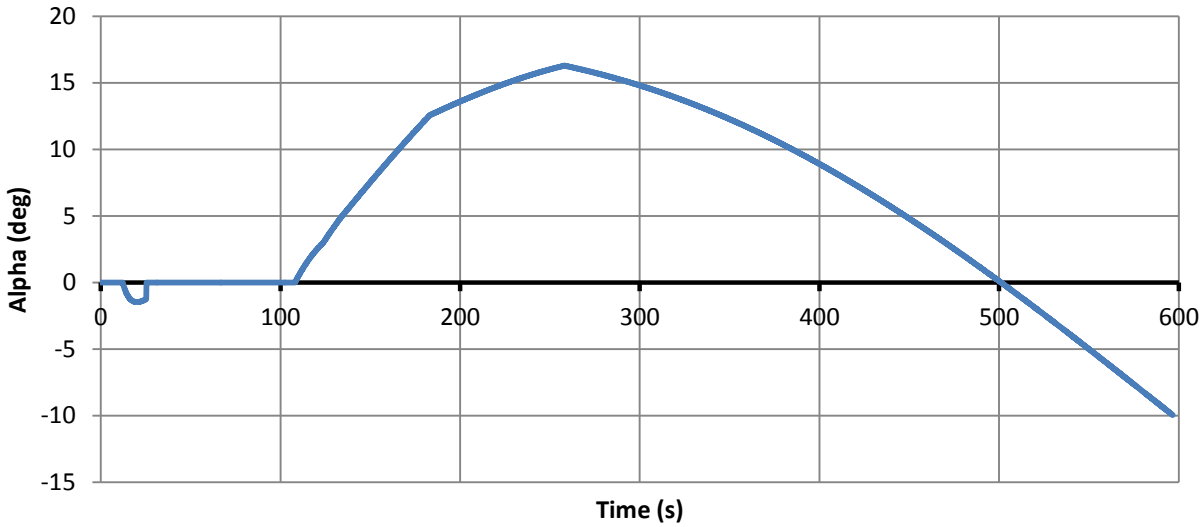

(a)

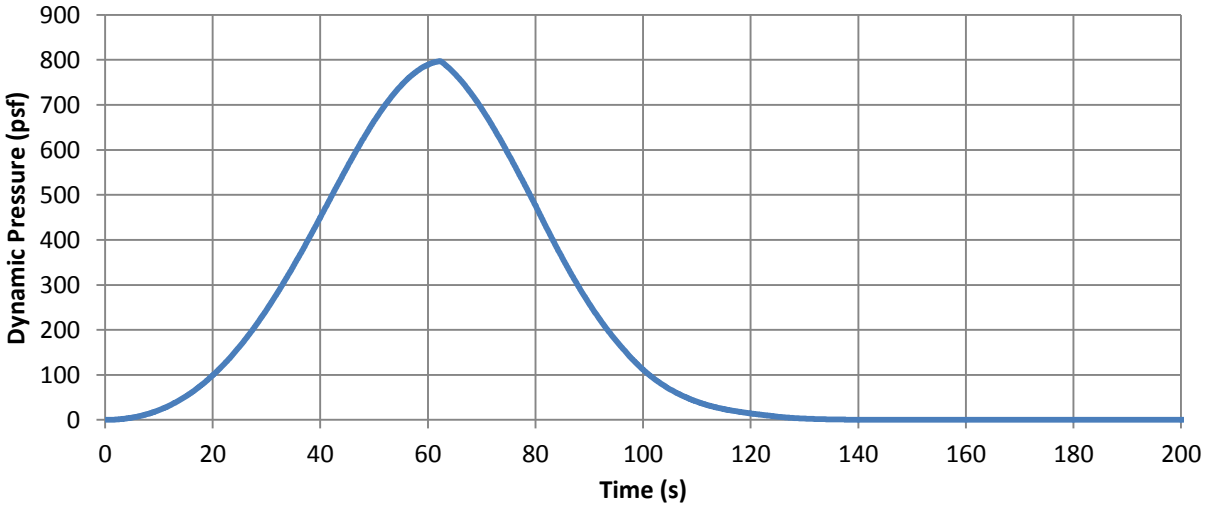

(b)

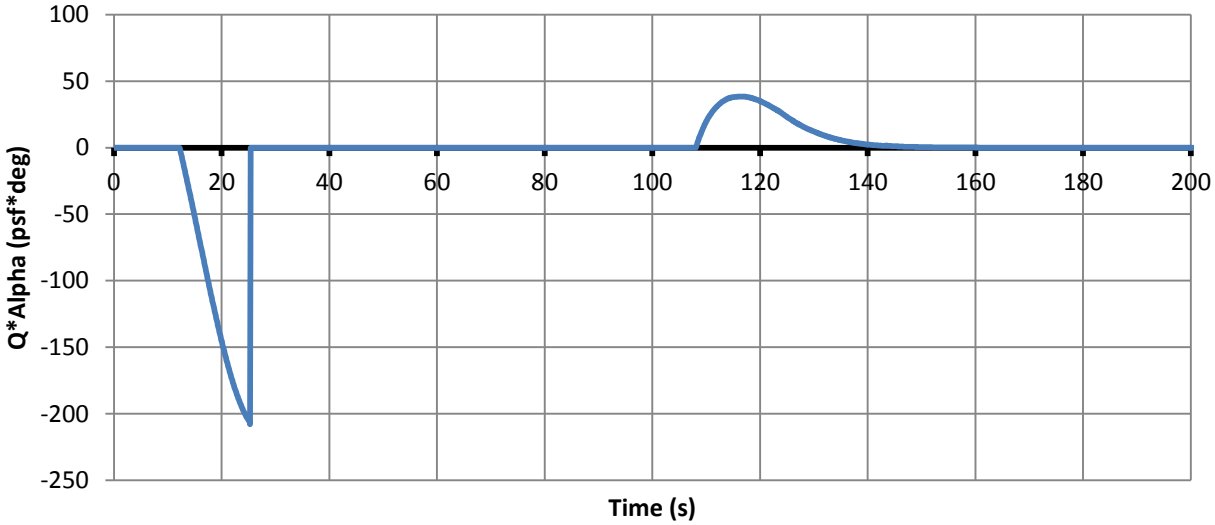

(c)

Figure 7.21a-c. 2.5 Stage RSRM V Aerodynamic Limits Check.

The effect of a ΔV variation on GLOW is shown in Figure 7.22. It is generated based on a total ΔV requirement of 9700 m/s, specific impulse for the engines, and the inert mass ratios specified of 0.06 and 0.08 for the first and second stage. Total ΔV is an estimation of necessary energy, in terms of velocity, to overcome adverse effects that are a result of drag, steering, and gravity losses. The velocity budget curve based on these parameters is shown in Figure 7.22. The minimum is shown in the figure and is also specified as case *1bb*.

Table 7.14. 100 mt Derivative of 2.5 Stage RSRM V Vehicle.

		Propellant			Engine				ΔV		Inertial Burnout			Max
Case	GLOW	Stage 1	f_1	Stage 2	Stage 1		Stage 2		Req	Avail	Vel.	Alt.	FPA	Q
-	*kg*	*kg*	-	*kg*	*Type*	#	*Type*	#	*m/s*	*m/s*	*m/s*	*m*	*deg*	*psf*
1bb	2011314	1037293	0.22	725086	-	-	-	-	9700	-	-	-	-	-
2bb	2016607	960289	0.196	805241	-	-	-	-	9700	-	-	-	-	-
3bb	2016528	960289	-	805241	F-1A	4	SSME	4	10365	9596	6898	400734	-0.07	952
4bb	2016528	960289	-	805241	F-1A	4	SSME	5	10149	9592	7109	399260	1.49	965
5bb	2142261	1466370	0.35	425609	-	-	-	-	9700	-	-	-	-	-
6bb	2142267	1466370	-	425609	F-1A	4	SSME	3	9462	9589	7789	400563	0.22	973
7bb	2142267	1466370	-	425609	F-1A	4	SSME	2	9336	9593	7916	399061	0.01	972
8bb	2361993	1789500	0.43	311507	-	-	-	-	9700	-	-	-	-	-
9bb	2361997	1789500	-	311507	F-1A	4	SSME	2	9288	9589	7958	399565	0.24	847
10bb	2479809	1935348	0.46	277154	-	-	-	-	9700	-	-	-	-	-
11bb	2479814	1935348	-	277154	F-1A	4	SSME	1	9322	9586	7906	400864	0.34	778

The propellant amount in case *1bb* is not equivalent to the values specified in Table 7.13. Adjusting the propellants is done by shifting the f_1 fraction. Matching the stage one propellant mass to the required 960 mt is done by shifting slightly left on the curve to case *2bb*. The stage 1 propellant is matched, but the shift has forced the stage 2 propellant to grow. This is acceptable as it is only a slight change in the original design. Case *2bb* is then run in THEO which generates the results shown in case *3bb*. As indicated by the burnout conditions, this particular configuration is incapable of bringing the vehicle to required burnout conditions. An attempt is then made to remedy this deficiency by adding a SSME engine. The addition helps, but the burnout velocity is approximately 500 m/s below the necessary velocity. Also notice that these two cases have a maximum dynamic pressure that is over the limit, which must be remedied one of two ways. The first method is to decrease the thrust to weight ratio by removing a stage one engine. Removal of a stage one engine decreases this ratio too much for this vehicle, and it falls back to the surface. The only other method is to increase GLOW of the vehicle which resultantly decreases the thrust to weight ratio.

Increasing GLOW is done by shifting to the right on the curve in Figure 7.22. A shift to an f_1 of 0.35 evaluates the next propellant requirements as case *5bb*. The propellant amounts are run in THEO with the results shown in case *6bb* and *7bb*. Burnout velocity is surpassed in both of these cases, indicating excessive energy contained within the propellant. Notice also that the dynamic pressure is higher for these two cases than in case *3bb* or *4bb*. Intuitively, these dynamic pressure values should be lower than previous cases as a result of the lower thrust to weight ratio. This is not the case here because case *6bb* and *7bb* require a very larger primary pitchrate which in turn forces the vehicle to remain in the atmosphere longer which increases maximum dynamic pressure. It serves to indicate that GLOW should be further increased.

Maximum dynamic pressure is decreased with the propellant requirements as a result of shifting f_1 to 0.43 and 0.46 in case *8bb* and *10bb*. These adjustments lead the vehicle to a configuration that is below the dynamic pressure limit. Unfortunately, these adjustments have required that the vehicle no longer resemble the configuration that was used for the 130 mt configuration. This eliminates the configuration from Table 7.13 as candidate for a 100 mt payload to orbit.

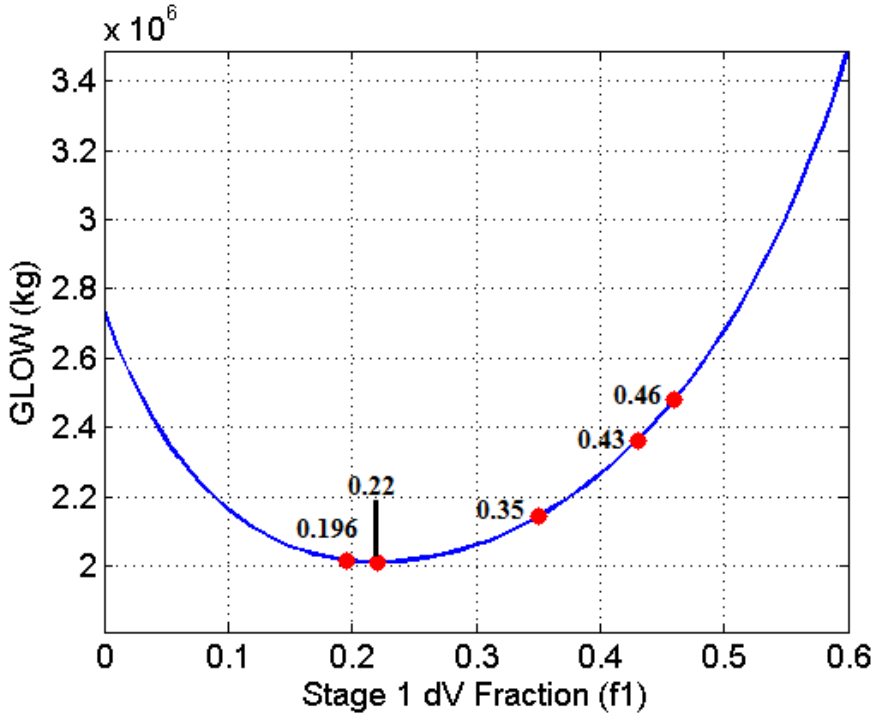

Figure 7.22. 100mt Derivative of 2.5 Stage RSRM V GLOW vs. ΔV Curve.

7.3.5 60 mt Payload Requirement for 2.5 Stage RSRM V Vehicle

A similar analysis is performed for the 60 mt payload configuration. The cases for this analysis are shown in Table 7.15 and are used to determine if the 130 mt configuration can be simplified to this lower payload. A velocity budget analysis with a specified total ΔV of 9700 m/s reveals the curve shown in Figure 7.23. The minimum is specified as case *1ba* and describes the minimum GLOW to bring the vehicle to orbit in terms of overcoming total ΔV. The propellant requirements are run in THEO with the results shown in case *2ba*, which shows that particular propellant and engine combination does not bring the vehicle to orbital conditions.

Table 7.15. 60 mt Derivative of 2.5 Stage RSRM V Vehicle.

		Propellant			Engine				ΔV		Inertial Burnout			Max
Case	GLOW	Stage 1	f_1	Stage 2	Stage 1		Stage 2		Req	Avail	Vel.	Alt.	FPA	Q
-	*kg*	*kg*	-	*kg*	*Type*	#	*Type*	#	*m/s*	*m/s*	*m/s*	*m*	*deg*	*psf*
1ba	1224165	611472	0.21	454469	-	-	-	-	9700	-	-	-	-	-
2ba	1224168	611472	-	454469	F-1A	2	SSME	2	11305	9578	5894	394065	0.60	643
3ba	1352525	960844	0.376	230623	-	-	-	-	9700	-	-	-	-	-
4ba	1352529	960844	-	230623	F-1A	3	SSME	1	10526	9595	6734	769644	-0.01	1182
5ba	1661927	1342107	0.500	142120	-	-	-	-	9700	-	-	-	-	-
6ba	1661927	1342107	-	142120	F-1A	3	SSME	1	9198	9582	8040	400860	0.11	992

An attempt to match the stage one propellant requirements to the 960 mt as specified in Table 7.13 is made by shifting f_1 to 0.376. The velocity budget analysis in case *3ba* reveals the propellant requirements for this particular ΔV fraction. Running these propellant amounts in THEO reveals the burnout conditions shown in case *4ba*. Not only is the burnout velocity insufficient, but the maximum dynamic pressure of 1182 psf is above the specified limit. As discussed in the 100 mt case, this can be remedied by the removal of a stage one engine or an

increase in GLOW. The removal of a stage 1 engine is not a viable option because the vehicle would fall back to the surface. Case *2ba* is able to approach altitude with two engines, but any increase in GLOW from that case will fall back to the surface. Using three engines is necessary to reach orbit.

Maximum dynamic pressure can only then be decreased by shifting the ΔV fraction and resultantly increasing GLOW. The velocity budget adjustment to an f_1 of 0.5 reveals new propellant requirements shown in case *5ba*. These are then run in THEO with the results in case *6ba*. This case shows that the modification does decrease the maximum dynamic pressure indicating that a further increase in GLOW should bring the maximum dynamic pressure below 800 psf. Unfortunately, the vehicle no longer resembles the original configuration, and further increases in GLOW only increase divergence from the original vehicle. It should also be noted that the curve in Figure 7.23 has a relatively steep slope after an f_1 of 0.5. As a result, the 2.5 stage RSRM V configuration can be eliminated from having potential payload variability.

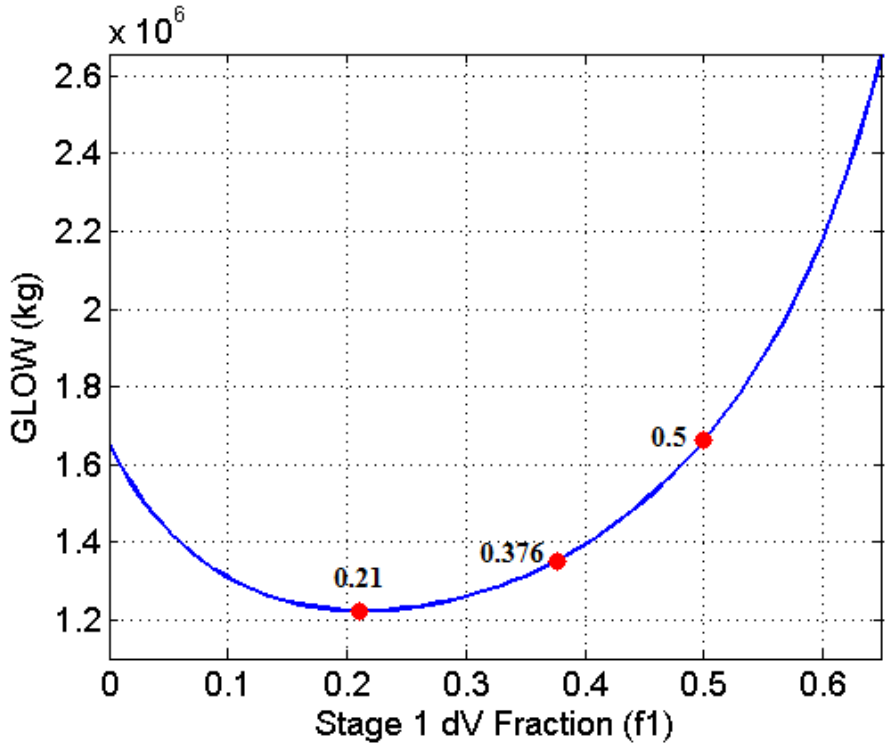

Figure 7.23. 60mt Derivative of 2.5 Stage RSRM V GLOW vs. ΔV Curve.

7.4 2.5 Stage M550 Vehicle

The next analysis is for configuration C from Table 7.1. The main difference between this and the previous cases is the booster. Monolithic 550 FW3 (M550) is a single segment booster designed to provide something cheaper and lighter than any of the RSRM family. This comes at a price, as the thrust profiles from Chapter 5 illustrate the M550 is approximately half of the RSRM family. Remedying this is done by attaching more boosters to the first stage. This introduces some unique considerations. The first is the increase in drag due to the proportional increase in cross sectional area. For a heavy lift launch vehicle this additional area does not have a significant effect on the trajectory. Remember from Table 4.1 in Chapter 4, the ΔV estimation to overcome drag is approximately 50 m/s. This is extremely small when compared to the total ΔV of 9613 m/s available within the propellant. As such, an area addition will result in only a slight increase for the total ΔV required. For an accurate simulation, this drag increase must still be considered.

The second consideration associated with this booster type is the variability that comes from using more than two boosters. In other words, payload to orbit can theoretically be varied by simply increasing or decreasing the number of boosters attached to the core. RSRM family boosters have very high thrust and mass, and as a result, it can be difficult to modify the vehicle to match different payloads with the use of only two boosters. Evidence of this conclusion was revealed in the analysis of the previous two cases. The M550 has the potential to eliminate this difficulty with the inherent variability of numerous boosters.

7.4.1 2.5 Stage M550 Vehicle Aerodynamic Coefficients

As discussed in Chapter 3, lift data is only available for those configurations that resemble a 2.5 stage vehicle with 2 RSRM or RSRM V boosters. The 2.5 Stage M550 does not resemble this configuration, and as a result, lift is assumed negligible. Figure 7.24 shows the drag profiles for this vehicle which are generated with Missile Datcom and are assumed to be a constant value from Mach 5 to the burnout condition.

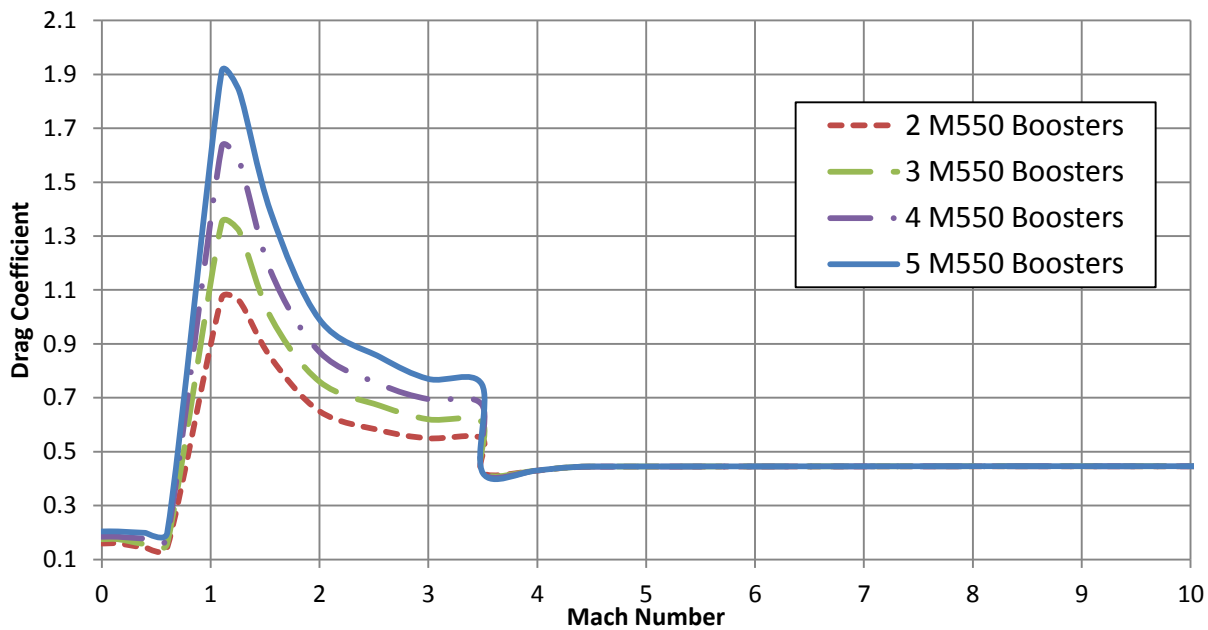

Figure 7.24. M550 Configuration Drag Coefficient Profile

7.4.2 2.5 Stage M550 General Analysis

The first step is to perform a general analysis of this 2.5 stage configuration with M550 boosters and a payload of 130 mt. The top results are shown in Table 7.16 for configurations with three, four, and five boosters. The possibility of these different booster configurations forces the selection process to be slightly more complicated than with the RSRM family evaluations. Instead of simply determining the lowest possible GLOW based on stage one and two propellant mass, it is imperative to consider varying the number of boosters. An initial overview of the data in Table 7.16 reveals that a successful configuration with five boosters has a much higher GLOW requirement than the other configurations. Note as well that case *12c* and *13c* have a maximum dynamic pressure that is above 800 psf. This serves to indicate that even if there were lighter cases for this particular engine configuration, they would have a maximum dynamic pressure above 800 psf. A smaller GLOW would increase the thrust to weight ratio and subsequently the maximum dynamic pressure. As a result of the high GLOW and dynamic pressure, a configuration with five boosters is ruled out as the minimized case.

Table 7.16. 2.5 Stage M550 General Analysis Top Configuations.

	Independent Variables						Burnout Conditions			
	Propellant Mass		Primary Pitch Event				Inertial Property			
	Stage 1	Stage 2	Start Time	Length	Pitchrate	GLOW	FPA	Velocity	Altitude	Max Q
Case	*kg*	*kg*	*s*	*s*	*deg/s*	*kg*	*deg*	*m/s*	*m*	*psf*
-	Booster: 3 M550 FW3 Booster			1st Stage Engine: 3 F-1A			2nd Stage Engine: 4 J-2X			
1c	1150000	600000	6.2	21	-0.7	2891314	0.51	7547.4	401803	873
2c	1300000	600000	6.2	19	-0.55	3050889	-0.06	7671.8	396051	776
3c	1400000	600000	6.2	17	-0.45	3157272	-0.11	7711.3	399811	718
4c	1400000	600000	10.2	21	-0.6	3157272	-0.01	7700.7	403247	717
5c	1450000	600000	9.2	13	-0.6	3210463	-0.06	7727.5	401030	691
-	Booster: 4 M550 FW3 Booster			1st Stage Engine: 2 F-1A			2nd Stage Engine: 4 J-2X			
6c	1150000	450000	7.2	15	-0.7	3016955	0.31	7616.3	400710	727
7c	1200000	450000	7.2	21	-0.55	3070146	0.18	7616.1	402190	696
8c	1250000	400000	9.2	21	-0.7	3068990	1.88	7680.9	402281	702
9c	1250000	450000	8.2	11	-0.7	3123338	-0.04	7621.8	398921	668
10c	1350000	400000	6.2	9	-0.55	3175373	1.6	7678.3	401284	646
11c	1400000	400000	9.2	15	-0.55	3228564	1.42	7676.1	397876	620
-	Booster: 5 M550 FW3 Booster			1st Stage Engine: 2 F-1A			2nd Stage Engine: 4 J-2X			
12c	950000	600000	6.2	15	-0.8	3255917	-0.12	7642.6	396399	838
13c	1000000	600000	6.2	19	-0.65	3309109	-0.13	7642.3	399605	807
14c	1050000	600000	9.2	25	-0.65	3362300	-0.31	7656.1	396155	776
15c	1100000	600000	8.2	21	-0.6	3415492	-0.34	7648.1	399128	750
16c	1150000	600000	7.2	17	-0.55	3468683	-0.51	7647.6	396492	724

The next step is to determine whether a case with three or four M550 boosters is the optimized configuration. Cases *1c – 5c* show the top results for a configuration with three M550 boosters. The data here reveals some pertinent information for this case. First of all, case *2c* is the lightest case from Table 7.16 that best achieves burnout conditions. The burnout velocity and burnout flight path angle are both very close to the required burnout conditions. The altitude is slightly outside of the 0.5% accuracy requirement but can be corrected with a minor secondary pitchrate adjustment. Notice that the maximum dynamic pressure for case *1c* is above 800 psf. Just like cases *12c – 16c*, this high maximum dynamic pressure indicates that any further decrease in the propellant masses will result in a higher thrust to weight ratio. A higher thrust to weight ratio will place the vehicle beyond the limits of dynamic pressure. Maximum dynamic pressure in case *2c* is 24 psf below the 800 psf limit, indicating there is room for it to increase. This trend guides the analysis and suggests that the minimized case potentially exists in between case *1c* and *2c*.

A pitch analysis of case *2c* is shown in Figure 7.25. The intersection curve groups show that the vehicle is stable in terms of the pitch properties. The next step is to perform a refined analysis around this particular configuration to determine if GLOW can be locally decreased. Any decrease is limited by dynamic pressure limits, and this refined search shows how much the propellant mass can be adjusted before an 800 psf dynamic pressure is surpassed. The results of this search are shown in Table 7.17.

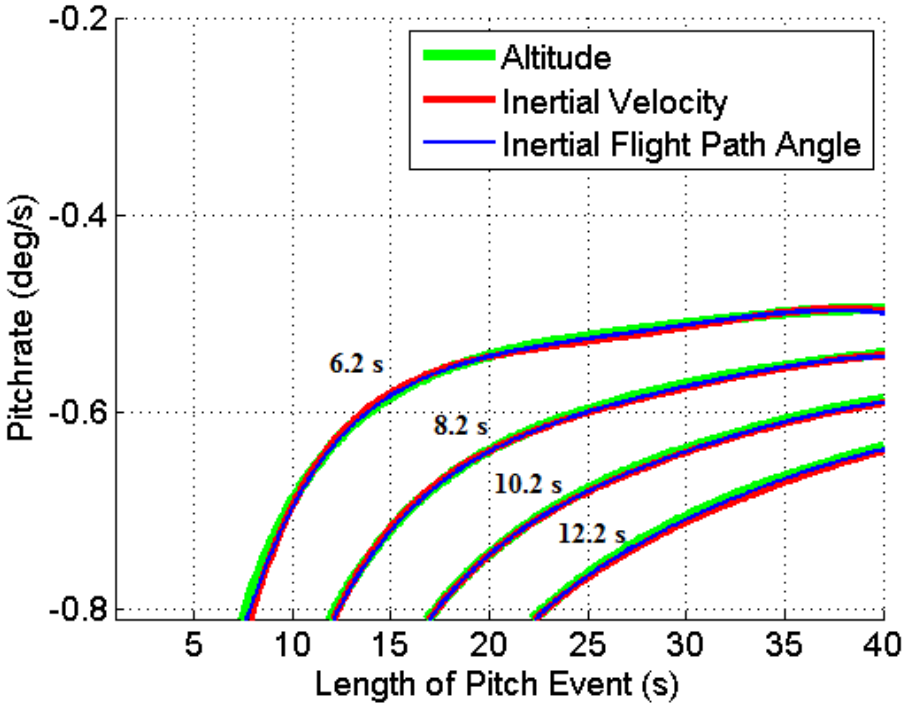

Figure 7.25. Case 2c Intersection Curve. Burnout curve groups for start time of 6.2-12.2 s.

7.4.3 2.5 Stage M550 Refined Analysis

Table 7.17. 2.5 Stage 3 M550 GLOW Minimization Cases. Minimized configurations based on Case 2c.

	Independent Variables						Burnout Conditions			
	Propellant Mass		Primary Pitch Event				Inertial Property			
	Stage 1	Stage 2	Start Time	Length	Pitchrate	GLOW	FPA	Velocity	Altitude	Max Q
Case	*kg*	*kg*	*s*	*s*	*deg/s*	*kg*	*deg*	*m/s*	*m*	*psf*
c1	1250000	580000	6.7	19	-0.7	2975958	0.59	7679.3	400593	825
c2	1260000	580000	7.7	21	-0.71	2986596	0.54	7688.5	399395	818
c3	1250000	600000	8.2	17	-0.75	2997697	0.17	7631.7	398961	806
c4	1260000	600000	7.7	21	-0.65	3008335	0.21	7630.4	401375	799
c5	1280000	590000	7.2	15	-0.71	3018742	0.31	7673.3	400290	797
c6	1290000	590000	6.2	11	-0.71	3029381	0.25	7688	398323	791
c7	1290000	600000	6.7	15	-0.63	3040250	0.16	7650	401809	782

The data shown in Table 7.17 reveals that GLOW can be decreased from case *2c* . Cases *c1-c4* have the lowest GLOW but are all disqualified because they have either high maximum dynamic pressure and/or a burnout condition that is outside of the 0.5% bounds. The first case that fulfills all requirements is case *c5*. As such, it can be considered the minimized case for a 2.5 stage vehicle with 3 M550 boosters, 3 F-1A stage 1 engines, and 4 J-2X engines.

The next step is to check the GLOW stability in terms of the ΔV for the different propulsion stages. A ΔV analysis is shown in Figure 7.26, and case *c5* is represented by the yellow point on the surface. As this point shows, the vehicle is on a moderately shallow portion of the surface indicating a somewhat stable vehicle. Even though it has been shown that GLOW is at a minimum, there is a possibility that the vehicle can be adjusted to an even shallower portion of the curve.

This can theoretically be done by adjusting certain vehicle properties. For example, consider the surface in Figure 7.26. The surface shows the stability location of the configuration based on the ΔV contribution for the portion of the trajectory when the boosters and first stage burn together, and for the first stage after booster separation. The position of case *c5* on this surface indicates that if the ΔV fraction from these two propulsion components were less, the case would shift to a more stable position. Unfortunately, this would result in a decrease in GLOW which would then place the dynamic pressure over the limit. Instead of trying to shift the point, it is in fact possible to readjust the surface by changing certain vehicle properties. To decrease the ΔV contribution from the boosters and first stage would require an increase in the stage 2 contribution which corresponds to an increase in the stage 2 propellant mass. An increase in propellant requires an increase in thrust which is done with the addition of one J-2X engine. The results of the reanalysis of this vehicle with 5 J-2X engines in the second stage is shown in Table 7.18.

Table 7.18. 2.5 Stage 3 M550 GLOW Minimization Cases Revised. Additional J-2X engine.

	Independent Variables						Burnout Conditions			
	Propellant Mass		Primary Pitch Event				Inertial Property			
	Stage 1	Stage 2	Start Time	Length	Pitchrate	GLOW	FPA	Velocity	Altitude	Max Q
Case	*kg*	*kg*	*s*	*s*	*deg/s*	*kg*	*deg*	*m/s*	*m*	*psf*
c1a	1150000	680000	6.2	11	-0.8	2978272	0.56	7651.8	398747	815
c2a	1160000	680000	7.2	19	-0.65	2988910	0.47	7661.5	397345	808
c3a	1170000	680000	6.7	19	-0.61	2999548	0.49	7661.4	399347	802
c4a	1180000	680000	6.2	17	-0.59	3010187	0.5	7663.3	400643	796
c5a	1190000	680000	6.2	21	-0.55	3020825	0.32	7680.6	396761	790
c6a	1180000	690000	6.7	11	-0.71	3021056	0.23	7645.1	398532	787
c7a	1190000	690000	6.7	11	-0.69	3031694	0.31	7639.6	402025	781

Notice how the results in Table 7.18 compare to those in Table 7.17. GLOW and maximum dynamic pressure are very similar. Then only major difference is the stage propellant mass, and as expected the configuration with the additional J-2X engine has higher second stage propellant masses. The minimized case out of Table 7.18 corresponds to the one that finds a balance between minimizing GLOW and remaining below the dynamic pressure limit. The minimized solution is case *c4a* which has a GLOW that is a few tons lighter than case *5c* from the previous analysis. Figure 7.27 illustrates the GLOW versus ΔV stability analysis of this case.

The position of case *c4a* is represented on this figure by the yellow dot. A comparison of Figure 7.26 and 7.27 reveals that this engine adjustment has brought the solution to a shallower region on the surface. As expected the increase in propellant mass of the second stage has resulted in a vehicle that is at a slightly more stable position on the curve. This search has revealed a case for a 2.5 stage vehicle with 3 M550 boosters that is capable of fulfilling all the necessary conditions.

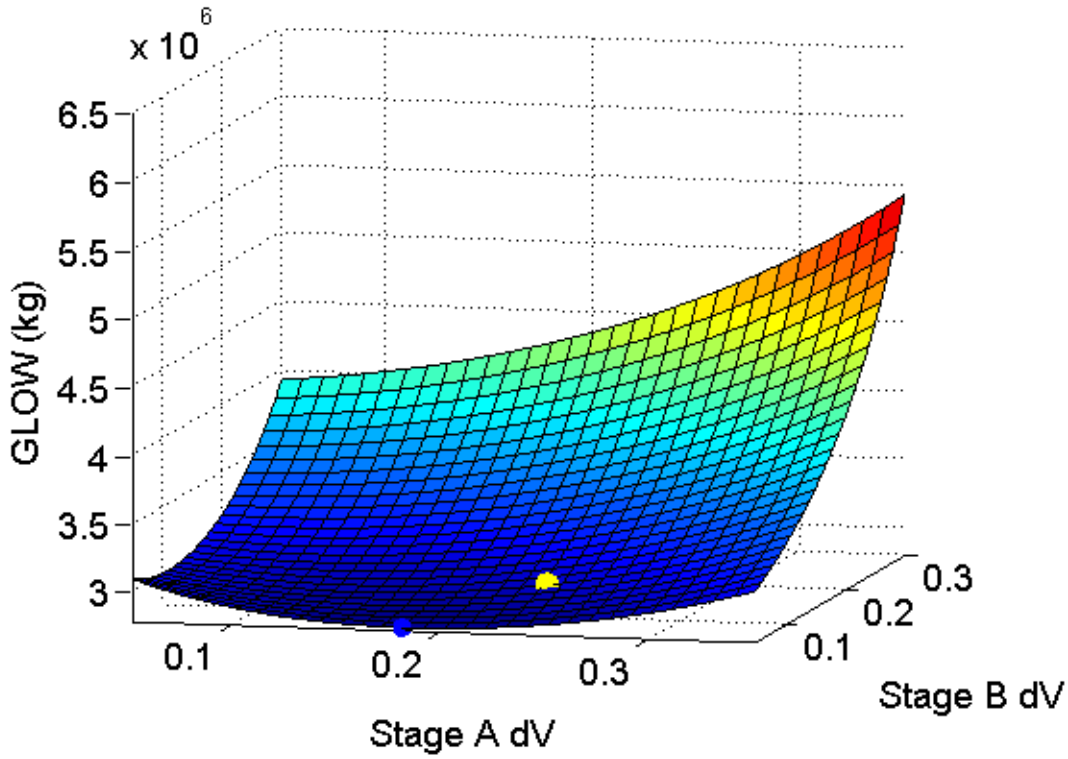

Figure 7.26. 2.5 Stage M550 Stability Surface for Case c5.

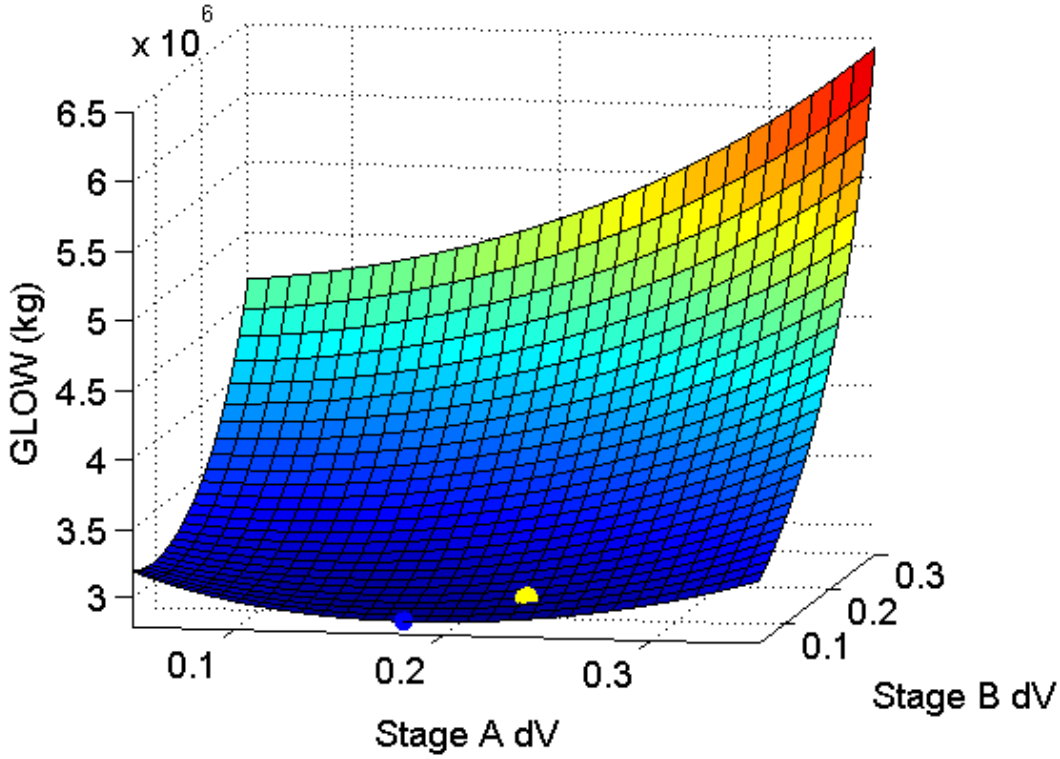

Figure 7.27. 2.5 Stage M550 Stability Surface for Case c4a.

The last step is to check the configurations represented by cases *6c-11c* in Table 7.16. These cases use four M550 boosters and as a result have a much lower stage two propellant mass than the other configurations. Notice that the dynamic pressure is not close to surpassing specified limits. This implies that there is substantial room for GLOW to decrease. The results for a refined search around cases *6c* and *7c* with an adjusted secondary pitch event are shown in Table 7.19.

Table 7.19. 2.5 Stage 4 M550 GLOW Minimization Cases .

	Independent Variables						Burnout Conditions			
	Propellant Mass		Primary Pitch Event				Inertial Property			
	Stage 1	Stage 2	Start Time	Length	Pitchrate	GLOW	FPA	Velocity	Altitude	Max Q
Case	*kg*	*kg*	*s*	*s*	*deg/s*	*kg*	*deg*	*m/s*	*m*	*psf*
c1b	1160000	400000	9.8	22	-0.8	2973245	0.51	7638.1	397630	753
c2b	1170000	400000	9.8	21	-0.83	2983883	0.54	7635.7	399536	747
c3b	1180000	400000	9.8	23	-0.78	2994522	0.49	7635.4	399441	740
c4b	1190000	400000	9.8	22	-0.78	3005160	0.45	7639.2	398925	734
c5b	1200000	400000	9.8	23	-0.75	3015798	0.36	7644.4	397830	728
c6b	1210000	400000	10	19	-0.81	3026437	0.44	7634.4	401110	722
c7b	1220000	400000	9.8	19	-0.78	3037075	0.39	7636.7	400992	716

The lightest configuration that meets the specified 0.5% bounds for the boundary condition is case *c3b*. It is also well below the dynamic pressure limit which implies that the thrust to weight ratio has some room to increase before the dynamic pressure limit is reached. An analysis similar to the previous case was performed to determine if varying the number of stage 2 engines would bring the vehicle to orbit. No cases were successful which suggests that case *c4b* is the minimized case for the vehicle with 4 M550 boosters. The GLOW versus ΔV analysis of this case is shown to be a relatively stable surface in Figure 7.28.

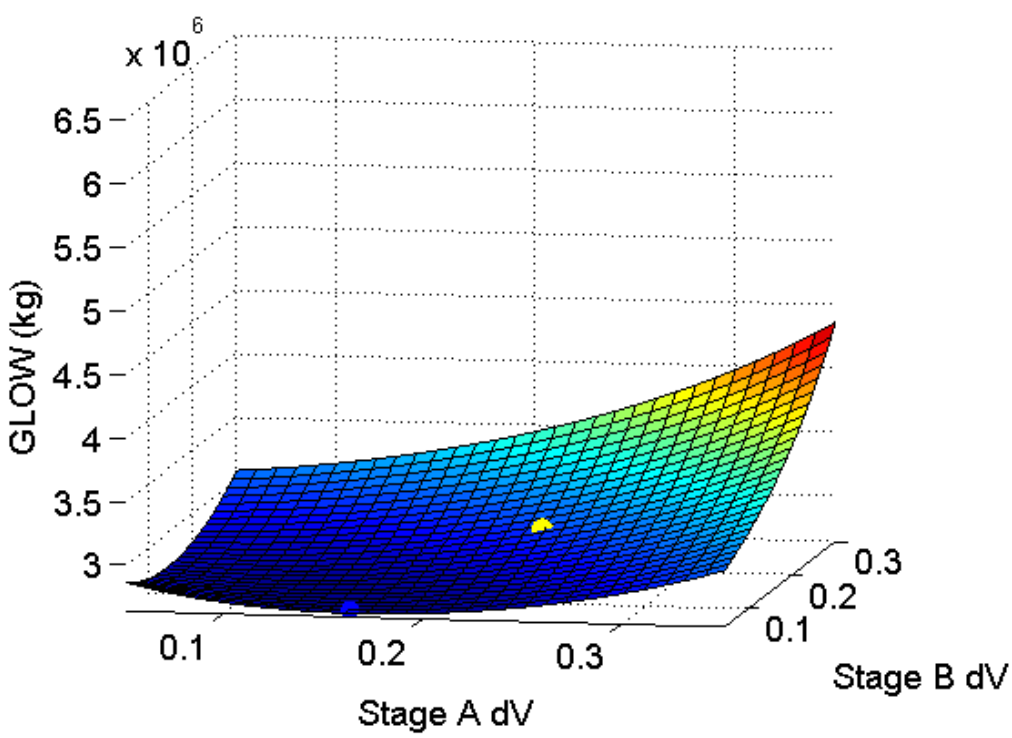

Figure 7.28. 2.5 Stage M550 Stability Surface for Case c3b.

The final selection for this vehicle with M550 boosters is down to the two cases shown in Table 7.20. There are a few differences that should be noted before presenting the decision. Case *c3b* is approximately 15 mt lighter than case *c4a*. Also, notice the difference between the velocity budget analysis shown in Figures 7.27 and 7.28. The surface shown for case *c3b* has a shallower slope than case *c4a* indicating an increased stability when using four M550 boosters instead of three. As the objective of this analysis is to search for a minimized GLOW case that is on a relatively stable ΔV surface , case *c3b* is deemed the solution for the 130 mt payload configuration.

Table 7.20. 2.5 Stage M550 130 mt Payload Vehicle Selections.

		Propellant		Engine					
Case	GLOW	Stage 1	Stage 2	Booster		Stage 1		Stage 2	
-	*kg*	*kg*	*kg*	*Type*	#	*Type*	#	*Type*	#
c4a	3010187	1180000	680000	M550 FW3	3	F-1A	3	J-2X	5
c3b	2994522	1180000	400000	M550 FW3	4	F-1A	2	J-2X	4

The final step is to check the physical dimensions and determine if radius and vehicle length should be adjusted from the original assumption. It can be advantageous to decrease the radius of the vehicle because of the resultant decrease in drag. A revaluation of this case in THEO indicates that the radius can be reduced from the initial radius assumption of 4.265 m to 3.7 m. Remember that a decrease in radius is inversely proportional to the velocity of the vehicle. In turn, velocity squared is proportional to an increase in maximum dynamic pressure. As a result, vehicle radius can only be decreased as long as maximum dynamic pressure is below 800 psf or until physical limitations are reached. For this case, the control variable is rocket length as the maximum dynamic pressure is well below the limit. Radius can be decreased only until length constraints are reached, which is a radius of 3.7 m for stage 1 and 3.15 m for stage 2. The results of the reevaluated case with new dimensions are shown in Table 7.21.

Table 7.21. 2.5 Stage M550 Configuration for 130 mt Payload.

	Length	Diameter	Propellant	Inert	Engine	# Engines	Burnout Alt	400000	m
130 mt	*m*	*m*	*kg*	*kg*	*(Shape)*	-	Burnout Vel	7643	m/s
Booster	13.72	4.06	1043260	111476	M550 FW3	4	Burnout FPA	0.003	*deg*
Stage 1	32.91	7.40	1180000	75321	F-1A	2	Max Q	754.9	*psf*
Stage 2	54.50	6.30	400000	34786	J-2X	4	GLOW	2994521	*kg*
Shroud	12.19	7.40	-	19674	Biconic	-	Start Pitch	9.8	*s*
Total	99.60	-	-	-	2.5 Stage	-	Pitch Length	23	*s*
Secondary Pitch Event Revision				3rd	-0.121536	*deg/s*	Pitchrate	-0.7920	deg/s
Secondary Pitch Event Revision				4th	-0.168014	*deg/s*			

A combination of minimizing GLOW and maintaining acceptable dynamic pressure levels has guided the analysis to a configuration that is capable of reaching the desired burnout conditions. The vehicle described in Table 7.21 also has been shown to be at a stable position on the GLOW vs ΔV surface, and as a result, is the solution for a 2.5 stage vehicle with M550 FW3 boosters. A check to ensure that the aerodynamic constraints are not surpassed is shown in Figure 7.29.

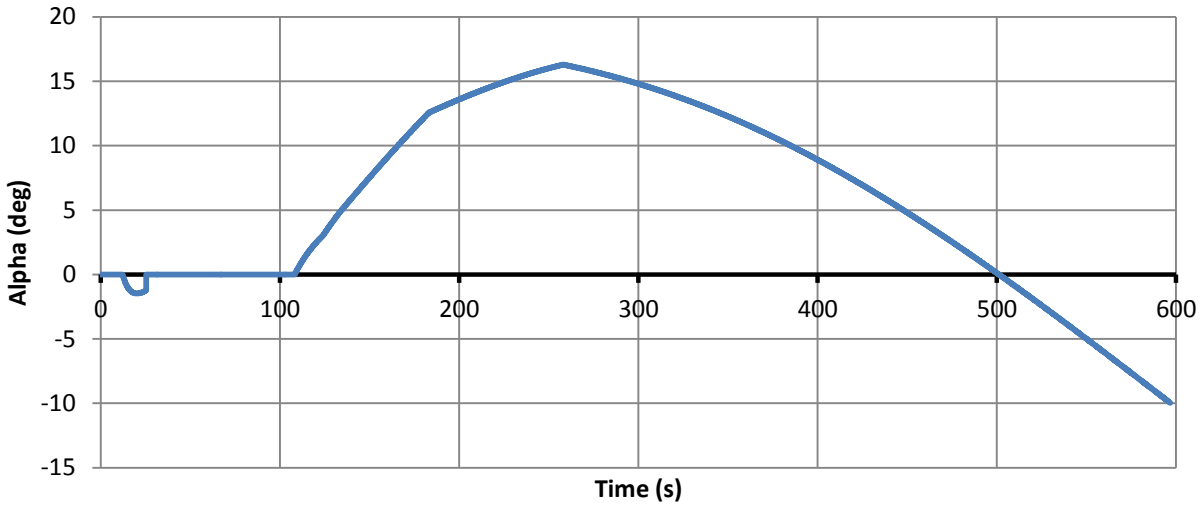

(a)

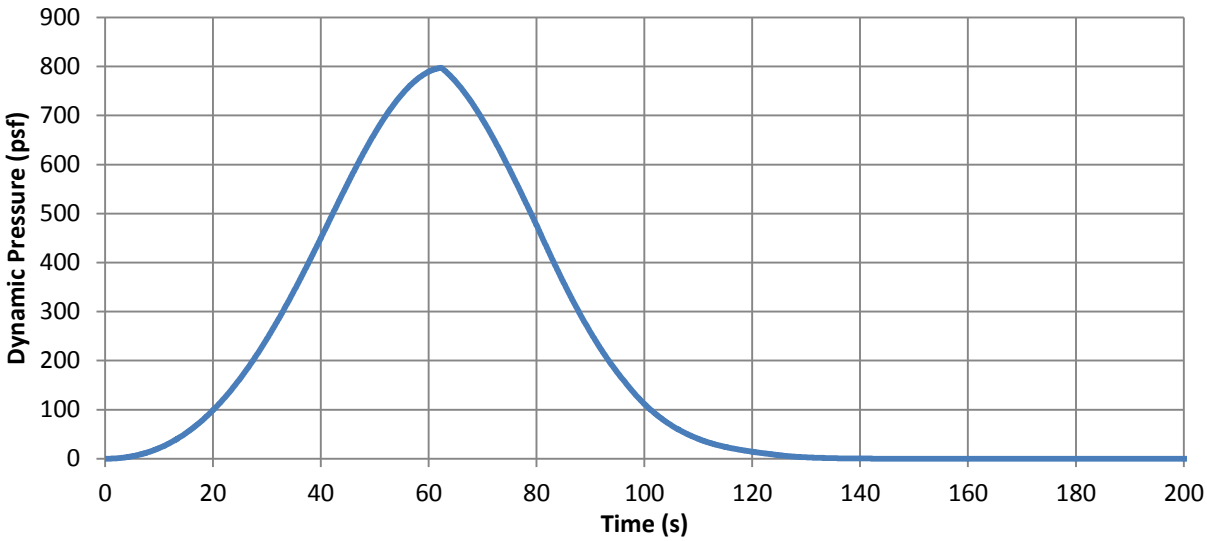

(b)

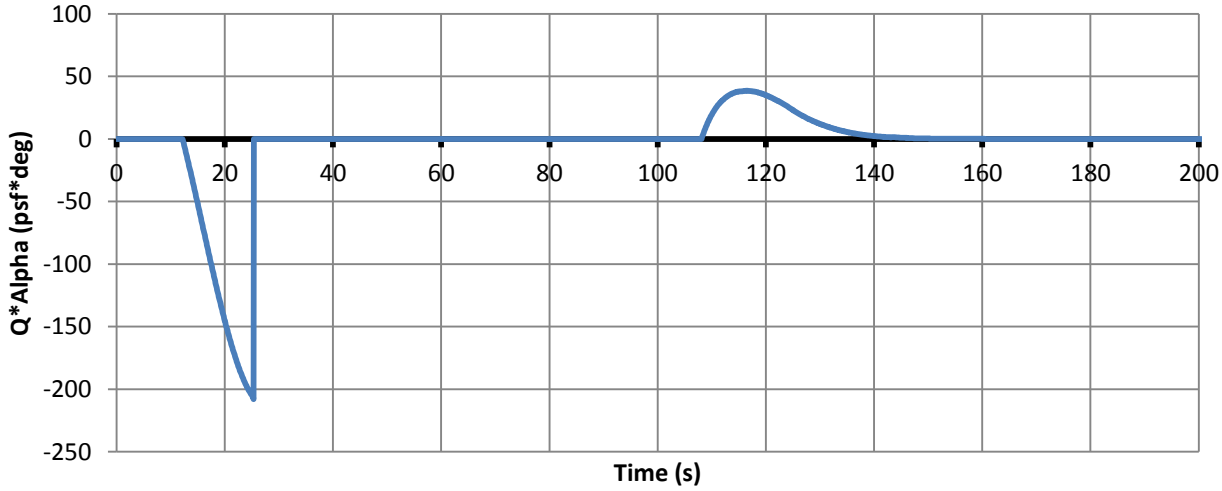

(c)

Figure 7.29. 2.5 Stage M550 Aerodynamic Limits Check

7.4.4 100 mt Payload Requirement for 2.5 Stage M550 Vehicle

The next task is to determine if the 130 mt payload configuration described in Table 7.21 can be modified to smaller payload configurations. As discussed in the analysis for a previous case, a configuration is considered adaptable to different payloads if the vehicle can be brought to orbit with only slight modifications in the design of the vehicle. The results shown in Table 7.22 describe if this capability is possible with this vehicle.

Utilizing a configuration with M550 boosters has advantages that the RSRM family vehicles do not. The high thrust and mass made it very difficult to use them efficiently for different requirements. M550 boosters introduce more variability to the different payload requirements by providing more manageable booster properties. Minimizing changes to the core can theoretically be done by adjusting the number of M550 boosters instead of changing the stage 1 and stage 2 vehicle components.

Table 7.22. 100 mt Derivative of 2.5 Stage M550 FW3 Vehicle.

		Propellant		Engine						ΔV		Burnout Condition			
Case	GLOW	Stage 1	Stage 2	Booster		Stage 1		Stage 2		Req	Avail	Vel.	Altitude	FPA	Q
-	*kg*	*kg*	*kg*	*Type*	#	*Type*	#	*Type*	#	*m/s*	*m/s*	*m/s*	*m*	*deg*	*psf*
1ca	2546294	1180249	268158	M550	3	-	-	-	-	9550	-	-	-	-	-
2ca	2532794	1180249	268158	M550	3	F-1A	2	J-2X	4	9359	9663	7964	401038	0.312	782
3ca	2525382	1180061	246654	M550	3	-	-	-	-	9450	-	-	-	-	-
4ca	2509219	1180061	246654	M550	3	F-1A	2	J-2X	3	9336	9582	7907	398410	0.476	804
5ca	2324174	1180036	347426	M550	2	-	-	-	-	9600	-	-	-	-	-
6ca	2330043	1180036	347426	M550	2	F-1A	2	J-2X	4	9802	9643	7500	400938	0.411	558
7ca	2358073	1180166	381637	M550	2	-	-	-	-	9700	-	-	-	-	-
8ca	2367368	1180166	381637	M550	2	F-1A	2	J-2X	4	9844	9735	7551	400162	0.174	555
9ca	2390659	1180100	402677	M550	2	-	-	-	-	9750	-	-	-	-	-
10ca	2390167	1180100	402677	M550	2	F-1A	2	J-2X	4	9902	9785	7542	400979	0.285	541
11ca	2454724	1179998	466981	M550	2	-	-	-	-	9900	-	-	-	-	-
12ca	2459956	1179998	466981	M550	2	F-1A	2	J-2X	5	10130	9915	7445	399314	0.025	499
13ca	2459956	1179998	466981	M550	2	F-1A	3	J-2X	4	9345	9808	8123	100103	-0.22	934
14ca	2376282	1180000	390000	M550	2	F-1A	2	J-2X	4	9886	9754	7528	401844	-0.08	549
15ca	2354543	1180000	370000	M550	2	F-1A	2	J-2X	4	9789	9705	7577	399595	0.75	564
16ca	2343673	1180000	360000	M550	2	F-1A	2	J-2X	4	9775	9679	7565	397081	0.338	572
17ca	2354541	1180000	370000	M550	2	F-1A	2	SSME	2	9809	9796	7646	399813	0.167	565

* Gray tinted rows signify a case that is a velocity budget analysis.

The search begins by performing a velocity budget analysis of the vehicle with a 100 mt payload requirement. An initial guess of 9550 m/s for the total ΔV is made to bring the vehicle to orbit. An analysis with this parameter and 3 M550 boosters reveals the propellant requirements and GLOW shown in case *1ca*. The results are favorable as the propellant amount for the first stage is approximately the same as those for the 130 mt payload configuration. This serves to indicate that decreasing the number of boosters on the vehicle minimizes changes to the core of the vehicle. The propellant requirements are then run in THEO with the results shown in case *2ca*. THEO shows that the case is able to reach orbit with a high burnout velocity indicating excessive amounts of energy contained within the propellant. An attempt is then made to decrease the total energy in the vehicle by revising the required ΔV to 9450 m/s as shown in case *3ca*. Reevaluating the budget analysis reveals the propellant requirements which are then run in THEO as shown in case *4ca*. The burnout velocity is again overshot, indicating that the amount of propellant should be decreased further. Unfortunately, the maximum dynamic pressure for the case has surpassed 800 psf, implying that a continued propellant decrease will result in high maximum dynamic pressure values.

An attempt to remedy this is made by removing one booster and reevaluating the propellant requirements based on a total ΔV assumption of 9600 m/s. Propellant requirements with these properties are shown in case *5ca*

and then evaluated with THEO as shown in case *6ca*. Burnout velocity is insufficient by approximately 150 m/s indicating that the energy contained within the propellant is too low. Total ΔV in case *7ca*, *9ca*, and *11ca* is then adjusted repeatedly to attempt overcoming this deficiency, but THEO shows in cases *8ca*, *10ca*, and *12ca* that the burnout velocity is still insufficient. An additional stage 1 engine is added in case *13ca*, but the burnout velocity is surpassed by 500 m/s.

Case *8ca* has a burnout velocity that is the closest to reaching the desired burnout condition with a velocity of 7551 m/s. As a result, the next task was to perform a localized search around this case by varying the stage 2 propellant mass. Varying the stage 2 propellant mass allows the first stage to remain unchanged which minimizes modifications to the vehicle. Reevaluated configurations with stage 2 propellant masses of 390, 370, and 360 mt are shown in cases *14ca-16ca*. Unfortunately, none are capable of reaching orbit, implying that instead of adjusting the propellant masses, it is necessary to improve the efficiency of the engines. This is performed by replacing the 4 J-2X engines with 2 SSME engines. There is an improvement in performance because the I_{sp} shifts from 448 s for the J-2X to 455 s for the SSME. The configuration with replaced stage 2 engines is run in THEO with the results shown in case *17ca*. The performance increase is enough to bring the vehicle to required orbital conditions. The analysis described here has shown that by adjusting the number of boosters and exchanging the stage 2 engines, a 100 mt payload can be brought to orbit with minimal changes to the configuration described in Table 7.21. The only other difference is a 30 mt decrease in the stage 2 propellant which requires only slight design changes to the vehicle. A GLOW versus ΔV stability check is illustrated in Figure 7.30 to show that it is stable on the ΔV surface.

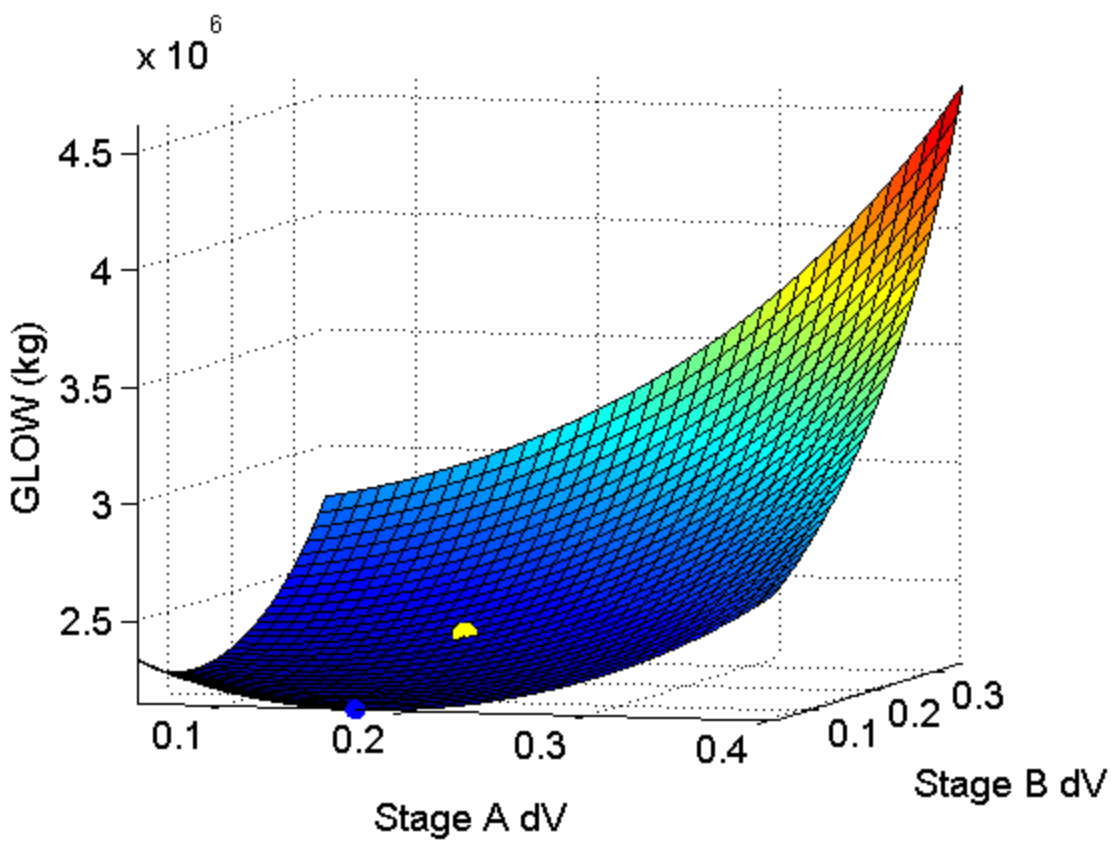

Figure 7.30. 2.5 Stage M550 100 mt Stability Surface for Case 17ca. Represented by yellow dot.

7.4.5 60 mt Payload Requirement for 2.5 Stage M550 Vehicle

The last step is to determine if the vehicle described in Table 7.21 can be modified for the smallest payload requirement of 60 mt. Performing this analysis is done in a way similar the previous case. The goal is to produce a vehicle that has only slight changes to the original vehicle. Minimizing these changes become more difficult as the payload requirement decreases. The results in Table 7.23 step through the process to determine which modifications bring the payload to orbital conditions.

Case *1cb* is an attempt to run the vehicle in THEO using the original vehicle described in Table 7.21 without any changes to the core. The only difference is that the M550 boosters are removed, which leaves a two stage vehicle. The burnout velocity is approximately 800 m/s above the required 7670 m/s for a 400 km orbit indicating excessive amounts of energy. The energy available can be reduced by reevaluating the propellant masses based on a new ΔV. The new ΔV of 9850 m/s is an initial guess as to what the energy requirements might be. The reevaluated propellant masses are shown in case *2cb*. Running these new propellant amounts in THEO reveals the results shown in case *3cb*. The burnout velocity has decreased, but notice that the maximum dynamic pressure has greatly surpassed limits. The decrease in propellant mass has increased the thrust to weight ratio which has in turn increased the maximum dynamic pressure. Decreasing the energy available within the rocket has forced the maximum dynamic pressure past 800 psf. This implies that simply removing all the M550s from the original vehicle is not a sufficient solution to bring 60 mt of payload to orbit.

Table 7.23. 60 mt Derivative of 2.5 Stage M550 FW3 Vehicle.

		Propellant		Engine						ΔV		Burnout Condition			Max
Case	GLOW	Stage 1	Stage 2	Booster		Stage 1		Stage 2		Req	Avail	Vel.	Altitude	FPA	Q
-	*kg*	*kg*	*kg*	*Type*	*#*	*Type*	*#*	*Type*	*#*	*m/s*	*m/s*	*m/s*	*m*	*deg*	*psf*
1cb	1769783	1180000	400000	-	-	F-1A	3	J-2X	3	9570	10389	8472	402064	-0.04	785
2cb	1559767	1180001	206791	-	-	-	-	-	-	9850	-	-	-	-	-
3cb	1559772	1180001	206791	-	-	F-1A	3	J-2X	2	9118	9738	8278	401583	-0.09	1106
4cb	1577184	648360	198571	M550	2	-	-	-	-	9800	-	-	-	-	-
5cb	1562629	648360	198571	M550	2	F-1A	1	J-2X	2	9592	9885	7953	400792	0.126	731
6cb	1503024	574154	214586	M550	2	-	-	-	-	9700	-	-	-	-	-
7cb	1501095	574154	214586	M550	2	F-1A	1	J-2X	2	9624	9792	7829	400901	-0.36	751
8cb	1453269	531283	209436	M550	2	-	-	-	-	9600	-	-	-	-	-
9cb	1449890	531283	209436	M550	2	F-1A	1	J-2X	2	9510	9667	7818	400360	0.38	820
10cb	1524607	659712	145689	M550	2	-	-	-	-	9400	-	-	-	-	-
11cb	1517226	659712	145689	M550	2	F-1A	1	J-2X	2	9528	9626	7760	399313	0.444	741
12cb	1528410	682976	129263	M550	2	-	-	-	-	9300	-	-	-	-	-
13cb	1524120	682976	129263	M550	2	F-1A	1	J-2X	2	9589	9566	7639	399759	0.163	732

* Gray tinted rows signify a case that is a velocity budget analysis.

Since a two stage vehicle does not work, two M550 boosters are added to the vehicle. The stage propellant masses are estimated in case *4cb* with an initial ΔV guess of 9800 m/s. Propellant amounts, along with two boosters, are then run in THEO with the results in case *5cb*. The burnout velocity of this case is 7953 m/s indicating the energy should be further reduced. This is done by reevaluating the propellant requirements with a decreased total ΔV. The ΔV value is reduced from 9700 m/s to 9300 m/s in cases *6cb*, *8cb*, *10cb*, and *12cb* to determine how much the propellant should be adjusted. Running each of these propellant adjustments in THEO reveals the results shown in cases *7cb*, *9cb*, *11cb*, and *13cb*. These results show that case *13cb* is the first case to bring the vehicle to orbit without overshooting the required inertial velocity.

Analysis of this vehicle has shown that a solution can be determined by stepping through different propellant masses until all burnout conditions are met. It does not resemble the original core vehicle, but it does utilize the boosters used for other payload configuration. The GLOW versus ΔV stability surface for case *13cb* is shown in Figure 7.31.

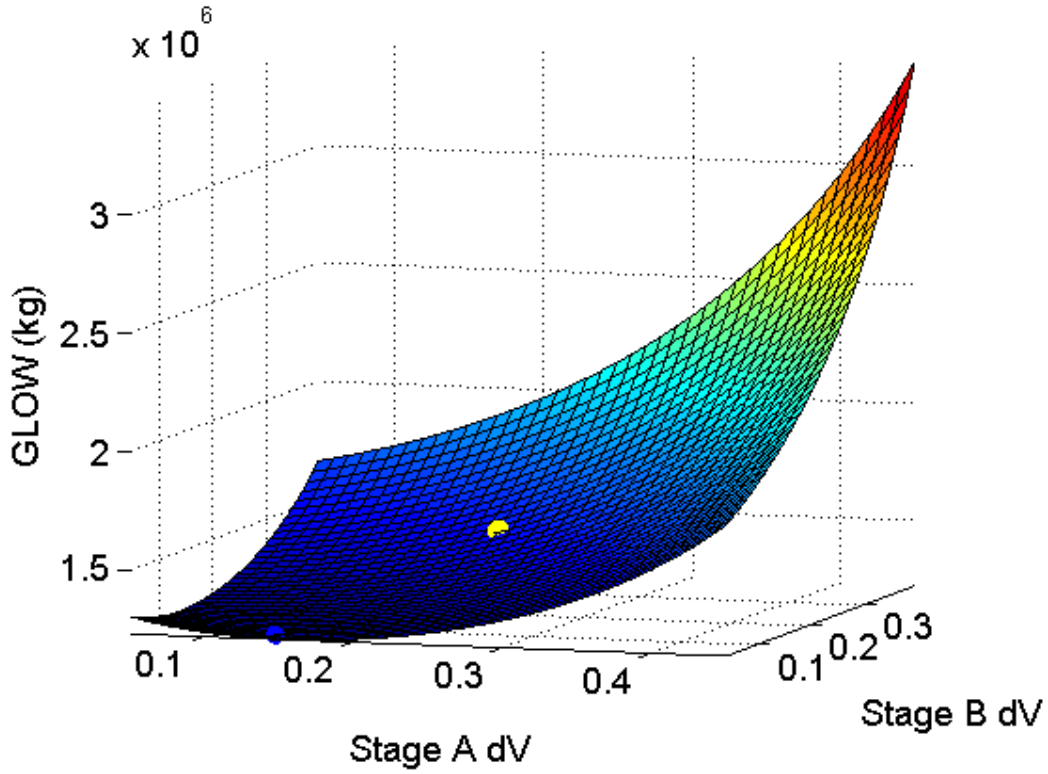

Figure 7.31. 2.5 Stage M550 60 mt Stability Surface for Case 13cb. Represented by yellow dot.

7.3.4a 2.5 Stage M550 FW3 Configuration Summary

A summary of the different payload configurations for a 2.5 stage vehicle using M550 FW3 boosters is displayed in Table 7.24. The use of this booster has proven to be favorable in terms of minimizing GLOW and also for bringing different payload masses to orbit. The M550 has introduced adaptability that is not achievable when using RSRM family boosters.

Table 7.24. 2.5 Stage M550 Vehicle Configuration Summary.

		Propellant		Engine					
Payload	GLOW	Stage 1	Stage 2	Booster		Stage 1		Stage 2	
mt	*kg*	*kg*	*kg*	*Type*	*#*	*Type*	*#*	*Type*	*#*
130	2994521	1180000	400000	M550 FW3	4	F-1A	2	J-2X	4
100	2354541	1180000	370000	M550 FW3	2	F-1A	2	SSME	2
60	1524120	682976	129263	M550 FW3	2	F-1A	1	J-2X	2

7.5 2.5 Stage P80 Vehicle

The next case begins with Configuration D in Table 7.1. This configuration is a 2.5 stage vehicle that uses the P80 strap on booster for additional thrust. A P80 is a small single segment booster similar to the M550 FW3 with a thrust profile displayed in Chapter 4. The thrust profile is approximately half of the M550, implying that a successful configuration will require a higher number of boosters than previous configurations to bring the vehicle to orbit. Using a large number of boosters has a significant advantage when designing launch vehicles. It allows the payload to be adjusted by removing or adding a booster. This was illustrated with the vehicle that used M550 boosters. The payload to orbit was modified from 130 mt to 100 mt by simply removing two boosters and performing other minor adjustments to the vehicle. The same principle with increased variability, should apply when using P80 boosters.

7.5.1 2.5 Stage P80 Vehicle Aerodynamic Coefficients

The aerodynamic drag properties for this vehicle are shown in Figure 7.32. This configuration is similar to the previous case in that it does not resemble the 2.5 stage vehicle used for the NASA tabulated wind tunnel data. Due to this, lift is assumed to be zero. Drag coefficient is assumed constant from M = 5 to the burnout condition.

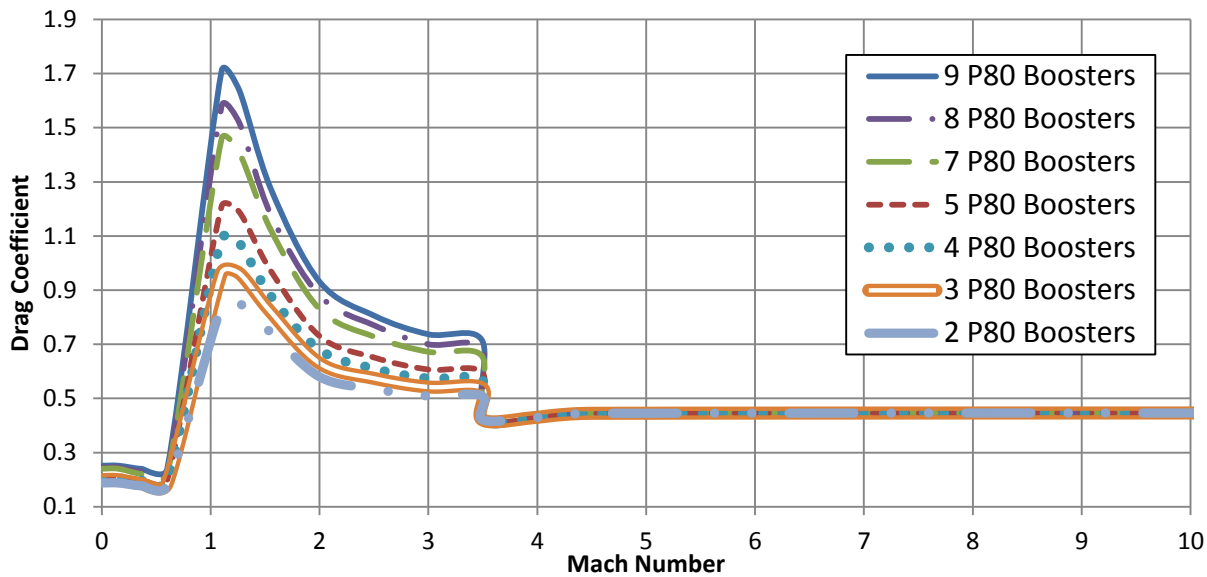

Figure 7.32. P80 Configuration Drag Coefficient Profile

7.5.2 2.5 Stage P80 General Analysis

The first step is to perform a general analysis of this configuration for the 130 mt payload configuration. Results of this analysis are shown in Table 7.25 for three configurations using seven, eight, and nine boosters. These booster configurations were chosen based on a few constraints. The first is the consideration of how many boosters can fit on the vehicle. Ten boosters approaches that limit, and as a result, the maximum considered here is nine. The lower limit is constrained by thrust to weight ratio. When the number of boosters decreases to six, the thrust to weight ratio is reduced to value that is not sufficient for bringing the vehicle to orbit. Another consideration for the lower limit is maintaining the high variability for this vehicle. High variability is maintained as long as there are sufficient boosters, and it is expected that decreasing below seven has an adverse effect on this variability.

Table 7.25. 2.5 Stage P80 General Analysis Top Configurations.

	Independent Variables						Burnout Conditions			
	Propellant Mass		Primary Pitch Event				Inertial Property			Max
	Stage 1	Stage 2	Start Time	Length	Pitchrate	GLOW	FPA	Velocity	Altitude	Q
Case	*kg*	*kg*	*s*	*s*	*deg/s*	*kg*	*deg*	*m/s*	*m*	*psf*
-	Booster: 7 P80		1st Stage Engine: 3 F-1A			2nd Stage Engine: 3 SSME				
1d	1150000	600000	7.2	12	-0.6	2690490	1.15	7524.4	396799	779
2d	1200000	600000	10.2	20	-0.6	2743681	0.92	7556.2	397706	752
3d	1250000	600000	11.2	18	-0.6	2796873	0.64	7589.8	396687	727
4d	1300000	550000	8.2	10	-0.6	2795717	2.25	7666.8	403872	741
5d	1350000	600000	12.2	12	-0.6	2903256	0.35	7627.2	399577	681
-	Booster: 8 P80		1st Stage Engine: 3 F-1A			2nd Stage Engine: 3 SSME				
6d	1050000	650000	6.2	19	-0.55	2733488	0.1	7462.1	399446	806
7d	1150000	600000	7.2	15	-0.65	2785523	0.99	7626.4	402702	795
8d	1200000	600000	9.2	19	-0.65	2838714	0.59	7672.5	398894	770
9d	1250000	600000	9.2	17	-0.6	2891906	0.44	7696.5	401346	745
10d	1300000	600000	6.2	13	-0.4	2945097	0.18	7725.6	399585	722
11d	1300000	650000	6.2	17	-0.3	2999445	-1.2	7625.4	397597	687
-	Booster: 9 P80		1st Stage Engine: 3 F-1A			2nd Stage Engine: 3 SSME				
12d	1050000	650000	6.2	15	-0.8	2828521	-0.74	7558	400692	817
13d	1100000	600000	6.2	19	-0.65	2827365	0.29	7692.1	397845	835
14d	1150000	600000	9.2	25	-0.65	2880556	0.08	7725.8	399988	808
15d	1150000	650000	8.2	21	-0.6	2934904	-1.22	7625.7	403793	766
16d	1200000	650000	7.2	17	-0.55	2988095	-1.47	7656.6	403893	743

For similar reasons, the number of stage one and two engines are not modified. Increasing the number of F-1A engines would push the vehicle past dynamic pressure limits, and decreasing them would result in low thrust to weight ratio. Remember from the M550 configuration, that it is possible to decrease the overall GLOW by increasing the ΔV fraction from the second stage. A high fraction is promoted by using configurations with more stage two engines. As a result, all three cases in Table 7.25 use no less than three SSMEs.

First consider the use of 7 P80 boosters to bring the vehicle to orbit. The top results of a general analysis for this configuration are represented by cases *1d-5d*. Case *1d* has an inertial velocity and flight path that is outside the specified bounds for the burnout conditions. These two deficiencies serve to indicate that there is not sufficient energy in terms of propellant to bring the vehicle to orbit. Notice that as propellant is added in both cases *2d* and *3d*, the vehicle begins to approaches the necessary burnout conditions but are still insufficient. It is not until case *4d* that the vehicle achieves necessary burnout velocity. The flight path angle for this case is outside of the necessary bounds which could be the result of two different issues. It is possible that the secondary pitch events used in this simulation do not correspond well with the actual vehicle. If this is the case, slight secondary pitchrate adjustments should bring the vehicle to the required flight path angle of 0.5 degrees. The other possibility is that the vehicle still has insufficient propellant within the stages. To determine this, a pitch analysis for case *4d* is shown in Figure 7.33.

The intersection groups for this case illustrate that the burnout flight path angle does not coincide with the other burnout conditions. For there to be a solution, all three curves must intersect on the plot. The flight path angle curve is offset from the rest. An attempt to correct this is made by slightly increasing the third and fourth secondary pitchrates. The results of this adjustment are shown in Figure 7.34.

The adjustment results in improved curve groups, but there is still a variable that is slightly offset. Notice that the altitude and flight path angle curves coincide very well, but the inertial velocity profile has shifted away from a solution. This velocity shift suggests that the cause is not a result of mismatched pitch properties but is related to the amount of energy contained in the propellant. A slight increase in propellant could bring the vehicle to the necessary burnout conditions.

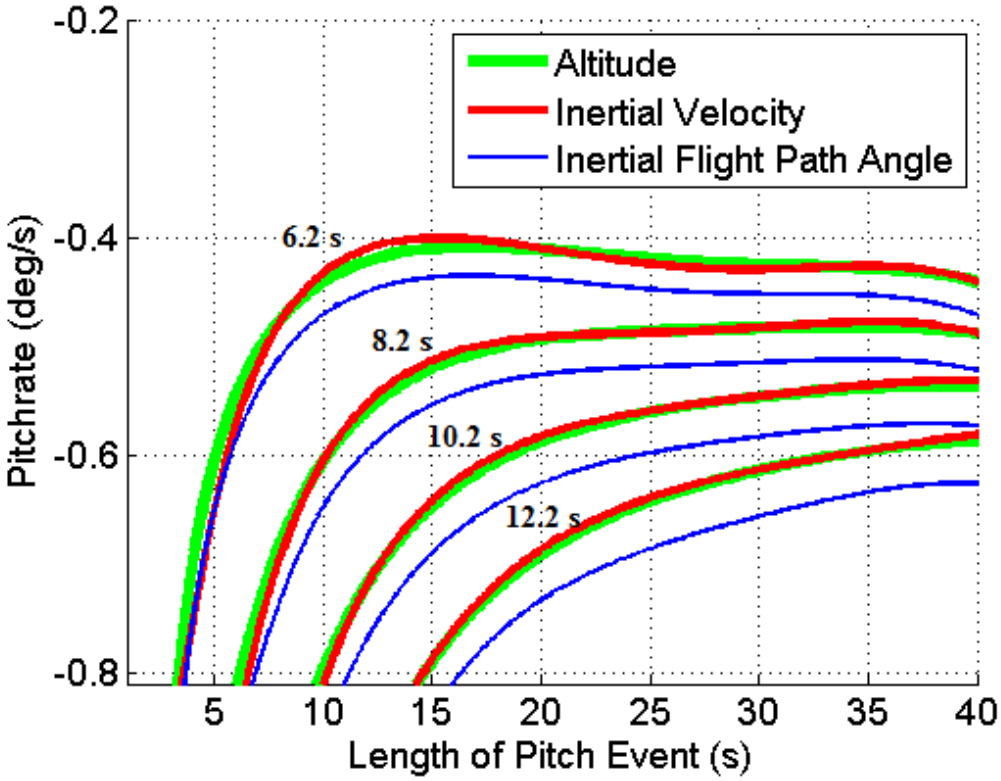

Figure 7.33. Case 4d Intersection Curves. Start time of 6.2 – 12.2 s.

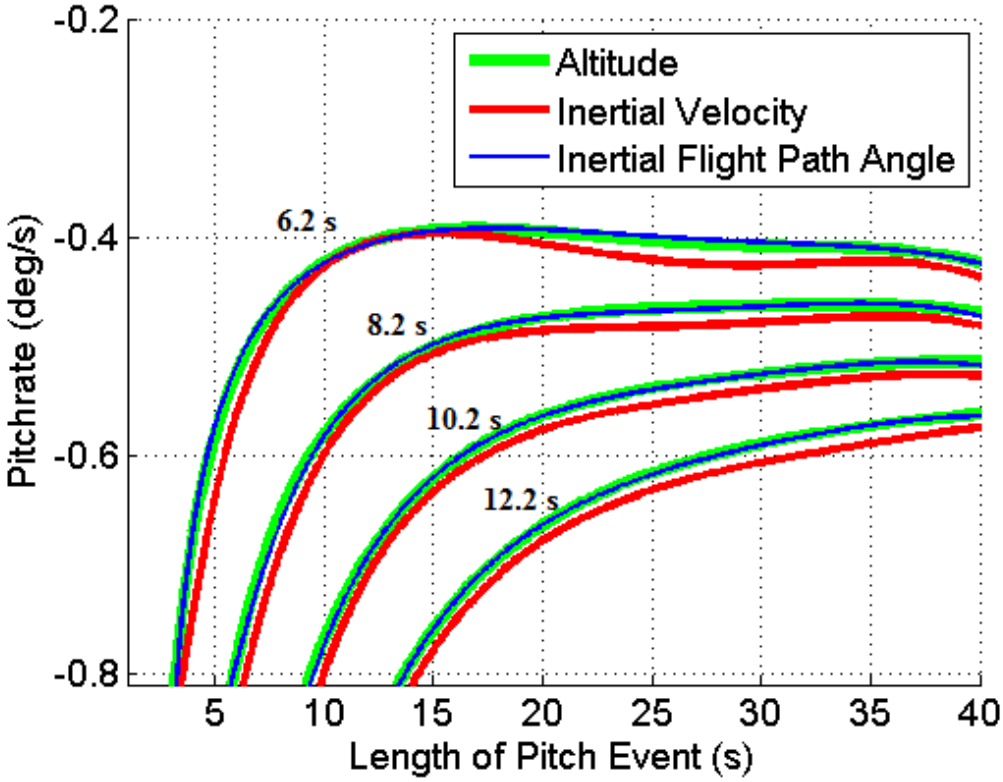

Figure 7.34. Case 4d Revised Intersection Curves. Start time of 6.2 – 12.2 s.

7.5.3 2.5 Stage P80 Refined Analysis

The next step is to perform a refined analysis around case *4d* to determine how the propellant should be adjusted to bring the vehicle to orbit. The results are shown in Table 7.26. The cases are arranged in order of increasing GLOW, and as such, it is easy to locate the case with minimized GLOW. To be considered a successful configuration the burnout velocity must be no less than 7631.7 m/s, the burnout flight path angle must be less than 0.5 deg, and the altitude no less than approximately 398000 m. The lightest case that meets all of these requirements is case *d4*. This is the configuration that minimizes GLOW for a 2.5 stage vehicle with 7 P80 boosters.

Table 7.26. 2.5 Stage 7 P80 GLOW Minimization Cases .

	Independent Variables						Burnout Conditions			
	Propellant Mass		Primary Pitch Event				Inertial Property			Max
	Stage 1	Stage 2	Start Time	Length	Pitchrate	GLOW	FPA	Velocity	Altitude	Q
Case	*kg*	*kg*	*s*	*s*	*deg/s*	*kg*	*deg*	*m/s*	*m*	*psf*
d1	1310000	520000	6.2	6	-0.6	2773746	0.34	7622.4	398610	751
d2	1320000	520000	6.2	18	-0.42	2784384	0.21	7632	396545	747
d3	1330000	520000	7.7	17	-0.48	2795023	0.22	7631.5	398245	741
d4	1320000	540000	6.7	13	-0.426	2806124	0.393	7638	398778	734
d5	1310000	550000	7.7	18	-0.45	2806355	0.08	7635.2	396102	732
d6	1320000	550000	8.7	13	-0.525	2816993	0.14	7631.2	398960	726
d7	1330000	550000	8.2	17	-0.45	2827631	0.06	7637.2	398103	722

Cases *6d-11d* are the top results of a vehicle with eight P80 boosters. The results illustrate how increasing the stage propellants affects the burnout conditions of the vehicle. Case *6d* is eliminated as a potential solution because the burnout velocity is well below the required burnout conditions and because the dynamic pressure is above 800 psf. To determine the source of this deficiency, the results of a pitch analysis are shown in Figure 7.35 for case *7d*. The curves in each start time group are relatively close together, but there are no intersection points. An attempt to correct this is made by increasing the secondary pitchrates in Figure 7.36.

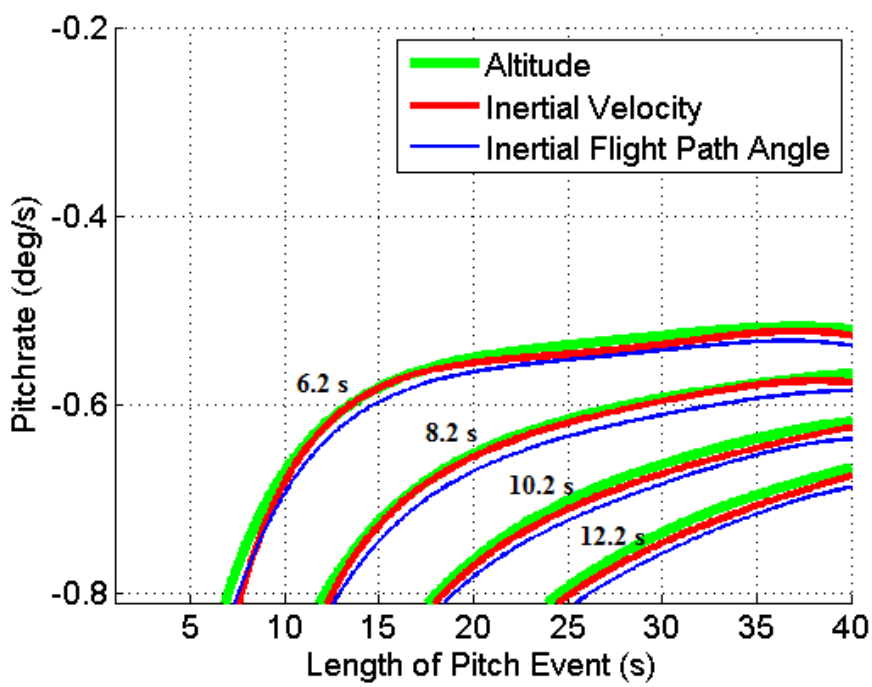

Figure 7.35. Case 7d Intersection Curves. Start time of 6.2 – 12.2 s.

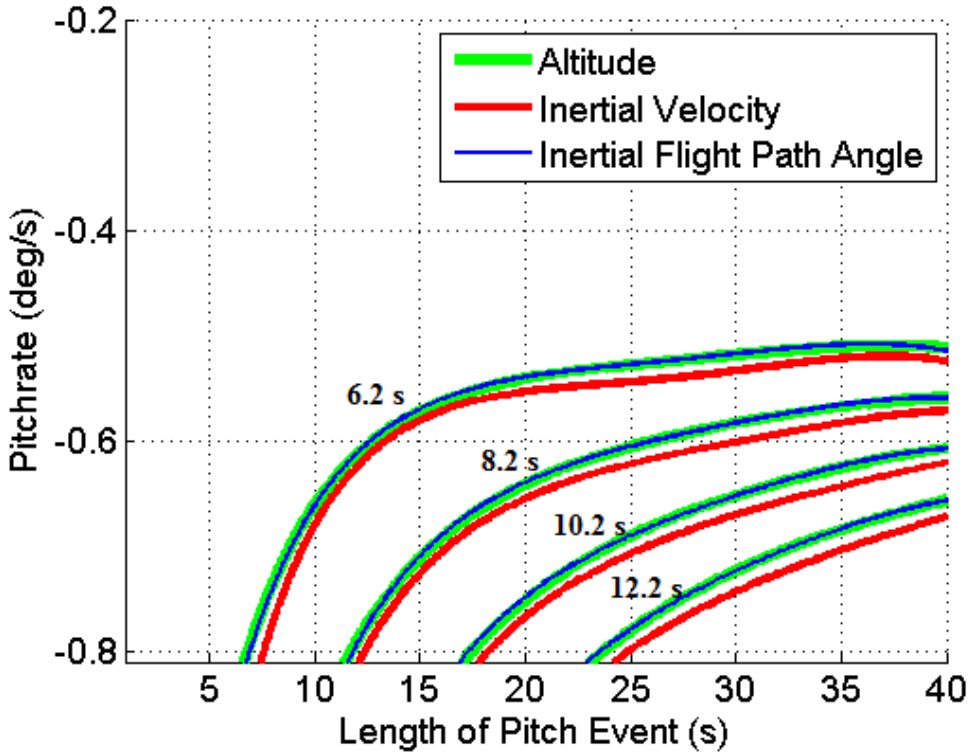

Figure 7.36. Case 7d Revised Intersection Curves. Start time of 6.2 – 12.2 s.

The adjustment corrects the burnout flight path angle but shifts the velocity curve away from the group. This indicates, just like case *4d*, the lack of intersection points is a result of insufficient propellant. Case *8d* is the next case and has a burnout velocity that is acceptable. A refined analysis between cases *7d* and *8d* should reveal a configuration that has the capability to bring the vehicle to orbit. The results of the analysis are in Table 7.27 and in order of increasing GLOW. When determining the minimized case for this configuration, it is also important to monitor dynamic pressure. Dynamic pressure here serves as a constraint, which rules out case *d1a*. The first to reach the necessary burnout conditions is case *d5a* which has a GLOW of approximately 2807 mt. This search has revealed the minimized GLOW case for the 2.5 stage vehicle with 8 P80 boosters.

Table 7.27. 2.5 Stage 8 P80 GLOW Minimization Cases .

	Independent Variables						Burnout Conditions			
	Propellant Mass		Primary Pitch Event				Inertial Property			Max
	Stage 1	Stage 2	Start Time	Length	Pitchrate	GLOW	FPA	Velocity	Altitude	Q
Case	*kg*	*kg*	*s*	*s*	*deg/s*	*kg*	*deg*	*m/s*	*m*	*psf*
d1a	1150000	590000	6.7	20	-0.6	2774653	0.88	7651	397617	804
d2a	1150000	600000	6.2	8	-0.74	2785523	0.61	7632.5	398459	796
d3a	1160000	600000	6.2	9	-0.68	2796161	0.47	7646.1	396057	791
d4a	1150000	610000	6.2	17	-0.54	2796393	0.4	7610.9	400714	787
d5a	1170000	600000	6.7	10	-0.68	2806800	0.47	7648.4	397466	785
d6a	1170000	610000	6.7	20	-0.53	2817669	0.37	7643.7	396308	777
d7a	1180000	610000	6.2	9	-0.61	2828307	0.34	7647.8	397112	772

The very last set of data in Table 7.25 is for the 2.5 stage vehicle with 9 P80 boosters. Case *14d* has a GLOW of 2881 mt and a maximum dynamic pressure of 808 psf. This implies that a successful case for this vehicle requires a GLOW that is greater than 2881 mt to maintain the dynamic pressure at acceptable levels. GLOW for this configuration is approximately 100 mt higher than others, eliminating it from the possible minimized cases.

The very last step is to compare the results of case *d5a* and *d4* to determine which best satisfies the condition for an optimized 2.5 stage vehicle. A comparison of the vehicle properties is shown in Table 7.28. Notice that GLOW for these two cases are within a few hundred kilograms of each other. A change in the number of boosters for this vehicle has not affected the overall GLOW, but does affect the size of the core. Notice the difference between the stage 1 and 2 propellant masses. Case *d4* has a total stage 1 and 2 propellant mass of 1860 mt while case *d5a* has a total of 1770 mt. Adding an extra booster has the effect of decreasing the size of the core by approximately 90 mt. This is advantageous when designing a vehicle with multiple payload requirements because a smaller core is well suited to the smaller payloads. Higher payloads can simply be achieved by attaching more boosters. A smaller core increases the potential variability of the vehicle. The last consideration is the vehicle stability with respect to the GLOW vs ΔV surface. The two surfaces are shown in Figures 7.37 and 7.38.

Table 7.28. 2.5 Stage P80 130 mt Payload Vehicle Selections.

		Propellant		Engine					
Case	GLOW	Stage 1	Stage 2	Booster		Stage 1		Stage 2	
-	*kg*	*kg*	*kg*	*Type*	*#*	*Type*	*#*	*Type*	*#*
d4	2806124	1320000	540000	P80	7	F-1A	3	SSME	3
d5a	2806800	1170000	600000	P80	8	F-1A	3	SSME	3

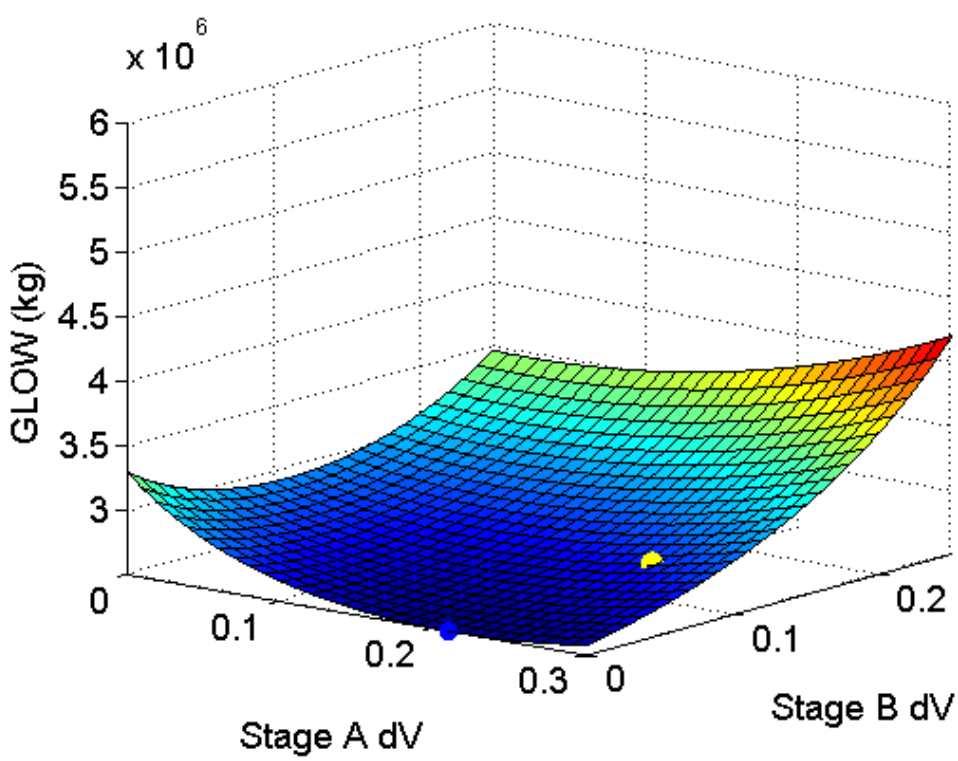

Figure 7.37. 2.5 Stage P80 Stability Surface for Case d4.

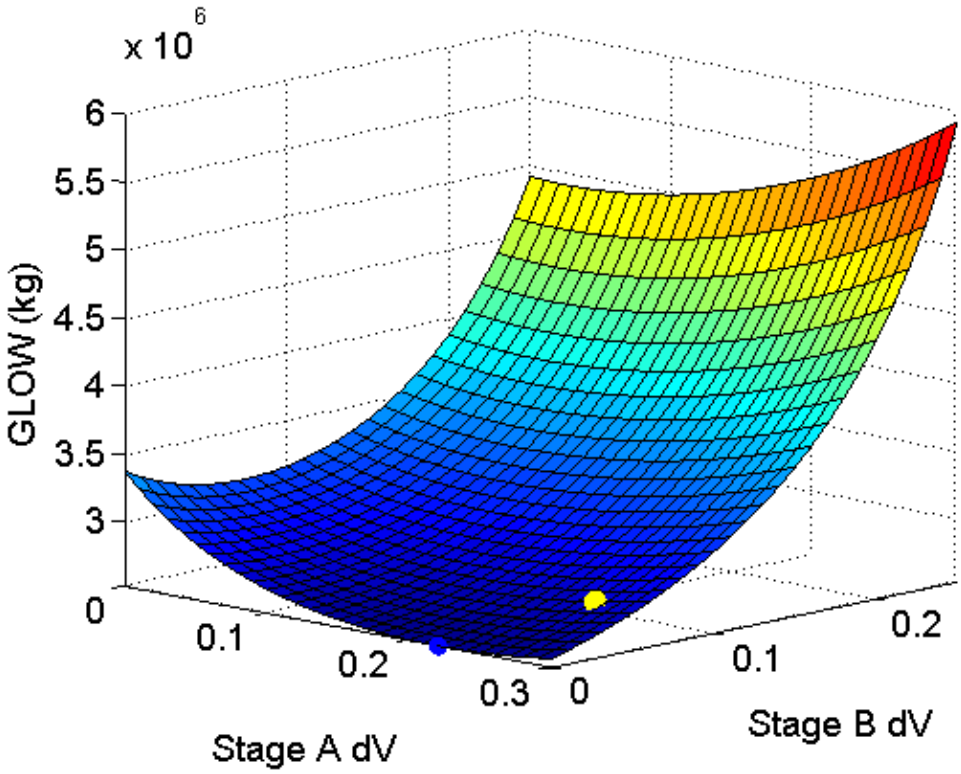

Figure 7.38. 2.5 Stage P80 Stability Surface for Case d5a.

The surface for case *d4* is graphically represented in Figure 7.37, and the surface for case *d5a* is shown in Figure 7.38. Overall, the surface for case *d4* has a shallower slope than the surface in case *d5a*. Generally, this would suggest that case *d4* is more stable as a vehicle in terms of GLOW versus ΔV. Notice though, that the yellow dot representing case *d5a* is closer to the minimum point on the surface than the point represented in Figure 7.37. As a result of this consideration, it is acceptable to assume that the stability of case *d5a* is very similar to case *d4* and can be assumed to be stable.

As stated earlier, the GLOW of these two cases is approximately equal, and as was just shown by the previous two figures, they have a very similar stability slope as well. The deciding factor then lies in using seven or eight P80 boosters. To promote variability for multiple payloads, the configuration selected as optimized for this particular vehicle is case *d5a* with eight boosters. The vehicle parameters and burnout conditions for this are described in Table 7.29. Dimensions have been adjusted to ensure the propellant fits within the dimensions, and the trajectory has been reevaluated based on the corrected dimensions. Angle of attack, dynamic pressure, and angle of attack*dynamic pressure are plotted in Figure 7.39 to ensure no limits were surpassed.

Table 7.29. 2.5 Stage P80 Configuration for 130 mt Payload.

	Length	Diameter	Propellant	Inert	Engine	# Engines	Burnout Alt	400000	m
130 mt	*m*	*m*	*kg*	*kg*	*(Shape)*	-	Burnout Vel	7646.1	m/s
Booster	10.00	2.99	705503	54762	P80	8	Burnout FPA	0	*deg*
Stage 1	31.34	7.60	1170000	74684	F-1A	3	Max Q	799.3	*psf*
Stage 2	55.90	7.60	600000	52177	SSME	3	GLOW	2806800	*kg*
Shroud	12.19	7.60	-	19674	Biconic	-	Start Pitch	6.7	*s*
Total	99.43	-	-	-	2.5 Stage	-	Pitch Length	10	*s*
Secondary Pitch Event Revision				3rd	-0.121536	*deg/s*	Pitchrate	-0.6847	deg/s
Secondary Pitch Event Revision				4th	-0.177588	*deg/s*			

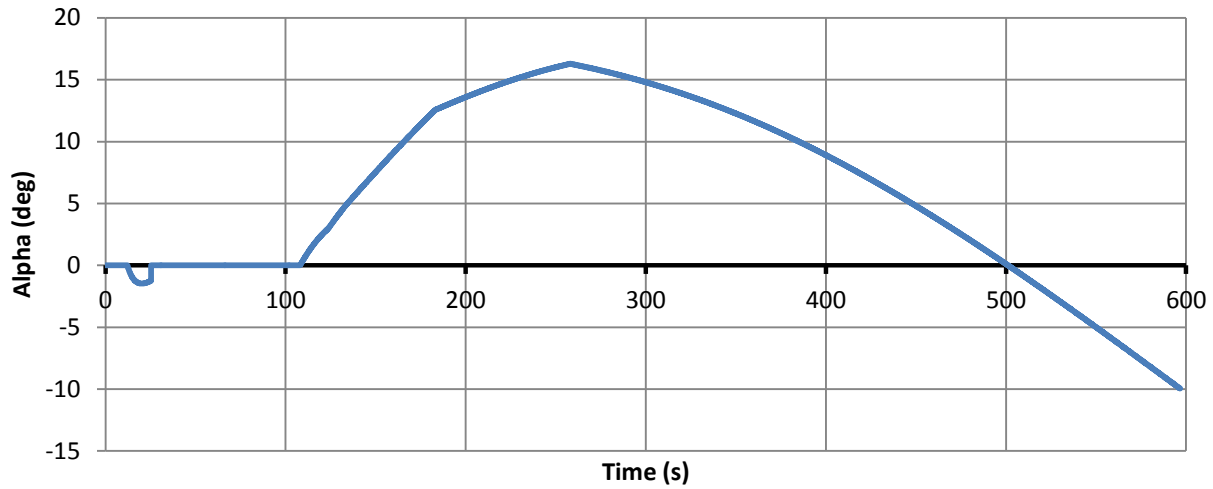

(a)

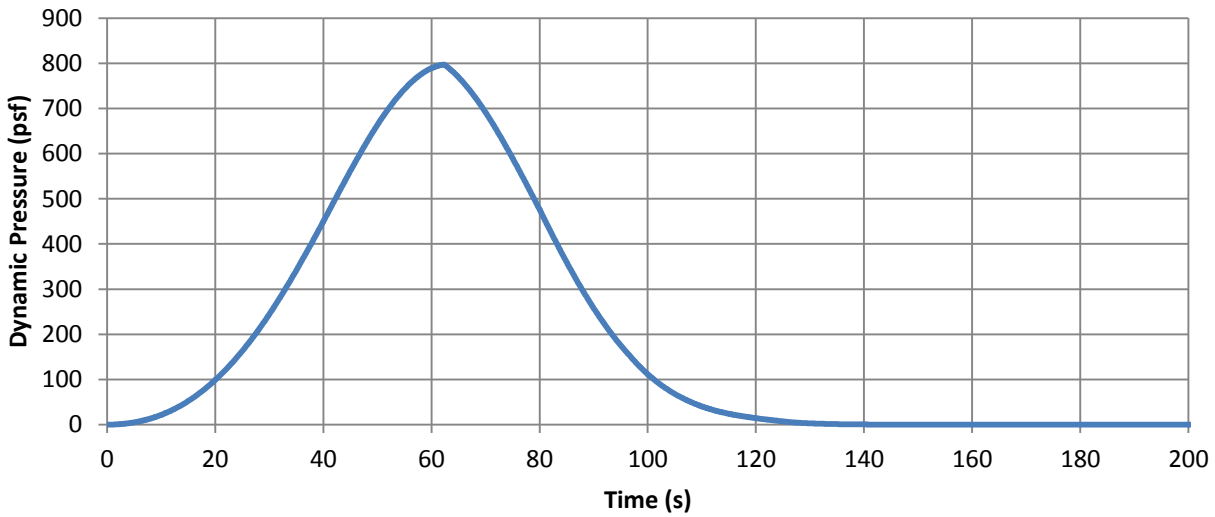

(b)

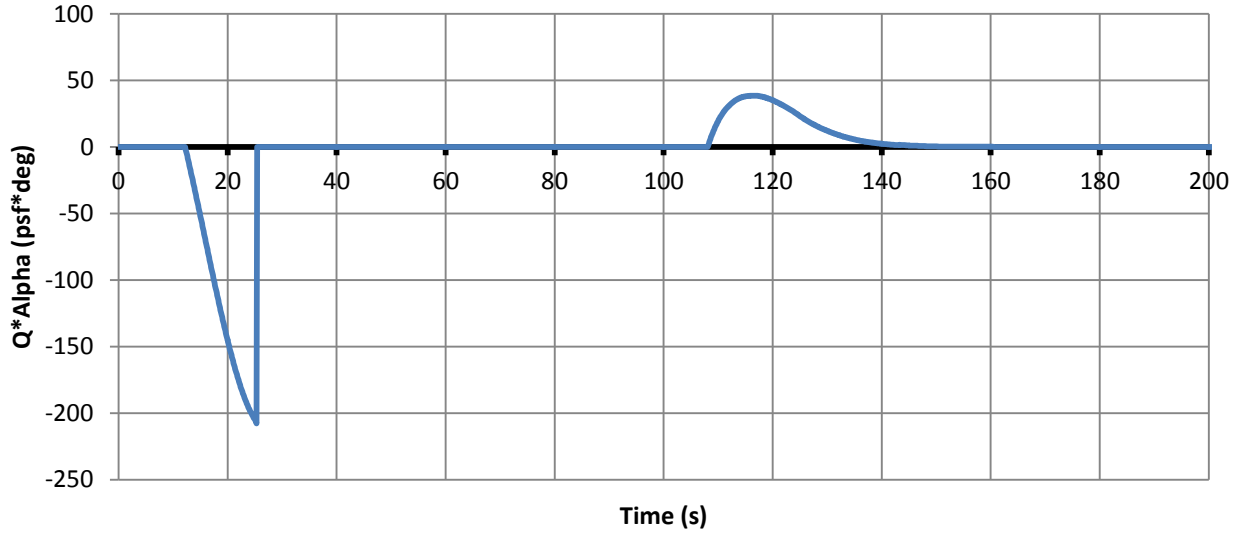

(c)

Figure 7.39. 2.5 Stage P80 Aerodynamic Limits Check.

7.5.4 100 mt Payload Requirement for 2.5 Stage P80 Vehicle

The goal in satisfying the lower payload requirements is to use a modified configuration of the vehicle described in Table 7.29. As discussed earlier, the modified configurations should minimize changes to the core of the vehicle by simply adjusting the number of boosters on the vehicle. If the booster adjustments cannot bring the payload to orbit, then modifications must be performed on stage 1 and 2. The P80 is a small booster and should support this booster variability for the different payloads.

Table 7.30 displays the results for different booster configurations run in THEO. Each of these cases is the exact same vehicle as described in Table 7.29 except for the number of boosters. Case *1dd* shows the results for five P80 boosters reaching altitude. A burnout velocity of 8003 m/s indicates the number of boosters should be further reduced. Case *2dd* uses one less P80 booster, and resultantly, the burnout velocity has shifted closer to the required burnout conditions. An attempt to remedy this high burnout condition is made in case *3dd* by removing one more booster. The burnout velocity here is corrected to the necessary burnout velocity. Also, note that the additional burnout conditions are met, and the maximum dynamic pressure is below the limit. This small procedure has shown that the vehicle can be adjusted without modifications to the core for a payload of 100mt. Lastly, a GLOW versus ΔV analysis is shown in Figure 7.40 to show that the vehicle lies on a relatively shallow portion of the surface.

Table 7.30. 100 mt Derivative of 2.5 Stage P80 Vehicle.

		Propellant		Engine						ΔV		Burnout Condition			Max
Case	GLOW	Stage 1	Stage 2	Booster		Stage 1		Stage 2		Req	Avail	Vel.	Alt.	FPA	Q
-	*kg*	*kg*	*kg*	*Type*	*#*	*Type*	*#*	*Type*	*#*	*m/s*	*m/s*	*m/s*	*km*	*deg*	*psf*
1dd	2491700	1170000	600000	P80	5	F-1A	3	SSME	3	9711	10053	8003	401	0.02	755
2dd	2396667	1170000	600000	P80	4	F-1A	3	SSME	3	9782	9966	7845	399	0.176	727
3dd	2301634	1170000	600000	P80	3	F-1A	3	SSME	3	9885	9875	7650	400	0.286	692

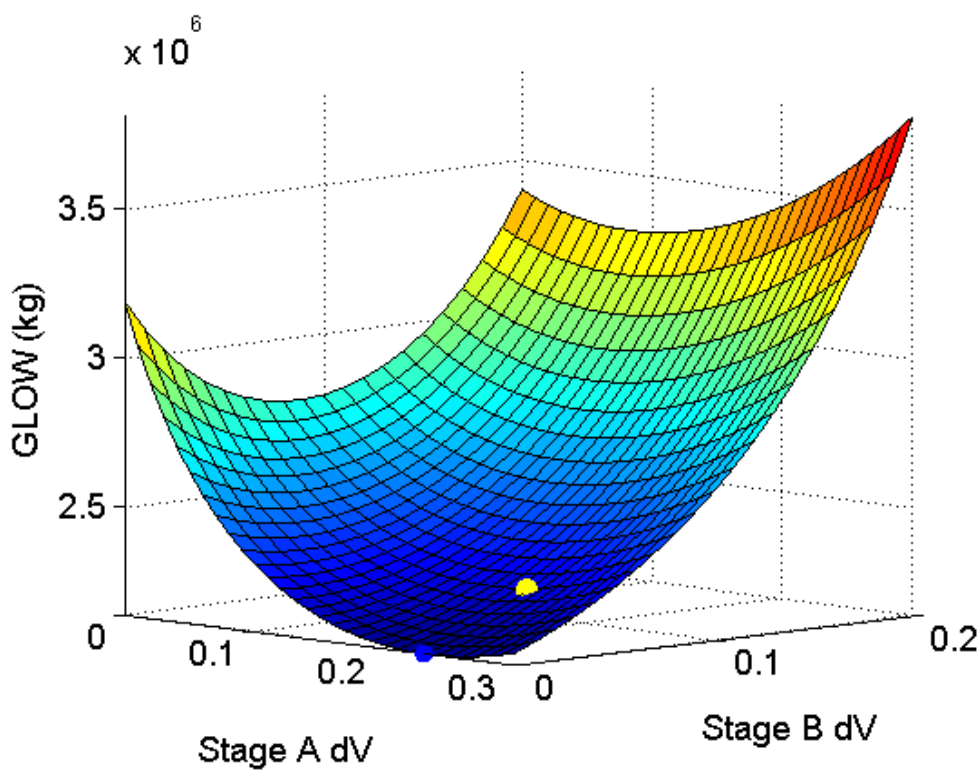

Figure 7.40. 2.5 Stage P80 100 mt Stability Surface for Case 3dd. Represented by yellow dot.

7.5.5 60 mt Payload Requirement for 2.5 Stage P80 Vehicle

A similar process is performed on the 60 mt payload requirement as shown in Table 7.31. In an attempt to preserve the core configuration, Case *1de* removes one more booster from case *3dd* described in Table 7.30. Both burnout altitude and flight path angle meet required conditions, but burnout velocity is approximately 1000 m/s past the required orbital speed. This indicates that the configuration must be further reduced. The next step removes the remaining two boosters, which leaves a two stage vehicle described in case *2de*. To provide a sufficient thrust to weight ratio, this configuration requires the addition of one stage 1 engine. Evaluation of this configuration with THEO reveals a burnout velocity of 8941 m/s which is approximately 1000 m/s over the necessary value. Also, notice the high maximum dynamic pressure for this case. Since the number of stage 1 engines cannot be reduced, the only solution to this high dynamic pressure would be a considerable increase in the weight of the vehicle. The results of these two cases indicate that the payload cannot be brought to orbit by simply modifying the number of boosters. Orbit can only be reached by performing modifications to the core.

Table 7.31. 60 mt Derivative of 2.5 Stage P80 Vehicle.

		Propellant		Engine						ΔV		Burnout Condition			Max
Case	GLOW	Stage 1	Stage 2	Booster		Stage 1		Stage 2		Req	Avail	Vel.	Alt.	FPA	Q
-	*kg*	*kg*	*kg*	*Type*	*#*	*Type*	*#*	*Type*	*#*	*m/s*	*m/s*	*m/s*	*km*	*deg*	*psf*
1de	2166601	1170000	600000	P80	2	F-1A	3	SSME	3	9841	10982	8798	401	-0.1	691
2de	1976536	1170000	600000	-	-	F-1A	4	SSME	3	9497	10779	8942	400	0.167	1097
3de	1362080	731015	305475	P80	2	-	-	-	-	9850	-	-	-	-	-
4de	1379457	731014	305475	P80	2	F-1A	2	SSME	2	9594	9759	7827	400	0.416	857
5de	1417218	815127	268048	P80	2	-	-	-	-	9850	-	-	-	-	-
6de	1428257	815127	268048	P80	2	F-1A	2	SSME	2	9635	9786	7812	400	0.212	812
7de	1438049	818599	273993	P80	2	-	-	-	-	9815	-	-	-	-	-
8de	1438411	818599	273993	P80	2	F-1A	2	SSME	1	9778	9822	7700	401	0.116	778

As a two stage vehicle would not be a good fit for this particular vehicle, the next cases are 2.5 stage vehicles with two boosters. This overcomes the need for four F-1A engines and also reduces the maximum dynamic pressure substantially. Performing a velocity budget analysis with an initial ΔV assumption of 9850 m/s reveals the propellant requirements shown in case *3de*. These propellants are then run in THEO with the results shown in case *4de*. Burnout velocity is much improved from the previous cases, but is still excessive. This is mostly likely due to the high thrust to weight ratio indicated by the high maximum dynamic pressure. GLOW of the vehicle is increased in case *5de* by performing a ΔV analysis with an increased velocity contribution from the first stage. The stage propellant requirements are then run in THEO with the results in case *6de*. The propellant adjustment decreases the maximum dynamic pressure and also shifts the burnout velocity closer to the required conditions. To further improve the burnout condition, the ΔV assumption is decreased to 9815 m/s, and the ΔV fraction for stage 1 is again increased slightly in case *7de*. Propellant requirements from this adjustment are then run in THEO revealing a configuration that is capable of achieving orbit at the required altitude.

The configuration described in case *8de* necessary for 60 mt payload required some substantial modifications from the original vehicle. Modifications were shown to be necessary as the cases *1de* and *2de* were excessive in terms of reaching orbital conditions. Notice also the decrease in GLOW that is a result of using case *8de* instead of case *2de* or *1de*.

To show the stability of the vehicle, the GLOW versus ΔV analysis is shown in Figure 7.41. The location of this vehicle is on a relatively shallow portion of the surface indicating that it is sufficient in terms of GLOW stability and velocity contribution.

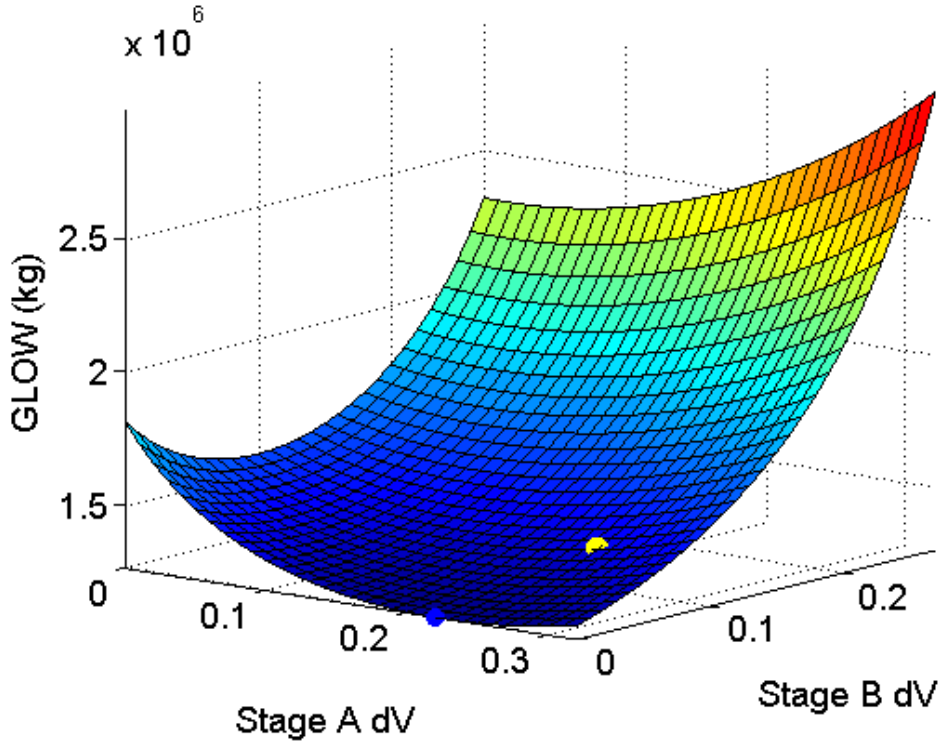

Figure 7.41. 2.5 Stage P80 60 mt Stability Surface for Case 8de. Represented by yellow dot.

7.5.6 2.5 Stage P80 FW3 Configuration Summary

A summary of the different payload configurations for a 2.5 stage vehicle using P80 boosters is displayed in Table 7.32. The use of this booster has proven to provide increased variability when minimizing GLOW and also for bringing different payload masses to orbit. The P80 has improved the vehicle adaptability to different payloads, and revealed configurations with the lowest GLOW.

Table 7.32. 2.5 Stage P80 Vehicle Configuration Summary.

		Propellant		Engine					
Payload	GLOW	Stage 1	Stage 2	Booster		Stage 1		Stage 2	
mt	*kg*	*kg*	*kg*	*Type*	*#*	*Type*	*#*	*Type*	*#*
130	2806800	1170000	600000	P80	8	F-1A	3	SSME	3
100	2396667	1170000	600000	P80	3	F-1A	3	SSME	2
60	1438411	818599	273993	P80	2	F-1A	2	SSME	1

7.6 2 Stage Vehicle

Configuration E from Table 7.1 is a 2 stage vehicles similar to the Saturn V rocket used for the Apollo missions. The Saturn V is technically classified as a 3 stage vehicle, but uses only two of the stages to bring the vehicle to a low earth orbit (LEO). The third stage is associated with the trajectory from LEO to the parking orbit, and then on to the moon. The payload to LEO can be considered the entire third stage.

7.6.1 2 Stage Vehicle Aerodynamic Coefficients

The aerodynamic drag properties for this vehicle are shown in Figure 7.42. This configuration is similar to the previous case in that it does not resemble the 2.5 stage vehicle used for the NASA tabulated wind tunnel data. Due to this, lift is assumed to be zero. Drag coefficient is assumed constant from M = 5 to the burnout condition.

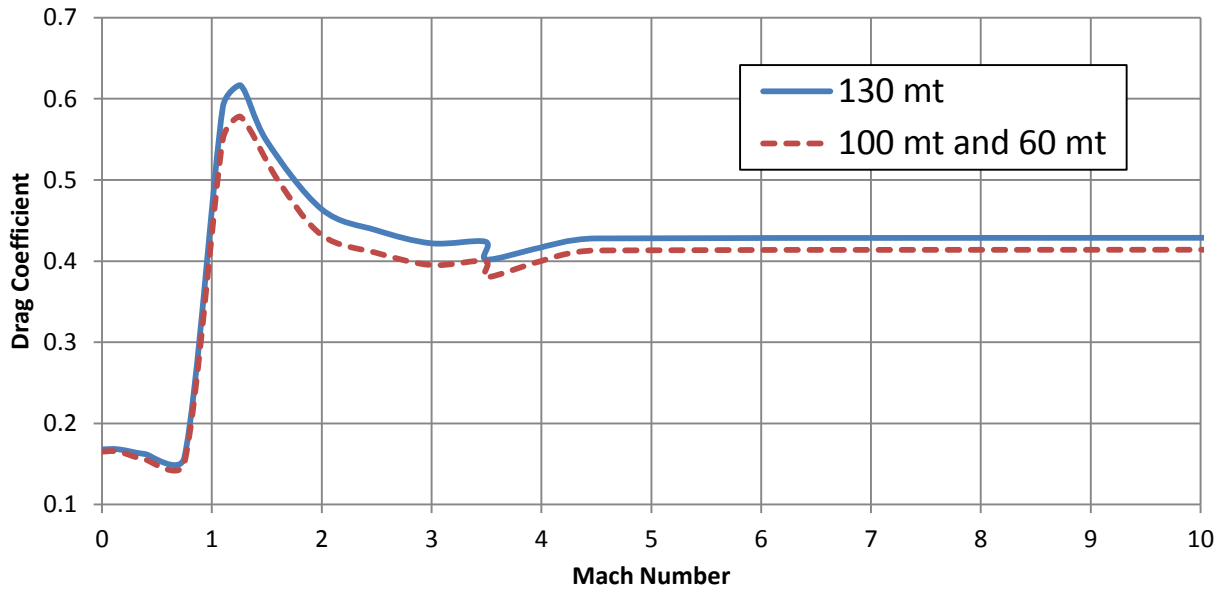

Figure 7.42. 2 Stage Configuration Drag Coefficient Profile.

7.6.2 2 Stage General Analysis

A 2 stage vehicle increases the simplicity of the vehicle and the optimization by eliminating a portion of the trajectory where two separate propulsion systems burn simultaneously. The top results of a general analysis for a 2 stage vehicle are shown in Table 7.33. For this configuration the vehicle has 5 F-1A first stage engines and 5 J-2X second engines. The selection of the number of first stage engines is driven by two factors. If the number of engines is increased above five, maximum dynamic pressure values are considerably past 800 psf. Likewise, stage 1 engines less than five result in an insufficient thrust to weight ratio, and the vehicle falls back to the planet shortly after liftoff. Remember from a previous discussion, that a high ΔV contribution from the second stage promotes a lower GLOW. In an attempt to utilize this concept, there are as many stage two engines on the vehicle that can fit.

Table 7.33. 2 Stage General Analysis Top Configurations.

	Independent Variables						Burnout Conditions			
	Propellant Mass		Primary Pitch Event				Inertial Property			
	Stage 1	Stage 2	Start Time	Length	Pitchrate	GLOW	FPA	Velocity	Altitude	Max Q
Case	*kg*	*kg*	*s*	*s*	*deg/s*	*kg*	*deg*	*m/s*	*km*	*psf*
1e	1750000	650000	8.2	17	-0.6	2717908	1.72	7685.4	402697	919
2e	1800000	650000	7.2	5	-0.65	2771099	1.58	7721	403492	887
3e	1800000	700000	13.2	15	-0.65	2825447	0.23	7629.7	396385	835
4e	1850000	700000	10.2	17	-0.4	2878639	0.05	7666.5	396091	808
5e	1900000	700000	6.2	15	-0.2	2931830	0.02	7682	400092	780
6e	1950000	700000	10.2	11	-0.3	2985022	-0.1	7713.1	400832	755

Cases *1e-4e* can bring the payload to orbit, but notice that the maximum dynamic pressure is high. The first case with an acceptable maximum dynamic pressure is case *5e*. Increasing GLOW from case *1e* is necessary to decrease the thrust to weight ratio and reduce the dynamic pressure to an acceptable value. This indicates that finding a minimized GLOW case for this configuration is constrained by maximum dynamic pressure. A balance between maintaining an acceptable dynamic pressure and minimizing GLOW suggests that the optimized case exists in between case *4e* and *5e*. A pitch check of case *5e* is shown in Figure 7.43 to ensure pitch stability.

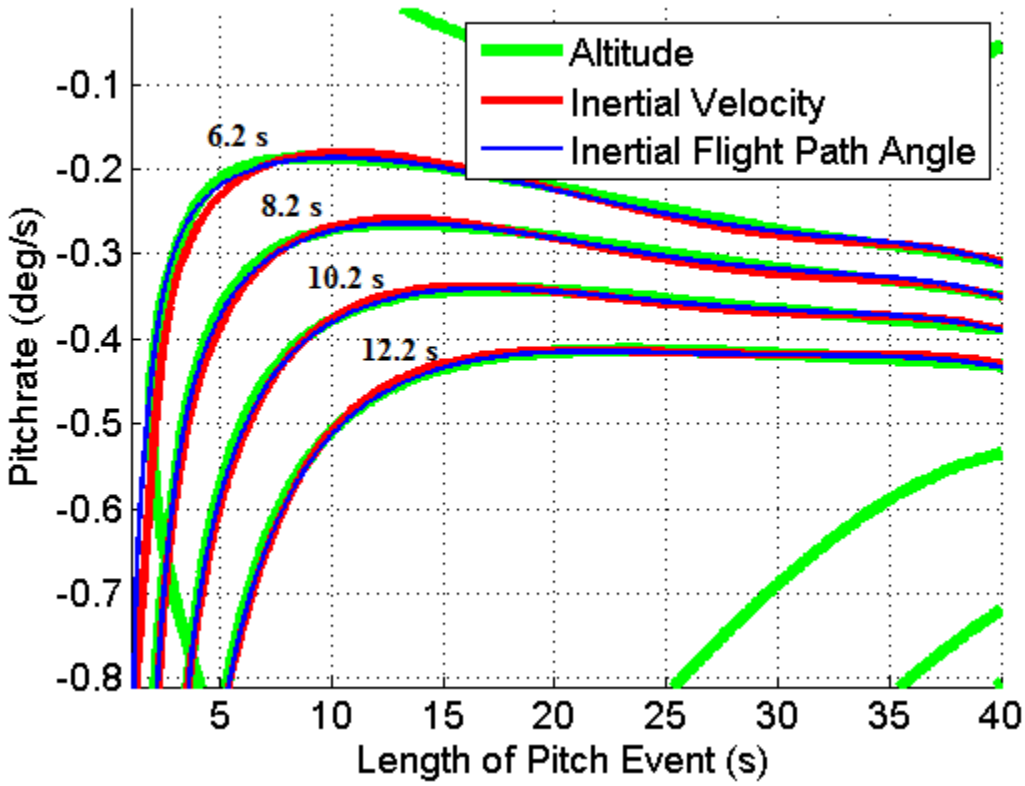

Figure 7.43. Case 5e Intersection Curves. Start time of 6.2 s to 12.2 s.

7.6.3 2 Stage Refined Analysis

Performing a refined analysis around cases *4e* and *5e* yields the results shown in Table 7.34. The cases are arranged in order of increasing GLOW and decreasing maximum dynamic pressure. As discussed earlier, the minimized case should be the first configuration to retain acceptable maximum dynamic pressure values. Case *e3* fulfills this condition but has a low burnout velocity. Moving to case *e4* remedies this deficiency, and provides a case that meets the required burnout conditions. A pitch analysis in Figure 7.44 of case *e4* reveals that the pitch properties are well suited to this vehicle. This process has revealed an optimized case for the 2 stage 130 mt payload configuration, and the parameters and final vehicle properties are shown in Table 7.35. To verify that the vehicle does not overshoot aerodynamic properties, angle of attack, dynamic pressure, and angle of attack*dynamic pressure profile are shown for the trajectory in Figure 7.45a-c.

Table 7.34. 2 Stage GLOW Minimization Cases.

	Independent Variables						Burnout Conditions			
	Propellant Mass		Primary Pitch Event				Inertial Property			
	Stage 1	Stage 2	Start Time	Length	Pitchrate	GLOW	FPA	Velocity	Altitude	Max Q
Case	*kg*	*kg*	*s*	*s*	*deg/s*	*kg*	*deg*	*m/s*	*km*	*psf*
e1	1850000	690000	6.2	5	-0.3	2867769	0.44	7673.2	401701	816
e2	1850000	700000	8.7	11	-0.35	2878639	0.29	7643.8	403333	806
e3	1850000	710000	10.2	9	-0.45	2889508	-0.08	7632.7	398142	798
e4	1870000	700000	12.2	13	-0.5	2899915	0.15	7662.9	401208	796
e5	1860000	710000	8.2	21	-0.3	2900147	-0.04	7632.9	400219	792
e6	1880000	700000	11.2	9	-0.5	2910554	0.12	7670.5	401034	791
e7	1890000	700000	8.7	19	-0.3	2921192	0.16	7670.1	402926	785
e8	1900000	700000	10.2	7	-0.45	2931830	0.05	7682	400864	780
e9	1900000	710000	12.2	17	-0.4	2942700	-0.14	7657.2	401127	771

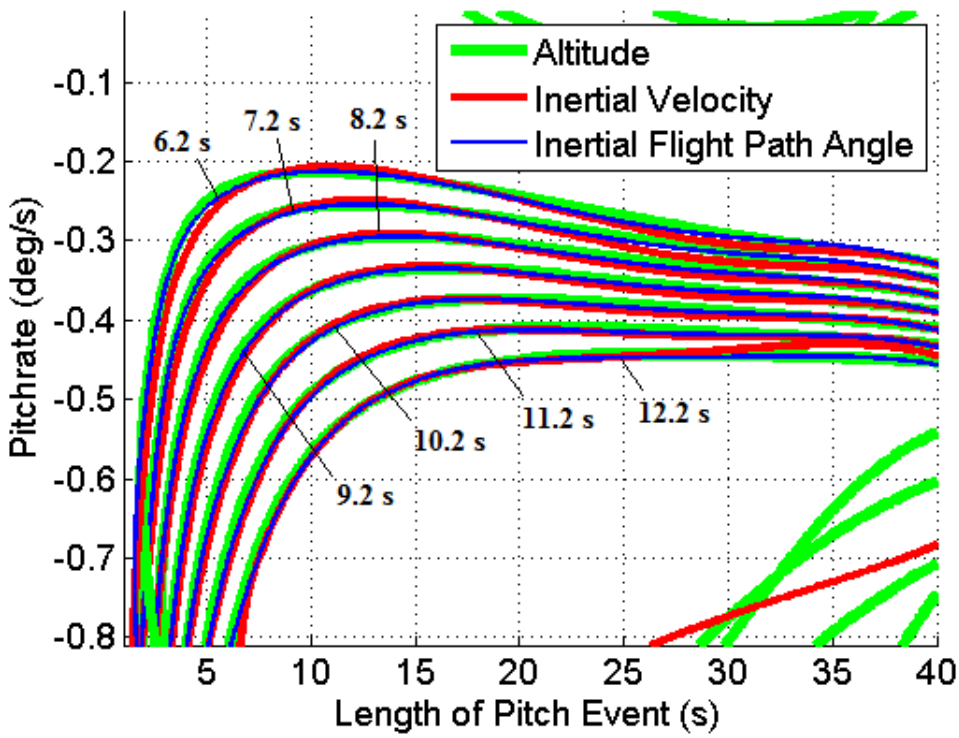

Figure 7.44. Case e4 Intersection Curves. Start time of 6.2 s – 12.2 s.

Table 7.35. 2 Stage Configuration for 130 mt Payload.

	Length	Diameter	Propellant	Inert	Engine	# Engines	Burnout Alt	399999	m
130 mt	*m*	*m*	*kg*	*kg*	*(Shape)*	-	Burnout Vel	7667	m/s
Stage 1	36.30	8.78	1870000	119367	F-1A	5	Burnout FPA	0.0305	*deg*
Stage 2	50.60	8.78	700000	60875	J-2X	5	Max Q	797.2	*psf*
Shroud	12.19	8.78	-	19674	Biconic	-	GLOW	2899915	*kg*
Total	99.09	-	-	-	2 Stage	-	Start Pitch	12.2	*s*
							Pitch Length	13	*s*
Secondary Pitch Event Revision				4th	-0.153722	*deg/s*	Pitchrate	-0.5010	deg/s

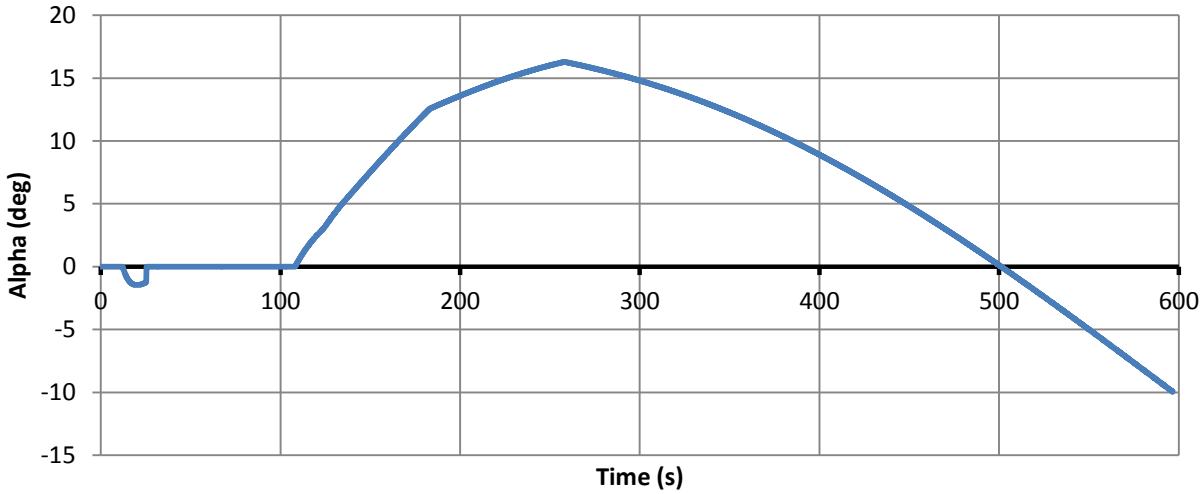

(a)

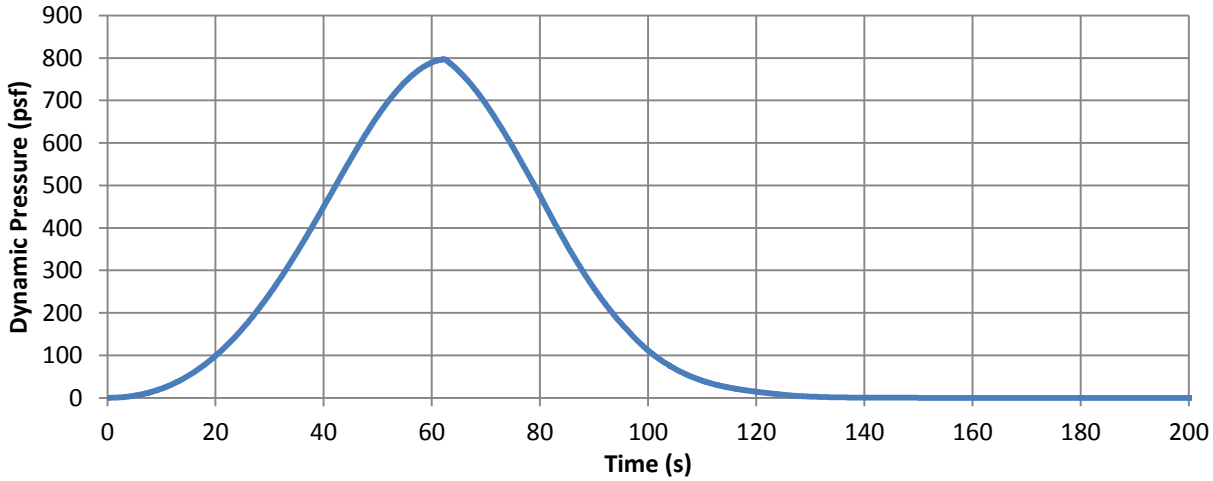

(b)

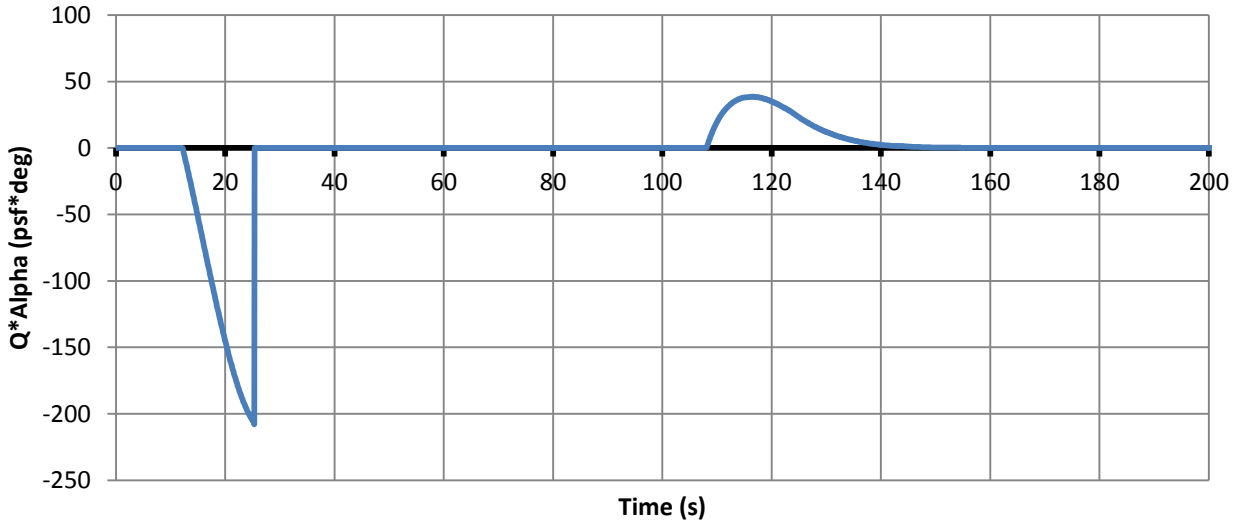

(c)

Figure 7.45a-c. 2 Stage Aerodynamic Limits Check.

Figure 7.46 shows the GLOW versus ΔV stability for the optimized case described in Table 7.35. The location of case *e4* is signified by the red point. Notice that the point is slightly offset from the curve. This is likely due to the simplicity of this ΔV tool. A velocity budget analysis is a simple method for predicting the propellant necessary to bring a payload to orbit as a function of the total ΔV (Humble, Henry, & Larson, 1995). As mentioned in an earlier section, this requires assumptions that can be a source of error when comparing to data generated with a trajectory simulation tool. In spite of the error, it is advantageous to consider the curve in Figure 7.46 as it represents a general idea as to the overall stability of this particular configuration.

For comparison, the velocity budget curve for the Saturn V is shown in Figure 7.47 (Saturn Flight Evaluation Working Group, 1973). The two vehicles have a lot of similarities conceptually, but notice the differences between these two curves. Both profiles have a similar minimum GLOW, but the overall curve for case *e4* has a shallower slope. The vehicle in Figure 7.46 is much closer to the minimum, and as a result it can carry more payload than the Saturn V with less propellant. Table 7.36 shows a comparison of the two vehicles. One of the most significant factors for the improvement over the Saturn V is the engine properties. These ΔV curves suggest that upgrading thrust and specific impulse significantly improves the performance and capability of the vehicles described here.

Table 7.36. Saturn V and 2 Stage Vehicle Comparison.

					Stage 1		Stage 2	
Vehicle	GLOW	Payload	Altitude	ΔV Required	Thrust/eng	I_{sp}	Thrust/eng	I_{sp}
-	*kg*	*kg*	*km*	*m/s*	*N*	*s*	*N*	*s*
Saturn V	3039000	120000	180 - 440	9312	7590000	263	1023000	424
2 Stage	2899739	130000	400	9671	8896440	300	1310000	448

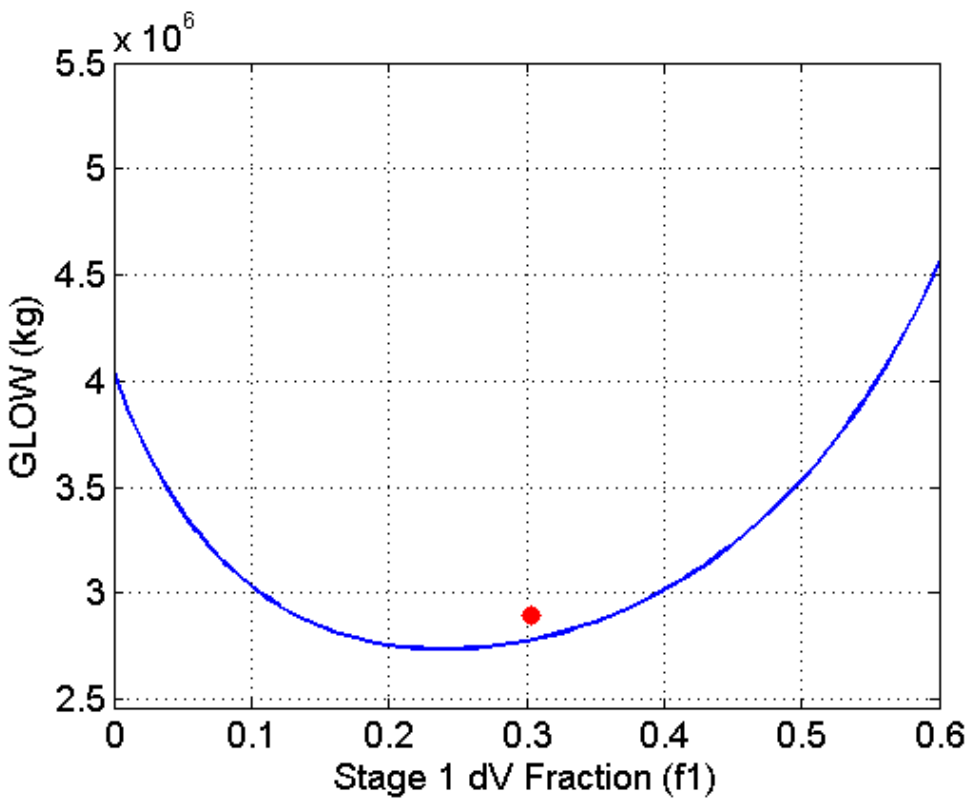

Figure 7.46. 130 mt 2 Stage Vehicle Stability. Variation of GLOW with 1st stage ΔV.

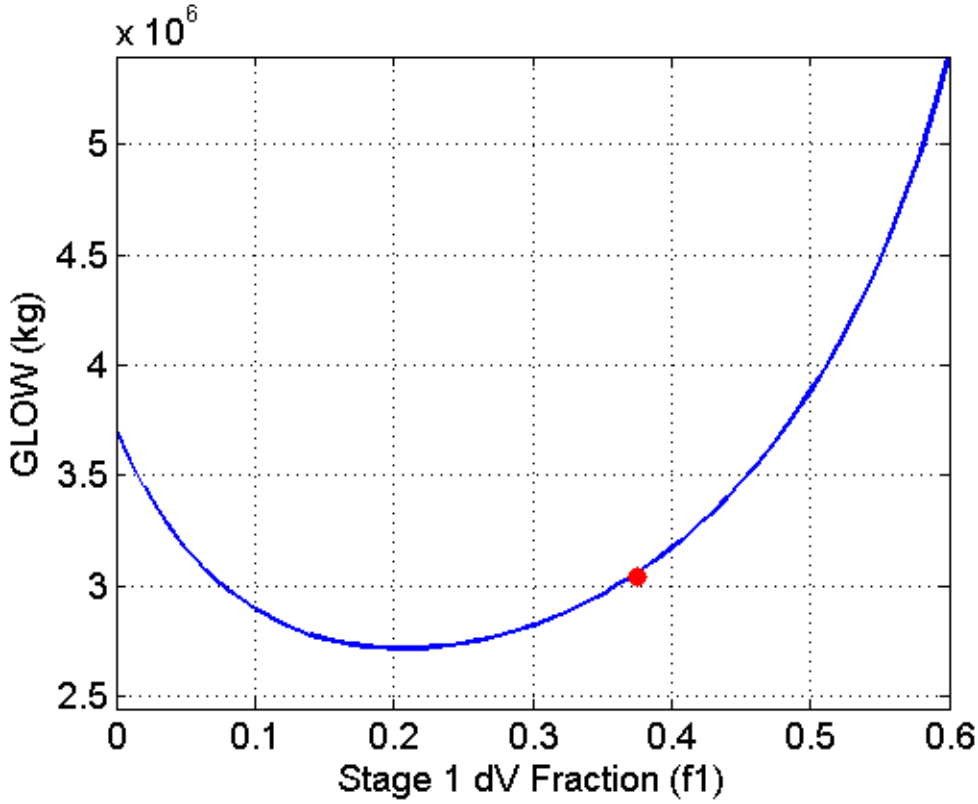

Figure 7.47. Saturn V Vehicle Stability. Variation of GLOW with 1st stage ΔV.

7.6.4 100 mt Payload Requirement for 2 Stage Vehicle

This two stage configuration is treated differently than the previous configuration. The 2.5 stage vehicles were designed to have high adaptability for different payloads based on booster adjustments. Two stage vehicles do not have this capability of being able to increase or decrease thrust based on booster addition or removal. As a result, the 2 stage versions for 100 mt and 60 mt payload are not necessarily variants. Minimizing changes to the vehicle is very difficult because the stage one and two propellant tanks must be modified to fit the different payloads to this vehicle. The only similarity is that there is an attempt to use the same engines as the 130 mt configuration.

The 100 mt and 60 mt payload configurations follow a similar method as the previous derivatives. The process is described with the cases in Table 7.37. Case *1ea* displays the results of a velocity budget analysis for the minimum propellant requirements with an initial total ΔV guess of 9800 m/s. The number of stage one engines has been reduced from five to four to maintain an acceptable maximum dynamic pressure and cannot be decreased below four to ensure adequate thrust to weight ratios. Running case *1ea* propellant requirements in THEO is shown in case *2ea*. All burnout conditions are met except for inertial velocity. This is a result of insufficient energy available in the vehicle and is remedied by increasing the velocity contribution (f_1) of the first stage from 0.24 to 0.3.

New propellant requirements are shown in case *3ea*, and evaluated in THEO as shown in case *4ea*. All burnout conditions are met, but notice the high maximum dynamic pressure of 863 psf. Since the number of stage one engines cannot be adjusted the only way to remedy this is to decrease the thrust to weight ratio by increasing GLOW. An adjustment is made in case *5ea* by shifting f_1 to 0.35. The new propellant requirements are then simulated in THEO with the results shown in case *6ea*. Maximum dynamic pressure is still high at 837 psf, indicating f_1 should be increased even further. Also, notice in case *6ea* that the burnout velocity is excessive, implying that a solution might be determined by decreasing the estimated total ΔV. The results of the reevaluated propellants with a new ΔV and f_1 are shown in case *7ea*. As displayed in case *8ea*, these adjustments reduce the

maximum dynamic pressure to acceptable values, but the burnout velocity is still high. This is remedied in case *9ea* by throttling the stage two engines to 84% thrust.

This process has led the analysis to the first case that is capable of reaching burnout conditions and fulfilling maximum dynamic pressure constraints. Determining the minimized case for the 100 mt configuration is difficult as it is hard to balance the high thrust output of the F-1A with the minimized weight of the vehicle. Notice the difference in GLOW between case *1ea* and *9ea* that is necessary due to the high thrust. A possible solution to this issue would be to throttle the F-1A, but it is currently unknown if it has that capability. Case *9ea* is shown in Figure 7.48, and is also offset from the curve. The slope is steep for this configuration, indicating that changes ΔV will have significant effects on GLOW. This would also be corrected if the F-1A was able to use a throttling capability.

Table 7.37. 100 mt Stage Vehicle.

		Propellant			Engine				ΔV		Inertial Burnout			Max
Case	GLOW	Stage 1	f_1	Stage 2	Stage 1		Stage 2		Req	Avail	Vel.	Alt.	FPA	Q
-	*kg*	*kg*	-	*kg*	*Type*	#	*Type*	#	*m/s*	*m/s*	*m/s*	*km*	*deg*	*psf*
1ea	2188386	1204278	0.24	724559	-	-	-	-	9800	-	-	-	-	-
2ea	2188394	1204278	-	724559	F-1A	4	J-2X	5	10259	9698	7102	401	0.08	835
3ea	2218955	1401815	0.3	559350	-	-	-	-	9800	-	-	400	-	-
4ea	2218963	1401814	-	559349	F-1A	4	J-2X	4	9685	9697	7672.9	400	0.19	863
5ea	2293657	1578555	0.35	455095	-	-	-	-	9800	-	-	-	-	-
6ea	2293665	1578555	-	455096	F-1A	4	J-2X	3	9538	9694	7812	399	0.12	837
7ea	2459508	1882708	0.440	309997	-	-	-	-	9700	-	-	-	-	-
8ea	2459514	1882708	-	309997	F-1A	4	J-2X	2	9317	9590	7919	400	0.48	781
9ea	2459514	1882708	-	309997	F-1A	4	J-2X(84.0%)	2	9533	9591	7702	400	-0.10	775

*Shaded rows represent velocity budget analysis that estimates propellant requirements based on ΔV.

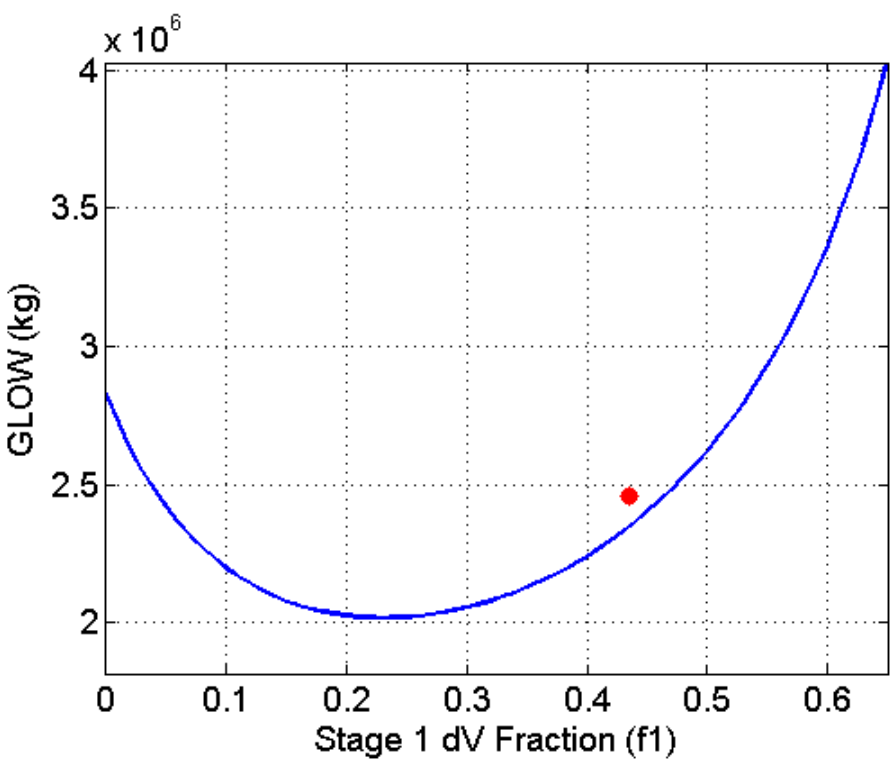

Figure 7.48. 100 mt 2 Stage Vehicle Stability. Variation of GLOW with 1st stage ΔV.

7.6.5 60 mt Payload Requirement for 2 Stage Vehicle

The process for the 60 mt payload configuration is very similar and is shown in Table 7.38. The minimized propellant requirements are determined with a velocity budget analysis and shown in case *1eb*. Evaluating this configuration in THEO with two stage one engines reveals the results in case *2eb*. The vehicle is unable to meet all burnout conditions, implying the need for an additional thrust. A stage one engine is added in case *3eb*; bringing the vehicle much closer to burnout conditions. The maximum dynamic pressure is excessive, indicating that a substantial increase in GLOW is necessary to decrease the thrust to weight ratio. An increase is made in case *4eb* by adjusting the stage one contribution to 0.48. The new propellant amounts are run in THEO with the results shown in case *5eb*. Burnout conditions are close, but dynamic pressure is still unacceptably high, implying an even higher increase in GLOW is necessary to correct the thrust to weight ratio. This would require an extreme divergence from the minimum, which disqualifies this vehicle for a 60 mt payload. The issue associated with the high thrust F-1A engines is amplified for this configuration, and an acceptable balance between the mass and thrust to weight ratio could only be achieved by changing the stage one engines.

Table 7.38. 60 mt Derivative of 2 Stage Vehicle.

		Propellant			Engine				ΔV		Inertial Burnout			Max
Case	GLOW	Stage 1	f_1	Stage 2	Stage 1		Stage 2		Req	Avail	Vel.	Alt.	FPA	Q
-	*kg*	*kg*	-	*kg*	*Type*	#	*Type*	#	*m/s*	*m/s*	*m/s*	*km*	*deg*	*psf*
1eb	1280916	680716	0.23	438909					9700					
2eb	1280922	680718		438909	F-1A	2	J-2X	3	10673	9567	6526.9	366	19.20	639
3eb	1280922	680718		438909	F-1A	3	J-2X	3	9961	9590	7295	402	0.43	1275
4eb	1628927	1294098	0.48	158748					9700					
5eb	1628930	1294098		158748	F-1A	3	J-2X	1	9023	9588	8211.6	400	0.15	1028

The analysis for these configurations has shown that it is difficult to create a two stage vehicle adaptable to different payloads. The main engines used on this vehicle are very powerful, and make it difficult to find a medium between minimizing mass and maintaining an acceptable dynamic pressure. Configurations able to reach orbital conditions are shown in Table 7.39.

Table 7.39. 2 Stage Vehicle Configuration Summary.

		Propellant		Engine			
Payload	GLOW	Stage 1	Stage 2	Stage 1		Stage 2	
mt	*kg*	*kg*	*kg*	*Type*	#	*Type*	#
130	2899915	1870000	700000	F-1A	5	J-2X	5
100	2459514	1882708	309997	F-1A	4	J-2X(84%)	2

7.7 2 Stage Booster Vehicle

Configuration F from Table 7.1 is a 2 stage vehicle with boosters in place of a standard first stage. The RSRM is already designed and as a result it would be efficient to use if it could successfully bring the vehicle to orbit. The analysis for this case is slightly different because the mass of the boosters is already specified. This implies that the ΔV contribution from stage one is preset and based on the number of boosters.

7.7.1 2 Stage Booster Vehicle Aerodynamic Coefficients

This vehicle does not resemble a 2.5 stage vehicle and as such, it is assumed to have zero lift. The drag data for this vehicle is generated in Missile Datcom and is shown in Figure 7.49.

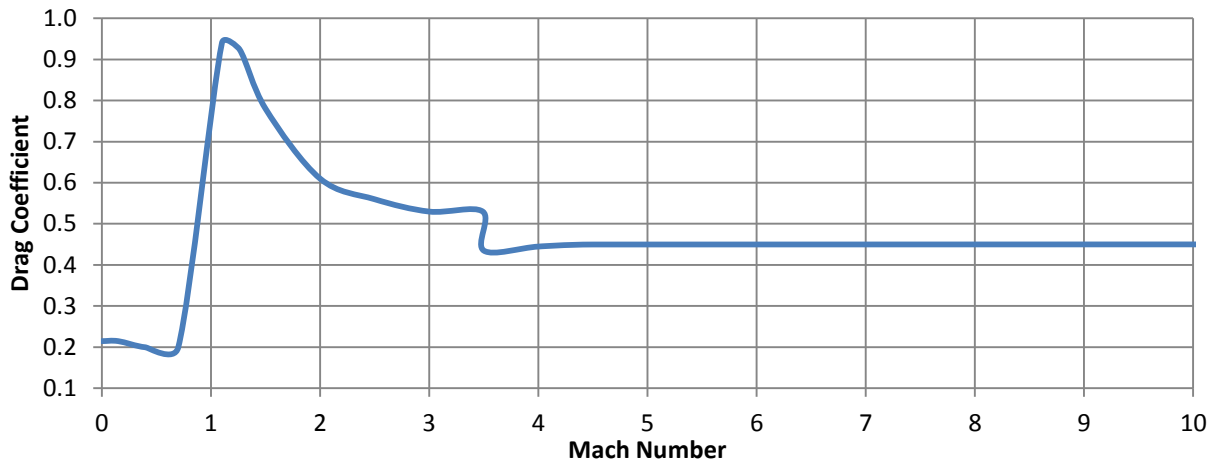

Figure 7.49. 2 Stage Configuration Drag Coefficient Profile.

7.7.2 2 Stage Booster Vehicle General Analysis

Table 7.40 contains the results of a general analysis for this configuration. There are few possibilities in terms of the number of booster and stage two engines that the vehicle can have. Cases *1f-4f* are the top cases for a configuration with 3 RSRM boosters and 5 SSMEs in the second stage. The burnout velocity ranges from being 1100 m/s to 1800 m/s short of the desired condition, indicating that this particular configuration is incapable of reaching orbit. The low maximum dynamic pressure suggests that the thrust to weight ratio is low for a vehicle with three RSRMs. An attempt to increase the number of SSMEs beyond five is impractical because of their expense and limited supply.

Table 7.40. 2 Stage Booster General Analysis Top Configurations.

	Independent Variables						Burnout Conditions			
	Propellant Mass		Primary Pitch Event				Inertial Property			
	Stage 1	Stage 2	Start Time	Length	Pitchrate	GLOW	FPA	Velocity	Altitude	Max Q
Case	*kg*	*kg*	*s*	*s*	*deg/s*	*kg*	*deg*	*m/s*	*km*	*psf*
	Stage 1: 3 RSRM Stage 2: 5 SSME									
1f	1505100	850000	8.7	2	-0.52	2851220	15.25	6512.8	402	476
2f	1505100	900000	8.7	2	-0.34	2905568	14.53	6412.5	395	443
3f	1505100	950000	8.7	1	-0.5	2959916	15.69	6170.7	403	415
4f	1505100	1000000	8.7	1	-0.3	3014264	16.11	5955.3	396	392
	Stage 1: 4 RSRM Stage 2: 4 SSME									
5f	2006800	680000	6.2	19	-0.49	3252312	4.94	7155.1	398	811
6f	2006800	680000	10.2	21	-0.65	3252312	4.9	7157.2	397	809
7f	2006800	700000	6.2	13	-0.5	3274052	4.34	7133.8	399	793
8f	2006800	700000	9.2	15	-0.65	3274052	4.25	7140.3	397	793
9f	2006800	750000	7.2	19	-0.4	3328399	4.1	7084	401	752
10f	2006800	750000	8.2	7	-0.75	3328399	4.01	7091.2	399	753
11f	2006800	750000	14.2	17	-0.75	3328399	3.85	7102.2	396	750
	Stage 1: 4 RSRM Stage 2: 5 SSME									
12f	2006800	880000	8.7	8	-0.5	3469705	4.92	7237.8	392	667
13f	2006800	890000	9.2	7	-0.56	3480574	5	7200.8	396	659
14f	2006800	900000	10.2	13	-0.4	3491444	4.95	7167.6	398	649
15f	2006800	900000	14.2	17	-0.5	3491444	4.87	7173.4	396	648

Cases *5f-11f* includes an additional RSRM booster to attempt improving the thrust to weight ratio for the vehicle. Notice that the burnout velocity for these cases is much closer to the desired burnout condition, but not without a substantial increase in GLOW. Even with this increase in propellant, the vehicle is still incapable of reaching the necessary orbit. Instead of trying to correct this just by increasing the propellant mass, an additional SSME is also added to the second stage in cases *12f-15f*. The velocity is modified by this adjustment but is still 400 m/s to 500 m/s inadequate. Notice also that GLOW has shifted to almost 3500 mt, which is substantially higher than any of the preceding configurations. An attempt to bring the payload to orbit would only be reached by further increasing GLOW.

Remember the thrust profile for the RSRM in Chapter 4. Each booster is designed to have a specific thrust profile, which has a negative effect when used as a first stage. The thrust profile for the RSRM is not designed to function as the primary thrust source for a vehicle, and events such as the thrust bucket have a negative effect on the performance of the rocket. During the thrust bucket regime on this vehicle, the thrust to weight ratio is decreased which forces the vehicle to accelerate at a slower rate. Inert mass ratio is also very high for this vehicle as it has the inert mass for each booster as well as additional 20 mt that is assumed necessary to attach the boosters to the second stage. These two factors imply that using any predesigned booster with larger thrust buckets for the first stage of a vehicle will most likely be incapable of bringing the vehicle to orbit. An adequate booster would require that it be designed specifically for a first stage.

The last consideration that eliminates the 2 stage booster from potential heavy lift configurations is the high thrust requirements for the 2nd stage. Stage 2 requires at least 5 SSME for the configurations in Table 7.40. Using SSME engines on this scale is wasteful as they are extremely expensive and originally intended for multiple reuses. Other boosters like the M550 FW3 would require even more stage two engines because the burn time for an M550 is almost 20 s less than the burn time for the RSRM. First stage separation would be earlier which would require a higher ΔV contribution from stage 2. A higher ΔV could only be provided by increasing the mass of the stage two propellant. This would then require even more thrust, and the situation would quickly diverge away from a minimized case.

These considerations as well as the data in Table 7.40 indicate that a 2 stage Booster configuration with prefabricated boosters is not a practical concept for a heavy lift launch vehicle. The necessary GLOW to bring the vehicle to orbit is incomparable to the minimized GLOW that preceding cases have achieved. Because of the inability to achieve orbit with a 130 mt payload, it is not even considered for the 60 mt and 100 mt payload configurations.

7.8 1.5 Stage RSRM Vehicle

The last case has a slightly different objective than the others. Optimization of the vehicle is still the goal, but it instead looks at in terms of varying the booster properties and holding the core at constant specifications. Configuration G from Table 7.1 is a 1.5 stage vehicle using two RSRM V boosters with 5 SSME engines. The optimization of this configuration is per the request of NASA with preset specifications. The core of the vehicle has a propellant mass of 984295 kg and an inert mass ratio of 0.066. Inert mass ratio is based on the 0.06 used in all other configurations but with an addition that accounts for propellant that remains unburned within the tanks. The objective is to start with RSRM V boosters and modify them to see how this preset core can reach burnout conditions. Alterations are made by adjusting the thrust profile, propellant mass, and burn time. This analysis is only performed for the 130 mt payload as the boosters are to be matched to this configuration. This section primarily discusses the effects of varying these parameters on the RSRM V.

7.8.1 1.5 Stage RSRM V Vehicle Aerodynamic Coefficients

The drag coefficient data for this vehicle is shown in Figure 7.50 and is generated in Missile Datcom. The lift for this vehicle is assumed to be zero as it is not a 2.5 stage vehicle.

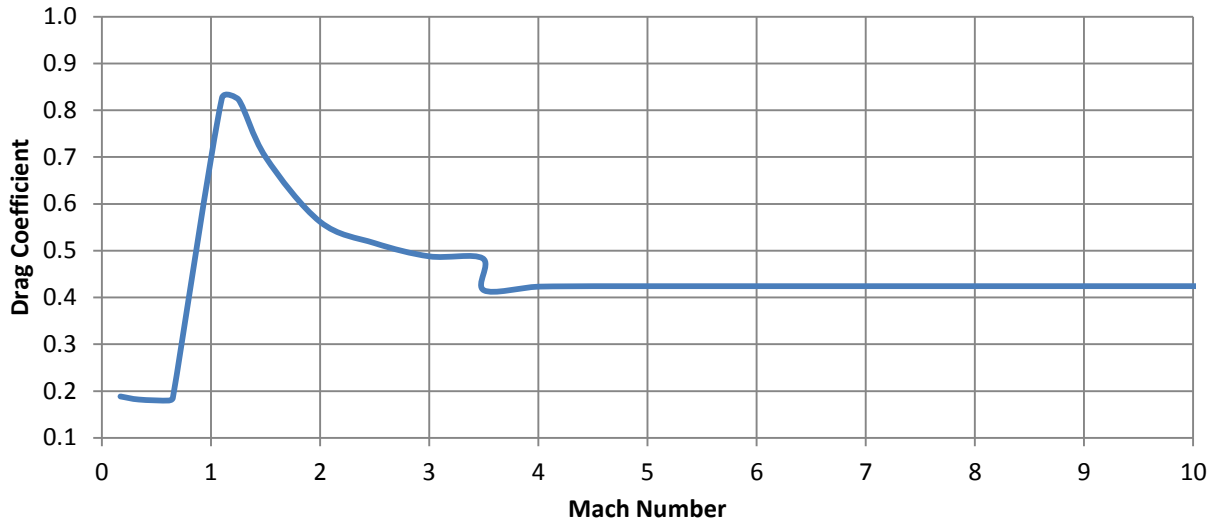

Figure 7.50. 1.5 Stage RSRM V Configuration Drag Coefficient Profile.

7.8.2 1.5 Stage RSRM V Analysis

Case *1g* in Table 7.41 represents the 1.5 stage configuration with unmodified RSRM V boosters. The ΔV required from the engines is almost 1300 m/s less than necessary for orbit. The deficiency here could be result of either a low thrust to weight ratio or insufficient energy contained within the propellant. Cases *2g-4g* demonstrate the effects of increasing the thrust profile of the RSRM V. The thrust profile for these cases is modified by multiplying the original RSRM V with a multiplication factor. For example, multiplying the original curve described in Chapter 4 by 1.1 increases the thrust output by 10 percent. Smaller adjustments are also made that increase the burn time or decrease the effect of the thrust bucket that was discussed in Chapter 4. When thrust is modified mass flow rate must be reevaluated using Eq. (7.1). The change in mass flow rate is proportional to thrust, and as such, will increase when using a multiplication factor greater than one. I_{sp} is held constant in the equation, as specific impulse is a function of the propellant properties.

$$I_{sp} = \frac{T}{\dot{m} g_0} \tag{7.1}$$

Cases *2g-4g* show the progression in thrust changes that shift the burnout velocity of the vehicle, and the results are shown for a multiplication factor of 1.1, 1.2, and 1.25. These upgrades are performed until the dynamic pressure constraint is reached in case *4g*. Burnout velocity is still insufficient, indicating that an increase in propellant mass is necessary to attempt improving the burnout velocity.

Table 7.41. 1.5 Stage RSRM V with Multiplication Factor.

		Propellant	Engine			ΔV		Burnout Condition			
Case	GLOW	Per Booster	Booster		Mult.	Req	Avail	Velocity	Alt.	FPA	Max Q
-	*kg*	*kg*	*Type*	#	*Factor*	*m/s*	*m/s*	*m/s*	*km*	*deg*	*psf*
1g	2661103	626729	RSRM V	2	1	10338	9125	6452	400	0.369	543.6
2g	2661103	626729	RSRM V	2	1.1	10193	9187	6661	401	-0.206	643.7
3g	2661103	626729	RSRM V	2	1.2	10054	9228	6843	401	-0.097	761.5
4g	2661103	626729	RSRM V	2	1.25	9983	9243	6929	399	-0.064	824.8

The next modifications that are considered on the RSRM V booster are a combination of propellant mass and thrust and burn time variation and are shown in Table 7.42. An attempt to overcome the deficiency of case *4g* is made by increasing the propellant mass per booster to 700 mt and by adjusting the original thrust profile to Variant 1 in Figure 7.51. The propellant change increases the energy available, and the thrust variation improves the performance of the booster in a low thrust region. These adjustments do improve the burnout velocity, but not to the necessary condition. 100 mt of propellant per booster is then added in case *g2*, but the results are 600 m/s below the required orbital velocity. An attempt to remedy this is made by adding another 100 mt of propellant per booster and with a multiplication factor of 1.4. Case *g3* shows that these modifications bring the vehicle to within approximately 210 m/s of the necessary burnout velocity. The maximum dynamic pressure is high, indicating a further increase in propellant mass is necessary to reduce the thrust to weight ratio. This increase is made in case *g4* which improves the velocity slightly and also reduces the maximum dynamic pressure to acceptable values. Case *g5* shows that an adjustment of the multiplication factor to 1.5 brings the payload to correct orbital conditions. By refining this case with a minor adjustment to the multiplication factor, the booster propellant requirement can be reduced to 891 mt.

Table 7.42. 1.5 Stage RSRM V with Booster Adjustments.

		Propellant	Engine			ΔV		Burnout Condition			
Case	GLOW	Per Booster	Booster		Mult.	Req	Avail	Velocity	Alt.	FPA	Max Q
-	*kg*	*kg*	*Type*	*#*	*Factor*	*m/s*	*m/s*	*m/s*	*m*	*deg*	*psf*
g1	2807645	700000	RSRM V	2	1.2	9945	9320	7041	399	0.439	686.3
g2	3007645	800000	RSRM V	2	1.2	10003	9421	7082	399	-0.144	587.8
g3	3007645	800000	RSRM V	2	1.4	9754	9508	7420	398	-0.222	803.2
g4	3207645	900000	RSRM V	2	1.4	9772	9614	7489	401	-0.168	692.5
g5	3207645	900000	RSRM V	2	1.5	9672	9652	7645	401	-0.090	797.0
g6	3189645	891000	RSRM V	2	1.488	9670	9637	7633	399	-0.105	799.6
g7	3307645	950000	RSRM V	2	1.35	9720	9764	7618	401	0.217	808.6
g8	3337645	965000	RSRM V	2	1.35	9720	9688	7632	400	0.153	795.5
g9	3389890	626729	RSRM V	3	1	9862	9488	7292	399	-0.101	670.0
g10	3537703	676000	RSRM V	3	1.13	9675	9643	7635	399	-0.169	792.0

A thrust multiplication factor of 1.448 is quite high, and might be slightly unrealistic when trying to design a booster. The question to ask is, is there a way to alter the vehicle so that it will still reach target conditions without such a high thrust multiplication factor? Case *g7 and g8* reveal the answer to this question. An attempt is made to decrease the multiplication factor by lengthening the burn time of the booster and further increasing the propellant. The revised thrust profile is shown as Variant 2 in Figure 7.51. The adjustment does require an increase in GLOW but fortunately allows the multiplication factor to decrease to 1.35. This implies that a longer burning booster can lead to lower overall thrust requirements.

Lastly, a three booster configuration is shown in cases *g9* and *g10* for comparison. Without any modifications to the RSRM V, the payload is able to come within 400 m/s of the desired burnout condition. To correct the deficiency, the propellant mass per booster is increased by 50 mt and a multiplication factor of 1.13 is used. Unfortunately, three boosters force GLOW to be very high negating the advantages of a booster that has minimal changes. A comparison of the top three cases is shown in Table 7.43, as well as the detailed results for the minimized case in Table 7.44. It should also be noted that the thrust profile including the multiplication factor for the minimize case is shown in Figure 7.51. To ensure that the aerodynamic properties of angle of attack, dynamic pressure, and angle of attack*dynamic pressure remain within the specified bounds, the trajectory plots are shown in Figure 7.52a-c.

Table 7.43. 1.5 Stage RSRM V Vehicle Comparison.

		Propellant		Engine				
Case	GLOW	Stage 1	Booster	Booster		Stage 1		Multi.
-	*kg*	*kg*	*kg*	*Type*	*#*	*Type*	*#*	*Factor*
g6	3189645	984295	891000	RSRM V	2	SSME	5	1.488
g8	3337645	984295	965000	RSRM V	2	SSME	5	1.35
g10	3537703	984295	676000	RSRM V	3	SSME	5	1.13

Table 7.44. Minimized GLOW for 1.5 Stage Vehicle.

	Length	Diameter	Propellant	Inert	Engine	# Engines	Burnout Alt	399124	m
130 mt	*m*	*m*	*kg*	*kg*	*(Shape)*	-	Burnout Vel	7632	m/s
Booster	50.00	4.16	1782000	204116	SSME	5	Burnout FPA	-0.105	*deg*
Stage 1	53.70	9.00	984295	69559	RSRM V	2	Max Q	799.6	*psf*
Shroud	12.19	9.00	-	19674	Biconic	-	GLOW	3189645	*kg*
Total	65.89	-	-	-	1.5 Stage	-	Start Pitch	7	*s*
Secondary Pitch Event Revision				3rd	-0.321536		Pitch Length	10	*s*
Secondary Pitch Event Revision				4th	-0.355014	*deg/s*	Pitchrate	-0.7770	deg/s

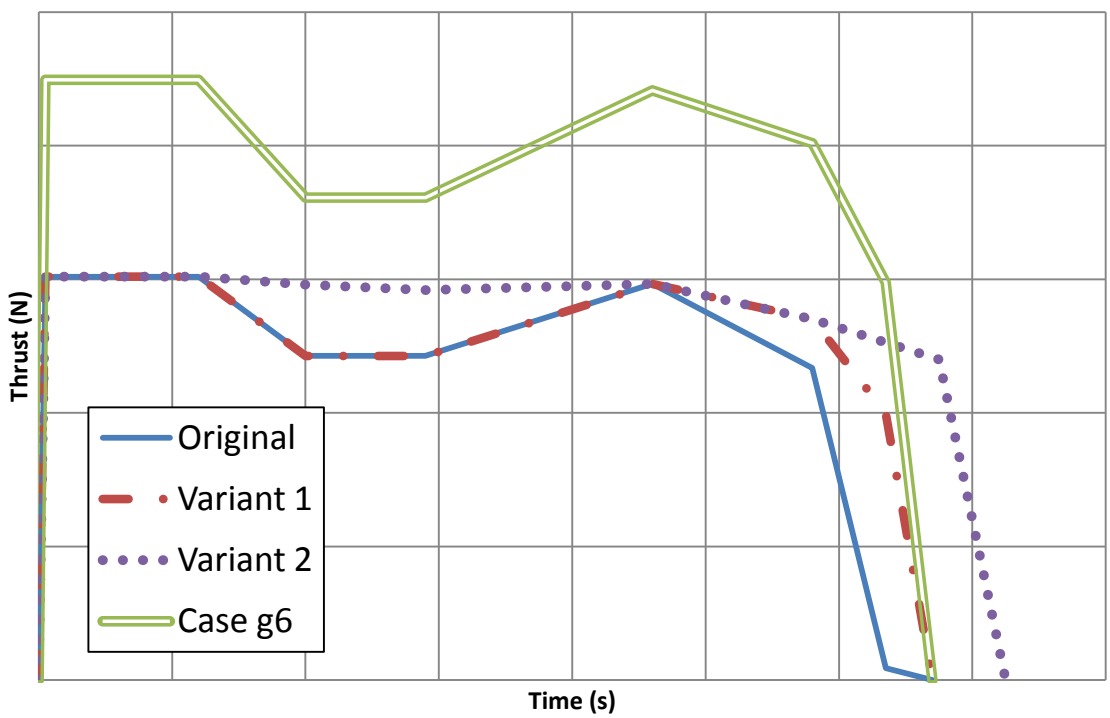

Figure 7.51. Modified Thrust Profiles for RSRM V booster. Axis removed for ITAR restrictions.

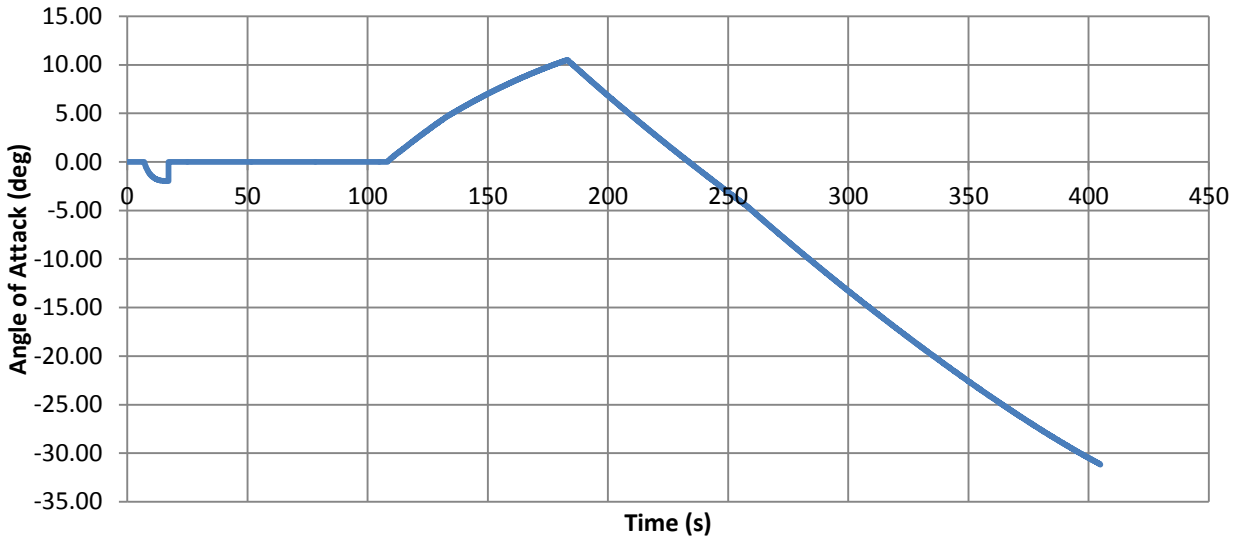

(a)

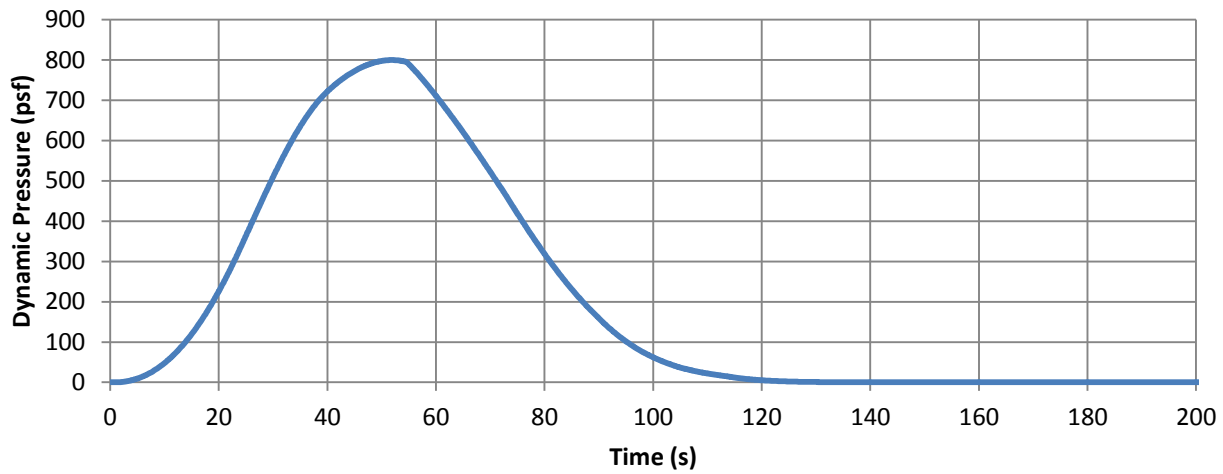

(b)

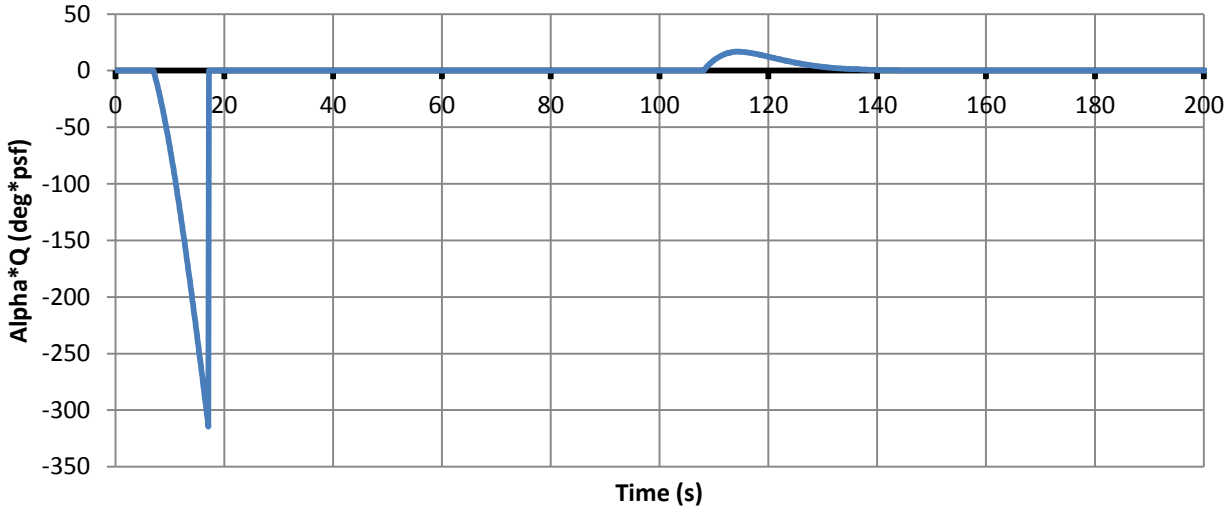

(c)

Figure 7.52a-c. 1.5 Stage RSRM V Aerodynamic Limits Check.

Chapter 8

Conclusion

Chapter 8

Conclusion

There are seven different configurations analyzed to minimize GLOW. Each of them has advantages and disadvantages specific to that configuration, and as a result, they perform differently than one another. Table 8.1 compares the vehicles that are capable of bringing the maximum payload to orbit with some historical vehicles.

8.1 Final Results

The RSRM family configurations have the highest GLOW out of any of the analyzed cases. This is directly a result of the booster size. The RSRM family boosters have high thrust output and heavy initial masses and as a result, no more than two can be used on a launch vehicle. More than this will result in a vehicle that surpasses maximum dynamic pressure values. Even with two boosters, the thrust to weight ratio is high, and the thrust to weight ratio can then only be decreased by increasing the weight of the vehicle. Also, notice the difference between the 2.5 Stage vehicle with RSRMs and RSRM Vs. The RSRM V is a more powerful engine than the RSRM and drives GLOW to be 117 mt heavier than the vehicle with 2 RSRMs. The high thrust from these boosters drives up the final optimized weight for these configurations. It was also determined that the 100 mt and 60 mt payload variants could not be derived from the original configuration. Considering this and the high GLOW, these configurations are removed from candidacy as the final optimized solution.

Table 8.1. Overall Configuration Comparison.

			Propellant		Engine					
Configuration	Payload	GLOW	Stage 1	Stage 2	Booster		Stage 1		Stage 2	
Historical Vehicles	*mt*	*kg*	*kg*	*kg*	*Type*	*#*	*Engine*	*#*	*Engine*	*#*
2.5 Stage RSRM	130	3283966	1150000	680000	RSRM	2	F-1A	3	SSME	3
2.5 Stage RSRM V	130	3401459	960000	710000	RSRM V	2	F-1A	3	SSME	3
2.5 Stage M550	130	2994521	1180000	400000	M550 FW3	4	F-1A	2	J-2X	4
	100	2354541	1180000	370000	M550 FW3	2	F-1A	2	SSME	2
	60	1524120	682976	129263	M550 FW3	2	F-1A	1	J-2X	2
2.5 Stage P80	130	2806800	1170000	600000	P80	8	F-1A	3	SSME	3
	100	2396667	1170000	600000	P80	3	F-1A	3	SSME	2
	60	1438411	818599	273993	P80	2	F-1A	2	SSME	1
2 Stage	130	2899915	1870000	700000	-	-	F-1A	5	J-2X	5
	100	2459514	1882708	309997	-	-	F-1A	4	J-2X(84%)	2
1.5 Stage RSRM V	130	3189645	984295	-	*RSRM V*	2	SSME	5	-	-
Space Shuttle	29	2030000	729007	-	RSRM	2	SSME	3	-	-
Delta IV Heavy	22.7	775643	658320	26014	RS-68	2	RS-68	1	RL-10B-2	1
					Stage 1		Stage 2		Stage 3	
Saturn V	120	3039000	2286217	490778	F-1	5	J-2	5	J-2	1

*(*RSRM V*) represents modified RSRM V booster.

The 2.5 stage M550 FW3 case shows major improvement over the RSRM configurations. The M550 booster has a lower thrust and propellant mass per booster. This implies that to reach orbit, the vehicle will require more boosters. A concept such as this is very useful as it allows thrust to be added in smaller increments as

compared to the RSRM family boosters. Smaller thrust and propellant mass increments imply that the vehicle can be tailored to a specific payload without greatly increasing the thrust to weight ratio. Use of the M550 booster allows the vehicle to have a GLOW 300 – 400 mt less than the RSRM configurations for a payload of 130 mt. Notice as well that the 100 mt payload can be brought to orbit by simply removing two M550 boosters and performing a slight modification to the stage two propellant mass. The 60 mt payload requires more significant adjustments to the core, but is still able to use the M550 for reaching orbital conditions.

The P80 is an even smaller booster, and as such, further increases the capability of a vehicle to be designed for a heavy lift configuration and still be adaptable for different payloads. The 130 mt payload case requires eight P80 boosters, and is able to decrease the required GLOW from the 2.5 stage M550 configuration by approximately 200 mt. Using a higher number of smaller boosters allows the vehicle to be matched better with the necessary propellant and engine properties which resultantly decreases GLOW. The 100 mt payload is capable of being brought to orbit by simply adjusting the number of boosters from eight to three. The 60 mt payload can also be brought to orbit, but does require modifications to the core vehicle.

The 2 stage vehicle is quite capable in optimizing the vehicle as it has been minimized to have the second lowest GLOW of 2899.9 mt. Compared to 2.5 stage vehicles, it is much simpler and is also able to bring the 100 mt payload to orbit. The disadvantage associated with this vehicle is that the core must be modified to bring different size payloads to orbit. This configuration has almost no variability in being able to minimize changes to the core of the vehicle. Also, when comparing to the Saturn V, there is approximately a 100 mt decrease in GLOW which is simply a result of upgrading the engines.

The last case is a 1.5 stage configuration using modified boosters. This case was tasked by NASA to determine how a RSRM V booster should be modified to bring a constant core configuration to orbit. Thrust, propellant mass, and burn time are adjusted in the modified booster to minimize GLOW of the vehicle and bring the payload to orbit. The minimized GLOW is high and as result can be eliminated for potential candidate. It is interesting to note that in comparison with the Space Shuttle, which is another 1.5 stage vehicle, a 60% increase in GLOW has increased the payload to four times that which the Shuttle was capable of.

In consideration of all this, the configuration that minimizes GLOW and also provides a large amount of adaptability to different payload requirements is the 2.5 Stage vehicle using the P80 booster. It has been proven using THEO and velocity budget optimization techniques to be a very capable vehicle. This is the final optimized configuration for this analysis, and is illustrated in Figure 8.1.

8.2 Continued Study and Improvements

A possible solution to increasing the capability of these different configurations would be to introduce throttling into the first stage engines and/or increase the maximum dynamic pressure constraint beyond 800 psf. Adjustments made to these properties might be enough to decrease the minimum GLOW and increase the capability for adaptable payloads. Continued research in these two areas could possibly provide and advantage.

There are a couple of short term improvements I would like to implement to THEO that will allow it to better model these trajectories. The first is a wind model which would improve the real world accuracy of these trajectories. The second would be to obtain a reliable tool such as OVERFLOW for estimating the aerodynamic properties of each vehicle. This is necessary for correct estimation of drag, lift, and center of pressure.

The next improvement would come from evaluating the CG of the vehicle at every new increment in the trajectory. This addition will pave the way for a long term goal of transferring this code into a 6 DOF analysis considering the rotational and translational movements of the vehicle. I would also like to introduce a GUI for easier user input.

Lastly, I would like to continue development of the secondary analysis tools. These aided in locating optimized solutions, and I am certain that a refinement of these tools will make it simpler to locate the configurations with the lightest GLOW.

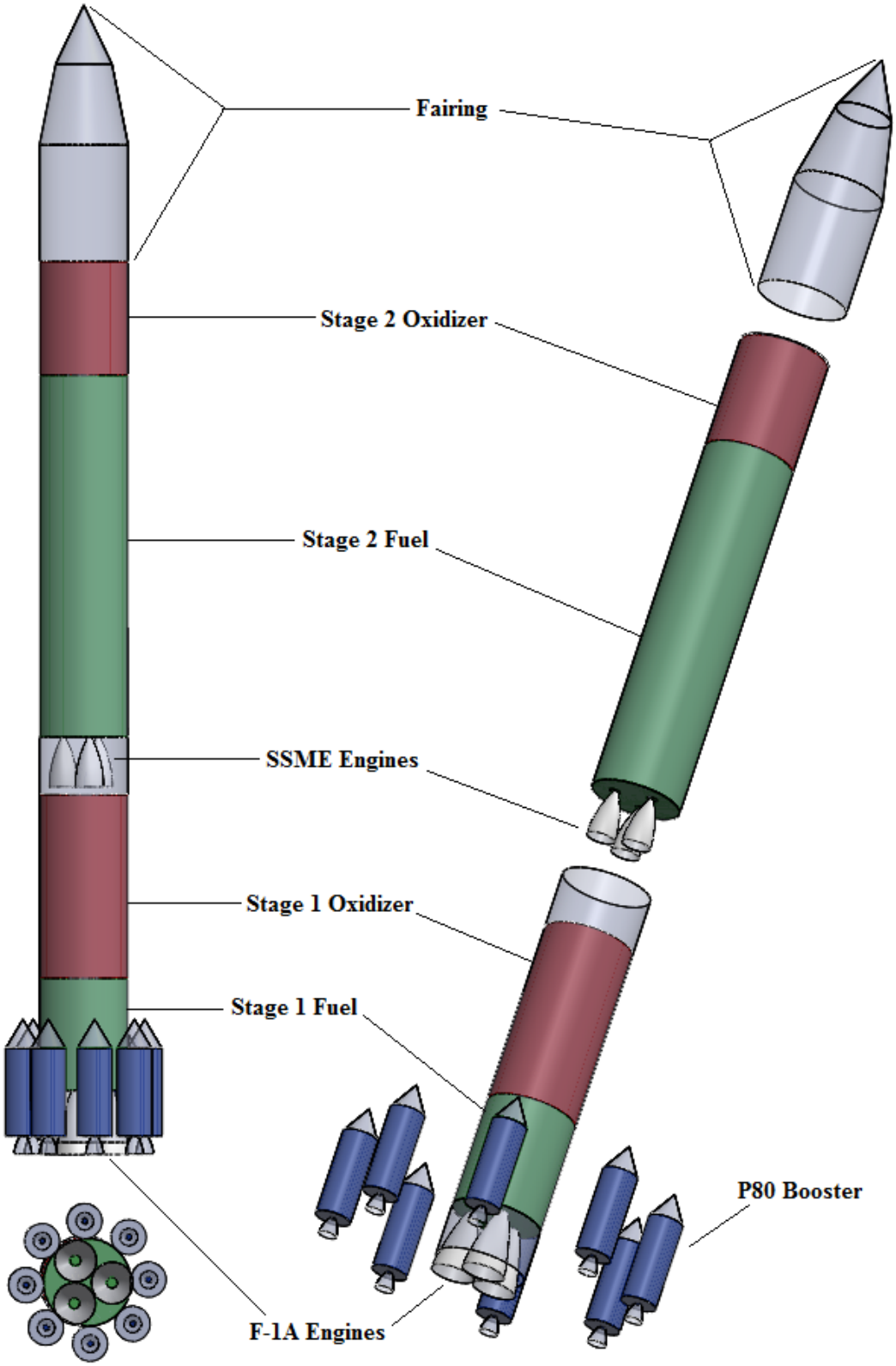

Figure 8.1. Overall Optimized Configuration. 2.5 Stage Vehicle with 8 P80 Booster. Illustrates side, bottom, and exploded view.

Appendices

Appendix A

These equations model the earth's atmospheric temperature (theta), pressure (delta) , and density (sigma) ratios based on altitude. This model breaks the atmosphere into nine sections, and assumes density and pressure effects are negligible after 120000 m. The altitude input (h_feet) must be in English units of feet. The local atmospheric condition of temperature, pressure, or density can then be determined by multiplying each ratio by the sea level standard values. Ratios are compatable across both unit systems.

```
Altitude is greater than 0 ft (0 m) and less than 36089 ft (11000 m)
    theta = 1 - h_feet / 145442.
    delta = (1 - h_feet / 145442.)^5.255876
    sigma = (1 - h_feet / 145442.)^4.255876
Altitude is greater than 36089 ft (11000 m) and less than 65617 ft (20000 m)
    theta = 0.751865
    delta = 0.223361*e1^(-(h_feet-36089.)/20806.)
    sigma = 0.297076*e1^(-(h_feet-36089.)/20806.)
Altitude is greater than 65617 ft (20000 m) and less than 104987 ft (32000 m)
    theta = 0.682457 + h_feet / 945374.
    delta = (0.988626 + h_feet / 652600.)^(-34.16320)
    sigma = (0.978261 + h_feet / 659515.)^(-35.16320)
Altitude is greater than 104987 ft (32000 m) and less than 154199 ft (47000 m)
    theta = 0.482561 + h_feet / 337634.
    delta = (0.898309 + h_feet / 181373.)^(-12.20114)
    sigma = (0.857003 + h_feet / 190115.)^(-13.20114)
Altitude is greater than 154199 ft (47000 m) and less than 167323 ft (51000 m)
    theta = 0.939268
    delta = 0.00109456*e1^(-(h_feet-154199.)/25992.)
    sigma = 0.00116533*e1^(-(h_feet-154199.)/25992.)
Altitude is greater than 167323 ft (51000 m) and less than 232940 ft (71000 m)
    theta = 1.434843 - h_feet / 337634.
    delta = (0.838263 - h_feet / 577922.)^12.20114
    sigma = (0.798990 - h_feet / 606330.)^11.20114
Altitude is greater than 232940 ft (71000 m) and less than 282148 ft (86000 m)
    theta = 1.237723 - h_feet / 472687
    delta = (0.917131 - h_feet / 637919)^17.08160
    sigma = (0.900194 - h_feet / 649922)^16.08160
Altitude is greater than 282148 (86000 m) and less than 393696 ft (120000 m)
    delta = (3E75*h^(-15.38))/P0
    sigma = (5E81*h^(-17.6))/rho0
    temp = (4.647E-12*h^3-1.183E-6*h^2+0.0995*h-2578.7)
Altitude is greater than 393696 ft (120000 m)
    temp = 5.014E-25*h^5-9.408E-19*h^4+7.027E-13*h^3-2.626E-07*h^2+0.04955*h-2825.9
    delta = 0
    sigma = 0
```

Appendix B

THEO to POST validation plots

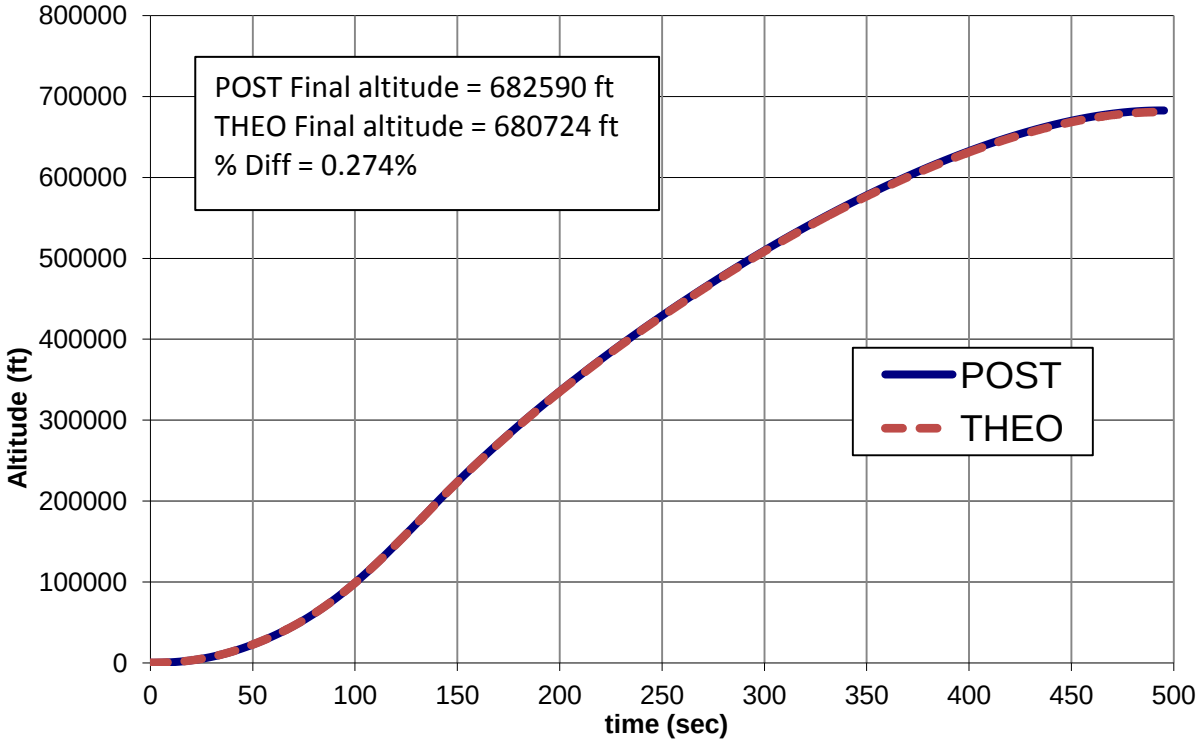

Figure B1. Altitude.

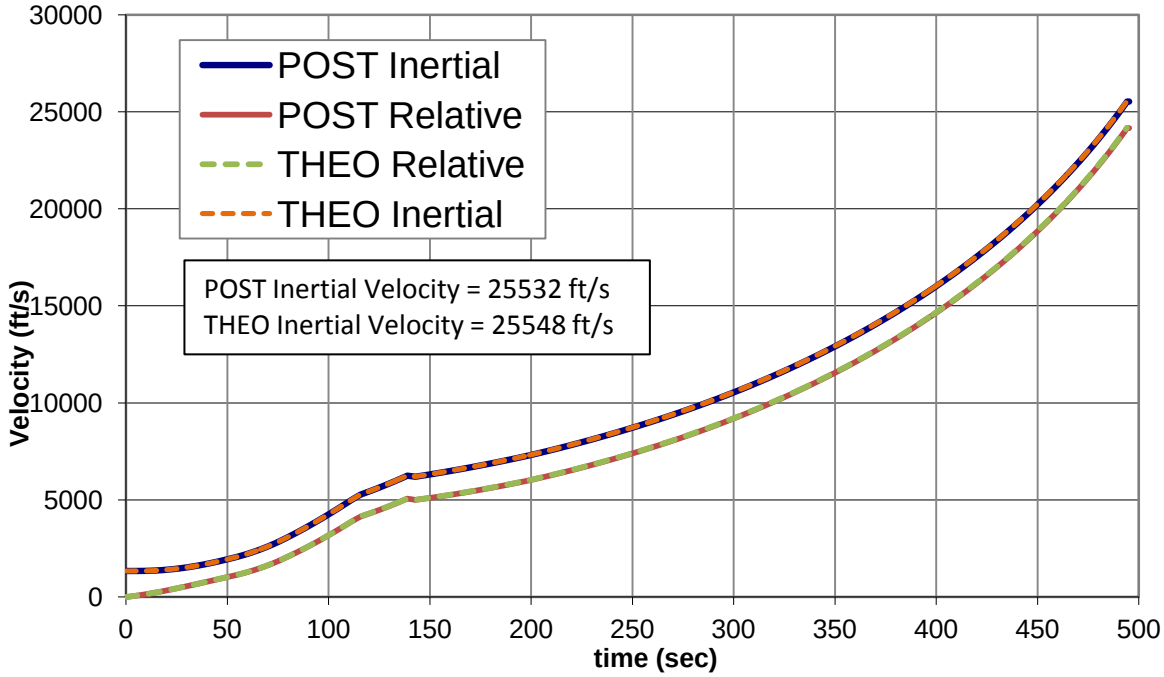

Figure B2. Inertial and Relative Velocity

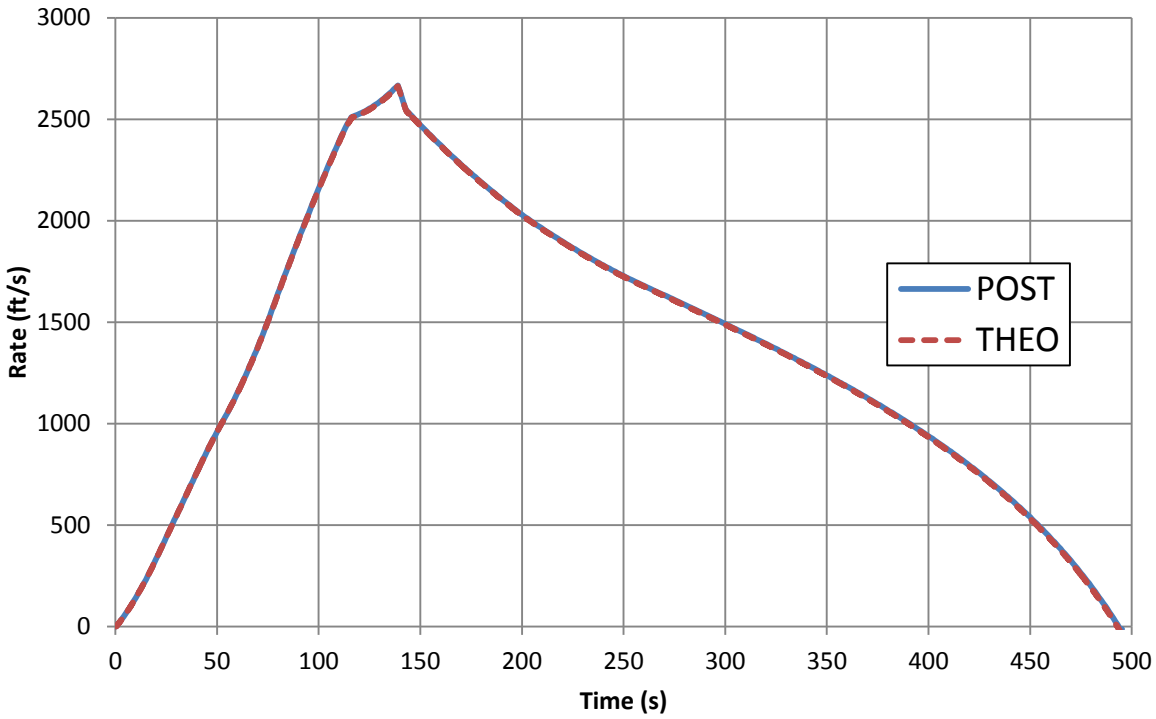

Figure B3. Rate of Change of Altitude.

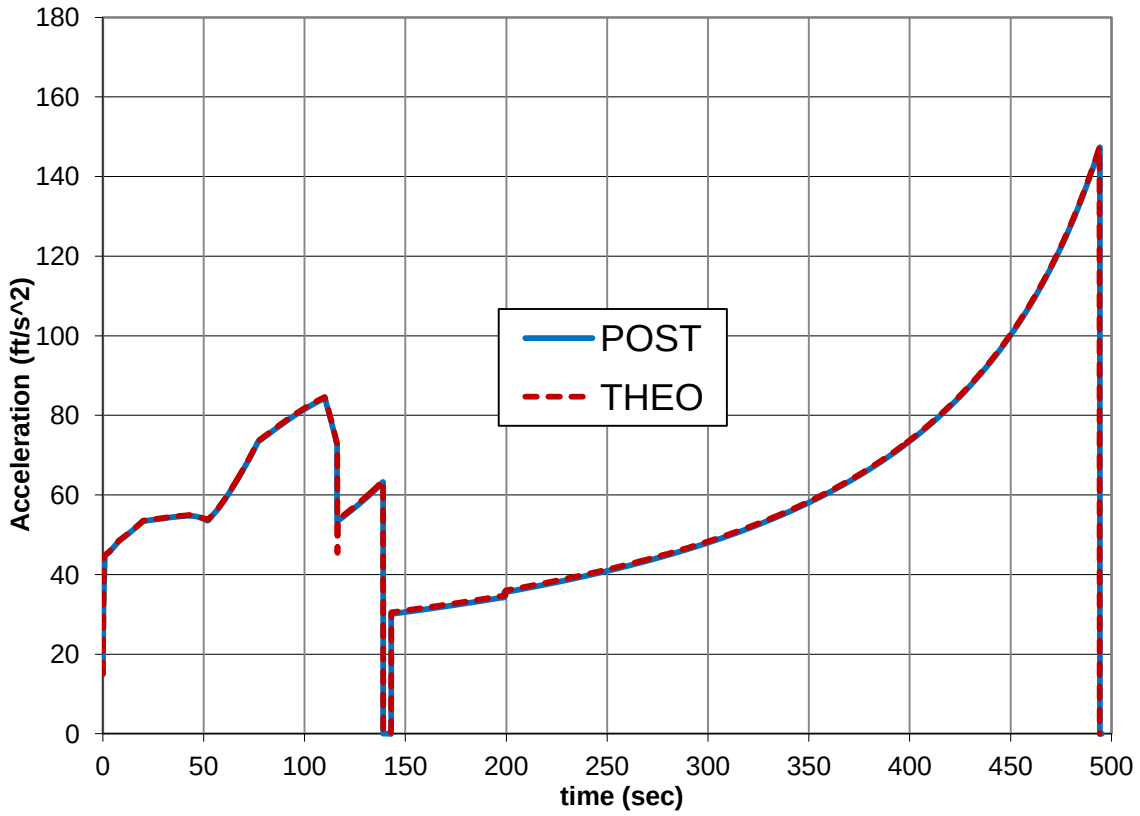

Figure B4. Sensed Acceleration.

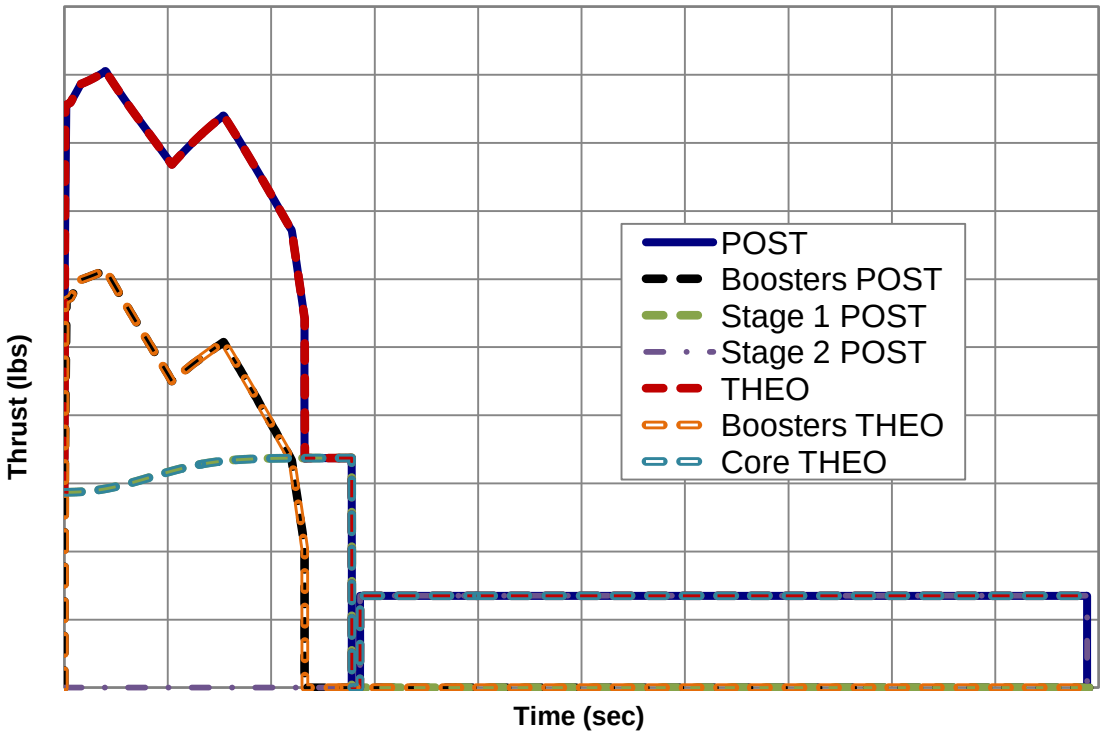

Figure B5. Stage Thrust Profile. Axes removed for ITAR regtulation.

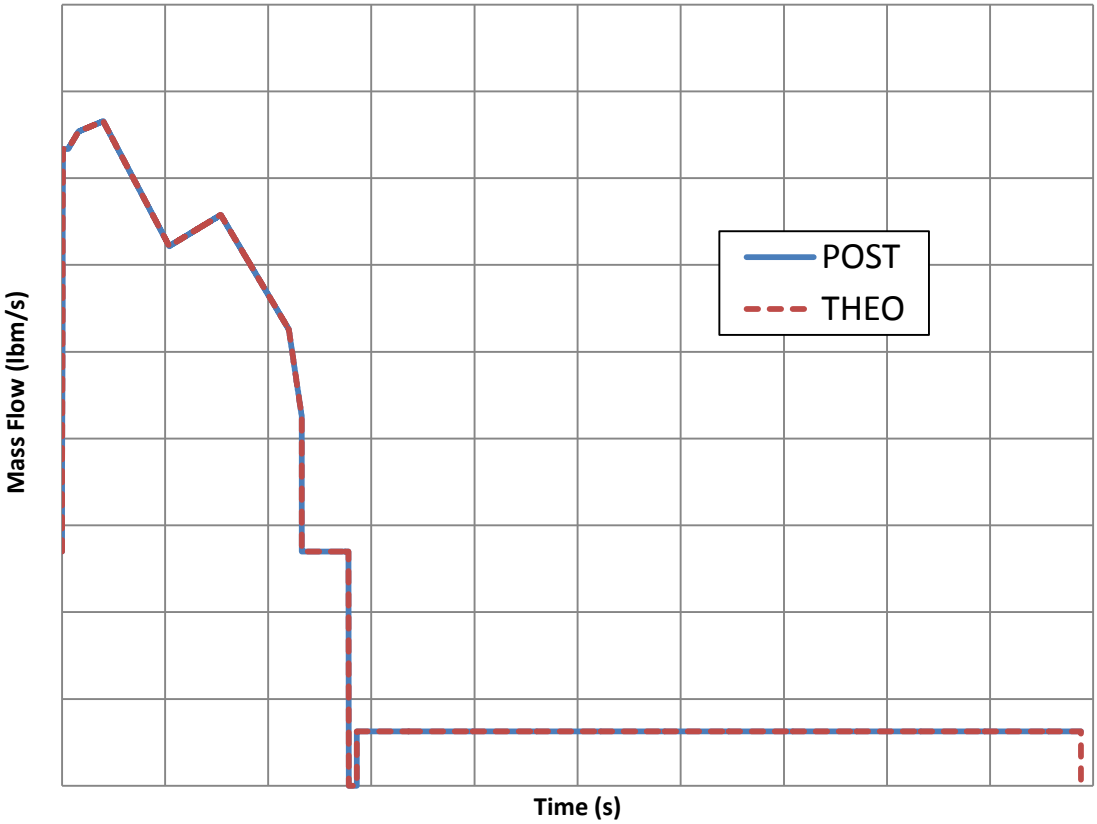

Figure B6. Mass Flow Rate. Axes removed for ITAR regualtion.

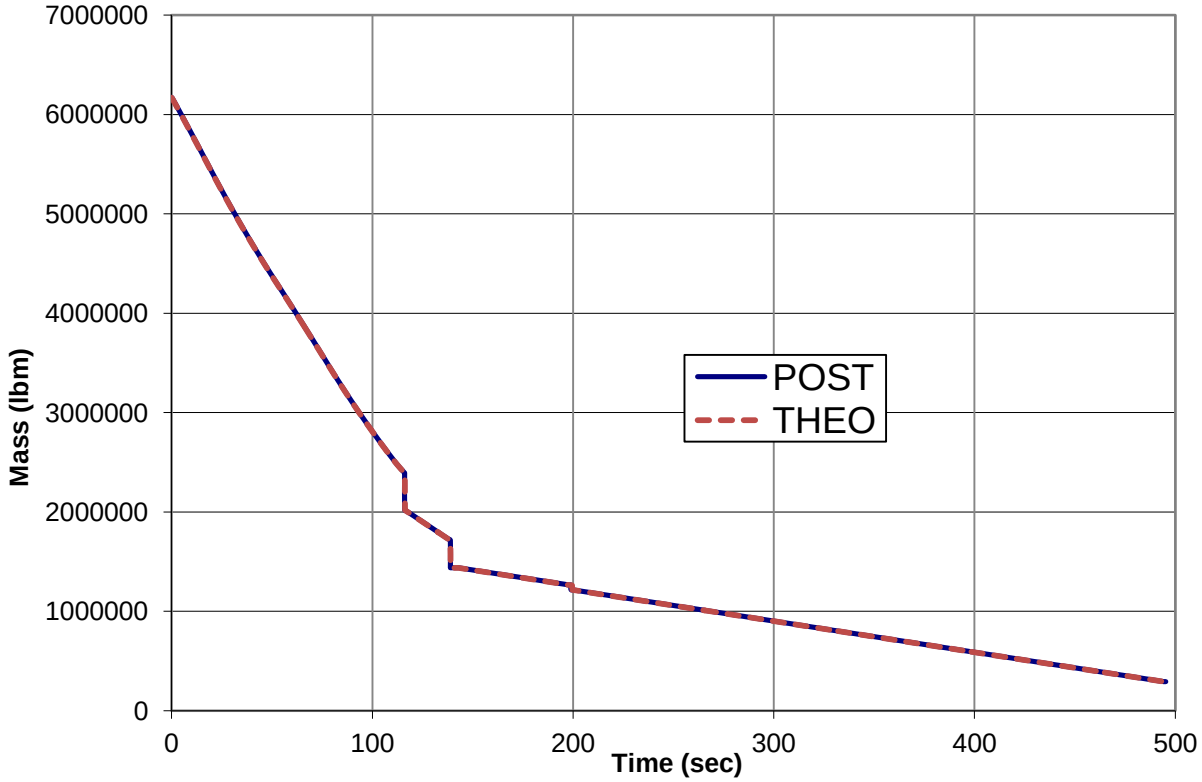

Figure B7. Mass.

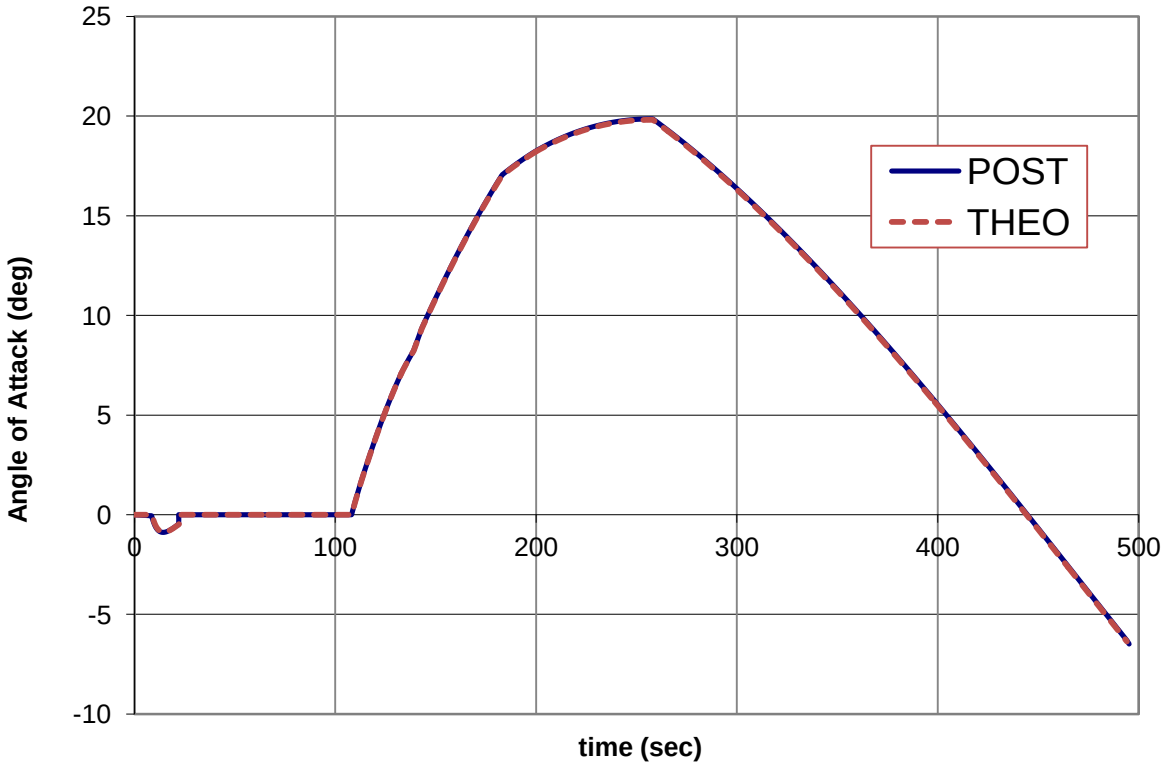

Figure B8. Angle of Attack.

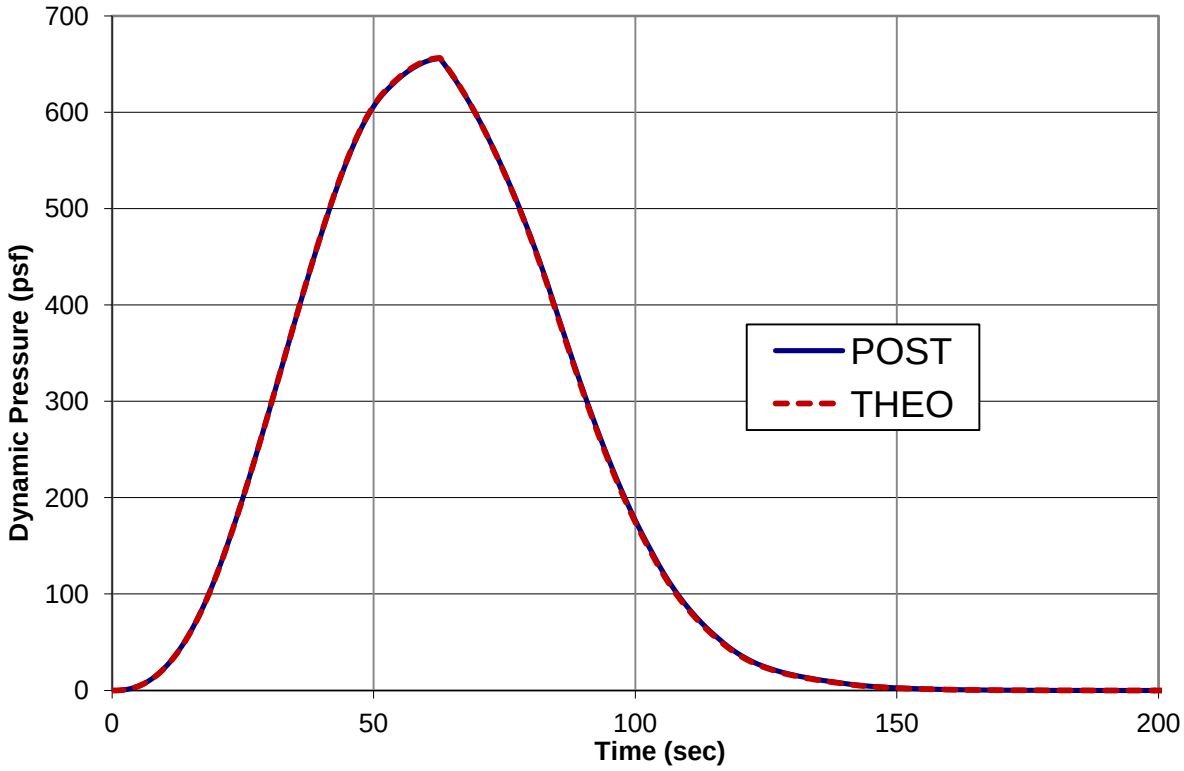

Figure B9. Dynamic Pressure.

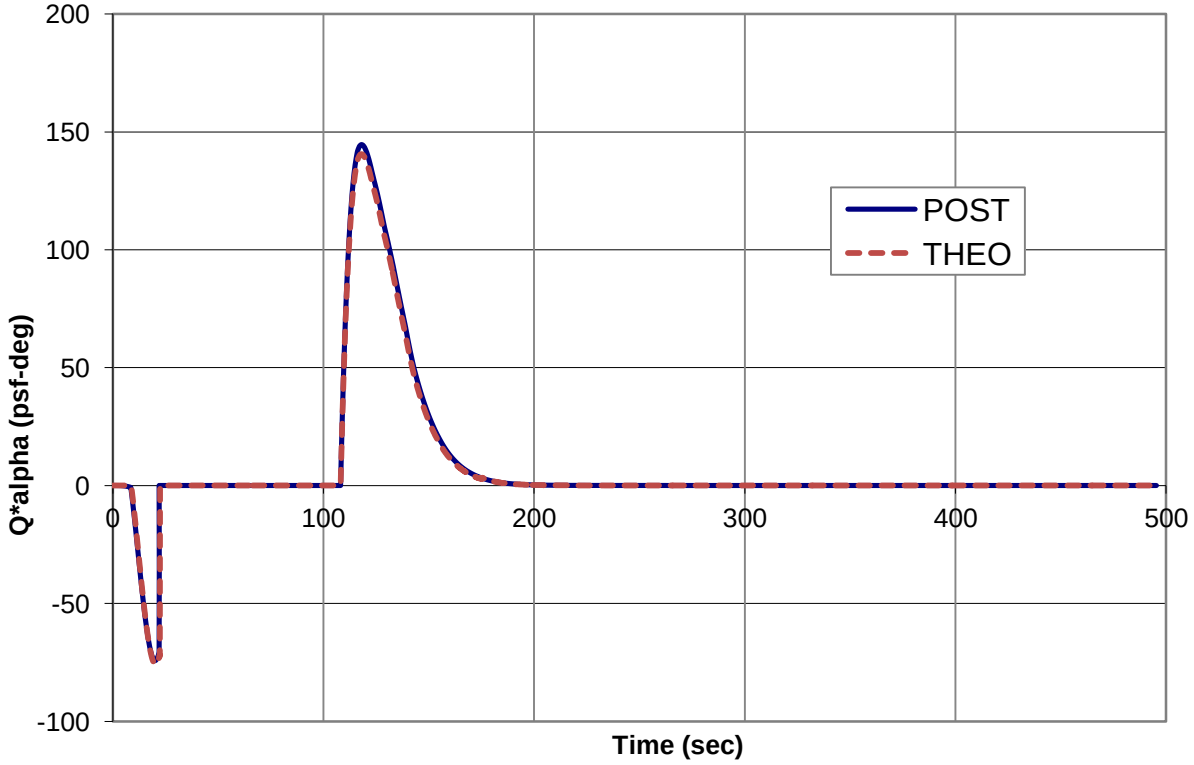

Figure B10. Dynamic Pressure * Angle of Attack (Q*alpha).

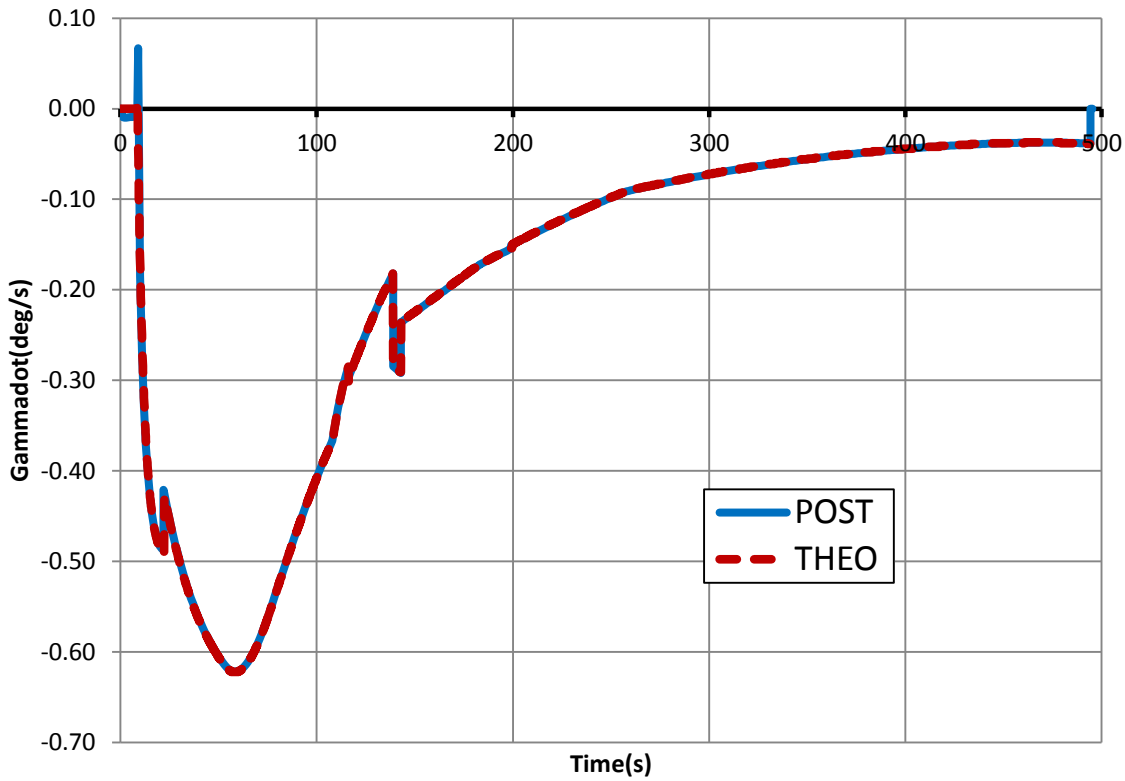

Figure B11. Rate of Change of Flight Path Angle.

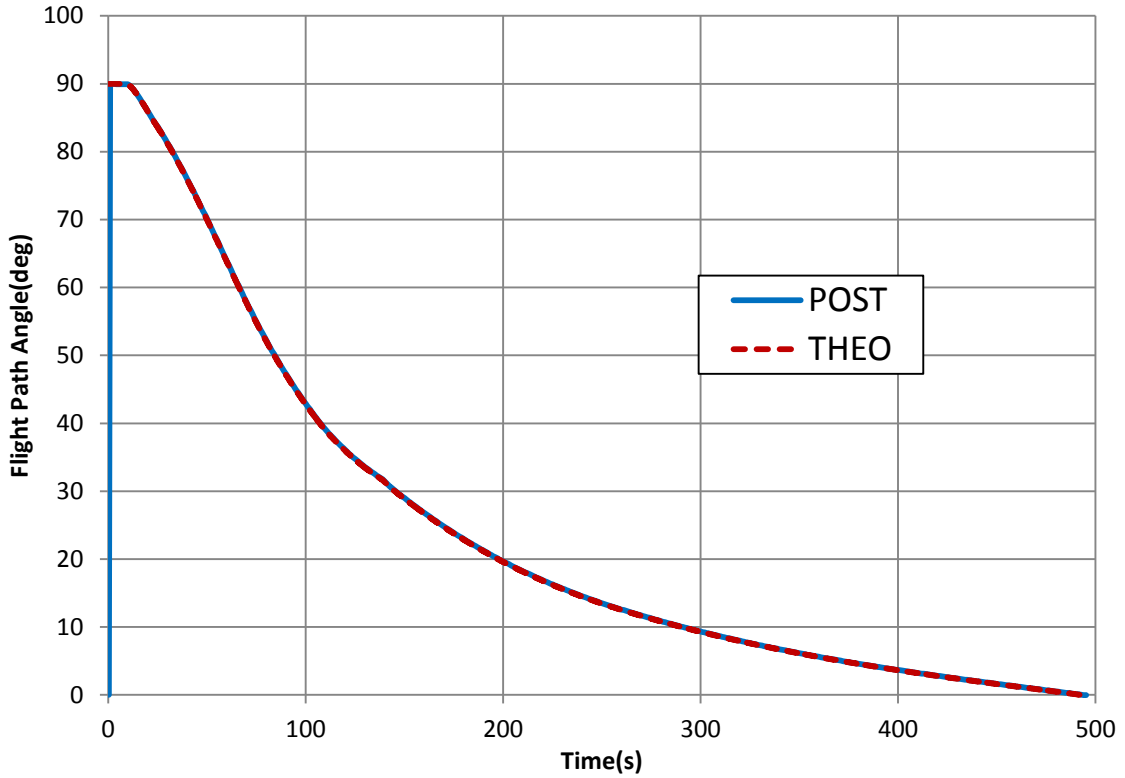

Figure B12. Relative Flight Path Angle.

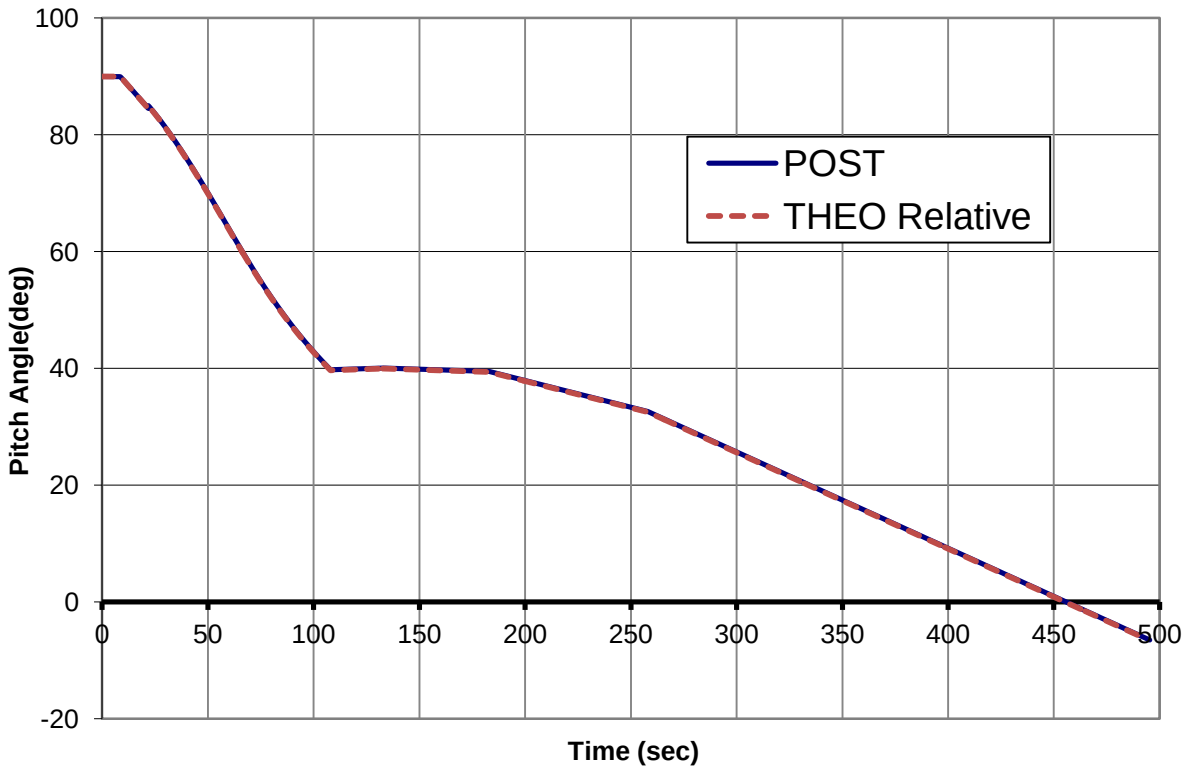

Figure B13. Pitch Angle.

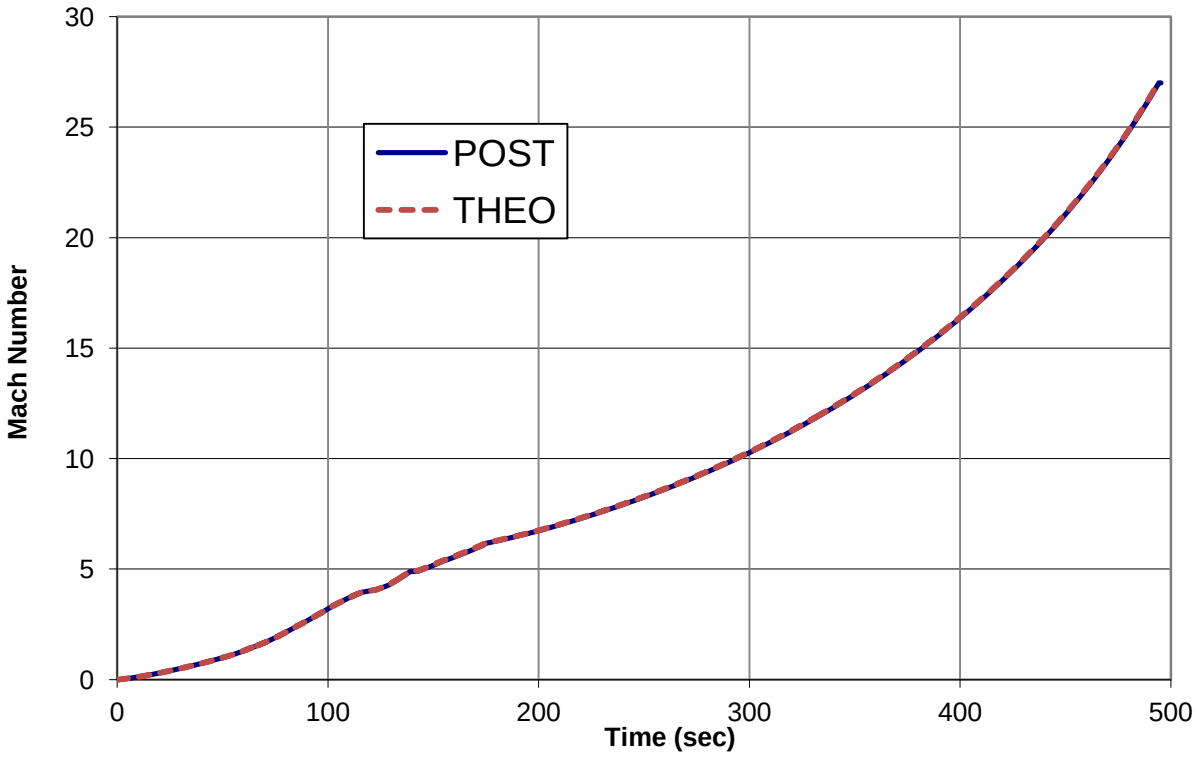

Figure B14. Mach Number

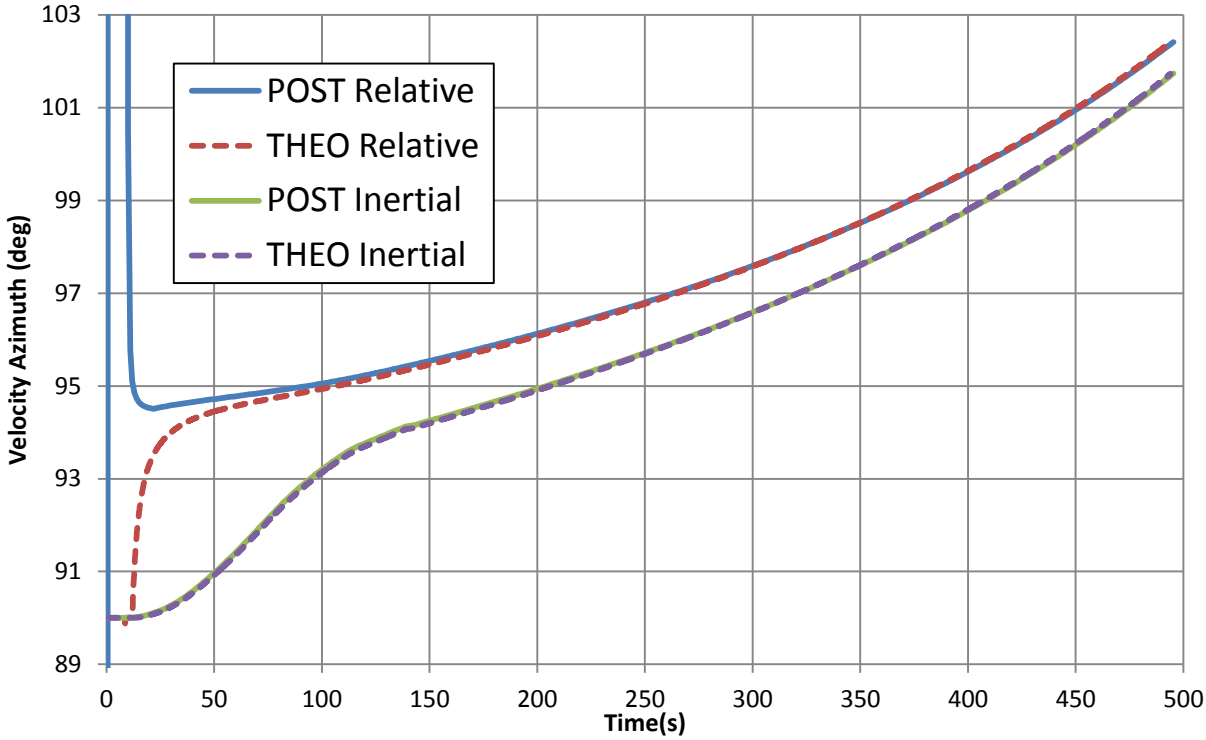

Figure B15. Velocity Azimuth.

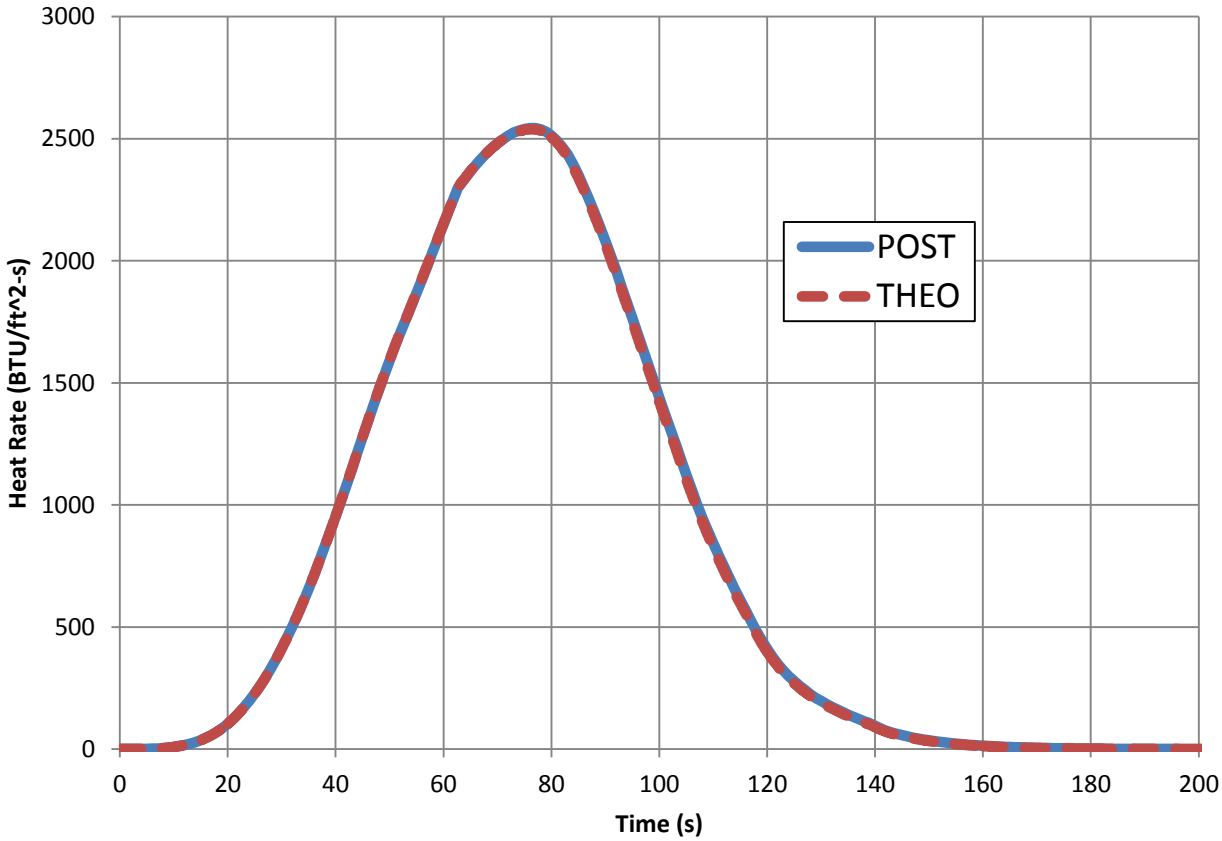

Figure B16. Heat Rate on the Vehicle.

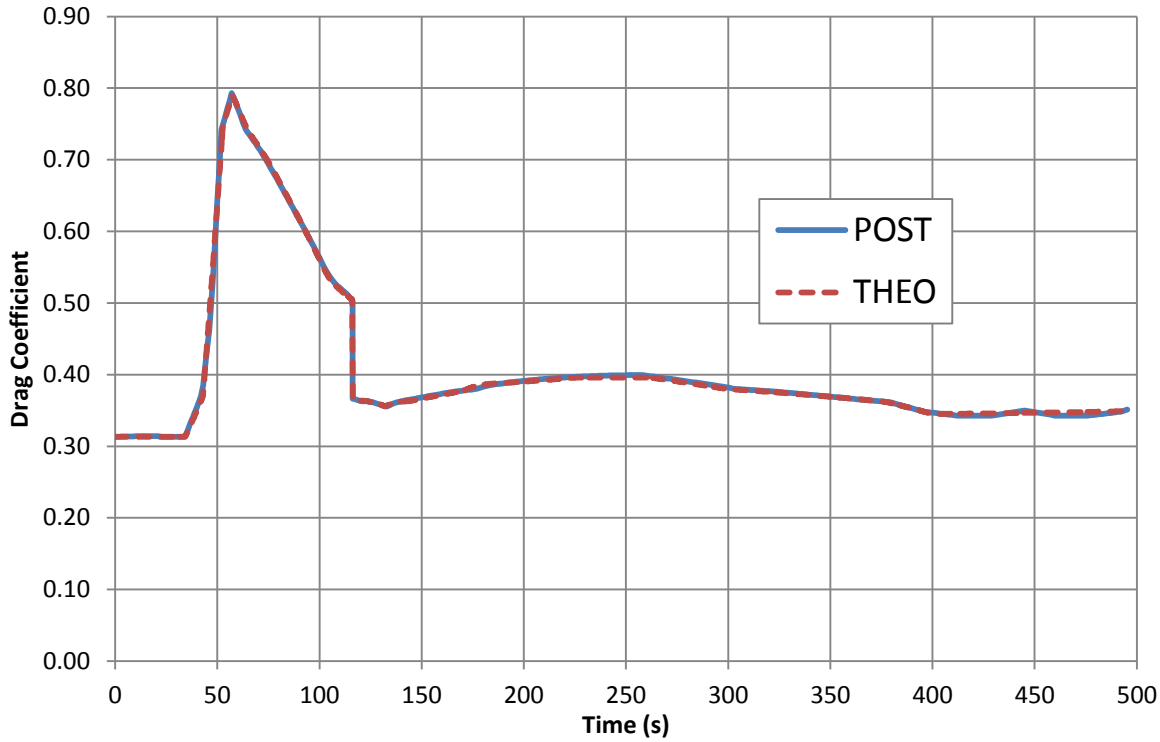

Figure B17. Vehicle Drag Coefficient.

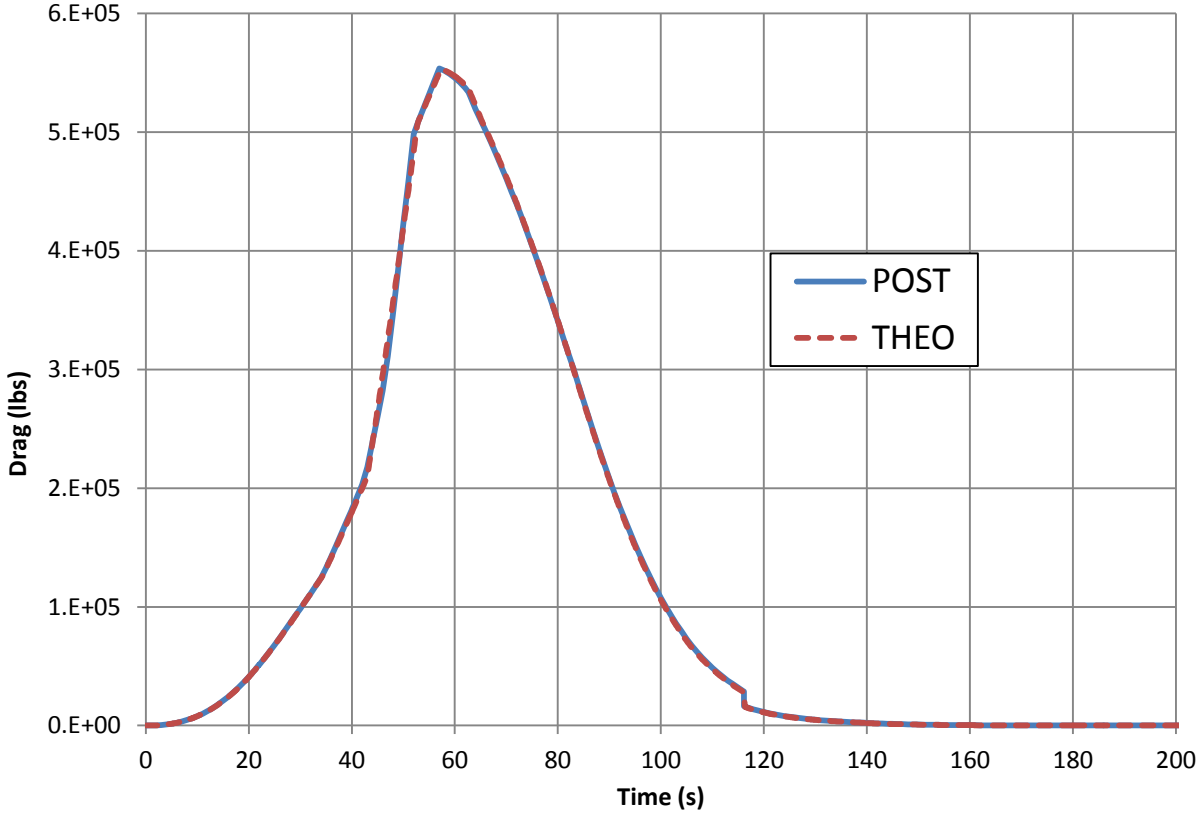

Figure B18. Vehicle Drag.

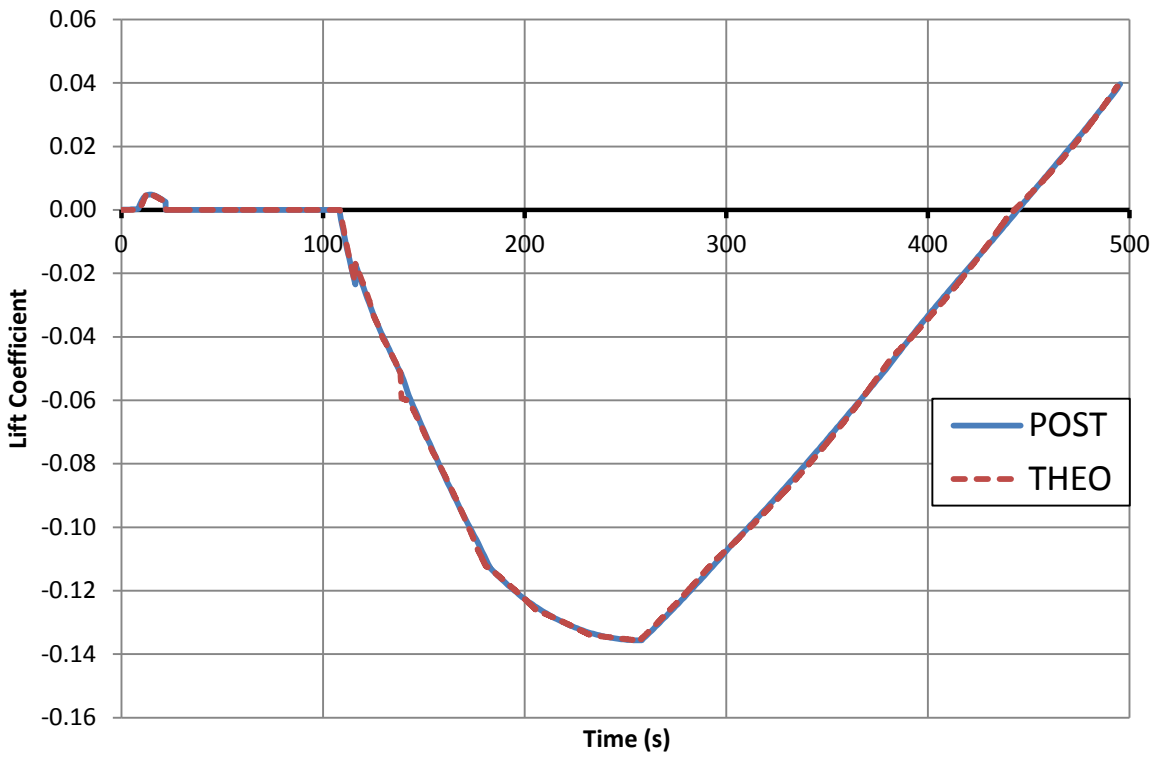

Figure B19. Lift Coefficient.

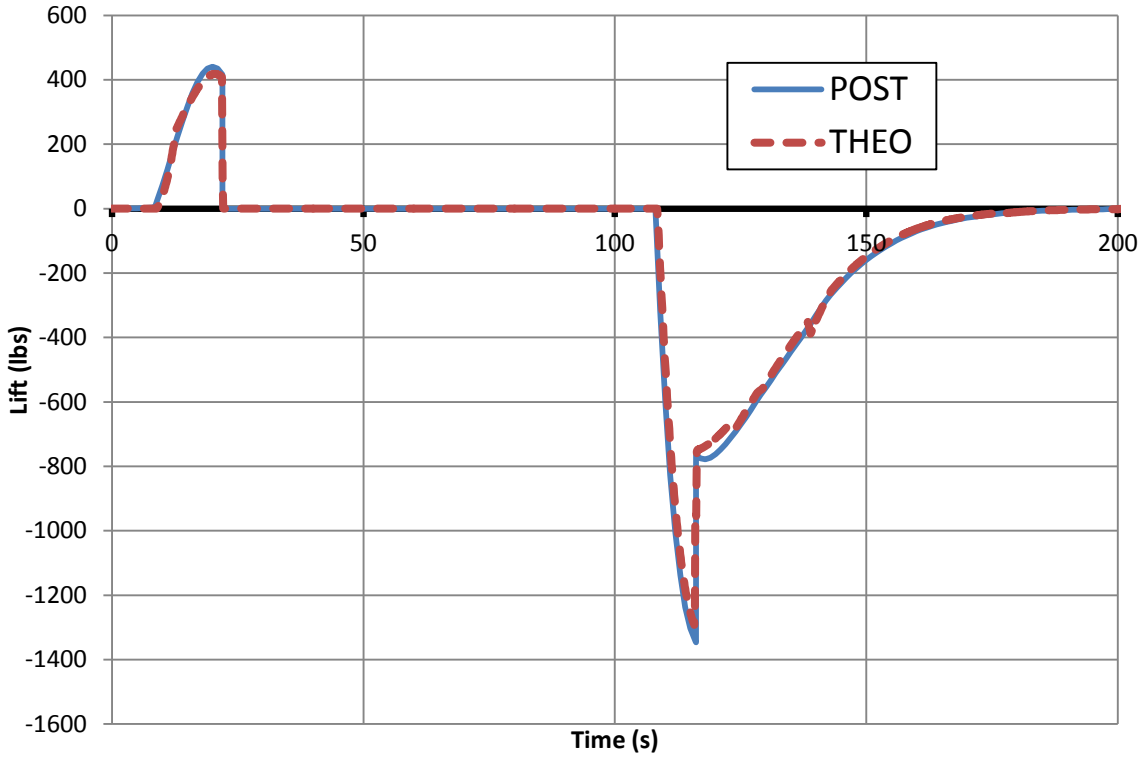

Figure B20. Vehicle Lift.

VITA

Paul Ritter was born as an army brat, the son of Michael and Patricia Ritter. As a child, he grew up moving around the world, experiencing many different lifestyles and cultures. Eventually his family settled in Clarksville, TN where he received his high school diploma at Clarksville High School. It was there that his passion for aerospace vehicles began to grow and drive him towards attending the University of Tennessee. It was there that he received his Bachelor of Science degree in Aerospace Engineering, and also where he was offered a Graduate Teaching Assistantship for a Master's program in Aerospace Engineering. He was then offered the opportunity to work with NASA on a heavy lift launch vehicle optimization which led to the results of this thesis.